THE UNIVERSITY
of EDINBURGH

Presynaptic dysfunction in CDKL5 deficiency disorder

Christiana Kontaxi

Thesis submitted for the degree of Doctor of Philosophy

University of Edinburgh

2021

"Any man could, if he were so inclined, be the sculptor of his own brain."

Santiago Ramón y Cajal

Declaration

I certify that this thesis has been composed entirely by myself. All experiments, analysis of data, and preparation of figures were conducted by me unless stated otherwise in the text. This work has not been submitted for any other degree or professional qualification.

30th September 2021

Abstract

Cyclin-dependent kinase-like 5 (CDKL5) deficiency disorder (CDD) is a monogenic developmental and epileptic encephalopathy with onset in early infancy that is caused by mutations in the *CDKL5* gene. CDD patients often exhibit profound neurodevelopmental delay, visual and motor deficits, and autistic-like manifestations, whereas epileptic seizures typically appear as early as the third week after birth. CDKL5 is a neuron-specific serine/threonine kinase that has been implicated in different cellular processes including neurite outgrowth, microtubule remodelling, and synaptogenesis. Animal models of CDKL5 deficiency have revealed phenotypes associated with defective neurotransmission. However, the potential role of CDKL5 in presynaptic processes and synaptic vesicle (SV) membrane trafficking remains unknown.

In this project, we used a novel CDKL5 KO rat model to detect potential phenotypes that are linked to loss of CDKL5 function. Using a genetically encoded fluorescent reporter, we revealed that absence of CDKL5 results in defective SV recycling in an activity-dependent manner in primary hippocampal neurons. Using a molecular replacement strategy, we showed that the kinase domain of CDKL5 was able to restore the speed of SV endocytosis indicating that the catalytic activity of CDKL5 is essential for its role in SV recycling. In agreement, we revealed that CDKL5 mutants either lacking the kinase domain or containing kinase-inactive mutations reported in CDD patients were unable to rescue this impairment suggesting that defective presynaptic processes may contribute to the CDD onset.

Since the kinase activity is critical for CDKL5-mediated SV recycling, we also explored whether the phosphorylation levels of its *in vitro* presynaptic substrate, amphiphysin 1 (Amph1), were altered in CDKL5 KO neurons. We revealed that CDKL5 does not exert its presynaptic role by phosphorylating Amph1 at S293. At the same time, this work showed that Amph1-mediated complexes are important for SV endocytosis in presynaptic terminals. Furthermore, we mapped the Amph1 motif that interacts with a different endocytosis protein, endophilin A1, and we demonstrated that the Amph1-endophilin A1 complex is essential for SV regeneration. Finally, the phosphorylation dynamics at Amph1-S293 dictates both Amph1-mediated interactions with endophilin A1 and SV endocytosis, indicating that phosphorylation-dependent Amph1-endophilin A1 interaction is essential for optimal SV endocytosis. Overall, this study offers the first evidence of a presynaptic role of CDKL5 that is mediated through its kinase activity and creates the basis for future research on presynaptic CDKL5 that could lead to potential treatments for CDD patients.

Lay summary

Cyclin-dependent kinase-like 5 (CDKL5) deficiency disorder (CDD) is an infant disorder that is characterised by intellectual disability and epilepsy. In CDD, modifications in the region of DNA that produces the human CDKL5 protein are responsible for constructing a damaged and dysfunctional version of the protein. CDKL5 is present in nerve cells (neurons) in the brain, and its role is to attach a chemical group called phosphate to other proteins to modify their function.

Neurons have the ability to transfer information from one to another. Two neurons meet each other at a junction called synapse that has two sides, a delivering presynaptic part and a receiving postsynaptic part. Small packs of chemical molecules, known as synaptic vesicles (SVs), are used for the delivery. The most important work of the presynaptic side is the preparation of SVs for delivery, the delivery itself, and then the reformation of SVs for the next round. Poor communication between the presynaptic and postsynaptic part leads to various disorders similar to CDD with the presynaptic part alone being critical for many of them. CDD is currently untreatable; as a result, it is very important to understand what roles the CDKL5 protein plays in the presynaptic side that could potentially assist the appearance of CDD.

In this study, we used neurons from rat brains that were not able to produce any CDKL5 protein to test if the SV cycle or any other process at the presynaptic side of the neuron was damaged. In neurons lacking CDKL5 protein, we found that the SV cycle becomes dysfunctional with the reformation of SVs taking more time compared to neurons producing CDKL5. Furthermore, we reported that inability of CDKL5 to add phosphate groups to

other proteins was key for slowing SV reformation. We tested whether one of these proteins was amphiphysin 1 (Amph1), since CDKL5 was previously shown to add phosphate to it. Amph1 generally assists the SV reformation at the presynaptic side, however we revealed that CDKL5-dependent phosphate addition to Amph1 played no role in SV reformation. At the same time, we explored the role of Amph1 in SV reformation by examining its ability to bind to a number of proteins. Changes in Amph1 that mimicked the addition of phosphate revealed that its interactions were altered with a different protein called endophilin. Furthermore, SV reformation was also affected, revealing that Amph1 binding to endophilin is important for this process. Overall, this project shows for the first time that CDKL5 is necessary for proper SV recycling at the presynaptic side and its loss might damage communication between neurons leading to CDD. This breaks new ground for future research on presynaptic CDKL5 that could lead to potential treatments for CDD patients.

Acknowledgements

Firstly, I would like to thank my supervisor, Prof Mike Cousin, who welcomed me in his group and gave me the opportunity to work on a project that I wanted a lot. I am very grateful for all the excellent scientific advice and for guiding my scientific development throughout my PhD. His generosity, kindness, and understanding have been remarkable. I feel very fortunate for having him as my supervisor and, in the future, I aspire to become a supervisor like him.

I would also like to thank my thesis committee, Prof Peter Kind and Dr Mandy Jackson, for the fruitful discussions and constructive feedback that I received in all our meetings. Also, Prof Peter Kind for allowing me to join his group's meetings. I really enjoyed them, and I have learnt a lot.

I am grateful to all the members of the Cousin lab for their help the past four years. Special thanks to Dr Elizabeth Davenport for introducing me to many of the techniques I have used; Dr Eva-Maria Blumrich for sharing her expertise in biochemistry and especially pull-down assays; Dr Daniela Ivanova for her help in the lab and our discussions; Dr Callista Harper for providing some templates for data analysis; and, lastly, Dr Rona Wilson for generating some of the mouse cultures that I used at the beginning of my PhD.

I would like to acknowledge the Kind lab for providing the CDKL5 KO rats for this project. Furthermore, special thanks to Lynsey Dunsmore and all the staff at the BVS facility at Hugh Robson Building that have been handling the *Cdkl5* KO LE line for their willingness to help and their dedication. I am very appreciative of their punctuality in providing the animals needed for my

project. Also, many thanks to all lab staff and especially Carol Wollaston and James Griffiths for the technical assistance.

I would also like to acknowledge the Principal's Career Development PhD Scholarship (The University of Edinburgh), the Loulou Foundation and the Simons Initiative for the Developing Brain for funding this work.

I would like to thank Dr Eugenia Goya for her encouragement and advice; Angeliki, for her company in the lab while we were working crazy hours; also, my friend, Dora, for her understanding and for sounding the alarm when I needed holidays.

I am very grateful to my parents and my sister, Natalia, for always listening uncomplainingly to all my concerns, supporting all my choices, and keeping me motivated.

A million thank-yous would not be enough to acknowledge the contribution of my partner, Marios, during my PhD. For sharing his coding expertise and his scientific advice, for his enthusiasm, for listening to my never-ending concerns, for making science more fun, for his understanding and all the movies we did not watch together at the weekends because I was acquiring movies in the microscope, for waiting with me in the lab every single night to finish my experiments, and all of these, while being an amazing scientist himself.

Last but not least, thanks to the latest recruit into my life, Hubert, that has been a great company while writing this thesis in the middle of a pandemic.

Table of contents

List of figures

List of tables

Abbreviations

aa	amino acids
ADBE	activity-dependent bulk endocytosis
AMPARs	α-amino-3-hydroxy-5-methyl-4-isoxazolepropionic acid-type glutamate receptors
Amph	amphiphysin
AP1	adaptor protein 1
AP2	adaptor protein 2
AP3	adaptor protein 3
AP5	2-amino-5-phosphonovaleric acid
APS	ammonium persulfate
APS	ammonium persulfate
ARP2/3	actin-related protein 2/3
ATP6V1B2	v-type proton ATPase subunit B
BAR	Bin/Amphiphysin/RVS
BDNF	brain-derived neurotrophic factor
BSA	bovine serum albumin
CALM	clathrin assembly lymphoid myeloid leukaemia

CBB	Coomassie Brilliant blue
CCV	clathrin-coated vesicle
CDD	CDKL5 deficiency disorder
Cdk5	cyclin-dependent kinase 5
CDKL5	cyclin dependent kinase-like 5
CHC	clathrin heavy chain
CLAP	clathrin-associated protein
CME	clathrin-mediated endocytosis
CNQX	6-cyano-7-nitroquinoxaline-2,3-dione
CNS	central nervous system
CV	coefficient of variance
DNMT1	DNA methyltransferase 1
Dyn1	dynamin 1
DYRK1A	dual specificity tyrosine-phosphorylation-regulated kinase 1A
EPS15	epidermal growth factor receptor substrate 15
EPS15R	EPS15-like 1
FAK	focal adhesion kinase
FCHO1/2	F-BAR domain only protein 1/2
GABA	γ-aminobutyric acid

GFP	green fluorescent protein
GluD1	glutamate D1 receptor
GSK3	glycogen synthase kinase 3
HDAC4	histone deacetylase 4
HSC70	heat shock cognate 70
iPSCs	induced pluripotent stem cells
IQGAP1	IQ domain-containing GTPase-activating protein 1
KO	knockout
MAPK	mitogen-activated protein kinases
mCer	mCerulean
mEPSCs	miniature excitatory postsynaptic currents
MES	2-(N-morpholino)ethanesulfonic acid
mIPSCs	miniature inhibitory postsynaptic currents
MT	microtubule
mTOR	mechanistic target of rapamycin
NA	numerical aperture
NDs	neurodevelopmental disorders
NES	nuclear export signal
NGL1	netrin-G1 ligand 1

NLS	nuclear localisation signal
NMDAR	N-methyl-D-aspartate receptor
NSF	N-ethylmaleimide-sensitive factor
N-WASP	neural Wiskott-Aldrich syndrome protein
PCR	polymerase chain reaction
PLD	phospholipase D
PRD	P-rich domain
PSD	postsynaptic density
RIM	Rab3-interacting molecule
rpS6	ribosomal protein S6
RRP	readily releasable pool
SDS	sodium dodecyl sulphate
SEM	standard error of the mean
SH3	Src homology 3
SNARE	soluble NSF-attachment receptor
SV	synaptic vesicle
SV2A	synaptic vesicle glycoprotein 2A
Syp1	synaptophysin 1
sypHy	synaptophysin-pHluorin

Syt1	synaptotagmin 1
TEMED	tetramethylethylenediamine
TGF-β	transforming growth factor β
TMR-dextran	tetramethylrhodamine-dextran
VAMP4	vesicle-associated membrane protein 4
VGLUT1	vesicular glutamate transporter 1
α-SNAP	α-soluble NSF-attachment protein

Chapter 1: Introduction

All animal central nervous systems (CNSs) consist of two cellular components, neurons and glial cells, that are initially organised into neural circuits and further into neural systems. Neural systems serve distinct purposes, including processing of different types of information from the environment (sensory), organisation and generation of actions (motor), or performing higher brain functions, such as memory, emotions, language, perception, and thinking.

Most neurons are specialised for long-distance electrical signalling and intercellular communication. These properties are attributed to the electrically excitable character of the neuronal membrane and the overall neuronal morphology. Two major features of neurons protrude from the cell body, the axon and the dendrites. The axon has numerous nerve terminals and can extend for a long distance from the cell body. On the other hand, the dendrites are characterised by extensive branching and can expand to a large surface in the vicinity of the cell body. Typically, the axonal terminal of a neuron reaches a particular region on the dendrites or cell body of a following neuron forming a specialised site, the synapse, that lacks physical connection, however. Intercellular communication occurs mainly in a unidirectional manner with postsynaptic elements being responsible for receiving inputs from the nerve terminals of presynaptic neurons that are then integrated and transmitted towards the axon. Axons, in turn, can deliver electrical activity towards nerve

terminals over long distances as "action potentials" due to regulated ion exchange across the neuronal membrane.

1.1 Neuronal communication at central synapses

Since the time of the "War of the Soups and the Sparks"[1], it is now well established that neuronal communication occurs mainly through chemical transmission at synapses. Synaptic signalling involves the release of chemical neurotransmitters, stored in synaptic vesicles (SVs) within the presynaptic nerve terminal, that bind to and activate receptors residing on the postsynaptic neuron triggering a cascade of intracellular reactions. The main excitatory neurotransmitter is the amino acid glutamate, whereas the main inhibitory neurotransmitter is γ-aminobutyric acid (GABA). Neurotransmitter secretion occurs in discrete quanta and is mediated by SV exocytosis in a calcium-dependent manner, usually after depolarization of the presynaptic membrane. After exocytosis, the membrane corresponding to fused SVs together with their molecular components is endocytosed via various modes and SVs are subsequently recycled. This membrane recycling that SVs undergo in nerve terminals is adequately fast and necessary to prevent any shortage due to continuous neurotransmission preserving thus neuronal activity.

[1] Reference is made here on the book "The War of the Soups and the Sparks" by Elliot S. Valenstein (Columbia University Press, 2005) that describes the debate over whether neuronal impulses are transmitted electrically or chemically that emerged between pharmacologists and electrophysiologists in the 1950s.

1.1.1 Neurotransmitter release

Neurotransmitters are released through SV exocytosis generally in response to excitation of the presynaptic membrane that occurs upon arrival of action potentials. During exocytosis, SVs fuse with the lipid bilayer of the plasma membrane allowing their content to be secreted into the surrounding presynaptic cleft. Although exocytosis is a common mechanism of membrane trafficking in cells, exocytosis of SVs differs as it is a calcium-dependent process and takes place exclusively at a specialised site of the presynaptic membrane, known as active zone, that spans opposite to the postsynaptic density (PSD). The depolarization of the presynaptic membrane results in opening of voltage-gated calcium channels that are organised in nano- or microdomains within the active zone leading to influx of calcium into the nerve terminal (Eggermann *et al.*, 2011; Dolphin & Lee, 2020). This initiates the fusion of SVs with the local neuronal membrane, but only those physically attached to the active zone. These requirements prior to fusion indicate that SV exocytosis is a complex multi-step cellular process.

One of the steps that precedes SV fusion is the physical translocation of SVs closer to the active zone. In general, SVs are organised into functionally distinct clusters within the cytoplasm of individual presynaptic boutons (Crawford & Kavalali, 2015). These vesicle subpopulations differ in size, mobility, position with respect to the active zone and are generally supplied by different modes of endocytosis (Fowler & Staras, 2015). Under prolonged stimulation, SVs composing the recycling pool move to the active zone to replenish vesicles as they are exocytosed. The recycling pool is considered to reside close to the active zone bound to a cytoskeletal matrix that includes various protein components, such as Rab3-interacting protein (RIM), ELKs,

bassoon, and piccolo (Schikorski & Stevens, 2001; Emperador-Melero & Kaeser, 2020). The remaining SVs form the reserve pool (or resting pool) that constitutes around 50 % of the total vesicle pool in rodent hippocampal synapses and is confined to a static state of unknown physiological significance (Crawford & Kavalali, 2015). SVs are held together with the help of synapsin, a peripheral vesicle protein, via phase separation (Shupliakov *et al.*, 2011; Orenbuch *et al.*, 2012; Milovanovic *et al.*, 2018; X. Chen *et al.*, 2020; Pechstein *et al.*, 2020). SV pools are dynamic entities both within and across synapses and evidence suggests that synapsin is the major regulator of vesicle mobility (Fernandez-Alfonso & Ryan, 2008; Bykhovskaia, 2011). Whether sorting of SVs originating from different cluster locations or endocytosis spots involves partly diffusion or is mediated entirely by actin and motor proteins, such as myosin V, has not been fully clarified (Ryan, 1999; Gramlich & Klyachko, 2017). Nevertheless, it has been supported that the interplay between Cdk5-mediated phosphorylation and calcineurin-mediated dephosphorylation of synapsin 1 is important for sorting newly endocytosed SVs (Fassio et al., 2016).

After being recruited to the active zone, SVs are subjected to docking and priming that refers to their physical attachment to the release site and activation of the release machinery, respectively. Docked and primed SVs are considered a distinct vesicle pool of the nerve terminal known as the readily releasable pool (RRP) and they are the first vesicles to be fused in response to brief stimulus. In cultured hippocampal neurons, ~4 docked vesicles are estimated to exist per synapse, whereas electron microscopy studies revealed that the RRP consists of ~10-15 (Ariel *et al.*, 2012; Kaeser & Regehr, 2017). Undocked vesicles close to empty docking sites form connections to the same active zone macromolecules that hold the docked vesicles at rest (Szule *et al.*,

2012). Docking is achieved by interaction of the vesicle protein VAMP2 or synaptobrevin 2 with the plasma membrane proteins SNAP-25 and syntaxin 1 forming a heterotrimeric complex known as soluble N-ethylmaleimide-sensitive factor (NSF)-attachment receptor (SNARE) complex and the assistance of proteins of the active zone, such as the Rab3-interacting molecule (RIM) and Munc13 (Dulubova *et al.*, 2005; Jahn & Fasshauer, 2012; Kaeser & Regehr, 2017). RIM interacts with the vesicle protein Rab3 tethering the SV at the release site (Wang *et al.*, 1997). Attached SVs undergo priming, a reaction to make them competent for fusion in a calcium-triggered manner, with the aid of Munc13 and Munc18 (Lai *et al.*, 2017). Munc18 is cytosolic protein interacting tightly with syntaxin 1 that adopts a "closed" conformation preventing possibly a premature SNARE complex assembly as well as controlling the timing of the SNARE activation (Verhage & Sorensen, 2008; Jahn & Fasshauer, 2012). Furthermore, Munc18 also participates in docking in chromaffin cells (Voets *et al.*, 2001), although the number of docked SVs remains unaltered in Munc18-deficient terminals (Verhage *et al.*, 2000). The Munc13-facilitated dissociation of Munc18 from syntaxin 1 allows the assembly of the SNARE complex where syntaxin 1 participates in an "open" state (Lai et al., 2017). The activation of the SNARE complex at the release site forces the lipid bilayer of the SV to closely associate with the lipid bilayer of the active zone. Two structures of four parallel α-helices from the SNARE proteins are formed on both sides of the attached vesicle (zippering) that extend into the membrane (Sutton *et al.*, 1998; Stein *et al.*, 2009; Sinha *et al.*, 2011). The docking and priming together require about 10-20 ms and are both reversible.

Calcium induces the completion of fusion in less than 0.5 ms involving the binding of multiple calcium ions at calcium binding C2 domains (Shao *et al.*,

1998; Ubach *et al.*, 1998; Ubach *et al.*, 2001). Several candidates bearing C2 domains are present at SVs and active zones, however, synaptotagmin 1 containing two C2 domains, C2A and C2B, constitutes the major calcium sensor for synchronous evoked release (Geppert *et al.*, 1994; Fernandez-Chacon *et al.*, 2001). Synaptotagmin 1 interacts with the SNARE complex through several interfaces including a large calcium-independent interface (Zhou *et al.*, 2015). Upon calcium binding, synaptotagmin 1 binds to curved membranes promoting the SNARE-mediated fusion of SVs (Martens *et al.*, 2007; Hui *et al.*, 2009). Despite that several mechanisms have been proposed for the synaptotagmin 1-SNARE complex cooperation (Rizo, 2018), this results in the opening of a fusion pore that expands as the SV membrane merges with the local neuronal membrane allowing the release of neurotransmitters. Another small cytosolic protein, named complexin, partially promotes the stabilization of the zippered SNARE complex and also activates it for synaptotagmin 1-regulated fusion (Xue *et al.*, 2008; Xue *et al.*, 2010; Jahn & Fasshauer, 2012; Yang *et al.*, 2013). After completion of fusion, conformational changes in NSF due to ATP hydrolysis result in the dissociation of the SNARE complex with the aid of the cytosolic factor α-SNAP (Sollner *et al.*, 1993; Hanson *et al.*, 1997; Rizo, 2018) allowing therefore for another round of exocytosis to occur.

1.1.2 Synaptic vesicle regeneration

The limited number of SVs in presynaptic terminals in combination with the altered surface tension established after SV fusion urges SVs to be reformed in order to avoid their depletion upon repeated rounds of exocytosis as well as to preserve membrane homeostasis. Retrieval of SVs occurs at the

periactive zone region through distinct endocytosis pathways that include the clathrin-mediated endocytosis (CME) and three clathrin-independent modes known as activity-dependent bulk endocytosis (ADBE), ultrafast endocytosis, and "kiss-and-run" depicted in Figure 1.1 (Milosevic, 2018). Except for their clathrin-dependency, these pathways differ in terms of the size of the internalised synaptic membrane: in CME, endocytosed clathrin-coated vesicles are of similar size to SVs (described in more depth in 1.1.2.1 Clathrin-mediated endocytosis); in ADBE, large membrane invaginations are observed, known as bulk endosomes (described in detail in 1.1.2.2 Activity-dependent bulk endocytosis); in ultrafast endocytosis, large endocytic vesicles are reported that do not reach the size of bulk endosomes; and lastly, in "kiss-and-run", a transient fusion pore closes to directly reform the exocytosed SV. The stimulation conditions, kinetics, temperature sensitivity, neuronal subtype, and presynapse maturity are additional aspects that determine the SV endocytosis route (Renden & von Gersdorff, 2007; Gan & Watanabe, 2018; Chanaday *et al.*, 2019). Newly endocytosed SVs are subsequently reacidified and refilled with neurotransmitters with the aid of the vacuolar-type H^+-ATPase that drives protons into the SV lumen upon ATP hydrolysis and vesicular neurotransmitter transporters that utilise the protonmotive force generated to accumulate neurotransmitters (Farsi *et al.*, 2017; Gowrisankaran & Milosevic, 2020). Neurotransmitter-filled SVs either supply the reserve pool for future use or return to the local recycling pool to enter another cycle of fusion. Since SV endocytosis is key for the SV regeneration and defines their fate in the presynaptic bouton, different mechanisms of SV endocytosis are reviewed in the following subsections with a special focus on CME and ADBE that have been explored in this thesis.

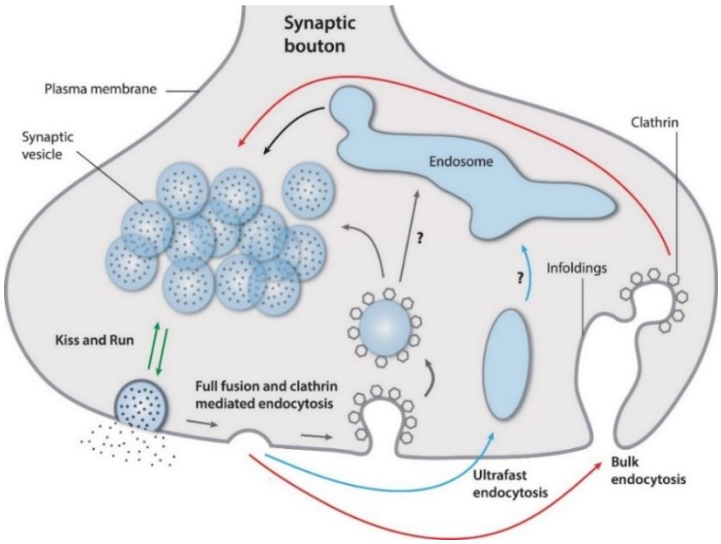

Figure 1.1 Main modes of SV endocytosis in nerve terminals

Schematic illustration of the major routes of SV endocytosis in nerve terminals that include "kiss-and-run", CME, ultrafast endocytosis, and ADBE as illustrated in the figure. "Kiss-and-run" involves the SV regeneration after closure of the fusion pore without having been preceded by a full fusion with the presynaptic membrane. CME occurs via clathrin-coated vesicles that bud directly from the plasma membrane. Ultrafast as well as bulk endocytosis involve the formation of large endosome-like structures from which SVs bud subsequently. Adapted from Jahne et al. (2015).

1.1.2.1 Clathrin-mediated endocytosis

CME is a ubiquitous process of eukaryotic cells that refers to the uptake of surface material into the cytoplasm employing clathrin-coated vesicles (McMahon & Boucrot, 2011). In nerve terminals, CME occurs with time constants over 5-10 s making CME a slow type of SV endocytosis with respect to other endocytosis mechanisms (Milosevic, 2018). Clathrin is composed of three clathrin heavy chains that form a trimeric structure known as triskelion and three clathrin light chains that have a regulatory role. Triskelia interact with each other to form polygonal "cages" that enclose invaginated endocytic pits. CME occurs in five successive stages that include initiation, cargo loading, membrane bending, vesicle scission, and disassembly of the coat (Kaksonen & Roux, 2018).

The process starts with the clustering of coat proteins in the cytosolic side of endocytic pits that display high local concentration of transmembrane proteins meant to be incorporated into the retrieved SV (cargo) and phosphatidylinositol 4,5-bisphosphate $PI(4,5)P_2$ phospholipids (Antonescu *et al.*, 2011). These two signatures of endocytic sites act as the seed for promoting the endocytic coat assembly at a specific location. Although CME is named after clathrin, this endocytic coat consists also of clathrin-associated adaptors that mediate the attachment of the clathrin "cage" to the plasma membrane and cargo, such as the heterotetrameric adaptor protein 2 (AP2) complex and the F-BAR domain only protein 1/2 (FCHO1/2) (Henne *et al.*, 2010; Kelly *et al.*, 2014). In addition, several scaffold proteins are recruited that participate in assembling the coat components together. Proteins with scaffolding activities are the epidermal growth factor receptor substrate 15 (EPS15), EPS15-like 1 (EPS15R) and intersectin (Marie *et al.*, 2004; Koh *et al.*, 2007). Binding of the

AP2 complex allows the recruitment of clathrin thus forming a clathrin-coated pit after being progressively polymerised to curved lattice. In parallel, interaction between the cytosolic region of cargo molecules and coat proteins results in cargo accumulation in the coated sites of the membrane and simultaneously induces membrane bending (Traub, 2009). Initiation-promoting adaptor and scaffolding proteins in addition to other cargo-associated adaptors, such as proteins of the clathrin assembly lymphoid myeloid leukaemia (CALM) family, AP180 and epsins, are essential for cargo loading and membrane bending (Ford *et al.*, 2001; Ford *et al.*, 2002; Miller *et al.*, 2015).

Following clathrin-coat assembly and cargo loading, the initial membrane bending deepens progressively enabling the budding of the clathrin-coated pit. Membrane curvature is mediated by several endocytic elements including coat-associated proteins, actin filaments as well as scission-related proteins (Saheki & De Camilli, 2012; Kaksonen & Roux, 2018). Although the way clathrin lattice contributes to forcing membrane to deform is still debatable, other coat proteins that bear amphipathic helices are involved including AP180 and epsin initially, while sorting nexin 9 and FBP17 arrive later as the membrane bending progresses (Ford *et al.*, 2002; Miller *et al.*, 2015). Evidence also supports a role for actin cytoskeleton in membrane shaping according to which regulatory proteins of the neural Wiskott-Aldrich syndrome protein (N-WASP) induce transient actin nucleation at endocytic sites mediated by actin-related protein 2/3 (ARP2/3) and other actin-related components (McMahon & Boucrot, 2011; Li *et al.*, 2015).

During vesicle scission, the neck of the mature clathrin-coated membrane is constricted and cut to detach the clathrin-coated vesicle (CCV) from the plasma membrane. The fission is assigned to the GTPase dynamin 1 (Dyn1)

that polymerises to a collar-like structure surrounding the neck of the budding vesicle upon GTP hydrolysis (Antonny *et al.*, 2016). Dyn1 is mainly recruited by the Bin/Amphiphysin/RVS (BAR)-containing proteins amphiphysin and endophilin that arrive at the site of the budding pit when the membrane there is highly bent (Daumke *et al.*, 2014). These proteins not only are able to detect and stabilise membrane curvature but also coordinate vesicle scission with actin assembly and recruit uncoating elements (Frost *et al.*, 2009; Milosevic *et al.*, 2011). However, whether they facilitate or block vesicle scission itself remains quite controversial (Boucrot *et al.*, 2012; Takeda *et al.*, 2018).

The cargo containing CCV undergoes uncoating that involves the dissociation of the endocytic machinery. Coat disassembly is mediated by synaptojanin 1, a phosphatase that dephosphorylates $PI(4,5)P_2$ to PI promoting thus the unbinding of clathrin adaptor proteins and heat shock cognate 70 (HSC70) chaperone that breaks the clathrin lattice in an energy-dependent manner and is recruited by the clathrin-binding auxilin cofactor (Massol *et al.*, 2006; Perera *et al.*, 2006; Kaksonen & Roux, 2018). The uncoated SV can fuse with its targeted endosomal compartment from which it is retrieved and reacidified afterwards as mentioned above in subsection 1.1.2. Alternatively, the SV can be acidified and directly supply the recycling pool, whereas endocytic components can be reused for another round of endocytosis (Milosevic, 2018).

1.1.2.2 Activity-dependent bulk endocytosis

While CME can support neurotransmission at a slow rate and under mild to moderate depolarising conditions, faster endocytosis processes are required upon increased neuronal activity. ADBE is the predominant pathway

employed during intense activity levels and involves the clathrin-independent internalisation of large plasma membrane regions (Clayton *et al.*, 2008; Kasprowicz *et al.*, 2008). These membrane invaginations undergo scission in a couple of seconds forming bulk endosomes often larger than 100 nm in diameter (Wu & Wu, 2007; Clayton *et al.*, 2008). After bulk endosomes are retrieved, SVs bud from their surface with the aid of a clathrin lattice comparable to that of the CME pathway although other patterns for regenerating endosome-derived SVs have been described (Cheung & Cousin, 2013; Milosevic, 2018).

ADBE acts as a highly regulated homeostatic mechanism for balancing the presynaptic net surface area upon increased excitation and restocking the SV pool when the neurotransmission demands are high. What seems to drive the formation of a large invagination instead of a clathrin-coated vesicle (as in CME) or a large endocytic vesicle (as in ultrafast endocytosis) is tightly associated with the dependence of ADBE on the strength of the stimulus. ADBE initiation is coupled with preceding calcium-induced SV fusion triggered by high stimulation frequencies (Wenzel *et al.*, 2012; Morton *et al.*, 2015). Firstly, high calcium influx due to elevated activity increases the presynaptic calcium concentration at such a level that can be detectable in the region adjacent to the active zone activating a series of downstream events that differentially switch on ADBE compared to other SV recycling pathways. EGTA-AM achieves to block ADBE proving that delocalised calcium is needed to trigger it (Morton *et al.*, 2015). Secondly, this calcium influx is likely to utilise preferentially ADBE-promoting calcium channels, such as the SV-associated calcium channel Flower that is transferred to the periactive zone where ADBE occurs upon fusion (Yao *et al.*, 2017).

Initially, calcium accumulation induces the calcium-dependent phosphatase calcineurin to form a complex with calmodulin and Dyn1 and dephosphorylate the latter (Clayton *et al.*, 2009; Xue *et al.*, 2011). The dephosphorylated form of Dyn1 at S774 and S778 interacts subsequently with syndapin 1 through utilising specific proline-rich protein motifs (Clayton *et al.*, 2009; Quan & Robinson, 2013). Knocking down syndapin 1 was shown to impair ADBE in neuronal cultures similarly to presynaptic microinjection of syndapin antibodies, pointing to a key role for syndapin 1 in mediating ADBE (Andersson *et al.*, 2008; Clayton *et al.*, 2009). Syndapin 1 contains an F-BAR domain that preferentially detects less curved membranes and thus it has been proposed that it facilitates and stabilises the bulk membrane bending (Andersson *et al.*, 2008; Clayton *et al.*, 2009). Reversibly, phosphorylation of Dyn1 at S774 by glycogen synthase kinase (GSK) 3 that requires prior phosphorylation at S778 by cyclin-dependent kinase (CDK) 5 abolishes the binding to syndapin 1 (Clayton *et al.*, 2010). During high frequency stimulation, GSK3 is phosphorylated itself by Akt and thus remains inactive (Smillie & Cousin, 2012). Whereas the stimulus-evoked Dyn1 dephosphorylation-rephosphorylation interplay dictates the binding to syndapin 1 and thus is important for ADBE, the contribution of other endocytic proteins whose phosphorylation state is also regulated in an activity-dependent manner, such as amphiphysin or synaptojanin, is still unknown.

The bulk membrane undergoes scission to form a bulk endosome that it is possibly mediated by the GTPase activity of Dyn1 (Clayton *et al.*, 2009; Nguyen *et al.*, 2012; Kasprowicz *et al.*, 2014). Whether syndapin 1 recruits dephosphorylated Dyn1 monomers at the neck of the bulk invagination to promote scission remains unclear. Besides, it is not unlikely that other Dyn-

binding proteins involved in CME are also implicated in ADBE. For example, overexpression of a dominant-negative mutant of endophilin in primary neuronal cultures impairs SV endocytosis after high frequency stimulation (Kononenko *et al.*, 2014). Moreover, a mutant of the *Drosophila* ortholog of intersectin lacking Dyn-interacting domains causes translocation of Dyn1 from the periactive zone and accumulation of large membrane invaginations there (Winther *et al.*, 2013). Except for Dyn1, other Dyn isoforms might also contribute to membrane scission in ADBE in the absence of Dyn1, since bulk endosomes are reported in Dyn1/3 double knockout (KO) neurons potentially due to the action of Dyn2 (Wu *et al.*, 2014). A role for actin polymerisation in both initiation and maturation of the bulk invagination has been also proposed (Nguyen *et al.*, 2012; Kononenko *et al.*, 2014; Wu *et al.*, 2016; Soykan *et al.*, 2017). Two regulatory molecules of ADBE, the promoting Rab GTPase Rab11 and the inhibitory synaptotagmin 11, have been identified but their activity extends to other retrieval modes implying that they are more general endocytosis regulators than ADBE-specific (Wang *et al.*, 2016; Kokotos *et al.*, 2018).

Several SV cargoes have been identified to be also retrieved by bulk endosomes (Kokotos *et al.*, 2018). To date, only the vesicle-associated membrane protein 4 (VAMP4) has been confirmed as an ADBE-specific cargo (Nicholson-Fish *et al.*, 2015). VAMP4 is sorted in bulk endosomes after interacting with the adaptor protein 1 (AP1) through a dileucine motif (Peden *et al.*, 2001; Nicholson-Fish *et al.*, 2015). In addition, it seems to be essential for ADBE itself since its downregulation inhibits ADBE in neuronal cultures (Nicholson-Fish *et al.*, 2015).

After their internalisation, bulk endosomes undergo slow acidification with the time constant to be estimated around 32 s (Nicholson-Fish *et al.*, 2015). Apart from ADBE, SVs regeneration from the endosomal membrane require

both calcium and calcineurin (Cheung & Cousin, 2013). The calcium source for SV reformation is considered to be the bulk endosome itself, since it contains high concentration of calcium imported during ADBE and released into the cytosol upon its acidification (Cheung & Cousin, 2013). This calcium efflux activates calcineurin and triggers the same Dyn/syndapin interaction needed to form bulk endosomes (Cheung & Cousin, 2019). Clathrin and different adaptor protein complexes including AP1, AP2 and adaptor protein 3 (AP3) are essential for facilitating SV budding from the endosomal membrane (Cheung & Cousin, 2012; Kononenko *et al.*, 2014). Following their retrieval, ADBE-derived SVs restock exclusively the reserve SV pool that is employed during high frequency stimulation (Cheung *et al.*, 2010).

1.1.3 Presynaptic deficits in neurodevelopmental disorders

Neurodevelopmental disorders (NDs) refer to a heterogeneous group of conditions with onset during the developmental period (American Psychiatric Association, 2017). Although the various classification systems for NDs are quite inconsistent, a broader grouping incorporates attention deficit hyperactivity disorder, autism spectrum disorders, intellectual disability, as well as psychiatric disorders, such as schizophrenia and bipolar disorder, and epilepsy (Thapar *et al.*, 2017). NDs usually involve disruption of proper brain development and lead to cognitive, social and motor deficits, whereas epileptic seizures are a frequently observed comorbidity (Zoghbi & Bear, 2012; Thapar *et al.*, 2017). NDs are attributed to diverse and still elusive etiologies, including both environmental factors and genetic causes of different inheritance. While genetic studies have revealed a large number of loci implicated in NDs, *de novo* mutations in key developmental genes make also a

major contribution to NDs onset with a prevalence of approximately 1 to 200-450 live births (Vissers *et al.*, 2016; Deciphering Developmental Disorders, 2017). For example, *de novo* mutations in single genes, such as *CDKL5*, *MeCP2*, and *SCN1A*, are responsible for some of the most severe neurodevelopmental conditions in infants (Fallah & Eubanks, 2020). However, despite their significant socioeconomic impact, the neuropathological mechanisms underlying NDs are still not understood in most cases.

Strong evidence supports that alterations in presynaptic processes can lead to NDs, such as autism and epilepsy (Waites & Garner, 2011; Fukata & Fukata, 2017). Genetic studies have identified pathogenic mutations in proteins associated with many aspects of the SV biology including SV recycling (Cortes-Saladelafont *et al.*, 2018). Remarkably, SV-related conditions are often characterised by severe early-onset neurodevelopmental delay and intellectual disability (Cortes-Saladelafont *et al.*, 2018). An example of an SV protein that has been associated with epilepsy is the synaptic vesicle glycoprotein 2A (SV2A), which is the target of multiple candidate antiepileptic drugs (Lynch *et al.*, 2004; Stephen & Brodie, 2018; Wood *et al.*, 2020). SV2A is an integral vesicular glycoprotein that regulates calcium-induced exocytosis at low stimulation frequencies by facilitating SV priming at the release sites and interacting with the main calcium sensor, synaptotagmin 1 (Custer *et al.*, 2006). It also enables the internalisation of synaptotagmin 1 in a phosphorylation-controlled way suggesting a potential role for SV2A in SV retrieval (Zhang *et al.*, 2015). Homozygous and heterozygous missense mutations on SV2A have been reported in humans to result in severe epilepsy and cognitive impairment (Serajee & Huq, 2015; Wang *et al.*, 2019). Likewise, *de novo* heterozygous mutations in the gene encoding for synaptotagmin 1 have been identified in patients that experience profound cognitive

impairment (Baker *et al.*, 2018). These mutations that cluster particularly within the C2B domain impact on SV recycling and display impaired exocytic rate after sustained stimulation (Baker *et al.*, 2018). Lastly, a nonsense mutation in the gene encoding for synapsin 1, a SV phosphoprotein that maintains the reserve pool and facilitates SV clustering, has been associated with epilepsy and autism-related behaviours (Garcia *et al.*, 2004). Neurons derived from synapsin 1-deficient mice, that exhibit seizure activity (Etholm *et al.*, 2012), display decreased RRP size coupled with impaired SV recycling rate (Baldelli *et al.*, 2007).

Epilepsy-related genes encoding for synaptic proteins that mediate SV endocytosis suggest that endocytic molecules are equally important for modulating neuronal excitability. Mice carrying *de novo* heterozygous mutation in *Dnm1* exhibit consistently recurrent seizures with the phenotype being more severe or even lethal in the homozygous state (Boumil *et al.*, 2010). Spontaneous patients mutations impact on SV endocytosis in a dominant-negative way *in vitro* (Dhindsa *et al.*, 2015). Mechanistically, Dyn1 variants demonstrate declining oligomerisation capability and fission activity (Dhindsa *et al.*, 2015). Pathogenic mutations are also reported in the gene that encodes for AP1 subunits resulting in severe intellectual disability (Tarpey *et al.*, 2006; Candiello *et al.*, 2016). Evidence shows that these mutations cause accumulation of early endosomes, reduced number of SVs, and slower SV recycling (Candiello *et al.*, 2016). Another endocytic molecule that has been linked to epilepsy is amphiphysin (Amph) 1 (Di Paolo *et al.*, 2002). Evidence for the epileptogenic role of Amph1 comes from a KO mouse model that displays increased susceptibility to seizures together with severe learning deficits (Di Paolo *et al.*, 2002). Absence of Amph1 accompanied by loss of an additional amphiphysin brain isoform, Amph2, causes a slowing in SV

endocytosis and priming, and results in decreased RRP (Di Paolo *et al.*, 2002). Generalised seizures are reported in a syndapin 1 KO mice affecting different aspects of SV recycling in addition to accumulation of endosomal intermediates and enlarged SVs (Koch *et al.*, 2011). Lastly, spontaneous epileptic activity has been also observed in endophilin 1/2 and 1/3 double KO mice, while total absence of endophilin results in impaired neurotransmission (Milosevic *et al.*, 2011).

1.2 CDKL5 deficiency disorder

In 1998, exon-trapping experiments led to the isolation of a novel transcript expressed by the Xp22 region with a highly homologous N-terminal kinase domain to that of eukaryotic serine-threonine kinases (Montini *et al.*, 1998). Due to its homology, Montini *et al*. initially named this newly identified product as serine-threonine kinase 9, only to be established later as cyclin-dependent kinase-like 5 (CDKL5) and be classified as a member of the CDKL family of kinases (Montini *et al.*, 1998). Although CDKL5 can be found in many tissues, it is robustly expressed in the brain and especially in neurons. Its preferable presence within neurons highlights only in part the potential importance of CDKL5 for proper brain function. Notably, it is the high occurrence of *CDKL5* mutations reported in various neurodevelopmental conditions that has brought CDKL5 to the forefront as a kinase essential for brain development.

Sporadic genetic mutations in the X-linked gene encoding for CDKL5 have been associated with a distinct early infantile epileptic encephalopathy (Fehr *et al.*, 2013; Mangatt *et al.*, 2016). Early infantile epileptic encephalopathies

represent a group of conditions in which epileptic seizures affect brain development and maturation resulting in cognitive, sensory and/or motor impairment occurring during the first 12 months of life (Dulac, 2001). *CDKL5* mutations have been identified in children diagnosed with various neurodevelopmental disorders, including X-linked infantile spasm syndrome (or X-linked West syndrome), an atypical variant of Rett syndrome, and Lennox-Gastaut syndrome (Kalscheuer *et al.*, 2003; Weaving *et al.*, 2004; Evans *et al.*, 2005; Mari *et al.*, 2005; Scala *et al.*, 2005). There is a high variability in pathogenic *CDKL5* mutations ranging from large rearrangements, such deletions and duplications, to point mutations including missense, nonsense, splice, and frameshift mutations. (Guerrini & Parrini, 2012).

Since most pathogenic mutations are found within the kinase domain and have been widely shown to result in loss of protein function, CDKL5-related pathogenic phenotypes have been termed collectively as CDKL5 deficiency disorder (CDD). Despite that CDD is commonly associated with early-onset epilepsy and severe intellectual disability, the clinical spectrum of CDD-related conditions is actually broad, and the identified pathogenic CDKL5 variants are abundant. Therefore, CDD has been only recently recognized as a distinct disorder. However, the ever-increasing frequency of patients being diagnosed with CDKL5 pathogenic mutations establishes CDD as one of the most common monogenic epileptic disorders in early childhood with the prevalence to be estimated around 1:40,000-60,000 live births (Lindy *et al.*, 2018; Jakimiec *et al.*, 2020).

1.2.1 Clinical features of CDD

In most CDD patients, refractory epileptic activity emerging during the first three months of life is the most outstanding clinical feature (Fehr *et al.*, 2013). Besides that, early disruption of the brain development accompanied by profound intellectual disability is the core phenotype that portrays CDD. So far, numerous studies have assessed the clinical profile of CDKL5 patients either by examining patient cohorts or individual cases, of which frequent CDD-related manifestations briefly involve: (1) cognitive delay, (2) visual impairments, (3) autistic-like features, such as poor eye contact and reduced social interaction, (4) bruxism (teeth grinding), (5) absent language skills, such as non-verbal communication, (6) motor impairments and hypotonia, (7) hand stereotypies, (8) scoliosis, (9) autonomic complications, such as respiratory disturbances and impaired sleep pattern, (10) hypsarrhythmia, (11) normal magnetic resonance imaging scan, and (12) mostly absent facial dysmorphisms, that are reviewed by (Guerrini & Parrini, 2012; Demarest *et al.*, 2019; Kadam *et al.*, 2019; Olson *et al.*, 2019; Jakimiec *et al.*, 2020).

CCD affects mostly heterozygous female patients with the severity of symptoms depending mainly on the pattern of X-chromosome inactivation (Bahi-Buisson & Bienvenu, 2012). However, despite the remarkably fewer cases of male patients diagnosed with CDD, they are more severely affected in relation to females possibly due to the presence of a single X chromosome in their genome (Mirzaa *et al.*, 2013; Fehr *et al.*, 2016a; Liang *et al.*, 2019). Except for the gender, the severity of CDD symptoms seems to rely also on the type and position of the pathogenic mutation, although this correlation has been difficult to prove, owning to the broad genetic and phenotypic spectrum in CDD. For example, it has been reported that individuals with a pathogenic

truncation towards the end of the CDKL5 protein are able to walk unaided and use more advanced communication compared to those with no functional protein (Russo *et al.*, 2009; Fehr *et al.*, 2016a). On the other hand, point mutations within the kinase domain as well as frameshift mutations have been linked to severe encephalopathy, inability to walk, and microcephaly (Bahi-Buisson *et al.*, 2012; Maortua *et al.*, 2012).

Different seizure types are observed in CDD and, in many cases, generalized tonic-clonic seizures are followed by epileptic spasms prior to myoclonic epilepsy, whereas a hypermotor-tonic-spasms pattern with frontal onset has been also reported as a distinctive seizure type (Klein *et al.*, 2011; Melani *et al.*, 2011; Bahi-Buisson & Bienvenu, 2012). Only few cases with milder epileptic encephalopathy have been responsive to antiepileptic drug administration with epilepsy in CDD being largely untreatable with conventional therapeutic approaches (Bahi-Buisson & Bienvenu, 2012; Melikishvili *et al.*, 2019).

1.2.2 The biology of CDKL5

1.2.2.1 Evolutionary history of CDKL5

Orthologs of the CDKL5 gene can be found among all three subphyla of Chordata with certain well-conserved sequences, including definitely the kinase domain, and protein structure (Fichou *et al.*, 2011; Fahmi *et al.*, 2019). The presence of a protein kinase sharing a highly homologous catalytic domain with CDKL5 in *Chlamydomonas*, a genus of green algae, indicates that CDKL5 might also be present in other kingdoms apart from animals as initially

thought (Tam *et al.*, 2013). However, no orthologs have been discovered in any prokaryotic species yet.

CDKL5 belongs to a large family of eukaryotic serine/threonine kinases known as the CMGC group from the initials of its most important subgroups that include the cyclin-dependent kinases (CDKs), mitogen-activated protein kinases (MAPK), glycogen synthase kinases (GSK) and CDK-like kinases (CDKLs). As its name reveals, CDKL5 is classified into the last kinase subgroup together with four closely-related kinases (CDKL1, CDKL2, CDKL3, CDKL4) with high-level sequence similarity within the N-terminal catalytic domains and C-terminal tails of variable lengths (Canning *et al.*, 2018). Although CDKLs contain cyclin-binding domains similarly to CDKs, there are no interactions with cyclin reported and they also seem to diverge evolutionarily from CDKs (Canning *et al.*, 2018).

1.2.2.2 CDKL5 distribution

In mammals, CDKL5 is highly expressed in the brain but it can be also found in a wide range of peripheral tissues including the testes, thymus, lung, heart, and liver (Lin *et al.*, 2005; Chen *et al.*, 2010). Within the brain, *in situ* hybridization and immunoblotting analysis has shown that CDKL5 is present in multiple regions including the cortex, hippocampus, and striatum, and, to a lesser extent, in cerebellum, brainstem, and olfactory bulb (Rusconi *et al.*, 2008; Chen *et al.*, 2010; Wang *et al.*, 2012; Schroeder *et al.*, 2019). CDKL5 is widely considered as a neuronal kinase and, despite it being suggested to be preferentially enriched in excitatory synapses in cultured hippocampal neurons, it can be found in both excitatory and inhibitory neurons (Rusconi *et al.*, 2011; Ricciardi *et al.*, 2012; Tang *et al.*, 2019). Though traces of CDKL5 have

been reported in glial cells, most of the studies do not detect any CDKL5 (Rusconi *et al.*, 2008; Chen *et al.*, 2010).

The temporal expression profile of CDKL5 in the brain has been assessed by various studies. CDKL5 expression seems to increase during perinatal and mainly early postnatal stages (Rusconi *et al.*, 2008; Chen *et al.*, 2010). However, whether CDKL5 isoforms start to express as early as the initial stages of embryogenesis is debatable, with studies detecting robust levels of CDKL5 mRNA in the foetal brain (Rademacher *et al.*, 2011; Hector *et al.*, 2016). In the mature brain, CDKL5 continues to express throughout adulthood.

1.2.2.3 CDKL5 gene and its regulation

In humans, CDKL5 is encoded by a single gene that was mapped to the chromosomal locus Xp22.13 comprising an area of 240 kb (Montini *et al.*, 1998; Kilstrup-Nielsen *et al.*, 2012). *CDKL5* consists of 27 exons numbered as presented in Figure 1.2A, of which exons 2-10, 12-16, and 18 are constitutive, whereas exons 1 and 1a-1e are untranslated. Five major mRNA transcripts (*hCDKL5_1*, *hCDKL5_2*, *hCDKL5_3*, *hCDKL5_4*, *hCDKL5_5*) are produced due to alternative splicing and variable untranslated region (UTR) lengths (Hector *et al.*, 2016). The various isoforms are differentially expressed relying on the tissue type, with the 9.7-kb *hCDKL5_1* variant that is transcribed from exon 1 predominantly expressed within the brain (Williamson *et al.*, 2012; Hector *et al.*, 2016). In the mature *hCDKL5_1* mRNA, exon 1 and part of exon 2 form the 5′-UTR, whereas part of exon 19 structures the 3-UTR with the polyadenylation signal (AATAAA) found 6.6 kb downstream of the stop codon (Hector *et al.*, 2016). Exons 1a-1e as well as exon 17 are excluded as depicted in Figure 1.2B. With the initiation codon located within exon 2,

translation of the brain-specific variant results in a large protein of 960 residues with an N-terminal catalytic domain encoded by exons 2-11 as shown in Figure 1.2C. This protein product has been previously defined as CDKL5$_{107}$ owning to its molecular weight (Williamson *et al.*, 2012). Repeated sequences, such as Alu elements, are detected within *CDKL5* and, despite their effect on its expression is not understood, they seem to facilitate pathogenic deletions (Erez *et al.*, 2009).

Some evidence is available about the regulation of *CDKL5* expression at the transcriptional level in contrast to the splicing or translational levels of regulation that have not been investigated yet. Upstream of exon 2, multiple transcription start sites spread across a region of over 18 kb and therefore the presence of multiple promoters has been predicted (Hector *et al.*, 2016). Two *CDKL5* promoters have been mapped so far, which are characterised by the presence of CpG islands in their vicinity and lack of TATA boxes (Vitezic *et al.*, 2014). The only detected active enhancer is sited in a region over 245 kb upstream of the *CDKL5* gene (Vitezic *et al.*, 2014). Several putative binding sites for transcription factors have been found, such as SP1, RREB1, FOXP1 and NFY (Vitezic *et al.*, 2014). In mice, the proliferation-promoting transcription factor MYCN has been reported to repress *Cdkl5* expression and this is achieved by interacting with an SP1-binding site (Valli *et al.*, 2012). Another repressor of *Cdkl5* transcription is MeCP2 that acts after CpG methylation of the 5'-UTR of rat *Cdkl5* in response to cocaine (Carouge *et al.*, 2010). Given that MYCN and MeCP2 have been shown to control the transcription of rodent orthologs, further studies are required to evaluate their impact on human *CDKL5* expression.

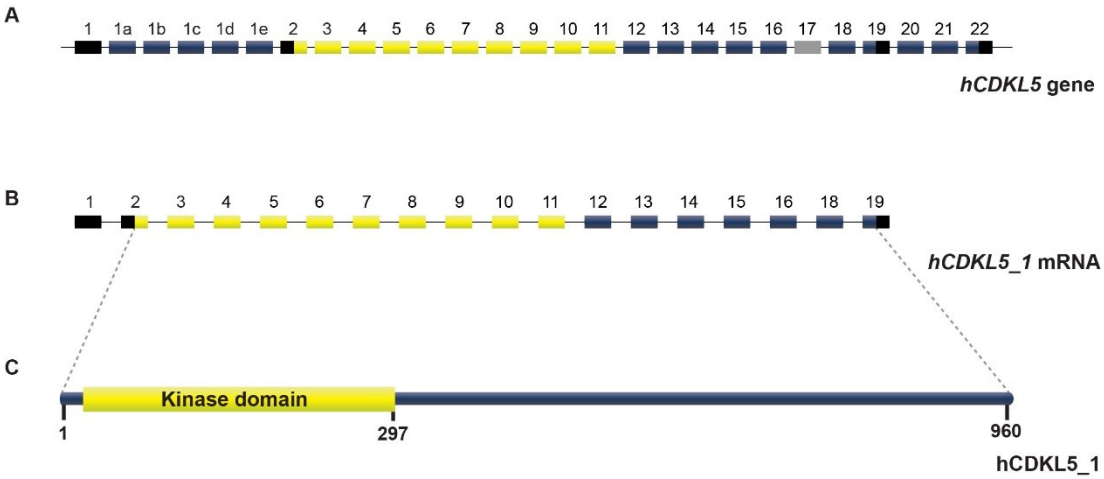

Figure 1.2 Expression of the human CDKL5 protein in the brain

Schematic presentation of the expression of the brain-specific isoform of CDKL5 in humans. (**A**) The human CDKL5 gene comprises of 27 exons, of which exons 2-10, 12-16, and 18 are constitutive. Exons 1, 1a-1e, part of 19, and part of 22 are untranslated (black). (**B**) CDKL5 undergoes alternative splicing producing a 9.7-kb transcript variant that is defined as hCDKL5_1 and expresses highly in the brain. The initiation codon is found within exon 2. The 5′-UTR consists of exon 1 and part of exon 2 (black), while the 3′-UTR is formed by part of exon 19 (black) with the polyadenylation site located 6.6 kb downstream of the stop codon. (**C**) Translation of hCDKL5_1 results in a large protein of 960 residues. The kinase domain (yellow) occupies the N-terminal region of the protein (13-297 aa) and is expressed by exons 2-12 (yellow). The numbering of CDKL5 exons and nomenclature follow the recommendations of Hector et al. (2016). The lengths of exon and intron sequences do not represent actual sizes.

1.2.2.4 CDKL5 structure

The brain-specific isoform of CDKL5 consists of 906 residues and is divided into two regions based on the functional role each one serves: the N-terminal kinase domain that phosphorylates targeted substrates and the long C-terminal tail that occupies the remaining two thirds of the molecule as depicted in Figure 1.3A. The kinase domain that is highly conserved across species is the only part of CDKL5 that has been crystallised (Protein Data Bank ID 4BGQ) as shown in Figure 1.3B (Canning *et al.*, 2018). It mostly consists of α-helices with the exception of an antiparallel β-sheet. CDKL5 bears three characteristic features of S/T kinases including a G-rich region close to a K residue following the pattern $GxGxxG{x_n}K$ that is involved in ATP binding (19-43 aa), a region with a conserved D residue required for its catalytic activity (131-141 aa), and, lastly, a conserved TEY motif (169-171 aa) that is a signature motif of the MAP kinase group (Montini *et al.*, 1998).

Regarding the C-terminal tail of CDKL5, there are no crystallographic data available so far. Likewise, attempts to predict the tertiary structure of the C-terminal tail have not been successful. What is known, however, is that it contains extensive amount of intrinsically disordered regions that provide additional interaction surfaces as well as accessible sites for posttranslational modifications (Fahmi *et al.*, 2019). Two nuclear localisation signals (NLS) and a single nuclear export signal (NES) can be found within the C-terminal tail that facilitate transport towards and from the nucleus (Bahi-Buisson & Bienvenu, 2012).

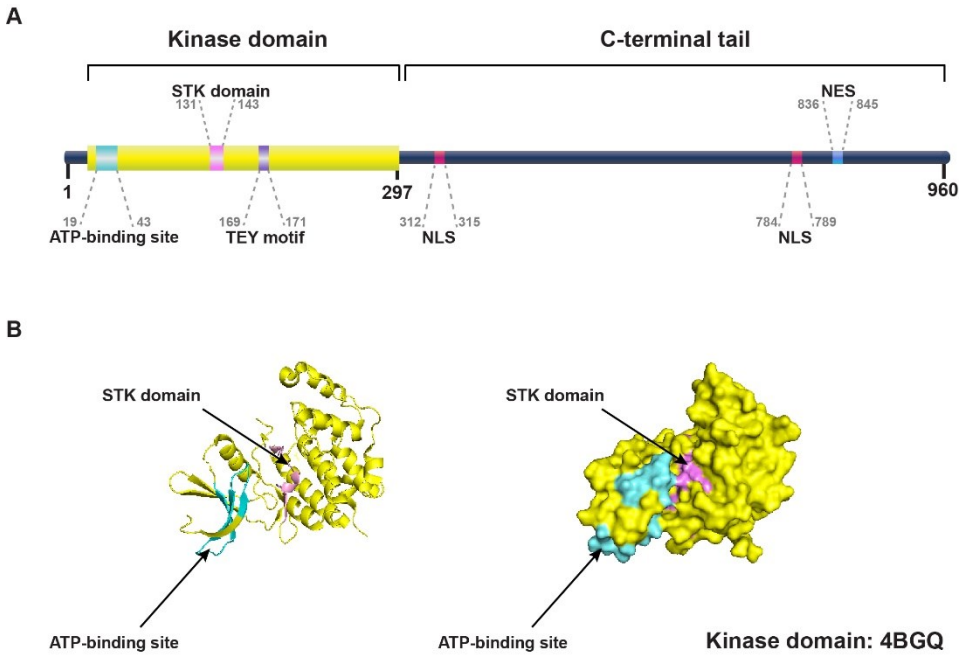

Figure 1.3 Structure of CKDL5 protein

Linearised and three-dimensional diagrams representing the structure of CDKL5. (**A**) CDKL5 is divided into the N-terminal kinase domain and the long non-domain C-terminal tail. Based on the amino acid sequence, a few typical kinase motifs are found within the kinase domain, such as the ATP-binding site (turquoise), the STK motif (pink), and the TEY motif (purple). Similarly, a few sequences required for nuclear transport are localised within the C-terminal tail including nuclear localisation sequences (NLS; fuchsia) and a nuclear export sequence (NES; light blue). (**B**) Two representations of the three-dimensional conformation of the kinase domain as was extracted from the Protein Data Bank (4BGQ). Both representations depict the kinase motifs that reside within the substrate docking groove (turquoise and pink highlights). Whereas the kinase domain consists of α-helices almost in its entirety, the ATP-binding site is structured by an antiparallel β-sheet.

1.2.2.1 Subcellular sorting and regulation of CDKL5

CDKL5 is primarily distributed into the cytoplasm and, to a lesser extent, to the nucleus (Rusconi *et al.*, 2011; Wang *et al.*, 2012; Schroeder *et al.*, 2019). Within the cytoplasm, CDKL5 has been detected at the postsynaptic density of dendritic spines (Ricciardi *et al.*, 2012; Zhu *et al.*, 2013), but it is likely to be widely distributed throughout the neuron. In the nucleus, CDKL5 localises preferably at nuclear speckles (Ricciardi *et al.*, 2009). It has been suggested that translocation of CDKL5 into or from the nucleus is mediated by its C-terminal tail and occurs in a phosphorylation- and activity-dependent manner (Rusconi *et al.*, 2008; Rusconi *et al.*, 2011; Oi *et al.*, 2017). During neurogenesis, CDKL5 is mainly present at the centrosome of cultured developing neurons (Barbiero *et al.*, 2017b).

Whether CDKL5 undergoes any posttranslational modifications has not been addressed exhaustibly. A few potential phosphorylation sites have been identified downstream of the kinase domain including S306, S308, S407, S529, S543, and S720 (Oi *et al.*, 2017; Munoz *et al.*, 2018; Fahmi *et al.*, 2019). The protein kinases that mediate CDKL5 phosphorylation remain largely unknown with the exception of dual specificity tyrosine-phosphorylation-regulated kinase 1A (DYRK1A) that has been identified to bind and phosphorylate CDKL5 at S308 exclusively (Oi *et al.*, 2017). Interestingly, CDKL5 has the ability to autophosphorylate itself within the kinase domain on Y171 that consists part of the TEY motif (Munoz *et al.*, 2018) and this modification is likely to be induced by brain-derived neurotrophic factor (BDNF) (Chen et al., 2010).

In hippocampal dendrites, it has been shown that dendritic CDKL5 levels are controlled in a depolarising-dependent way since KCl-mediated stimulation appears to be able to induce local translation of CDKL5 mRNA (La

Montanara *et al.*, 2015). However, sustained glutamate activation of N-methyl-D-aspartate receptor (NMDAR) triggers proteasomal degradation of CDKL5 after the latter was dephosphorylated by phosphatase 1 (Rusconi *et al.*, 2011; La Montanara *et al.*, 2015). Similarly, both deprivation of neurotrophic factors and hydrogen peroxide treatment promote proteasomal degradation of CDKL5 (Rusconi *et al.*, 2011).

1.2.3 Mammalian models for studying CDKL5

A number of genetic models has been produced in order to unravel the *in vivo* biological role of CDKL5. The first mouse line deficient of CDKL5 was developed by targeting exon 6 of the mouse *Cdkl5* gene causing thus an early truncation within its kinase domain (Wang *et al.*, 2012). Despite the absence of spontaneous seizures, this mouse model exhibits CDD-like features, such as hyperactivity, motor defects, reduced anxiety, decreased social interaction, respiratory deficiencies and impaired learning and memory that can associate with the severe intellectual disability commonly reported in CDD patients (Wang *et al.*, 2012; Lee & Liao, 2018). A similar CDKL5 KO mouse line was generated by targeting exon 4 of the *Cdkl5* gene (Amendola *et al.*, 2014). Although these CDKL5-null mice do not display any spontaneous seizures either, they have phenotypes mirroring CDD features, like hypoactivity, elevated sleep apnoea occurrence, increased limb clasping, impaired hippocampus-related memory, and altered electroencephalogram profiles in response to kainate-induced seizures (Amendola *et al.*, 2014; Fuchs *et al.*, 2014; Trazzi *et al.*, 2016; Lo Martire *et al.*, 2017). Moreover, both constitutive mouse models display altered sensory information processing indicative of impaired

neuronal connectivity as well as disruption of signal transduction underlying the loss of CDKL5 (Wang *et al.*, 2012; Amendola *et al.*, 2014).

Another mouse model developed by floxing exon 2 of *Cdkl5* demonstrates increased susceptibility to NMDA-induced -but not kainate-induced- seizures, altered long-term potentiation, enhanced anxiety, altered social behaviour and spatial memory in the absence of CDKL5 (Okuda *et al.*, 2017; Okuda *et al.*, 2018). Recently, a novel knockin model was developed bearing the CDD patient nonsense mutation R59X (Tang *et al.*, 2019; Yennawar *et al.*, 2019). R59X mice display autistic-like features as well as learning and memory impairment (Tang *et al.*, 2019; Yennawar *et al.*, 2019). Moreover, these mice are predisposed to pentylenetetrazol-induced seizures implying elevated underlying hyperexcitability (Yennawar *et al.*, 2019). Given that reporting spontaneous epileptic activity in murine models has been challenging, this leads to the notion that loss of CDKL5 causes epilepsy in ways that might differ across species and neural network complexity and that further studies are needed in order to explore the epileptogenic mechanisms of CCD.

Since epileptic seizures are attributed largely to excitatory/inhibitory imbalance, several studies have followed alternative approaches that involve the conditional eradication of CDKL5 expression from either glutamatergic or GABAergic neuronal subpopulations of certain brain regions. A few independent studies have used such conditional KO models generated by targeting different exons of the *Cdkl5* gene (Amendola *et al.*, 2014; Tang *et al.*, 2017; Schroeder *et al.*, 2019; Tang *et al.*, 2019). Firstly, findings indicate that different behavioural deficits due to loss of CDKL5 emanate from distinct brain regions and/or neuronal type. For example, significantly reduced locomotion is observed when CDKL5 expression is ablated in cortical interneurons or striatal spiny neurons, but remains unaltered when removed

in cortical or hippocampal pyramidal neurons (Amendola *et al.*, 2014). Accordingly, deficits in memory and learning associated with deletion of CDKL5 from glutamatergic neurons of the Nex-conditional KO mice are not observed in CDKL5-deficient GABAergic neurons of the Dlx-conditional KO mice (Tang *et al.*, 2017; Tang *et al.*, 2019). Secondly, impairment of cellular events, such as signal transduction, or altered protein levels due to loss of CDKL5 can also vary between excitatory and inhibitory neurons (Schroeder *et al.*, 2019).

Induced pluripotent stem cells (iPSCs) technology offers an alternative tool for investigating pathogenic mechanisms in patient-specific neurons (Amenduni *et al.*, 2011; Negraes *et al.*, 2021). Human iPSC-derived neurones developed from patients carrying pathogenic *CDKL5* mutations seem to preserve X-chromosome inactivation upon differentiation with some clones expressing the mutant and other clones the wild-type allele of the *CDKL5* gene (Amenduni *et al.*, 2011). Patient-derived neuronal systems display compromised proliferation and glutamatergic synaptogenesis, loss of synaptic contacts, elongated dendritic spines, reduced levels of CDKL5-mediated phosphorylation of microtubule (MT)-binding proteins in agreement to phenotypes observed in animal models (Ricciardi *et al.*, 2012; Baltussen *et al.*, 2018; Negraes *et al.*, 2021). Lastly, a few studies have employed patient-derived fibroblasts as model system to study the pathogenetic profile of CDD revealing CDKL5-related RNA splicing deficits and deregulation of molecules implicated in cholesterol homeostasis (Ricciardi *et al.*, 2009; Pecorelli *et al.*, 2015).

1.2.4 CDKL5 subcellular functions

Since all known pathogenic missense mutations cluster within the kinase domain of CDKL5, much of the research into its neuronal role has understandably focused on its catalytic activity. Despite that absent or aberrant CDKL5 expression has been associated with altered phosphorylation levels of several molecules, it is not clear whether CDKL5 directly catalyses these reactions with the exception of a limited number of confirmed substrates. As its structure reveals, CDKL5 is an active kinase and it has been suggested that recognises and preferentially phosphorylates substrates bearing an RPX(S/T)(A/G/P) motif (Canning *et al.*, 2018; Munoz *et al.*, 2018). All proposed *in vivo* and *in vitro* substrates of CDKL5 can be found in Figure 1.4.

Despite the biological significance and clinical relevance of the kinase activity of CDKL5, assessing its role in the developing brain needs to extend beyond its catalytic activity. The C-terminal tail of CDKL5 is equally essential as it performs multiple roles in neurons. Firstly, it is involved in subcellular sorting of CDKL5 (Rusconi *et al.*, 2008; Zhu *et al.*, 2013). Secondly, a growing number of interacting molecules have been identified to bind to it exclusively (Figure 1.4). Thirdly, it has been proposed that the C-terminal tail is critical for the stability of CDKL5 (Lin *et al.*, 2005; Williamson *et al.*, 2012). Lastly, it contains multiple putative phosphorylation sites that could regulate CDKL5 activity post-translationally (Oi *et al.*, 2017; Munoz *et al.*, 2018). Indeed, an early study shows that loss of the C-terminal tail enhances the autophosphorylation ability of CDKL5 *in vitro* (Lin *et al.*, 2005). Whether the C-terminal tail serves any other regulatory roles in relation to the kinase activity of the protein towards various putative substrates is still unclear.

Several cellular functions have been attributed to CDKL5 in murine neurons, patient-derived iPSCs, or various cell lines depending on the developmental stage, subcellular compartment, substrate, signal cascade and interactions that are established. A summary of different physiological roles of neuronal CDKL5 is outlined below.

Cell proliferation. Some evidence suggests that CDKL5 is involved in cell proliferation. In the human neuroblastoma cells SH-SY5Y, blocking CDKL5 expression results in enhanced proliferation activity (Valli *et al.*, 2012). Flow cytometric analysis reveals that CDKL5 might regulate proliferation by inhibiting the cell cycle in the G1/G0 phase, rather than inducing apoptosis (Valli *et al.*, 2012). Similarly, in the dentate gyrus, primary neural progenitor cells proliferate at higher rate when CDKL5 is absent (Fuchs *et al.*, 2014). However, the impact of CDKL5 on cell division in various cell lines has been shown to be different. Immunofluorescence analysis detects CDKL5 at the centrosome and midbody of proliferating cells (Barbiero *et al.*, 2017b). This indicates that CDKL5 is potentially important for stages of the cell cycle other than interphase. Indeed, silencing CDKL5 expression results in several defects during mitosis, such as mitotic spindle multipolarity, chromosome segregation impairment, and cytokinesis arrest (Barbiero *et al.*, 2017b). CDKL5-mediated cytokinesis seems to be particularly associated with phosphorylation of the extrachromosomal histone H2B at S14 by the HIPK2 kinase at the midbody (Barbiero *et al.*, 2017b). In agreement with a proliferation-promoting role, overexpression of CDKL5 stimulates proliferation in glioma cells through the PI3K/AKT signalling pathway (Jiang *et al.*, 2019). Therefore, further studies are required to assess whether CDKL5 is a positive or negative regulator of cell division during neuronal development.

Neuronal differentiation. Independently of its role in proliferation, CDKL5 expression seems to strongly increase upon differentiation although its absence does not seem to affect the differentiation rate itself (Ricciardi *et al.*, 2012; Valli *et al.*, 2012). Nevertheless, there is only little evidence supporting a primary role of CDKL5 in inducing differentiation (Valli *et al.*, 2012). Instead, CDKL5 is likely to have a downstream activity in the neurodevelopmental course and even modulate apoptotic cell death (Fuchs *et al.*, 2014).

Neuronal migration. Defects in neuronal migration during the perinatal and early postnatal stages have been linked to CDKL5 downregulation. In rat brains, silencing of CDKL5 expression results in delayed migration of neurons into the cortical layers (Chen *et al.*, 2010). The migrating ability of glioma cells has been also tested *in vitro*, where CDKL5 seems to have a promoting role (Jiang *et al.*, 2019). CDKL5 interacts *in vivo* with the IQ domain-containing GTPase-activating protein 1 (IQGAP1), a scaffold protein participating in cytoskeleton stabilisation (Barbiero *et al.*, 2017a). Using a wound-healing assay in HeLa cells, it was shown that CDKL5 silencing hinders the accumulation of IQGAP1 at the leading edge during migration. Moreover, CDKL5 downregulation disrupts the interaction of IQGAP1 with both the Rho GTPase Rac1, a well-known regulator of actin dynamics, and the MT plus-end tracking protein CLIP70 (Barbiero *et al.*, 2017a). These findings indicate that CDKL5 might modulate neuronal migration by influencing cytoskeleton dynamics.

Neuronal polarisation. A substantial body of work points towards an involvement of CDKL5 in different aspects of neuronal morphogenesis, such as axon growth and dendritic arborisation, whereas a potential role in establishing axonal specificity has been hypothesised. CDKL5 has been reported to regulate axonal specificity since aberrant CDKL5 levels are related to less polarised hippocampal neurons in culture. These neurons display either

multiple or even no axons (Nawaz *et al.*, 2016). This is accomplished through the interaction of CDKL5 with the brain-specific protein shootin 1, that regulates the axonal generation during polarization (Nawaz *et al.*, 2016). Although the phosphorylation levels of shootin 1 seem to decrease upon CDKL5 downregulation, it is not clear yet whether CDKL5 plays any direct role in shootin 1 phosphorylation (Nawaz *et al.*, 2016). Apart from neuronal polarity, these two proteins that colocalise at the distal tip of growing axons also regulate the axonal elongation since silencing either CDKL5 or shootin1 causes the formation of significantly shorter axons (Nawaz *et al.*, 2016). Whether the ternary complex IQGAP1-Rac1-CLIP170, which was introduced earlier, and shootin 1 share any complementary roles in CDKL5-mediated axonal growth has not yet been addressed. However, CLIP170 is mislocalised and fails to bind effectively to MTs in growth cones when CDKL5 is silenced, leading to shorter and less polarised axons and abnormal growth cones in neurons (Barbiero *et al.*, 2017a; Barbiero *et al.*, 2019b).

Neuronal morphogenesis. In neuroblastoma cells and cultured cortical neurons, knocking down CDKL5 leads to the formation of shorter axons and dendrites that also appear less branched (Chen *et al.*, 2010; Valli *et al.*, 2012). In agreement with this, cortical pyramidal neurons exhibit defects in apical dendritic morphology during the early postnatal stages upon CDKL5 downregulation using *in utero* electroporation (Chen *et al.*, 2010). CDKL5 deficient mice present abnormal dendritic branching of both cortical and hippocampal neurons *in vivo* as well as subsided dendritic length of newly generated granule cells (Amendola *et al.*, 2014; Fuchs *et al.*, 2014; Okuda *et al.*, 2018). The growth-promoting effect of CDKL5 on dendritic length may be assisted by Rac1 via its C-terminal tail (Chen *et al.*, 2010). Overexpression of a kinase-dead mutant of CDKL5 fails to promote dendrite growth in cultured

cortical neurons suggesting that the kinase activity is possibly implicated in determining dendritic length (Chen *et al.*, 2010).

CDKL5-mediated regulation of neuronal morphogenesis and maturation is also likely to occur by altering gene expression. An indirect involvement of CDKL5 in these nuclear processes occurs through its substrate histone deacetylase 4 (HDAC4) (Trazzi *et al.*, 2016). CDKL5-mediated phosphorylation of HDAC4 at S632 traps HDAC4 within the cytoplasm, preventing it from performing its nuclear tasks that include histone 3 deacetylation. This results in altered expression of target genes, such as BDNF (Trazzi *et al.*, 2016). In mice lacking CDKL5, HDAC4 is capable of translocating into the nucleus of neural progenitor cells, pointing towards a mechanism for regulating neuronal morphogenesis and maturation at the DNA level (Trazzi *et al.*, 2016).

Synaptogenesis. CDKL5 is important for dendritic spine formation, growth, and stabilisation (Ricciardi *et al.*, 2012; Zhu *et al.*, 2013; Della Sala *et al.*, 2016). Evidence provided by CDKL5 downregulation either in cultured neurons or *in vivo* suggests that mushroom-shaped spines are replaced by longer and thinner ones that display a more dispersed distribution along dendrites (Ricciardi *et al.*, 2012; Okuda *et al.*, 2018). Two molecules have been implicated in CDKL5-mediated spine formation, PSD95 and the cell adhesion molecule, netrin-G1 ligand 1 (NGL1) (Ricciardi *et al.*, 2012; Zhu *et al.*, 2013). CDKL5 binds and phosphorylates NGL1 specifically at S631, thus stabilising its interaction with PSD95, while CDKL5 itself also interacts with palmitoylated PSD95. In cultured hippocampal neurons, disruption of the CDKL5-PSD95 interaction reduces the accumulation of CDKL5 at spines, affecting both the spine density and length (Zhu *et al.*, 2013). In accordance with this, overexpression of a phospho-null mutant of NGL1 at S631 impacts

on spine elongation, possibly modifying the NGL1-PSD95 interaction (Ricciardi *et al.*, 2012).

Except for spine formation, it is likely that CDKL5 is also involved in the specificity of the presynaptic compartment. Expression of *GRID1* that encodes for glutamate D1 receptor (GluD1) has been reported to be dysregulated in human iPSC neurons derived from CDKL5 patients (Livide *et al.*, 2015). Interestingly, GluD1 is a neurexin-associated adhesion molecule that usually induces the inhibitory presynaptic differentiation of cortical neurons indicating thus a potential role of CDKL5 in presynapse development (Yasumura *et al.*, 2012; Fossati *et al.*, 2019).

Microtubule assembly. Since neurodevelopmental processes depend heavily on MT dynamics (Lasser *et al.*, 2018), effort has been aimed recently on investigating a putative involvement of CDKL5 in MT reorganization and/or stabilisation. This has been reinforced by the identification of the MT-associated protein MAP1S (S812 and S900), the MT end-binding protein EB2 (S222), the centrosome-related protein CEP131 (S35) and DLG5 (S1115), a protein involved in MT-based signalling, as direct CDKL5 substrates (phosphorylation sites in brackets) (Baltussen *et al.*, 2018; Munoz *et al.*, 2018). The CDKL5-mediated phosphorylation of MAP1S impacts on its affinity for MTs, possibly impeding thus cargo trafficking (Baltussen *et al.*, 2018). However, there is no evidence regarding the impact of phosphorylation on the remaining substrates. Moreover, CDKL5 might largely regulate MT-based structures, since involvement of CDKL5 in both cilia and flagella length control has been also reported (Tam *et al.*, 2013; Canning *et al.*, 2018).

Nuclear roles. In the nucleus, CDKL5 appears to perform activities related to different aspects of gene expression. It has been suggested that nuclear CDKL5 is involved in regulating alternative splicing (Ricciardi *et al.*, 2009). There, CDKL5 is enriched in nuclear speckles where several splicing factors reside (Ricciardi *et al.*, 2009). CDKL5 is important for maintaining nuclear speckle morphology and organisation, since aberrant CDKL5 levels either result in a more diffuse distribution of speckles components in the nucleus or prompt the assembly of abnormal speckles (Ricciardi *et al.*, 2009). It has been proposed that its kinase activity targets different splicing factors, therefore regulating splicing at the pre-mRNA level. However, there are not any identified targets yet.

An indirect involvement of CDKL5 in regulating gene expression occurs through phosphorylation of cytoplasmic HDAC4 (Trazzi *et al.*, 2016). As mentioned earlier, phosphorylated HDAC4 at S632 fails to translocate to the nucleus, where it catalyses histone 3 deacetylation thus impacting on gene expression during neuronal maturation (Trazzi *et al.*, 2016). In agreement to this, transcriptomic analysis in neural progenitor cells derived from CDKL5 patients has shown differential expression of various genes, indicating that CDKL5 might also participate in transcriptional regulation (Jagtap *et al.*, 2019). Besides, the nuclear proteins MeCP2, a known epigenetic factor, and DNA methyltransferase 1 (DNMT1) that is responsible for maintenance of DNA methylation patterns have been identified as potential CDKL5 binding partners as well as substrates (Mari *et al.*, 2005; Kameshita *et al.*, 2008), although any possible phosphosites are yet undetermined. However, according to different studies, the ability of CDKL5 to phosphorylate these substrates *in vitro* is not robust (Lin *et al.*, 2005; Sekiguchi *et al.*, 2013). Lastly, it is likely that CDKL5 modulates protein translation as well, since CDKL5-null mice display

reduced phosphorylation of the ribosomal protein S6 (rpS6) modulatory subunit at 240/244 in the somatosensory cortex (Amendola *et al.*, 2014).

Presynaptic role. While CDKL5 localises at the distal tip during axonal elongation and has been implicated in inducing presynaptic specificity, little is known about any involvement in biogenesis or function at the nerve terminal. The one exception is that it phosphorylates Amph1 at S293 *in vitro*, impacting on its affinity for endophilin (Sekiguchi *et al.*, 2013; Katayama *et al.*, 2015). As discussed in 1.1.2.1, Amph1 facilitates SV recycling through CME, indicating that CDKL5 might be implicated in SV endocytosis. According to a couple of early studies, amphiphysin is also involved in neurite outgrowth (Mundigl *et al.*, 1998), whereas it localises in growth cones and can undergo mitotic phosphorylation in dividing cells (Floyd *et al.*, 2001). Therefore, it has been hypothesised that Amph1 phosphorylation may alter actin dynamics regulating thus dynamic properties of developing neurons as well as the function of mature synapses (Floyd *et al.*, 2001).

Other roles. CDKL5 has been also implicated in preserving cholesterol homeostasis and regulating cellular responses to oxidative stress (Pecorelli *et al.*, 2015; Jagtap *et al.*, 2019). Mitochondrial abnormalities and altered oxygen consumption rate in combination with aberrant expression of redox-related genes that were reported in CDD-derived neural cells might underlie partly the generation of oxidative stress (Jagtap *et al.*, 2019). Defective mitochondrial function and decreased ATP production are also reported in CDKL5 KO mice (Vigli *et al.*, 2019; Carli *et al.*, 2021). This implies that CDKL5 possibly regulates brain energy metabolism and/or has antioxidative role during neurodevelopment.

1.2.5 Signal transduction pathways

A potential role in coordinating signalling pathways has been proposed for CDKL5 owning to evidence provided by either animal models or cell lines. In support of this, mice lacking CDKL5 display impaired phosphorylation profiles of various S/T kinases that are involved in different cellular cascades, such as the protein kinase A and Akt (Wang *et al.*, 2012). The major signalling pathway that is affected due to loss of CDKL5 is the PI3K/Akt/mTOR pathway, that is typically known to contribute to neurodevelopmental disorders and epileptogenesis (Costa-Mattioli & Monteggia, 2013). Reduced phosphorylation levels of Akt-S473 and the mechanistic target of rapamycin (mTOR)-S2448 sites have been reported, pointing to a dysregulation of the PI3K/Akt/mTOR signaling cascade in the absence of CDKL5 (Wang *et al.*, 2012; Amendola *et al.*, 2014; Fuchs *et al.*, 2014; Jiang *et al.*, 2019). Another member of the PI3K/Akt/mTOR pathway that is affected is the glycogen synthase kinase 3β (Fuchs *et al.*, 2014). Less phosphorylated GSK3β at S9 displays enhanced activity, resulting in hippocampal neurodevelopment defects coupled to CDKL5 loss that can be restored only after GSK3β inhibition (Fuchs *et al.*, 2015). However, whether CDKL5 is implicated in this pathway as an intermediate or direct kinase remains elusive. Intriguingly, it has been suggested that the PI3K/Akt/mTOR signalling is differentially altered in excitatory compared to inhibitory neurons (Schroeder *et al.*, 2019).

CDKL5 is also involved in the BDNF-Rac1 signalling pathway during the early postnatal stages (Chen *et al.*, 2010). As mentioned earlier, CDKL5 can form complexes with Rac1 in cortical neurons through its C-terminal tail. Under growth-inducing conditions, BDNF preferentially triggers CDKL5-dependent activation of Rac1 that is involved in modulating actin remodelling

(Chen *et al.*, 2010). In addition, BDNF induces tyrosine-specific phosphorylation of CDKL5, highlighting that CDKL5 can be regulated posttranslationally for performing actin-related functions (Chen *et al.*, 2010). However, mice lacking CDKL5 do not display altered BDNF expression or function (Amendola *et al.*, 2014). More recently, it has been reported that CDKL5 also regulates the transforming growth factor β (TGF-β) signaling pathway by phosphorylating the SMAD3 protein mediator *in vivo* (Fuchs *et al.*, 2019b). This pathway is responsible for various cellular processes, such as cell proliferation, axonal specification and protection against cell death, that are disrupted upon loss of CDKL5 supporting a possible crosstalk between CDKL5 and TGF-β in neurons.

1.2.6 Neuronal excitability and plasticity

Several studies point to the idea that an imbalance of excitatory-inhibitory signalling underlies CDD, similar to other epilepsy-related disorders. This indicates that CDKL5 may participate in mechanisms of neuronal excitability and neurotransmission. For example, loss of CDKL5 from forebrain inhibitory neurons results in increased excitatory, but unaltered inhibitory transmission and hyperexcitability at the circuit level, owning to increased levels of the GluN2B subunit of NMDARs at the PSD (Tang *et al.*, 2019). Aberrant paired-pulse facilitation as a presynaptic short-term mechanism of synaptic plasticity is also observed when CDKL5 is knocked out from inhibitory neurons (Tang *et al.*, 2019). On the other hand, deletion of CDKL5 from glutamatergic pyramidal neurons is accompanied by hyperexcitability and increased frequency of both miniature excitatory postsynaptic currents (mEPSCs) and miniature inhibitory postsynaptic currents (mIPSCs) (Tang *et al.*, 2017).

Intriguingly, spontaneous glutamate/GABA efflux ratio is considerably increased in the absence of CDKL5, in contrast to evoked release that remains unchanged (Sivilia *et al.*, 2016).

Decreased levels of the GluA2 subunit of α-amino-3-hydroxy-5-methyl-4-isoxazolepropionic acid-type glutamate receptors (AMPARs) have been reported in R59X knockin mice, modifying therefore both AMPAR-related function and plasticity (Yennawar *et al.*, 2019). Data also suggest that alterations in serotonergic neurotransmission may contribute to the pathophysiology of CDD (Fuchs *et al.*, 2019a; Vigli *et al.*, 2019). In the primary visual cortex, disturbance of circuit organisation with a higher density of parvalbumin-positive interneurons being hyperconnected to pyramidal neurons, dysregulation of pre- and post-synaptic elements and circuit hypoactivity are observed in CDKL5-deficient mice (Pizzo *et al.*, 2016). CDKL5-downregulated neurons display reduced frequency and amplitude of mEPSCs, indicating that CDKL5 contributes to regulation of excitatory synaptic strength (Ricciardi *et al.*, 2012). Lastly, impaired LTP and synapse maintenance have been also reported in CDKL5 KO neurons suggesting that plasticity is compromised after loss of CDKL5 (Della Sala *et al.*, 2016; Ren *et al.*, 2019).

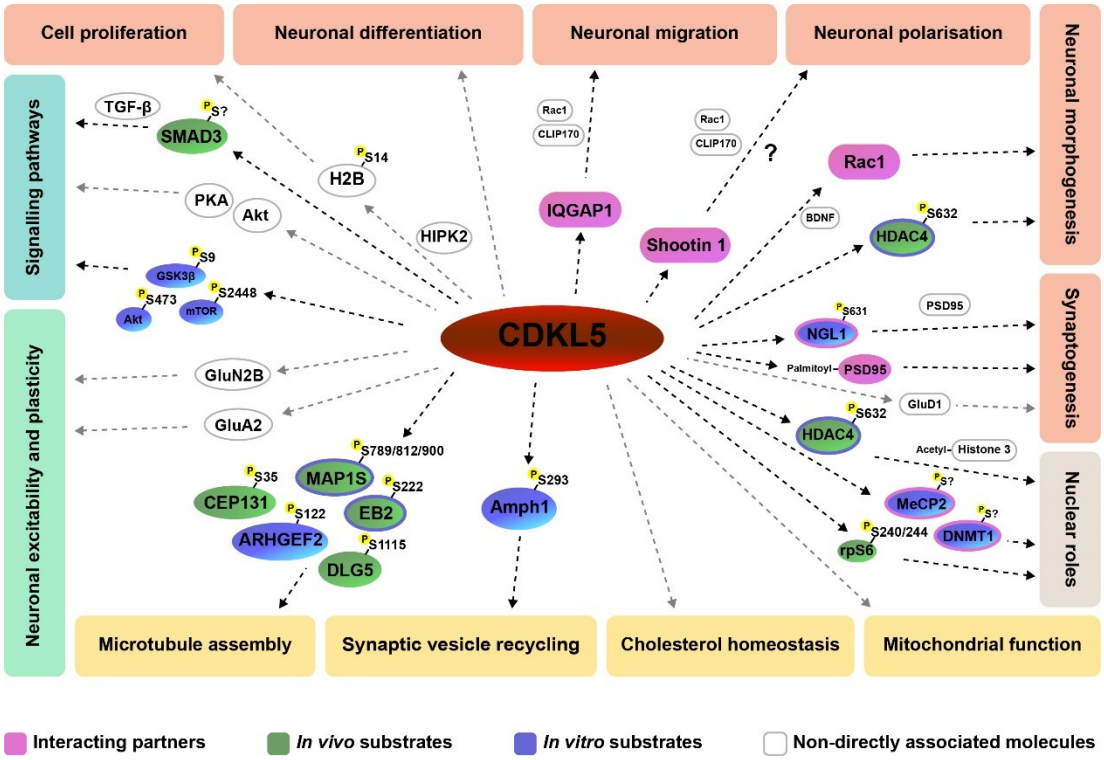

Figure 1.4 CDKL5 is implicated in various biological processes in the brain

CDKL5 is involved in distinct biological process both in the developing and mature neuron through various molecules, including interacting partners (magenta), *in vivo* and *in vitro* substrates (green and blue, respectively), and others (grey frame). Phosphosites are also reported with numbering according to the human isoforms.

1.3 Amphiphysin 1

Amph1 is a cytosolic protein belonging to a family that includes also Amph2 in vertebrates. Amph1 is mainly expressed in the brain, where it is significantly enriched in presynaptic terminals (Lichte *et al.*, 1992). Amph1 can be also detected in a range of tissues, including the retina, pancreas, liver, pituitary gland, testes, albeit considerably less abundant (Lichte *et al.*, 1992; De Camilli *et al.*, 1993; Yamamoto *et al.*, 1995; Floyd *et al.*, 1998; Grabs *et al.*, 2000; Terada *et al.*, 2002). In humans, the gene encoding for Amph1 is located on the short arm of chromosome 7 (7p13-14) and is transcribed into six splice variants, of which one is mainly neuron-specific and four are exclusively expressed in ribbon synapses in the retina (Yamamoto *et al.*, 1995; Floyd *et al.*, 1998; Terada *et al.*, 2002; Hosoya *et al.*, 2004). The remaining splice variant can be found in a variety of tissues outside of the central nervous system at low levels (Floyd *et al.*, 1998). Mouse and rat Amph1 genes are mapped on chromosome 13 and 17, respectively, and express proteins that share highly homologous N- and C-terminal regions with human Amph1 (85.1 % and 86.4 % total sequence similarity, respectively) (Jenkins *et al.*, 1995).

The neuron-specific isoform of Amph1 consists of 695 residues and has characteristic structural architecture based on its amino acid composition (Lichte *et al.*, 1992; Yamamoto *et al.*, 1995). The N-terminal domain is characterised by the presence of long stretches of amphiphilic α-helices. This module consists of an N-BAR domain and is a common feature of several proteins in addition to Amph1 (Peter *et al.*, 2004). The domain C-terminal to the N-BAR domain is overall positively charged and consists of several P residues. As a result, it is known as proline-rich domain (PRD). Apart from P

residues, it also contains other small aa, such as A and S residues, and has a high predisposition for β-turn secondary structures. Lastly, the remaining C-terminal region of Amph1 is pronouncedly acidic and contains two additional domains. The first one is known as clathrin-associated protein binding region (CLAP) domain, whereas the other has been identified as a Src homology 3 (SH3) domain (David *et al.*, 1994). In between, Amph1 contains a short hydrophobic region of 12 residues that is prone to form a transmembrane helix, although it is highly hydrophilic overall (David *et al.*, 1994). The domain structure of Amph1 can be found in Figure 1.5A. The pattern of domains, their amino acid sequences as well as their physicochemical properties, such as the charge distribution, appear to be well-conserved across vertebrate species with the exception of the region spanning between the CLAP and SH3 domains that differs considerably (David *et al.*, 1994; Yamamoto *et al.*, 1995).

Amph1 is a well-researched presynaptic protein implicated in different aspects of CME, an SV endocytosis pathway that has been described in more detail in subsection 1.1.2.1. The different stages of CME are presented in Figure 1.5B. During CME, Amph1 senses the membrane curvature that triggers its recruitment in the vicinity of the clathrin-coated pit (Evergren *et al.*, 2004; Peter *et al.*, 2004). The scission of the clathrin-coated pit requires the GTPase activity of Dyn1 (Pucadyil & Schmid, 2008) and Amph1 is important for recruiting Dyn1 around the deeply invaginated pit (Yoshida *et al.*, 2004). Furthermore, it has been suggested that Amph1 coordinates invagination and scission by remodelling the actin cytoskeleton (Yamada *et al.*, 2009). To perform the above activities, Amph1 forms multiple domain-specific interactions pointing therefore to the notion that it acts as multifunctional adaptor (Slepnev *et al.*, 2000). These interactions are discussed later in subsection 1.3.2. Lastly, Amph1 has been implicated both in epilepsy and tau-mediated neurodegeneration

indicating the importance of this endocytic protein in proper presynaptic function. Mice lacking Amph1 display presynaptic defects in SV recycling and are more prone to seizures (Di Paolo *et al.*, 2002). In another mouse model, accumulation of pathological tau aggregates has been associated with dysregulation of Amph1, similarly to multiple endocytic proteins that contribute to the early pathogenesis in Alzheimer's disease (De Jesus-Cortes *et al.*, 2012; Marsh & Alifragis, 2018; Xu *et al.*, 2018).

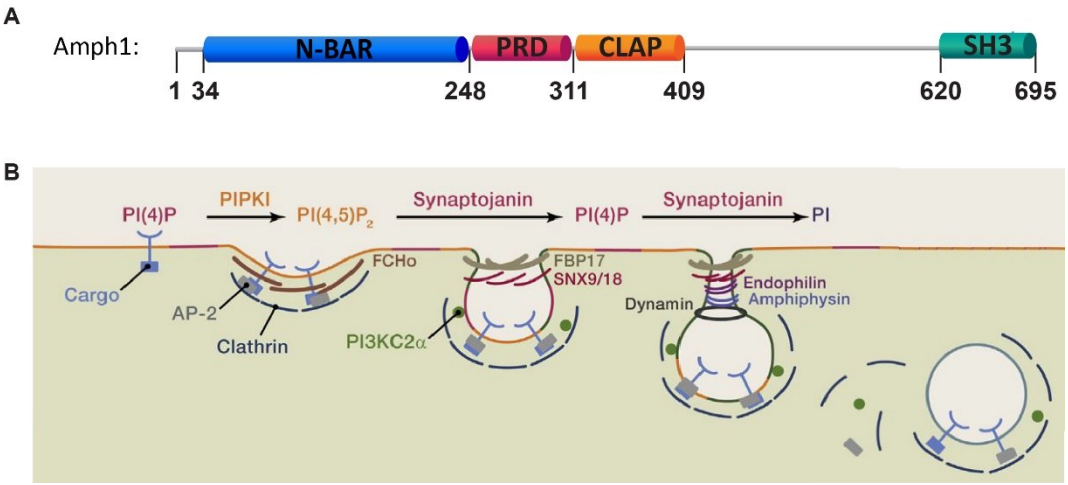

Figure 1.5 Amph1 has characteristic molecular structure that facilitates its involvement in CME

(**A**) Schematic illustration of the domain structure of Amph1. The N-BAR domain (blue) comprises the N-terminal region of Amph1 and is responsible for membrane bending. This is followed by the PRD (purple), the CLAP domain (yellow), and the SH3 domain (green) that is located at the most distant part of the C-terminal region. The residues that define each domain follow the human Amph1 numbering. (**B**)

Different stages of CME include nucleation, invagination, fission, and uncoating of SVs. Amph1 is recruited at the endocytic pit during late invagination and scission. Adapted from Daumke et al. (2014).

1.3.1 Activity-dependent modifications of Amph1

Several potential phosphorylation sites are present throughout the sequence of Amph1 suggesting that this posttranslational modification might dictate Amph1 activity in nerve terminals (Lichte *et al.*, 1992). Amph1 is detected as a double band by western blot analysis that is attributed to different phosphorylation states of the protein (Bauerfeind *et al.*, 1997; Craft *et al.*, 2008). Different studies reveal that it is a substrate of various protein kinases either *in vivo* or *in vitro*, including Cdk5, MAPK, minibrain kinase/dual-specificity tyrosine phosphorylation-regulated kinase (Mnb/Dyrk1A), casein kinase 2 and CDKL5 (Floyd *et al.*, 2001; Shang *et al.*, 2004; Doring *et al.*, 2006; Murakami *et al.*, 2006; Liang *et al.*, 2007; Sekiguchi *et al.*, 2013). In CHO cells, another member of the Cdk family, the mitotic cdc2/cyclin B kinase complex, has been reported to also phosphorylate Amph1 (Floyd *et al.*, 2001). A mass spectrometric study using rat brain synaptosomes detected 13 *in vivo* phosphorylation sites, of which S293 and T310 are the most abundant (Craft *et al.*, 2008). A list of the known phosphosites of Amph1 can be found in Table 1.1 together with the *in vitro* kinases that potentially mediated some of these reactions.

Amph1 undergoes reversible dephosphorylation that is facilitated by the calcium/calmodulin-dependent phosphatase calcineurin *in vitro* causing a

clear electrophoretic shift of its upper band (Bauerfeind *et al.*, 1997). In contrast to calcineurin, the protein phosphatases 1 and 2B fail to catalyse this reaction (Bauerfeind *et al.*, 1997). Amph1 dephosphorylation occurs in an activity-dependent manner with calcium influx being critical while SV exocytosis is not important *per se* (Bauerfeind *et al.*, 1997; Micheva *et al.*, 1997b). Notably, Amph1-S293 has been revealed as a major dephosphorylation site on KCl-stimulation of synaptosomes (Craft *et al.*, 2008).

Amph1 is also subjected to m-calpain-mediated cleavage mainly at S333, S377, and V392 residues distributed within the CLAP domain (Wu *et al.*, 2007). Calpain is a calcium-dependent cysteine protease that cleaves Amph1 in response to extensive calcium influx induced by either strong stimulation or kainate-induced hyperexcitation (Wu *et al.*, 2007). Despite that N-terminal fragments of Amph1 are still capable of binding to lipids, the interaction of truncated Amph1 with Dyn1 is impaired and ring formation is blocked, suggesting that Amph1 truncation is an additional mechanism for regulating SV endocytosis in rodent nerve terminals following high-frequency stimulation (Wu *et al.*, 2007).

Table 1.1 Phosphorylation sites on Amph1

Site	Domain	Kinase *in vitro*	*in vitro*	*in vivo*	References
S250	PRD	not known	-	+	(Craft *et al.*, 2008)
S252	PRD	not known	-	+	(Craft *et al.*, 2008)

T260	PRD	not known	-	+	(Choudhury *et al.*, 2008)
S262	PRD	not known	-	+	(Craft *et al.*, 2008)
S268	PRD	not known	-	+	(Craft *et al.*, 2008)
S272	PRD	Cdk5, Cdc2	+	+	(Floyd *et al.*, 2001) (Craft *et al.*, 2008)
S276	PRD	Cdk5, Cdc2	+	+	(Floyd *et al.*, 2001) (Liang *et al.*, 2007) (Craft *et al.*, 2008)
S285	PRD	Cdk5, Cdc2, MAPK	+	+	(Floyd *et al.*, 2001) (Liang *et al.*, 2007) (Shang *et al.*, 2004) (Craft *et al.*, 2008)
S293	PRD	Dyrk1A, MAPK, CDKL5	+	+	(Shang *et al.*, 2004) (Murakami *et al.*, 2006) (Craft *et al.*, 2008) (Sekiguchi *et al.*, 2013)
S295	PRD	Dyrk1A	+	-	(Murakami *et al.*, 2006)

T310	PRD	Dyrk1A	+	+	(Murakami *et al.*, 2006) (Craft *et al.*, 2008)
T350	CLAP	casein kinase 2	+	-	(Doring *et al.*, 2006)
T387	CLAP	casein kinase 2	+	-	(Doring *et al.*, 2006)
S496	-	not known	-	+	(Craft *et al.*, 2008)
S514	-	not known	-	+	(Craft *et al.*, 2008)
S539	-	not known	-	+	(Craft *et al.*, 2008)
S626	SH3	not known	-	+	(Craft *et al.*, 2008)

1.3.2 Molecular interactions of Amph1

Each of the major modules that comprise Amph1 not only bears unique structural features but is also essential for mediating distinct protein-protein or protein-lipid interactions within presynaptic terminals. The contribution of Amph1 in SV endocytosis as a multifunctional adaptor will be reviewed next per domain and a summary table can be found in Table 1.2.

N-terminal-mediated interactions. BAR domains are dimeric membrane-binding modules forming characteristic crescent-shaped structures. Based on their length, intrinsic curvature, and binding affinity to the membrane, BAR

domains are categorised in three subtypes: the N-terminal amphipathic helix-containing BAR (N-BAR), Fes/CIP4 homology BAR (F-BAR), and inverse BAR (I-BAR) (Simunovic *et al.*, 2015). Amph1 belongs to the first group of BAR-containing proteins and can either homodimerize or form heterodimers with Amph2, with the latter being the predominant form in the brain (Wigge *et al.*, 1997; Slepnev *et al.*, 1998). Amph2 is an isoform of 90 kDa with similar tissue expression, subcellular distribution, and structural organization with Amph1 (Wigge *et al.*, 1997), whereas it shares interacting partners with Amph1 (Ramjaun *et al.*, 1997) assisting the role of Amph1 as a scaffolding protein.

The Amph1 N-BAR domain is characterised by the ability to sense highly curved membrane formations with a diameter of 220 Å (Peter *et al.*, 2004). Apart from curvature sensor, it has been suggested that Amph1 N-BAR can tubulate membranes fitting them to the curvature of its own crescent structure depending on its density (Sorre *et al.*, 2012). However, this occurs only when the membrane has already reached a certain degree of curvature since Amph1 binds to the highly-curved membrane of the clathrin-coated pit just prior to scission (Taylor *et al.*, 2011). The mechanism through which Amph1 N-BAR shapes the membrane involves most probably the interaction of positively charged areas located throughout its curved-in surface with negatively charged phospholipids rather than helix insertion (Blood & Voth, 2006; Arkhipov *et al.*, 2009).

Apart from Amph2, three additional proteins have been reported to interact with Amph1 through its N-terminal region. The first one is the Cdk5-activating subunit p35 that interacts with Amph both *in vivo* and *in vitro* (Floyd *et al.*, 2001). Amph1 undergoes Cdk5-mediated phosphorylation and this modification has been related to actin remodelling during neuronal outgrowth (Floyd *et al.*, 2001). The second interacting partner on Amph1 is phospholipase

D (PLD) that hydrolyses phosphatidylcholine, producing the signalling molecule phosphatidic acid and soluble choline. Amph1 binding to PDL results in its inhibition, thus controlling the production of phosphatidic acid that is possibly important for regulating clathrin-coat assembly (Lee *et al.*, 2000). Finally, both the N-BAR and SH3 domains contribute to the interaction of Amph1 with the actin regulatory protein N-WASP triggering the N-WASP- and Arp2/3-dependent actin assembly (Yamada *et al.*, 2009).

PRD-mediated interactions. Downstream of the N-BAR domain, an overall basic PRD is found that contains, except for several P residues, other small amino acids. This domain displays high susceptibility to phosphorylation by various kinases implying its importance for regulating Amph1 function. Similarly to PRDs found in other endocytic proteins, the PRD of Amph1 binds to SH3 modules with high affinity. Interestingly, given that Amph1 comprises both a PRD and an SH3 domain, it has been hypothesized that an intramolecular interaction can be potentially formed between them hindering therefore binding to other interactors (Farsad *et al.*, 2003). To date, endophilin A1 has been identified to bind to the PRD of Amph1 through its SH3 domain (Micheva *et al.*, 1997b) and this interaction is possibly regulated by Dyrk1A- and/or CDKL5-mediated phosphorylation of Amph1 (Murakami *et al.*, 2006; Sekiguchi *et al.*, 2013). Altered phosphorylation of Amph1 at S293 by either kinase reduces its affinity for endophilin A1 (Murakami *et al.*, 2006; Sekiguchi *et al.*, 2013). Endophilin A1 is another N-BAR- and SH3-containing protein that is linked to SV endocytosis (Kjaerulff *et al.*, 2011). Apart from Amph1, several interactions with endocytic proteins have been revealed suggesting that it also acts as a scaffolding protein. Moreover, owning to its N-BAR domain, endophilin A1 is associated with membrane bending prior to scission (Gallop *et al.*, 2006). Endophilin A1 also facilitates the uncoating of

newly generated SVs (Gad *et al.*, 2000; Verstreken *et al.*, 2003; Sullivan, 2011). Lastly, it has been linked to regulation of fusion kinetics in chromaffin cells, independently of its endocytic roles (Gowrisankaran *et al.*, 2020).

CLAP-mediated interactions. Via the CLAP domain, Amph1 was reported to interact with the clathrin adaptor complex AP1 at the *trans*-Golgi and AP2 at the plasma membrane through the ear domain of the α-adaptin subunit as well as with clathrin heavy chain (CHC) *in vitro* (Wang *et al.*, 1995; Slepnev *et al.*, 2000; Huser *et al.*, 2013). These interactions are crucial for CME, since truncation of Amph1 within the CLAP domain results in inhibiting SV endocytosis as well as depression of synaptic transmission (Wu *et al.*, 2007). Two phosphorylation sites have been identified to be located within the CLAP domain, T350 and T387 (Doring *et al.*, 2006). The double phosphomimic mutant T350E/T387E results in reduced binding of clathrin triskelia to Amph1 implying possibly that clathrin has lower affinity for phosphorylated Amph1 (Doring *et al.*, 2006).

SH3-mediated interactions. The SH3 domain is a short module of around 60 aa that is present in several proteins serving a wide range of biological processes, such as altering the local concentration of various components or facilitating the assembly of multiprotein complexes (McPherson, 1999). The SH3 domain of Amph1 occupies the C-terminal region and can bind with high affinity to both Dyn1 and synaptojanin 1 in their C-terminal polyproline tail harbouring a PXXP motif (David *et al.*, 1996; McPherson *et al.*, 1996; Micheva *et al.*, 1997a; Cestra *et al.*, 1999). Multiple interactions between the amphiphysin SH3 domain and Dyn are required for Dyn recruitment to clathrin-coated pits *in vivo* (Rosendale *et al.*, 2019), whereas disruption of their interaction has been shown to block SV fission (Shupliakov *et al.*, 1997). Amph1 does not only recruit Dyn1 into the neck of the endocytic pit, but it also contributes to the

fission itself either physically or by stimulating the GTPase activity of Dyn1 (Meinecke *et al.*, 2013; Takeda *et al.*, 2018).

Another interacting partner of Amph1 SH3 domain is the focal adhesion kinase (FAK), a stimulus-dependent tyrosine kinase present in the presynaptic terminals (Messina *et al.*, 2003). This interaction has been suggested to enable the FAK-induced recruitment of amphiphysin to the plasma membrane and its disruption seems to impact on actin cytoskeleton and calcium-dependent endocytosis (Messina *et al.*, 2003). Last but not least, the calcineurin inhibitor (Cain) that regulates SV endocytosis through calcineurin activity and synapsin 1 are two additional interacting partners of the SH3 domain of Amph1 in the nerve terminal (Lai *et al.*, 2000; Onofri *et al.*, 2000). In the case of synapsin 1, interaction with Amph1 SH3 impairs its binding to protein components of SVs and also weakens its ability to trigger actin polymerisation (Onofri *et al.*, 2000).

Table 1.2 Established interacting partners of Amph1 and their role in endocytosis

Interacting partner	Known interaction site/domain	Known interaction site/domain on Amph	Role in endocytosis
Amph2 (Wigge et al., 1997)	N-terminal region	N-terminal region	Membrane remodelling Scaffold protein

Cdk5-activating subunit p35 (Floyd et al., 2001)	Unknown	N-terminal region	Phosphorylation of Amph1 by Cdk5
PLD (Lee et al., 2000)	Unknown	N-terminal region	Clathrin-coat assembly
N-WASP (Yamada et al., 2009)	Unknown	N-terminal region and SH3 domain	Arp2/3-dependent actin polymerization.
Endophilin (Micheva et al., 1997b)	SH3 domain	PRD domain Unknown (in Amph2: RKGPPVPPLP)	Membrane remodelling Scaffold protein Possibly scission Uncoating
CHC (Slepnev et al., 2000)	N-terminal domain	CLAP domain DLD and WD	Clathrin coat assembly

AP2 (Slepnev et al., 2000)	ear domain of α-adaptin subunit	CLAP domain FFED (and DPF)	Clathrin recruitment Clathrin coat assembly Interaction with dynamin
AP1 (Huser et al., 2013)	Unknown	CLAP domain WDLW (Amph1/2 heterodimer)	Clathrin coat assembly (trans-Golgi network)
Dyn1 (David et al., 1996; Grabs et al., 1997)	PRD PS**R**PN**R**	SH3 domain PXRPXR(H)R(H)	Scission via GTPase-dependent mechanochemical activity and release of CCVs
Synaptojanin 1 (Micheva et al., 1997a; Cestra et al., 1999)	PIR**PS**R PTI**PP**R	SH3 domain	Fission Uncoating

Focal adhesion kinase (Messina et al., 2003)	C-terminal proline-rich region	SH3 domain	Actin cytoskeleton remodelling Role in endocytosis?
Cain (Lai et al., 2000)	Proline-rich region	SH3 domain	Inhibition of calcineurin activity
Synapsin 1 (Onofri et al., 2000)	Proline-rich C-terminus?	SH3 domain	Actin cytoskeleton remodelling Attachment to SVs

1.4 Project objectives

Whilst the impact of CDKL5 deficiency on the development of human brain is evident given the severity of conditions associated with CDD, neither the physiological role nor the pathological defects of CDKL5 are well understood. This is exaggerated when the presynapse is considered, since the presence of CDKL5 there has not been properly established, and, thus, a putative role for

CDKL5 in presynaptic terminals has been poorly addressed. However, the evidence that Amph1, a highly enriched endocytic protein in nerve terminals, is a putative substrate of CDKL5 *in vitro* points to a possible presynaptic role for CDKL5. Also, many other neurodevelopmental epileptic conditions have been linked to defects of well-known presynaptic molecules, including endocytic proteins, which makes the task of examining the presynaptic role of CDKL5 necessary. This would allow us to achieve a better understanding of the basic CDKL5-related neurobiology and neuropathology. Moreover, the knowledge of the molecular events that involve CDKL5 -similar to other epileptic molecules- can be beneficial for the development of potential therapeutic strategies for CDD and, at the same time, help establish common approaches for similar epileptic disorders. To this end, our hypothesis was that CDKL5 deficiency at the presynapse impairs SV recycling and this is possibly mediated by altering the ability of neuronal activity to control the interaction between Amph1 and endophilin A1 due to phosphorylation of Amph1 at the S293 residue.

The aims of this project as addressed per chapter are:

- Chapter 3: Characterise a novel KO rat model of CDKL5 deficiency (*Cdkl5* KO Long-Evans) presynaptically focusing on various parameters of the SV cycle that might be affected due to the loss of CDKL5

- Chapter 4: Follow a structure-function approach to examine whether presynaptic deficits can be restored using a molecular replacement strategy with different exogenous CDKL5 constructs and investigate whether Amph1 is an interacting partner and substrate of CDKL5 focusing specifically on the S293 residue

- Chapter 5: Determine the functional role of Amph1 complexes in SV recycling at central presynaptic terminals and further elucidate the interaction between Amph1 and endophilin A1.

Chapter 2: Materials and methods

2.1 Materials

Synaptophysin-pHluorin was obtained from Prof L. Lagnado (University of Sussex, UK). The full-length rat Amph1 was gifted from Dr H. T. McMahon (MRC Laboratory of Molecular Biology, Cambridge, UK). The Amph1-mCerN1 expression vector was generated by the Cousin lab by cloning full-length rat Amph1 into an mCerulean (mCer) N1 vector with the sense CTC GAG ATG GCC GAC ATC AAG ACG GGC ATC T and antisense TGG ATC CCG TTC TAG GTG TCG TG TGA AGT TCT C primers and the restriction enzymes XhoI and BamHI (sites underlined), respectively. The full-length human CDKL5_1 (hCDKL5_1; hereafter referred to as CDKL5) was gifted from Dr V. Kalscheuer (Max Planck Institute for Molecular Genetics, Berlin, Germany). CDKL5-mCerC1 was generated by the Cousin lab by cloning CDKL5 into an mCerC1 vector with the sense CAT CAT CTC GAG GAA TGA AGA TTC CTA ACA TTG GTA ATG and antisense CAT CAT GGT ACC TTA CAA GGC TGT CTC TTT TAA ATC primers and the restriction enzymes XhoI and KpnI (sites underlined), respectively. Lastly, the pGEX-KG plasmid vector was gifted by Dr C. Rickman (Heriot-Watt University).

General reagents and chemicals were obtained from Sigma-Aldrich or Thermo Fisher Scientific. Specific reagents used for each method can be found in the following subsections.

2.2 DNA cloning

2.2.1 DNA recombination

2.2.1.1 Polymerase chain reaction

DNA amplification was achieved by polymerase chain reaction (PCR) using a pair of sense and antisense primers that were designed to introduce specific restriction enzyme recognition sites on either side of the DNA fragment. All the primers were generated by Eurogentec (Belgium) and a list of them can be found in Table 2.1. The reaction mix consisted of a Pfu 10x Reaction Buffer with 20 mM $MgSO_4$ (Promega, USA; M776A), a sense and antisense primer (1 μM), dNTPs (10 mM; Invitrogen™), Pfu DNA polymerase (5 U/μl; Promega, USA; M774A), and the DNA template (100 ng). PCR was carried out in a SimpliAmp Thermal Cycler machine (Thermo Fisher Scientific) under the following conditions: 95°C for 2 min, 40 cycles of 95°C for 30 s, 55°C for 1 min, and 72°C for 1 min/kilobase plasmid, and 72°C for 10 min followed by cooling to 4°C.

2.2.1.2 Agarose gel electrophoresis

To estimate the purity and identity of PCR amplified samples, gel electrophoresis was performed, where DNA fragments were separated based on their size. A small amount of PCR samples was loaded onto an 1 % (w/v) agarose gel (UltraPureTM Agarose; Invitrogen™) with SYBR® Safe DNA gel stain (10,000x; Invitrogen™) in Tris/Borate/EDTA buffer that consisted of 44.6

mM Tris, 44.4 mM boric acid and 1.6 mM EDTA. Apart from the samples, the HyperLadder™ 1kb DNA ladder (Bioline; BIO33026) was also loaded. Gel electrophoresis was performed at 120 V constant for 35 min. The DNA bands were visualized using ultraviolet light in a Syngene InGenius3 imaging system (Cambridge, UK) and GeneSys software (Syngene; Cambridge, UK).

2.2.1.3 Digestion with restriction enzymes

The PCR amplified insert as well as the vector of interest were digested by the appropriate pair of restriction enzymes to create compatible sticky ends. All restriction enzymes used were purchased from Thermo Fisher Scientific and can be found in Table 2.1. The digestion mix consisted of a 10x FastDigest Green Buffer (Thermo Fisher Scientific), 1 µl of each restriction enzyme, and 1 µg of either the insert or the vector. Three different types of controls were also prepared, including one with either the first or the second restriction enzyme and another one without any restriction enzymes. The digestion was performed in a water bath at 37°C for 1.5 h or at room temperature overnight. The digested DNA fragments were separated by gel electrophoresis (see above in 2.2.1.2 Agarose gel electrophoresis) and the bands representing the digested insert and vector, respectively, were cut out of the gel. The DNA was extracted using the Zymoclean™ Gel DNA Recovery Kit (Zymo Research) according to the manufacturer's instructions and ultrapure H_2O for the elution step.

2.2.1.4 Quantification of DNA concentration

The concentration of extracted DNA was estimated by measuring optical density at 260 nm using a NanoDrop spectrophotometer (Thermo Fisher Scientific). The absorbance ratios 260/280 and 260/230 were also evaluated as they indicate the presence of proteins and other contaminants evaluating thus the purity of the DNA samples. The values ~1.8 for the 260/280 and 2.0-2.2 for the 260/230 ratios were considered acceptable for the purity of DNA samples.

2.2.1.5 Introduction of DNA insert into expression vectors

Insert DNA was introduced into an expression vector bearing complementary sticky ends, using a T4 DNA Ligase (Promega; USA; M180A) and a 2x Rapid Ligation Buffer (Promega; USA; C6711) after the two molecules were mixed in a ratio 3:1 of insert:vector. The amount of insert DNA (ng) that was necessary for the ligation reaction was determined with the help of the NEBioCalculator v1.10.1 online calculator, for which the insert DNA length (bp), vector DNA length (bp) and vector DNA mass (ng) were required. CDKL5 truncated constructs were incorporated into mCerC1 expression vector, whereas Amph1 mutated constructs lacking the F-BAR domain were inserted into pGEX-KG plasmids. The ligation solution was incubated at room temperature for 30 min followed by overnight incubation at 4^{o}C.

2.2.1.6 Bacterial transformation

DNA constructs were mixed with either XL10 or BL21 competent bacterial cells and incubated on ice for 30 min. A sample of competent cells in which no DNA construct was added served as a negative control. Introduction of plasmid DNA into the bacterial host cells was achieved by the heat shock method at 42°C for 45 s followed by incubation on ice for 2 min. Pre-warmed lysogeny broth media containing 10 g tryptone (Merck), 5 g yeast extract and 171 mM NaCl, pH 7.4, was added aseptically to the transformed bacteria, which were then incubated at 37°C for 1 h in a shaking incubator. Pre-warmed agar plates containing the appropriate antibiotic (ampicillin, 100 ng/ml; kanamycin, 30 μg/ml) were inoculated aseptically and incubated at 37°C overnight. The plates were kept inverted to prevent any condensed water interfering with the growth of the bacteria. The following day the plates were checked for bacterial colonies and stored at 4°C. The plasmid vectors mCerC1 and mCerN1 were resistant to kanamycin (Fisher Bioreagents; BP 906-5), whereas the pGEX-KG plasmids to ampicillin.

2.2.1.7 Isolation of recombinant plasmid from bacteria

After transformation and growth of bacterial cells, colonies of identical plasmid clones were selected randomly and allowed to grow in lysogeny broth media containing the appropriate antibiotic (see above in 2.2.1.6 Bacterial transformation) at 37°C overnight in a shaking incubator. The bacterial culture was then lysed, and the plasmid DNA was purified chemically. Depending on the volume of the culture and the subsequent yield of plasmid DNA, either the GeneJET Plasmid Miniprep Kit (Thermo Fisher Scientific) or the HiSpeed®

Plasmid Maxi Kit (Qiagen) was used for this purpose, according to the manufacturer's instructions. The yield and purity of the recombinant DNA was estimated as described above (2.2.1.4 Quantification of DNA concentration).

2.2.1.8 DNA sequencing

Sanger sequencing was conducted by Source BioScience, UK, to verify that the nucleotide sequence of purified DNA constructs was correct. Primers used for sequencing were either designed and supplied together with the samples (listed in Table 2.1) or were provided by Source Bioscience, UK, such as the EGFP C F or PGEX 5' generic primers. Chromatographs were subsequently analysed using the A plasmid Editor v2.0.60 software created by Dr W. Davis (University of Utah).

Table 2.1 List of primers.

Name	**Sequence 5′-3′**
Primers for cloning Amph1 constructs into pGEX-KG vector	
Sense_PRD	CATCATGAATTCTAGGAGCTCCCAGTGATTCGGGTC Restriction enzyme: EcoRI (FD0274)
Antisense_SH3	ATGATGCTCGAGCTATTCTAGGTGTCGTGTGAAGTTCTC Restriction enzyme: XhoI (FD0694)

Antisense_ΔSH3	ATGATGCTCGAGCTAAGGAGGCAGTTCCTGAGCGG Restriction enzyme: XhoI

Primers for generating truncated versions of CDKL5-mCerC1

Sense_aa1	CATCATCTCGAGTAATGAAGATTCCTAACATTGG Restriction enzyme: XhoI
Sense_aa298	CATCATCTCGAGTACAAACCCAGAGACTTCTGG Restriction enzyme: XhoI
Sense_aa353	CATCATCTCGAGTACTGCCCCGGGCTGACGAAG Restriction enzyme: XhoI
Antisense_aa297	ATGATGGAATTCCTAAAATGTAGGGTGATTCAAAC Restriction enzyme: EcoRI
Antisense_aa352	ATGATGGAATTCCTAGCCTACACTCAGGTTCTG Restriction enzyme: EcoRI
Antisense_aa960	ATGATGGGTACCTTACAAGGCTGTCTCTTTTAAATC Restriction enzyme: KpnI (FD0524)

Sequencing primers

For sequencing the SH3 domain of Amph1	GAAGCAGGAACTGGCTACAG
For sequencing the C-terminus domain of CDKL5	CTTATGGACTGGGCTACACC, GTTACATCTCTCTTCGGCCTC

2.2.2 Site-directed mutagenesis

Point mutations were introduced in full-length rat Amph1 or human CDKL5 protein by PCR using a pair of sense and antisense primers that contain the respective modification. Some of these mutations located in different domains of Amph1 were shown to disrupt protein-protein interactions with different endocytic molecules (Cestra *et al.*, 1999; Slepnev *et al.*, 2000). These mutations were introduced in rat Amph1, using the full-length Amph1-mCerN1 plasmid as template of the PCR reaction. Similarly, single-base pair mutations were introduced in human CDKL5, using the full-length CDKL5-mCerC1 vector as DNA template. The missense mutation R178P that was reported in CDD patients (Elia *et al.*, 2008; Nemos *et al.*, 2009) as well as the K42R mutation that was shown to block the kinase activity of CDKL5 (Lin *et al.*, 2005) were both generated by the Cousin lab. The primers that were used for introducing point mutations were all purchased from Eurogentec (Belgium) and can be found in Table 2.2. The PCR reaction was performed as described in 2.2.1.1 Polymerase chain reaction, and was followed by digestion at 37^{o}C for 1 h with 1 µl DpnI endonuclease (Biolabs; R0176L) that cleaves selectively methylated DNA. XL10 competent cells were transformed by heat shock and mutated DNA constructs were purified either by miniprep or maxiprep as per manufacturer's instructions. The presence of the desired point mutations was confirmed by Sanger sequencing.

Table 2.2 List of primers used in site-directed mutagenesis.

Name	Sequence 5′-3′
Primers for the site-directed mutagenesis of Amph1-mCerN1	
AP2 (FFE→SSR) Sense	GAGAACATCATCAATTCCTCTAGGGAC AACTTTGTACCAG
AP2 (FFE→SSR) Antisense	CTGGTACAAAGTTGTCCCTAGAGGAAT TGATGATGTTCTC
CL_I (DLD→HSR) Sense	GGAGACTTTGCTGCATTCGCGCTTTGA CCCTTTCAAAC
CL_I (DLD→HSR) Antisense	GTTTGAAAGGGTCAAAGCGCGAATGC AGCAAAGTCTCC
CL_II (WD→SR) Sense	CAGACATTGCCCTCGCGCTTATGGACG ACAAG
CL_II (WD→SR) Antisense	CTTGTCGTCCATAAGCGCGAGGGCAAT GTCTG
PRD_I (PP_I→AA) Sense	GACAAGGAAAGGGGCTGCTGTCCCAC CTCTGC
PRD_I (PP_I→AA) Antisense	GCAGAGGTGGGACAGCAGCCCCTTTC CTTGTC
PRD_II (PP_II→AA) Sense	GAAAGGGCCTCCTGTCGCAGCTCTGCC TAAAGTC

PRD_II (PP_II→AA) Antisense	GACTTTAGGCAGAGCTGCGACAGGAG GCCCTTTC
PRD_III (PPVPP→AAVAA) Sense	CAAGGAAAGGGGCTGCTGTCGCAGCT CTGCCTAAAG
PRD_III (PPVPP→AAVAA) Antisense	CTTTAGGCAGAGCTGCGACAGCAGCC CCTTTCCTTG
PRD_IV (PVRP→AVRA) Sense	GCATCTCCTGCCGCAGTGCGAGCCAGA TCACCTTCAC
PRD_IV (PVRP→AVRA) Antisense	GTGAAGGTGATCTGGCTCGCACTGCGG CAGGAGATGC
SH3 (G→R, P→L) Sense	GCCACATACAAACGCCTCTTTCTAGAG AACTTCACAC
SH3 (G→R, P→L) Antisense	GTGTGAAGTTCTCTAGAAAGAGGCGTT TGTATGTGGC
S293A Sense Generated by the Cousin lab	CCAGTGCGACCCAGAGCACCTTCACA GACAAGG
S293A Antisense Generated by the Cousin lab	CCTTGTCTGTGAAGGTGCTCTGGGTCG CACTGG
S293E Sense Generated by the Cousin lab	CCAGTGCGACCCAGAGAACCTTCACA GACAAGG

S293E Antisense Generated by the Cousin lab	CCTTGTCTGTGAAGGTTCTCTGGGTCGC ACTGG

Primers for the site-directed mutagenesis of CDKL5-mCerC1

K42R Sense Generated by the Cousin lab	GAAATTGTGGCGATCCGGAAATTCAA GGACAGT
K42R Antisense Generated by the Cousin lab	ACTGTCCTTGAATTTCCGGATCGCCAC AATTTC
R178P Sense Generated by the Cousin lab	GCCACCAGATGGTATCCGTCCCCAGAA CTCTTA
R178P Antisense Generated by the Cousin lab	TAAGAGTTCTGGGGACGGATACCATCT GGTGGC

2.2.3 Cloning short hairpin RNA sequences

For knocking down Amph1, a short hairpin RNA sequence (shRNA) was cloned into a pSUPER.neo+gfp vector (Oligoengine) modified to express mCer instead of the original green fluorescent protein (GFP) probe (Clayton *et al.*, 2010). The shAmph1 expressing vector was generated by ligating annealed custom-made oligonucleotides with a pSUPER vector that was previously

digested using BglII (FD0083) and XhoI at 37°C for 30 min and gel purified. The annealing reaction was prepared by mixing a pair of sense and antisense oligonucleotides (3mg/ml) corresponding to the mouse Amph1 sequence in the appropriate annealing buffer (100 mM NaCl and 50 mM HEPES, pH 7.4) and was performed at 90°C for 4 min followed by 70°C for 10 min. The annealed oligonucleotides were cooled down to 10°C in 5°C steps, with 3 min for each step. A scrambled control was also generated using a pair of oligonucleotides that do not match any mouse Amph1 sequence. All the oligonucleotides used were purchased from Eurogentec (Belgium) and can be found in Table 2.3. The pSUPER vector used also expressed sypHy, which was mutated within its BglII site to avoid digestion there (mutated and cloned by the Cousin lab). The expression of mCer was prevented by introducing an early stop codon to the mCer sequence using site-directed mutagenesis. A map of the pSUPER vector used to silence Amph1 expression is presented in Figure 2.1. XL10 competent cells were transformed by heat shock and shRNA expressing pSUPER vectors were purified either by miniprep or maxiprep as per manufacturer's instructions. The presence of the shAmph1 was confirmed by Sanger sequencing.

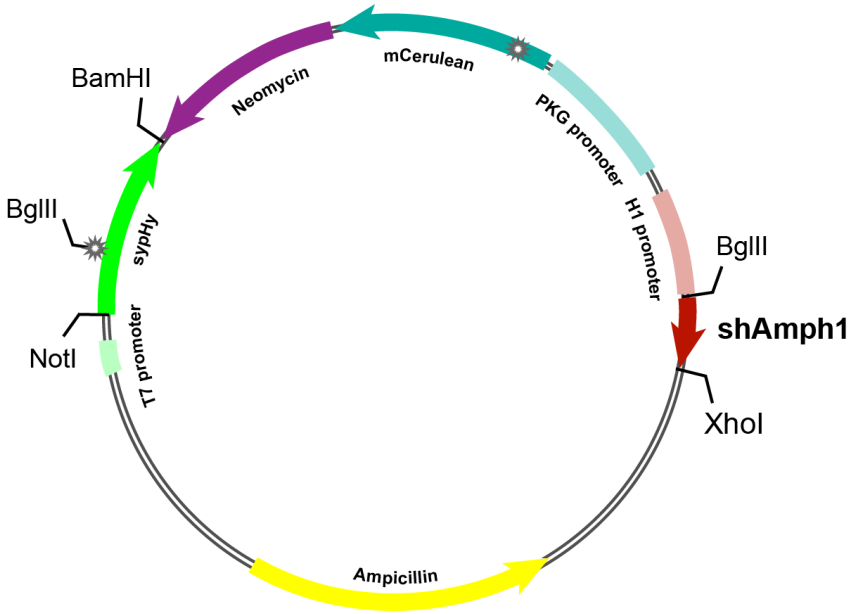

Figure 2.1 pSUPER vector expressing shAmph1

Schematic presentation of the pSUPER plasmid vector that was used to silence the expression of Amph1. The shAmph1 (red) and sypHy (green) expression is controlled by the H1 (light red) and T7 (light green) gene promoters, respectively. The expression of mCer (turquoise) was interrupted by introducing an early stop codon (star). The BglII site within sypHy was modified to prevent digestion (also star).

Table 2.3 List of oligonucleotides for knocking down Amph1.

Primer	Sequence 5′-3′
shAmph1 Sense	GATCCCCGGAAGCTTGTGGATTATGATTCAAGA GATCATAATCCACAAGCTTCCTTTTTC
shAmph1 Antisense	TCGAGAAAAAGGAAGCTTGTGGATTATGATCTC TTGAATCATAATCCACAAGCTTCCGGG
Scrambled Sense	GATCCCCTCGCGATTAGTTCATTAGGTTCAAGAG ACCTAATGAACTAATCGCGATTTTTC
Scrambled Antisense	TCGAGAAAAATCGCGATTAGTTCATTAGGTCTCT TGAACCTAATGAACTAATCGCGAGGG

2.3 Animals

All experimental procedures were conducted according to the Animals (Scientific Procedures) Act 1986 on the protection of animals used for scientific purposes, with approval of institutional animal welfare guidelines. Animals were maintained on a 12-hour light/dark cycle under temperature-controlled environment, with food and water provided when needed.

2.3.1 *Cdkl5* KO Long-Evans breeding colony

All the animals used for studying the role of CDKL5 at nerve terminals belonged to the *Cdkl5* KO Long-Evans rat breeding colony. This model was generated by Horizon Discovery, USA, by deleting a 10-bp sequence in exon 8 of the CDKL5 gene (138367-76 in genomic sequence) that results in the introduction of an early stop codon. CDKL5 heterozygous females (*Cdkl5*$^{+/-}$) and WT Long-Evans males (*Cdkl5*$^{+/y}$) were set up for timed matings and rat embryos were obtained from pregnant females at E17-E19. Embryos were sexed by dissecting the abdomen to reveal their inner reproductive organs. Only male *Cdkl5*$^{-/y}$ embryos (hereafter referred to as CDKL5 KO) and littermate controls (hereafter referred to as WT) were used for neuronal cultures given that *Cdkl5* is an X-linked gene. Adult male rats of both WT and CDKL5 KO background were used for biochemistry experiments.

2.3.2 Genomic DNA extraction

Genomic DNA was extracted from nose or tail (a couple of millimetres) biopsies of rat embryos following the HotShot method. Briefly, DNA was prepared by boiling tissue samples at 95^{o}C for 50 min in alkaline lysis reagent consisting of 25 mM NaOH and 0.2 mM disodium EDTA in double-distilled H_2O, pH 12. After cooling to 4^{o}C, neutralising reagent was added containing 40 mM Tris-HCl in double-distilled H_2O, pH 5 and the extracted DNA was stored at -20^{o}C.

2.3.3 Genotyping

The DNA sequence of interest was amplified by PCR using a pair of sense-antisense primers and an additional sense primer matching a 10 bp sequence present only in the genomic DNA derived from WT tissues that can be found in Table 2.4. Prior to PCR, a master mix was prepared including 1x Green GoTaq® Reaction Buffer, the above primers (500 nM), dNTPs (200 μM), GoTaq® DNA Polymerase (0.03125 U/μl), 1 μl DNA and double-distilled H_2O up to final volume 20 μl. PCR was carried out in a SimpliAmp Thermal Cycler machine (Thermo Fisher Scientific) under the following conditions: 94°C for 3 min, 94°C for 20 s, 56°C for 30 s (40 cycles), 72°C for 1 min, 72°C for 2 min and cooling to 4°C. PCR amplified samples were loaded onto a 0.6 % (w/v) agarose gel (UltraPureTM Agarose; Invitrogen) in 1x Tris/Borate/EDTA buffer using RedSafe Nucleic Acid Staining Solution (20,000x; GH Science). Apart from the samples, the HyperLadder™ 1kb (Bioline) DNA ladder, a WT, a KO, and a water control were also loaded. Gel electrophoresis was performed at 120 V constant for 35 min. The DNA bands were visualized using ultraviolet light in the Syngene InGenius3 imaging system (Cambridge, UK) and the GeneSys software (Syngene; Cambridge, UK). WT samples were represented as a double band of 335 bp and 135 bp, whereas CDKL5 KO samples as a single band of 325 bp due to the 10-bp deletion from exon 8, as shown in Figure 2.2. Since the sense primer matching this deletion was not able to bind, the low molecular weight band was absent from CDKL5 KO samples.

Table 2.4 List of primers used for genotyping.

Primer	Sequence 5′-3′	Location
Sense	GGGCTTGTAGCAAATCCATCC	Intron 6
Sense; matching a 10 bp deletion	ATACGTGGCTACTCGGTGGTAC	Exon 8
Antisense	AGCAAGCAGAGTTCTATTTTCCT	Intron 7

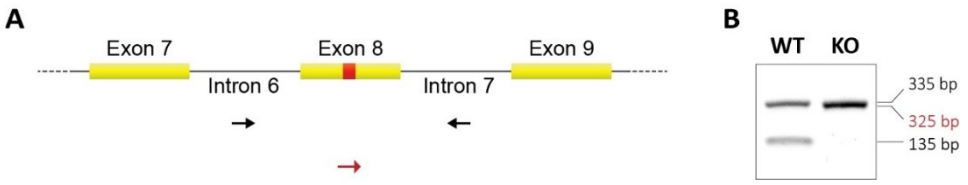

Figure 2.2 Genotyping strategy

(**A**) Schematic representation of the Cdkl5 gene region that encompasses the 10-bp deletion (red box) in exon 8 as well as the binding sites for the genotyping primers (black arrows). The genotyping strategy includes a third primer that recognizes the region containing the 10-bp deletion (red arrow). (**B**) Two PCR-amplified fragments of the Cdkl5 gene are detected at 335 bp and 135 bp, respectively, in WT embryonic tissues. A single 325-bp fragment lacking the 10-bp deletion is detected in CDKL5 KO embryonic tissue.

2.3.4 Wildtype animals

Wildtype mice from the C57Bl/6J colony were set up for timed matings and mouse embryos were obtained from pregnant females at E16-E17. Mouse embryos of both sexes were used for neuronal cultures. Adult Sprague Dawley rats were preferably used for biochemistry experiments (see 2.9.1 Crude synaptosome purification) due to the larger starting material that can be obtained compared to mice.

2.4 Cell culture

2.4.1 Preparation of primary hippocampal neurons

Primary neuronal cultures were prepared from the hippocampus of *Cdkl5* LE KO rat male embryos at E17-19 or C57Bl/6J wildtype mouse embryos of both sexes at E16-17. Dissected hippocampi were incubated in papain (10 U/ml; Worthington Biochemical; LK003178) at 37°C for 20 min before trituration in Dulbecco's Modified Eagle Medium/Nutrient Mixture F-12 (Thermo Fisher Scientific) supplemented with penicillin/streptomycin solution (Life Technologies; 15140-122) and filter-sterilised foetal bovine serum (Biosera; S1810-500). The solution was spun at 350 x *g* for 5 min at room temperature and resuspended in Neurobasal medium (Thermo Fisher Scientific) containing penicillin/streptomycin solution, L-glutamine (0.5mM; Life Technologies; 25030-024) and B27 supplement (1% v/v; Life Technologies; 17504-044). Cells were counted with a Marienfeld Neubauer counting chamber and loaded onto pre-warmed 25 mm coverslips containing 50 μL of laminin

(Sigma-Aldrich; L2020)-enriched Neurobasal in 6-well plates at a density of 4.0 × 10^6 cells/ml. The coverslips were previously coated in poly-D-lysine (0.05 μg/μl; Sigma-Aldrich; P7886-50MG) dissolved in 100 mM boric acid solution, pH 8.5, overnight at room temperature. After 1-h incubation at 37°C, each well was filled with 2 mL of Neurobasal medium. Cytosine β-D-arabinofuranoside (Sigma-Aldrich; C1768-100MG) was added to the cells to a final concentration 1 μM after 3 days to avoid proliferation of glia. Cells were kept in a humidified incubator at 37 °C/5% CO_2 for up to 15 days.

2.4.2 Transfection

Hippocampal neurons were transfected between 8-10 days *in vitro* (DIV) using 1-2 μl of Lipofectamine® 2000 Transfection reagent (Thermo Fisher Scientific) and 1 μg of plasmid per well incubated together for 20 min before transfection. In the case of the mCer, 0.7 μg of the plasmid were used per well. Transfection was performed using unsupplemented Neurobasal medium (Thermo Fisher Scientific) for 2 h at 37°C/5 % CO_2 prior to being replaced by the initial supplemented Neurobasal medium of the culture.

2.5 Imaging assays and microscopy

2.5.1 Synaptophysin-pHluorin live-cell imaging

For monitoring the kinetics of the SV cycling in nerve terminals of primary hippocampal neurons in real time, a GFP-derived tag was used called

pHluorin (Miesenbock *et al.*, 1998). This probe is characterized by high pH-sensitivity and is fused to lumenal domains of synaptic vesicle proteins, such as synaptoptophysin (Granseth *et al.*, 2006). Synaptophysin-pHluorin (sypHy) is a fusion SV protein with four transmembrane domains that bears the pHluorin tag in an intravesicular loop (Granseth *et al.*, 2006). The fluorescence of sypHy is dictated by the differences in pH between the lumen of SVs and that of the extracellular fluid under 488-nm excitation. At rest, the sypHy fluorescence is quenched by the acidic pH intralumenally (pH ~ 5.5). Upon stimulation, SV fusion with the plasma membrane leads to an increase in fluorescence due to the exposure of pHluorin molecules to the basic environment outside of the neuron (pH 7.4) and their subsequent deprotonation. The retrieval of the vesicular membrane and its protein components is followed by rapid reacidification (τ ~3-5 s) of the newly internalised SVs resulting in fluorescence being quenched again (Atluri & Ryan, 2006; Kwon & Chapman, 2011). Since reacidification occurs fast compared to endocytosis, this decay in fluorescence can be used to estimate the speed of SV endocytosis following stimulation (Sankaranarayanan & Ryan, 2000).

Two properties of sypHy have been crucial for studying the exocytosis-endocytosis dynamics in cultured neurons: its high sensitivity to pH changes, and low background fluorescence. The magnitude of the fluorescence signal depends on the fraction of pHluorin molecules in the deprotonated state at a given pH change (Sankaranarayanan *et al.*, 2000). Since the dissociation constant (pKa) of pHluorin has been determined to be ~7.1, pH changes from 5.5 to 7.4 result in approximately a 20-fold increase in the fluorescent light emitted upon single SV fusion events (Sankaranarayanan *et al.*, 2000). In addition to its optimal response to pH differences, the precise localization of

sypHy to SVs in combination with its low expression on the neuronal surface results in an enhanced overall signal-to-noise ratio (Granseth *et al.*, 2006). This makes sypHy an excellent tool for exploring different parameters of the SV cycle.

Primary hippocampal neurons at DIV 13-15 were mounted in a closed bath imaging chamber with two parallel wires attached to the sides 6 mm apart (RC-21BRFS; Warner) allowing electrical stimulation of the neurons. Two coverslips were tightly sealed to the top and bottom of the chamber fixed with silicone grease (medium viscosity; Acros Organics) with the latter carrying the neuronal specimen. Thin tubes (Warner) attached to the chamber ensured the smooth continuous perfusion of buffers within the chamber. The imaging buffer that was used included 119 mM NaCl, 2.5 mM KCl, 2 mM $CaCl_2$, 2 mM $MgCl_2$, 25 mM HEPES, 30 mM D-glucose, pH 7.4, supplemented with 10 μM 6-cyano-7-nitroquinoxaline-2,3-dione (CNQX) and 50 μM 2-amino-5-phosphonovaleric acid (AP5) to block glutamate receptors activity. This prevents recurrent network activity due to spontaneous neuronal firing. Neurons were stimulated with a train of action potentials of 1-ms pulse width and 100 mA current output at different frequencies based on the protocol applied using a D330 MultiStim Digitimer stimulator. The protocols used for depolarising hippocampal neurons are presented in Figure 2.4. At the end of each recording, neurons were perfused with NH_4Cl (pKa 9.24) solution, pH 7.4, consisting of the imaging buffer prepared as described above with 50 mM NH_4Cl instead of 50 mM NaCl. Ammonia can diffuse through cell membranes causing all sypHy molecules to unquench allowing therefore an evaluation of the total SV pool size. A typical response of sypHy-expressing boutons during field stimulation and NH_4Cl perfusion is presented in Figure 2.3A. All recordings were performed at room temperature.

Transfected neurons were visualized using a Zeiss Axio Observer D1 inverted epifluorescence microscope (Zeiss Ltd., Germany) and a 40x 1.3 numerical aperture (NA) oil immersion objective at 488 nm and 510 nm excitation and emission wavelengths, respectively (like GFP). Neurons co-expressing sypHy with mCer-tagged constructs were imaged at 500 nm excitation wavelength using a 525-nm dichroic and a 535-nm emission filter as mCer can be excited at 433 nm and detected at 475 nm (presence of mCer was always confirmed prior to imaging). In this way, the fluorescent light emitted represents sypHy and not mCer fluorescence. Images were acquired using a Hamamatsu Orca-ER CCD digital camera and the acquisition rate was set at 4 s constantly pre- and post-stimulus as this offers adequate temporal resolution for monitoring the exocytosis and endocytosis events.

2.5.1.1 Analysis of sypHy traces

Time-lapse stacks of image slices were analysed using the Fiji is just ImageJ (Fiji) software (Schindelin *et al.*, 2012; Schneider *et al.*, 2012). These were initially aligned using the StackReg plugin by selecting the Rigid Body as the transformation type (Thevenaz *et al.*, 1998). Regions of interest (ROIs) 0.8 μm in diameter were placed on each presynaptic bouton (~1-2 μm in diameter) of transfected axons that was responsive to stimulation within a field of view. Fluorescence intensity was measured for all image slices using the Times Series Analyzer plugin created by Dr J. Balaji (University of California, Los Angeles). The ROI Trace Selection v0.10 software generated by D. Stewart (University of Edinburgh) was employed for the manual removal of outlier ROI traces. The ratio $\Delta F/F_0$ was calculated, where ΔF represents the change in fluorescence intensity due to stimulation and F_0 the initial fluorescence

intensity prior to stimulation (baseline). When necessary, a one-phase exponential fit was used to correct baseline for bleaching that was then subtracted from all time points. The average $\Delta F/F_0$ data for each coverslip (~80-120 ROIs) were normalised to the maximum fluorescence intensity either during stimulation or NH_4Cl perfusion. Peak height was calculated as $\Delta F/F_0$ to the maximum fluorescence intensity in response to ammonia. The N refers to the number of individual coverslips analysed. In Figure 2.3B, examples of graphs produced during data analysis are presented.

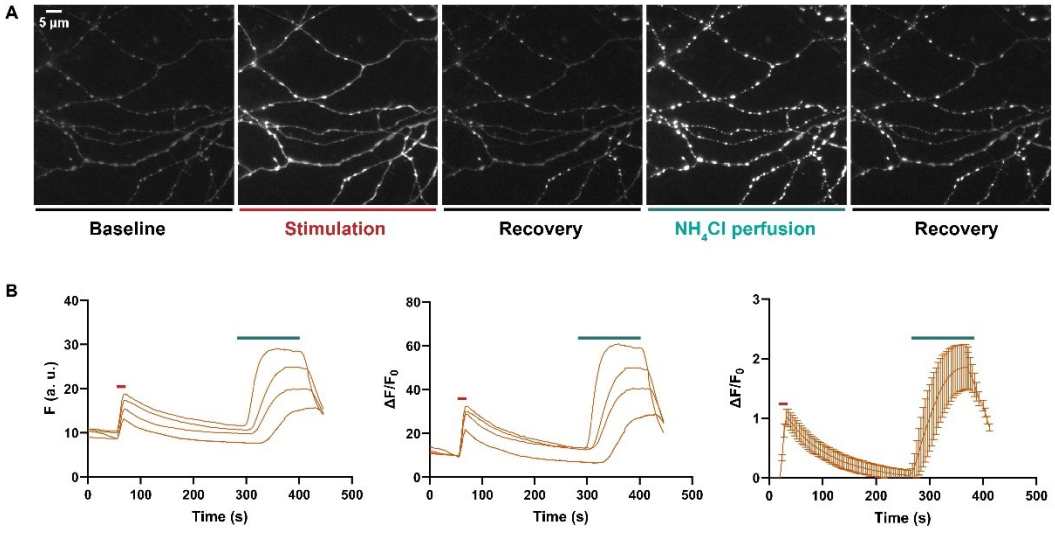

Figure 2.3 Imaging and analysis of sypHy expressing neurons

(**A**) Example response from sypHy expressing axons in primary hippocampal neuronal cultures that were subjected to 400 APs at 40 Hz and perfused with NH_4Cl solution. Representative image slices were selected from the whole time-course that was recorded. (**B**) Subsequent stages of sypHy analysis of 5 randomly picked coverslips in response to stimulation (400 APs at 40 Hz; red bars) and alkaline

solution (turquoise bars). Left, the fluorescence intensity of each coverslip is plotted in time. Middle, the fluorescence intensity is plotted in time following subtraction of the baseline fluorescence and normalisation with the latter. Right, the mean ± SEM of the normalised changes in fluorescence intensity in time is shown after being decay corrected and normalised for the stimulation peak.

2.5.2 Bafilomycin A1

To measure exocytosis independently of endocytosis, sypHy imaging was performed in the presence of bafilomycin A1 (ALFA AESAR, J61835.MX). This antibiotic acts as a specific inhibitor of the SV proton pump, V-ATPase, that is responsible for acidifying newly reformed SVs and, as a result, the pH intralumenally remains neutral preventing sypHy fluorescence from being quenched after endocytosis (Floor *et al.*, 1990). Neurons were subjected to 900 APs at 10 Hz under the continuous perfusion of imaging buffer (as described in 2.5.1 Synaptophysin-pHluorin live-cell imaging) supplemented with 1 μM bafilomycin A1 dissolved in DMSO and glutamate receptor blockers. The imaging was performed using the same imaging setup and parameters described in 2.5.1 Synaptophysin-pHluorin live-cell imaging. At the end of each recording, neurons were perfused with NH_4Cl solution to evaluate the total pool size. The average $\Delta F/F_0$ data for each coverslip were normalised to the average fluorescence intensity of the last 60 s during stimulation, when the sypHy trace reaches a plateau.

2.5.3 Acid perfusion

To examine the SV reacidification kinetics separately from the endocytosis kinetics, sypHy-expressing neurons were subjected to 300 APs at 10 Hz and perfused with acidic solution immediately after their stimulation. The acidic solution, that was prepared by replacing HEPES in the imaging buffer (as described in 2.5.1 Synaptophysin-pHluorin live-cell imaging) with 2-(N-morpholino)ethanesulfonic (MES) acid (pKa 6.1), pH 5.5, quenches the fluorescence of sypHy molecules residing on the plasma membrane. Therefore, all the newly formed synaptic vesicles (still basic intralumenally) contain sypHy molecules protected from the acidic extracellular environment. It is the fluorescence quenching of these sypHy molecules that can be used to estimate the speed of reacidification (Atluri & Ryan, 2006).

Since the reacidification of newly-endocytosed SVs is a rapid process, the acquisition rate was set at 2 s, as this offers sufficient temporal resolution (Atluri & Ryan, 2006; Kwon & Chapman, 2011). The imaging was performed using the same imaging setup and parameters described in 2.5.1 Synaptophysin-pHluorin live-cell imaging. At the end of each recording, neurons were perfused with NH_4Cl solution to evaluate the total pool size. An initial perfusion with acid was also applied prior to stimulation resulting in all sypHy molecules residing on the neuronal membrane at resting conditions to be quenched. This also serves as a control to estimate the speed of surface sypHy quenching, in comparison to surface quenching plus SV acidification during stimulation.

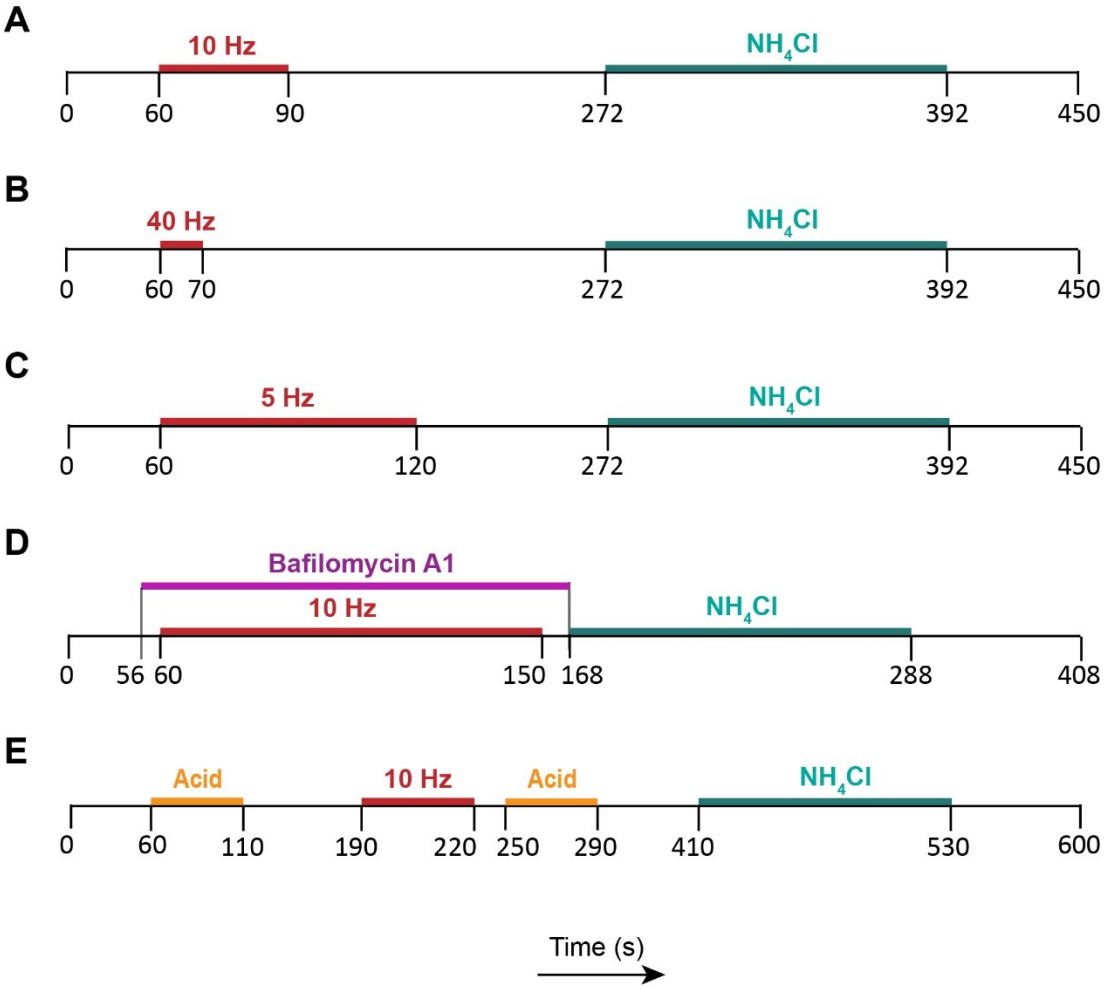

Figure 2.4 Imaging protocols using sypHy

Protocols employed to examine different parameters of SV recycling in hippocampal neurons expressing sypHy. (**A, B, C**) Neurons were stimulated at different frequencies (10 Hz for 30 s, 40 Hz for 10 s, 5 Hz for 60 s; red bars) and left to recover prior to perfusion with a NH_4Cl solution (turquoise bars). (**D**) Protocol for measuring exocytosis separately from endocytosis using bafilomycin A1 to block SV re-acidification. Neurons were stimulated at 10 Hz for 90 s (red bar) in the presence of bafilomycin A1 (purple bar) prior to perfusion with a NH_4Cl solution (turquoise bar). (**E**) Protocol for examining the re-acidification kinetics separately

from endocytosis. Neurons were stimulated at 10 Hz for 30 s (red bar) and were perfused with an acid solution pre- and post-stimulus for 50 s and 40 s, respectively (yellow bars). At the end, a NH_4Cl solution was also perfused (turquoise bar).

2.5.4 TMR-dextran uptake

Dextrans are hydrophilic polysaccharides of high molecular weight that are formed by α-1,6-polyglucose linkages. Fluorescently labelled dextrans, such as tetramethylrhodamine-dextran (TMR-dextran), can be used as markers for the fluid uptake of extracellular solutes through endocytosis. TMR-dextran is an anionic conjugate of 40 kDa characterised by excitation and emission wavelengths at 555 nm and 580 nm, respectively. Based on its molecular weight, the hydrodynamic radius (or Stoke's radius) of TMR-dextran in solution has been determined to be around 4.32 nm (Aimar *et al.*, 1990). Due to their large size in combination with low enrichment on the surface of the plasma membrane, TMR-dextran probes are less likely to be endocytosed by single SVs but can selectively label bulk endosomes after strong electrical stimulation (Holt *et al.*, 2003; Clayton & Cousin, 2009).

Neurons were stimulated with 400 APs at 40 Hz in the presence of 50 μM TMR-dextran in imaging buffer supplemented with glutamate receptors blockers and washed for at least 2 min to remove excess TMR-dextran. Under continuous perfusion with imaging buffer, TMR-dextran fluorescence was excited at 550 nm and detected at > 575 nm using a 565 nm dichroic filter. The imaging was performed using the same imaging setup described in 2.5.1 Synaptophysin-pHluorin live-cell imaging. Stacks of image slices were

acquired from 8-10 fields of view with the same axonal density per coverslip and analysed using the Fiji software. A maximum projection was applied according to which the final image was formed by pixels of the largest value across all slices. As a result, the dextran puncta that were bright in different focus planes became visible and, thus, quantifiable. MaxEntropy thresholding was applied and dextran puncta 0.64-2.24 μm in diameter were counted using the Analyze particles plugin of Fiji (Kapur *et al.*, 1985). Unstimulated coverslips were also imaged and analysed for all conditions. Since dextran is internalised into presynaptic boutons following strong stimulation selectively, the number of puncta from unstimulated coverslips provided an estimate of the background uptake and, therefore, were subtracted from all stimulated coverslips. The N refers to the number of individual coverslips analysed.

2.5.5 Immunofluorescence

Immunolabelling was performed using primary hippocampal neurons, which were initially fixed with 4 % (w/v) paraformaldehyde/PBS solution for 10 min and then neutralized with 50 mM NH_4Cl/PBS for 10 min. After three washes with PBS, cells were permeabilized in 0.1% (v/v) Triton X-100, 1% (w/v) BSA/PBS for 5 min and then blocked in 1% (w/v) BSA/PBS for 30 min. Following blocking, cells were incubated with the appropriate primary and secondary antibodies for 1-2 hours each at room temperature. A list of primary and secondary antibodies used can be found in Table 2.5. Transfected neurons were visualized using a Zeiss Axio Observer Z1 inverted epifluorescence microscope (Zeiss Ltd., Germany) and either a 40x 1.3 NA or 63x 1.4 NA oil immersion objective at both 475 nm and 555 nm excitation wavelengths. Fluorescent light was detected at 500-550 nm and 570-640 nm using a 495-nm

and a 570-nm dichroic filter, respectively. Neurons expressing mCer-tagged constructs were visualized at 475 nm excitation wavelength using an anti-GFP antibody with appropriate secondary antibody to increase the signal. Images were acquired using a Zeiss AxioCam 506 camera and the Zeiss ZEN 2 software. Data analysis was performed using the Fiji software as indicated in the following chapters.

Table 2.5 List of antibodies used for immunofluorescence.

Antibody against	Host	Dilution	Manufacturer
Primary antibodies			
Amph1	Rabbit	1:250	Synaptic Systems #120 003
GFP	Chicken	1:5000	Abcam ab13970
SV2A	Rabbit	1:200	Abcam ab32942
CDKL5	Sheep	1:200	Rouse lab (University of Dundee)

VGLUT1	Guinea pig	1:1000	Synaptic Systems #135 304
	Secondary antibodies		
Rabbit Alexa Fluor 488	Donkey	1:1000	Molecular Probes, Thermo Fisher Scientific
Chicken Alexa Fluor 488	Goat	1:1000	Molecular Probes, Thermo Fisher Scientific
Rabbit Alexa Fluor 568	Goat	1:1000	Molecular Probes, Thermo Fisher Scientific
Rabbit Alexa Fluor 568	Donkey	1:1000	Molecular Probes, Thermo Fisher Scientific
Guinea pig Alexa Fluor 568	Goat	1:1000	Molecular Probes, Thermo Fisher Scientific
Sheep Alexa Fluor 568	Donkey	1:1000	Molecular Probes, Thermo Fisher Scientific

2.6 Cell lysis

Primary hippocampal neurons in culture were washed with PBS and lysed on ice using RIPA buffer (50 mM Tris pH 7.8, 1 mM EDTA, 2 mM EGTA, 150 mM NaCl, 1 % (v/v) NP40, 0.5 % (w/v) deoxycholate, 0.1 % (w/v) sodium dodecyl sulphate (SDS), protease inhibitors cocktail (500x)). Lysed cells were collected and incubated at 4°C for 50 min while rotating. Cells were then centrifuged at 21,500 x *g* for 10 min at 4°C. The clear supernatant was collected and stored at -80°C. The total protein concentration of the samples was measured (see 2.7 Protein quantification) and adjusted to 5 mg/ml prior to western blotting. When adjustment of the protein concentration prior to analysing the samples by western blotting was not necessary, a different approach to produce cell lysates was followed according to which single coverslips were directly lysed with 20 µl 2x sample buffer (prepared as in 2.8.1 Gel electrophoresis) followed by immediate boiling at 95°C for 5 min.

2.7 Protein quantification

2.7.1 Bradford assay

For quantifying the total protein content of samples, the Bradford-Solution for Protein Determination (AppliChem; A6932) was used. A stock solution of bovine serum albumin (BSA; 100 µg/ml) was diluted accordingly in water to give the concentrations 0, 10, 20, 40, 60, 80, 100 µg/mL of protein standards and in duplicates. Distilled water was used as control (does not contain protein),

which served as blank. Samples were diluted 20 times and assayed in duplicates. Bradford reagent was added to the standards and samples followed by gentle vortexing and, after 10 min, the absorbance was measured at 595 nm using a Pharmacia Biotech Ultrospec 2000 spectrophotometer. The average values of the standards and samples were calculated. A standard curve was produced in Microsoft Excel by plotting the average values of each protein standard relative to its concentration (μg/μl), which was used to determine the total protein concentration of each unknown sample. Since BSA is a non-optimal protein standard for the Bradford assay, the protein concentrations were multiplied by 2.1 for a closer approximation, as per manufacturer's instructions.

2.7.2 BCA assay

For quantifying the total protein content of samples in solutions that interfere with the Bradford assay, the Pierce™ BCA Protein Assay Kit (Thermo Scientific; 23227) was used. The Albumin Standard (BSA) provided by the kit (2 mg/mL) was diluted accordingly to give the concentrations 25, 125, 250, 500, 750, 1,000, 1,500, 2,000 μg/mL of protein standards. The protein concentration was determined for the protein standards and samples in duplicates according to the manufacturer's instructions provided for a Standard Protocol. The absorbance was measured at 562 nm using a Pharmacia Biotech Ultrospec 2000 spectrophotometer. The average values of the standards and samples were calculated, and the blank (0 μg/mL BSA) average absorbance was subtracted subsequently. A standard curve was produced in Microsoft Excel by plotting the average values of each Protein Standard relative to its concentration

(μg/mL), which was used to determine the total protein concentration of each unknown sample.

2.8 Immunoblotting

2.8.1 Gel electrophoresis

Protein samples were separated by SDS polyacrylamide gel electrophoresis, which was performed using the Protean 3 system (Bio-Rad). Sample loading buffer, which was prepared as a 3x stock containing 200 mM Tris pH 6.8, 6 mM EDTA, 200 mM SDS, 28 % (v/v) glycerol, 0.7 % (w/v) bromophenol blue and 0.14 % (v/v) β-mercaptoethanol, was added in equal volumes with the samples. Proteins were denatured by heating at 95°C for 5 min. Samples were loaded into 10 % (v/v) gels in a Protean 3 system gel box, where running buffer containing 24.8 mM Tris, 192 mM glycine and 1 % (w/v) SDS was added. A 10 % (v/v) gel consisted of a resolving and a stacking layer. For 5 ml of the resolving layer 1.625 ml of 30 % Acrylamide/Bis Solution, 37.5:1 (Bio-Rad), 1.25 ml resolving solution (1.5 M Tris-HCl pH 8.8, 0.4 % (w/v) SDS), 50μl of 10 % (w/v) ammonium persulfate (APS), and 5 μl tetramethylethylenediamine (TEMED) were combined. Accordingly, for 2.5 ml of the stacking layer 0.375 ml of 30 % Acrylamide/Bis Solution, 37.5:1 (Bio-Rad), 0.625 ml stacking solution (0.5 M Tris-HCl pH 6.8, 0.4 % (w/v) SDS), 25 μl of 10 % (w/v) APS, and 2.5 μl TEMED were used. Except for lanes with protein samples, the PageRuler™ Prestained Protein Ladder (Thermo Fisher Scientific) was loaded into the gels. Gel electrophoresis was performed at 120 V constant for 90 min. For assessing the amount of protein per lane/band,

proteins were stained with Coomassie Brilliant blue (CBB; Instant Blue™ Protein Stain, CBS Scientific Company, Inc). After being washed overnight in a de-staining solution (40 % (v/v) methanol, 10 % (v/v) acetic acid) to reduce background, images of the stained proteins were acquired using a gel scanner.

2.8.2 Wet transfer

After gel electrophoresis, the gel as well as a Supported nitrocellulose membrane (0,45 μm; Bio-Rad) cut into the appropriate size for the gel (usually 6 cm x 8.5 cm) were soaked for 15 min in transfer buffer, which consisted of 2.5 mM Tris, 19.2 mM glycine and 20 % (v/v) methanol. Several pieces of thin blotting paper (VWR® Grade 703 Blotting Paper), cut into pieces of size 7 cm x 9.5 cm, and sponges of the same size were also soaked in transfer buffer for 15 min and stacked together to produce a 0.75-cm-thick layer. Transfer stacks were prepared in gel holder cassettes consisting of a bottom layer of a sponge and four blotting papers, the gel, the membrane and a top layer of four blotting papers and a sponge. Transfer was carried out at 100 V constant for 180 min on ice. Ponceau S (0.1 % (w/v) in 5 % acetic acid; Sigma-Aldrich) staining was performed to visualize the total protein content per lane.

2.8.3 Immunostaining

Following transfer, nitrocellulose membranes were blocked in a ratio 1:1 for LI-COR Odyssey Blocking Buffer (PBS):PBS for at least 1 h. After removing the blocking buffer, membranes were incubated overnight at 4°C rotating with primary antibody diluted in a ratio 1:1 of Odyssey Blocking Buffer (PBS):PBS

containing 0.1 % (v/v) Tween-20. Membranes were washed three times with PBS containing 0.1 % (v/v) Tween-20 and then incubated in dark with secondary antibody diluted again in 1:1 ratio of Odyssey Blocking Buffer: PBS containing 0.1 % (v/v) Tween-20 for 2h at room temperature rotating. Three washes with PBS containing 0.1 % (v/v) Tween-20 were then performed, which were followed by one additional wash with PBS to remove residual detergent. In the instances a phospho-antibody was used, PBS and LI-COR Odyssey Blocking Buffer (PBS) were replaced by TBS and LI-COR Odyssey Blocking Buffer (TBS), respectively, in all steps. Immunoblotting imaging was performed by using the LI-COR Biosciences Odyssey Infrared Imaging System as well as the ImageStudio Lite Ver 5.2 software. Lists of the primary and secondary antibodies used can be found in Table 2.6. The fluorescence intensity of protein bands was quantified using either the LI-COR or Fiji software. For LI-COR quantifications, rectangles were drawn around bands of interest and the median background fluorescence intensity was subtracted. For quantification using Fiji, images exported from LI-COR were converted to 16-bit greyscale and rectangles were dawn around bands of interest prior to plotting their intensities. Using the wand tool, the intensity peaks were selected for each band excluding the background signal.

Table 2.6 List of antibodies used for immunoblotting.

Antibody against	Host	Dilution	Manufacturer
Primary antibodies			
hCDKL5 Antigen: aa 350-650	Sheep	1:500	Rouse lab (University of Dundee)
msCDKL5 Antigen: aa 300-600	Sheep	1:500	Rouse lab (University of Dundee)
hCDKL5 Antigen: aa 636-758	Rabbit	1:500	Atlas Antibodies HPA002847
Amph1	Goat	1:500	Santa Cruz Biotechnology sc-8536
Endophilin A1	Goat	1:1000	Santa Cruz Biotechnology sc-10874
α-AP2 (a and c subunits)	Mouse	1:1000	Sigma Aldrich A 4325

CHC	Goat	1:250	Santa Cruz Biotechnology sc-6579
Syndapin 1	Goat	1:1000	Santa Cruz Biotechnology sc-10412
VGLUT1	Guinea pig	1:2000	Synaptic Systems #135 304
ATP6V1B2	Rabbit	1:5000	Abcam ab183887
Dyn1	Goat	1:500	Santa Cruz Biotechnology sc-6402
Syp1	Rabbit	1:500	Abcam ab14692
PSD95	Mouse	1:1000	BioLegend #810401

β-actin-peroxidase	Mouse	1:30000	Sigma-Aldrich A3854
Primary phosphoantibodies			
pAmph1-S293 Antigen: PVRPRS^{293}PSQTRC	Rabbit	1 mg/ml	MRC Protein Phosphorylation Unit, University of Dundee
pDyn1-S774	Sheep	1:1000	AbD Serotec (Bio-rad) AHP899
pAkt-S473	Rabbit	1:1000	Cell signalling D7F10
pMAP1S-S900	Rabbit	1:50	Abcam BOZ-2-F2-3
pGSK3α/β-S9/S21	Rabbit	1:1000	Cell signaling #9331
Secondary antibodies			
sheep IRDye800 conjugated	Rabbit	1:10000	Rockland Immunochemicals # 613-732-168

guinea pig IRDye 680RD	Donkey	1:10000	LI-COR Biosciences
mouse IRDye 680RD	Donkey	1:10000	LI-COR Biosciences
rabbit IRDye 680RD	Donkey	1:10000	LI-COR Biosciences
goat IRDye 680RD	Donkey	1:10000	LI-COR Biosciences
mouse IRDye 800CW	Donkey	1:10000	LI-COR Biosciences
rabbit IRDye 800CW	Donkey	1:10000	LI-COR Biosciences
goat IRDye 800CW	Donkey	1:10000	LI-COR Biosciences

2.9 Synaptosome purification

2.9.1 Crude synaptosome purification

The biochemical isolation of a crude synaptosome fraction from rat brains was performed according to Huttner *et al*. (Huttner *et al.*, 1983). Rat brains excluding the cerebellum were homogenized in ice-cold sucrose/EDTA (0.32 M sucrose, 1 mM EDTA, 5 mM Tris, pH 7.4) to obtain a 10 % (w/v) suspension with a glass homogenizer (Wheaton). The lysate (L) was centrifuged at 950 x *g* for 10 min at 4°C using an Avanti J-25 Beckman centrifuge and the JA 25.50 rotor and the supernatant was collected. The pellet was re-homogenized, and

after additional centrifugation, the supernatants were combined (S1), and then spun at 20,400 x *g* for 30 min at 4°C. The pellet (P2) represents the crude synaptosome fraction. For pull-down experiments (see 2.10.2.2 Pull-down assay), the P2 pellets were resuspended in lysis buffer containing 1 % Triton X-100, 25 mM Tris-HCl, 150 mM NaCl, 1 mM EGTA, 1 mM EDTA, pH 7.4 and store at -80°C for future use.

2.9.2 Synaptic vesicle isolation

For isolating the SV fraction from rat brains, the P2 pellet was resuspended in 1mL of ice-cold 0.32 M sucrose per brain and incubated with 1 M HEPES/NaOH solution (pH 7.4) on ice for 30 min. After spinning at 32,900 x *g* for 20 min at 4°C, the lysate pellet (LP1) and lysate supernatant (LS1) emerged, of which LS1 was spun at 135,000 x *g* for 2 h at 4°C. The pellet (LP2) that represents the crude SV fraction, was collected and resuspended in 40 mM sucrose. The protocol followed for the isolation of crude SVs is presented schematically in Figure 2.5. Aliquots of the intermediate fractions were kept for analysis. The total protein concentration of the samples was identified and adjusted to 1 mg/ml prior to immunoblotting. Samples were stored at -20°C.

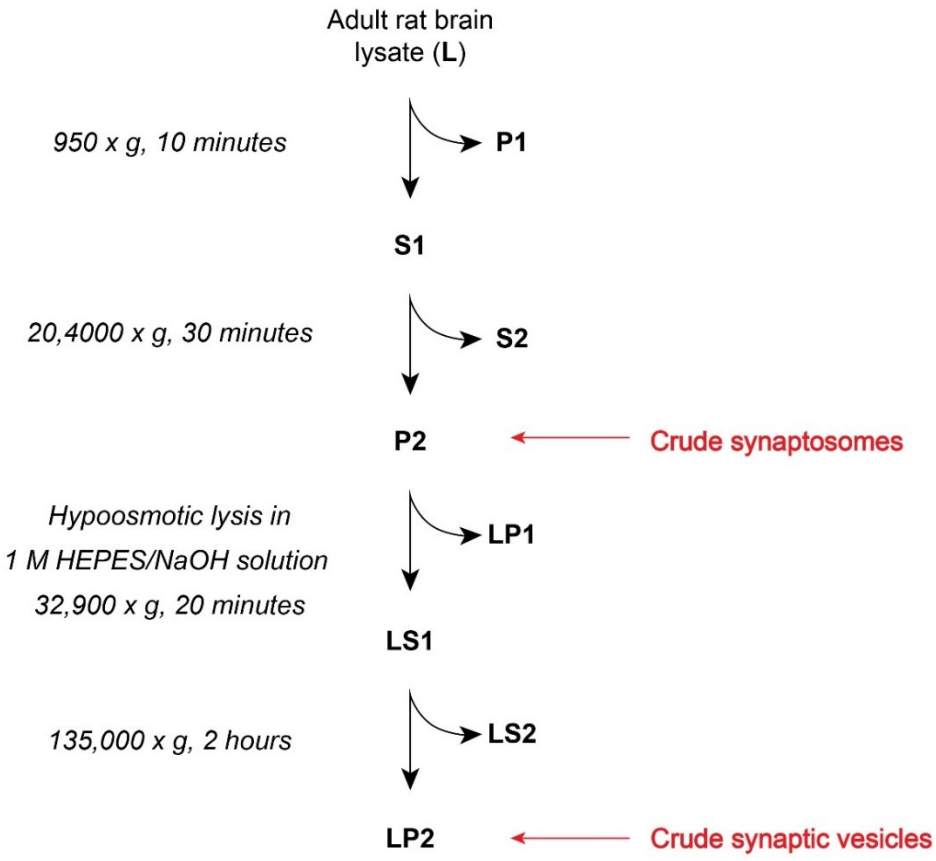

Figure 2.5 Protocol for the biochemical purification of crude synaptosome and SV fractions

Adult rat brains (L) were lysed in sucrose/EDTA solution and were subsequently separated by two successive low-speed centrifugations to produce the crude synaptosome fraction (P2) followed by a hypoosmotic lysis in 1 M HEPES/NaOH solution (pH 7.4). Lysed synaptosomes were then subjected to two centrifugation steps to produce the crude SV faction (LP2). The intermediate fractions that were produced include: (P1) tissue debris, nuclei, and large myelin fragments, (S2) microsomes, some small mitochondria, and synaptosomes, (LP1) synaptic membrane, large mitochondria, and myelin fragments, and (LS2) synaptosomal cytoplasm.

2.10 Protein-protein interaction assays

2.10.1 Immunoprecipitation

Adult mouse brains were homogenized in HEPES buffer (50 mM HEPES, pH 7.5, 0.5 % (v/v) Triton, 150 mM NaCl, 1 mM EDTA, 1 mM EGTA, 1 mM PMSF, protease inhibitors) using a glass homogenizer. The homogenate was incubated for 1-2 hours at 4°C rotating and then centrifuged at 75,500 x g for 40 min at 4°C in a Beckman centrifuge using a JA 25.50 rotor. The supernatant was collected and pre-cleared with Protein G Agarose beads (Sigma-Aldrich) for 1-2 hours at 4°C rotating. After a low-speed spin, the supernatant was collected, and the total protein content was assessed by Bradford (see 2.7.1 Bradford assay). The appropriate amount of brain lysate (2 mg of protein) was incubated with 2-3 μg of the antibody of interest overnight at 4°C rotating. The following day Protein G Agarose beads (about 20 μl) were added to the antibody-containing brain lysate and left rotating for 1-2 hours at 4°C before being centrifuged at 110 x g for 1 min at 4°C. The supernatant was then discarded and after three washes in HEPES buffer, sample buffer was added directly to the beads followed by heating at 95°C for 5 min. An antibody against the endocytic Dyn-like C-terminal Eps15 Homology Domain protein (EHD; Santa Cruz Biotechnology, sc-23452) was used as a control.

2.10.2 Pull-down assay

2.10.2.1 Purification of recombinant proteins from bacteria

For generating GST-fused Amph1 recombinant proteins, pGEX-KG vectors were used with all constructs being inserted C-terminally of the GST tag. Following the heat shock approach, BL21 DE3 bacteria were transformed with the recombinant vectors and individual colonies were selected and allowed to grow overnight at 37°C. This was used to start a large-volume culture of LB media containing ampicillin (1:1000), which was incubated at 37°C shaking for 1-2 h. The optical density of the culture at 600 nm was regularly measured until it reached a value around 0.6-0.8. The expression of the GST-fused proteins was then induced by isopropyl β-D-1-thiogalactopyranoside (1 mM; Calbiochem; 420322) and incubated at 37°C shaking. Pre- and post-induced samples were collected and processed for CBB staining to assess the level of success of the induction step. After 4 h, the induced bacterial cultures were spun at 5000 x g for 5 min at 4°C and the pellets were stored at -80°C for future use.

The pellets were resuspended in 40 ml ice-cold sodium chloride/tris/EDTA (STE) buffer containing 10 mM Tris, 150 mM NaCl, 1 mM EDTA, pH 8. Protease inhibitors and 1 mM PMSF were also added to prevent any protein degradation and lysozyme (0.0675 μg/μl; Sigma-Aldrich) to enable the deconstruction of the bacterial cell wall. The resuspended solution was left on ice for 30 min with occasional stirring and then dithiothreitol (4 mM; Sigma-Aldrich) and 4.5 ml 10% Triton X-100 were added. Sonication was performed at 10 kHz for 30 s on ice followed by a 30 s break and the process was repeated 5 more times. The lysates were spun at 17420 x g for 10 min at 4°C before being

transferred to prewashed Glutathione Sepharose 4B beads (GE Healthcare) and left rotating overnight at 4°C to allow binding of the GST tag. Prior to incubation with the lysates, the beads were successively washed in PBS, 0.1 % Triton-supplemented PBS and again PBS to remove excess Triton and finally resuspended in PBS to create a 50 % suspension. The bead-coupled GST-fused proteins were spun at 27 x g for 5 min followed by 5 washes in PBS, one wash in NaCl-containing PBS (1.2 M) and two additional washes in PBS. A small volume of PBS was added to the beads to create a 50 % suspension, where protease inhibitors were also added to prevent protein degradation. The yield of purified protein was estimated by gel electrophoresis followed by CBB staining.

2.10.2.2 Pull-down assay

Based on the level of purification that was achieved, a small volume (usually 100 μl) of the 50 % suspension containing the GSH-coupled GST-fused proteins was loaded into a ProbeQuant G-50 Micro Column (GE Healthcare) and washed once in ice cold lysis buffer. The lysis buffer contained 1 % Triton X-100, 25 mM Tris-HCl, 150 mM NaCl, 1 mM EGTA, 1 mM EDTA, pH 7.4. The beads were incubated with synaptosomal lysates for 2 h at 4°C rotating to enable the *in vitro* interaction with possible partners. The columns were centrifuged at 850 x *g* for 20 s in a Hettich 22R benchtop centrifuge and the beads were washed successively in ice cold lysis buffer, in NaCl-supplemented lysis buffer (500 mM) and in 20 mM Tris, pH 7.4. After being washed, 50 μl of sample buffer was added into the beads and left for 10 min at room temperature. The columns were spun at 19,720 x *g* for 1 min in a Hettich

22R benchtop centrifuge. The eluted proteins were boiled at 95°C for 5 min and stored at -20°C.

2.11 Statistical analysis

Statistical calculations were conducted using GraphPad Prism 8.4.2 software (GraphPad Software Inc). The normality of the data distribution was assessed by performing D'Agostino and Pearson omnibus normality test with significance level set at $\alpha = 0.05$. Datasets following a Gaussian distribution were presented as mean ± standard error of the mean (SEM) and statistical significance was assessed by unpaired two-tailed t test for comparison between two groups or analysis of variance (ANOVA) followed by Tukey's, Dunnett's or Sidak's post hoc analysis for multiple comparisons. Datasets following a non-Gaussian distribution were presented as median with interquartile range (IQR) indicating min to max whiskers and statistical significance was evaluated by Mann-Whitney test for comparison between two groups or Kruskal-Wallis followed by Dunn's post hoc analysis for multiple comparisons. For experiments with a small number of replicates for a normality test to be performed, a parametric test was assumed. Asterisks refer to p-values as follows: *; $p \leq 0.05$, **; $p \leq 0.005$, ***; $p \leq 0.001$, ****; $p \leq 0.0001$. All experiments consisted of at least three independent biological replicates and each replicate contained all the conditions being compared. For comparisons between CDKL5 KO and WT neurons, primary neuronal cultures were prepared in parallel from CDKL5 KO embryos and littermate controls. Live-imaging data were analysed blindly for experiments consisting of two

groups. Random variation or effect size were not estimated. Sample size and statistical test are indicated in the figure legends.

Chapter 3: Presynaptic characterization of a *Cdkl5* KO rat model

3.1 Introduction

Mutations in the X-linked gene encoding for CDKL5 kinase have been associated with a severe epileptic encephalopathy in infants known as CDD. Whilst the range of clinical features is broad, early-onset seizure activity is admittedly the most profound hallmark and neurodevelopmental impairment and intellectual disability are the most common outcomes in CDD. In an attempt to understand the biological importance of CDKL5 *in vivo*, a few CDKL5 KO murine models have been developed by targeting exon 2, 4 or 6 of the mouse *Cdkl5* gene causing thus an early truncation (Wang *et al.*, 2012; Amendola *et al.*, 2014; Okuda *et al.*, 2017). In a CDKL5 knockin murine model, the CDD-related nonsense mutation R59X has been introduced also resulting in an early stop codon (Tang *et al.*, 2019). CDKL5 mouse models display various CDD-like phenotypes such as motor defects, altered social interaction, limb clasping, anxiety, impaired memory and learning, or increased seizure susceptibility; however, no spontaneous epileptic activity has been observed in these models with the exception of a group of aged female heterozygous *Cdkl5* mice (Mulcahey *et al.*, 2020). Nevertheless, while human CDKL5 deficiency results in early-onset seizures and profound neurodevelopmental delay, loss of mouse Cdkl5 generally fails to recapitulate the severity of CDD phenotypes. Hence, this leads to the notion that loss of CDKL5 might affect

brain function differently across species and subsequent neural network complexity imposing the need for the development of non-murine mammalian model organisms.

In an attempt to identify robust phenotypes that can overcome the species barrier and allow for study of CDKL5 (patho)physiology, a *Cdkl5* KO rat model was developed by deleting exon 8 (Simões de Oliveira et al., in preparation). In support, genetically modified rats provide certain benefits as an alternative model organism in neurodevelopmental disorders. At first sight, rats have anatomically similar brains to mice, but they exhibit basic functional variations, such as different distribution of proteins, that could possibly affect studies elucidating pathogenic mechanisms of human diseases (Ellenbroek & Youn, 2016). Interestingly, rats show higher rate of neurogenesis and maturation in hippocampus than mice, albeit during adulthood, indicating fundamental divergence in memory and learning potential between the two organisms (Snyder *et al.*, 2009). Moreover, the enhanced sociability that characterises rats in combination with efficient cognitive behaviours can have greater translational relevance with respect to neurodevelopmental conditions that typically demonstrate social and cognitive deficits (Aitman *et al.*, 2016; Homberg *et al.*, 2017), such as CDD.

An established model of epileptogenesis highlights the excitatory/inhibitory imbalance as the leading mechanism of seizure onset (Staley, 2015). At the circuit as well as single-neuron levels, neurotransmission is essential for preserving the excitatory/inhibitory equilibrium and defects in multiple steps can result in seizures. A large body of work suggests that loss of CDKL5 leads to dysregulation of various elements of neurotransmission. These include altered levels of subunits of postsynaptic glutamate receptors (Tang *et al.*, 2019; Yennawar *et al.*, 2019), altered frequency of mPSCs and sPSCs

(Tang *et al.*, 2017; Wang *et al.*, 2021), hyperexcitability in both inhibitory- and excitatory-conditional *Cdkl5* KO mice (Tang *et al.*, 2017; Tang *et al.*, 2019), increased spontaneous glutamate/GABA efflux ratio (Sivilia *et al.*, 2016), and impaired serotonergic transmission (Fuchs *et al.*, 2019a; Vigli *et al.*, 2019). In addition to neurotransmission-related defects, altered plasticity is also reported upon absence of CDKL5 including both long- and short-term adaptations, while in most studies the number of synaptic connections is not preserved (Della Sala *et al.*, 2016; Ren *et al.*, 2019; Tang *et al.*, 2019). In agreement, elevated LTP and decreased mEPSCs frequency are reported in the CDKL5 KO rat model (Simões de Oliveira et al., in preparation). Yet, efficient neurotransmission depends also on presynaptic mechanisms and reliable SV recycling. However, whether CDKL5 deficiency impairs aspects of SV recycling remains largely unknown.

This chapter aims to characterise the *Cdkl5* KO rat model presynaptically by exploring possible phenotypes associated with SV recycling due to loss of CDKL5. Initially, we validated different antibodies against CDKL5 by fluorescent western blotting and immunolabelling. Then, we attempted to describe the spatiotemporal expression of CDKL5 in the rat brain. Since there is no clear evidence that CDKL5 is delivered to the presynapse, we tested whether CDKL5 is sorted to the presynaptic cytoplasm. To explore possible presynaptic defects, we started by examining whether CDKL5 loss impacts on the levels of known presynaptic proteins and/or their phosphorylation or the preservation of presynaptic boutons. Neuronal cultures were prepared from embryonic rat hippocampi to explore possible defects in SV recycling with sypHy-pHluorin imaging assays and dextran uptake.

3.2 Results

3.2.1 Validation of CDKL5 antibodies

Before describing the expression profile of CDKL5, we validated three antibodies against CDKL5 that have been previously used with mouse models in order to assess their immunoreactivity in the rat brain. Two of them were sheep polyclonal antibodies generated by the Rouse lab (University of Dundee) using GST-fused antigens adjacent to the CDKL5 kinase domain comprising aa 350-650 of the human or aa 300-600 of the mouse protein, respectively (Munoz *et al.*, 2018). An additional antibody was also tested as a commercially available option reacting with a C-terminal epitope on CDKL5 (Okuda *et al.*, 2017). To evaluate these antibodies, we used cortices from WT and KO rat brains that were dissected at P14, lysed in RIPA buffer, and provided by the Kind lab to examine CDKL5 expression. All antibodies detected CDKL5 as a band of 110 kDa, which was absent from the KO tissue (Figure 3.1A). Notably, several bands of lower molecular weight were also detected in both WT and KO tissues. The likelihood these bands to represent other members of the CDKL kinase group is low, since their molecular weights do not match those of known CDKLs and, nonetheless, it is the sequence of the C-terminal tail, where all antibody epitopes reside, that differs amongst CDKLs. Furthermore, mass spectrometric analysis failed to detect any CDKL5 products in the KO tissue excluding the possibility these bands representing other isoforms in the rat brain or even truncated versions of CDKL5 also confirming the validity of the KO rat model (data not shown)[2]. These bands

[2] The mass spectrometric analysis was performed by Matthias Trost's group (Newcastle University) in WT and CDKL5 KO synaptosomes prepared by the Cousin and Kind labs.

possibly result from the antibody polyclonality and/or the high sensitivity offered by fluorescent visualisation of western blot bands compared to chemiluminescence that has been previously employed with these antibodies. Since all three antibodies are specific to CDKL5, we selected the sheep polyclonal antibody against human CDKL5 to perform all experiments in this project.

Next, we examined the expression of CDKL5 in primary hippocampal neuronal cultures in order to evaluate whether the above CDKL5 antibody could be an efficient tool for immunolabelling. Primary hippocampal neurons derived from WT and KO animals were fixed at 15 DIV and stained for endogenous CDKL5 and SV2A as a random staining control between genotypes (Figure 3.1B). Also, all neuronal cultures were stained simultaneously to avoid possible staining deviations between different repeats. The expression level of CDKL5 was estimated by quantifying average CDKL5 fluorescence intensity of cell bodies normalised to that of SV2A. CDKL5 expression was significantly reduced in CDKL5-deficient neurons in comparison with WT neurons (Figure 3.1C). Although the CDKL5 fluorescence is not entirely eliminated in the case of KO neurons as it would have been anticipated, the significant decrease observed suggests that this CDKL5 antibody could be used as a reliable tool for immunolabelling.

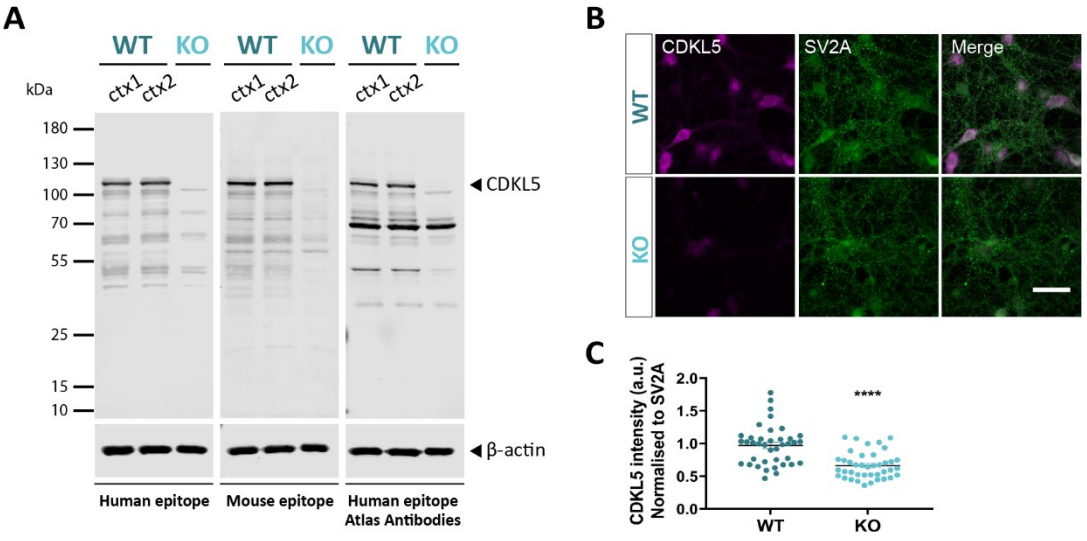

Figure 3.1 CDKL5 protein is absent from *Cdkl5* KO LE rat brains

(**A**) Immunoblots of cortical lysates generated from WT and CDKL5 KO animals at P14 using three different antibodies against CDKL5. The first two antibodies were raised against a human (aa 350-650) and a mouse (aa 300-600) epitope on CDKL5, respectively, whereas the Atlas CDKL5 antibody was tested as a commercially available alternative. CDKL5 is detected as a 110-kDa band that is absent from KO tissues. All three antibodies detect numerous non-specific bands that are found in both WT and CDKL5 KO tissues. In all cases, β-actin was used as a loading control. (**B**) Representative images of WT and CDKL5 KO primary hippocampal neurons fixed at 15 DIV and labelled for CDKL5 and SV2A. Scale bar, 50 μm. (**C**) Quantification of CDKL5 fluorescence intensity normalised to SV2A. Background was subtracted in all cases. Scatter plots indicate mean ± SEM. ****$p < 0.0001$ by unpaired two-tailed t test. WT $n = 39$, KO $n = 40$ fields of view from 4 independent preparations of neuronal cultures.

3.2.2 CDKL5 is expressed in different brain regions during development and adulthood

A number of studies have described the expression pattern of CDKL5 in the mouse brain. *In situ* hybridization and immunoblotting analysis have revealed that CDKL5 can be found in several regions, such as the cortex, hippocampus, striatum, and olfactory bulb (Rusconi *et al.*, 2008; Chen *et al.*, 2010; Wang *et al.*, 2012; Schroeder *et al.*, 2019). Given that loss of CDKL5 function has been linked to neural circuit deficits in different mouse models of CDD, it is also critical to characterise the expression profile of CDKL5 in the rat brain to determine potential variations across species in the level of the protein. To gain insight into the regional profile of CDKL5 in the rat brain, different brain regions were dissected and lysed in RIPA buffer, including the cerebral cortex, hippocampus, cerebellum, thalamus and archicortex (Figure 3.2A). The different lysates were generated and provided by the Kind lab for western blot analysis. Exploring CDKL5 expression involves an additional parameter, that of time. The temporal expression pattern of CDKL5 in the mouse brain seems to increase during perinatal and mainly early postnatal stages (Rusconi et al., 2008; Chen et al., 2010). Therefore, we focused our study mainly on the postnatal developmental stages until adulthood with dissections occurring at different time points including 0, 7, 14, 21, 28, 35, and 60 postnatal days (P). Fluorescent western blotting revealed that CDKL5 was robustly expressed in all regions of the rat brain that were examined in this study (Figure 3.2B). Quantification of the total amount of CDKL5 at each time point normalised to β-actin levels revealed that it was gradually increased during the early postnatal stages and remained high until adulthood for all brain regions tested with the only exemption of the cerebellum (Figure 3.2C).

This suggests that CDKL5 is widely expressed in the rat brain and is essential for postnatal neurodevelopment and possibly neuromaintenance.

Given that primary hippocampal neuronal cultures were selected as the experimental system to study the impact of CDKL5 deficiency on presynaptic mechanisms, we also tested the expression profile of CDKL5 in culture. Neuronal lysates were collected at different time points including 0, 4, 11, 14, 18, 21, and 25 DIV that mark both developing and mature neurons and concentrated to increase the total protein amount per sample. The level of CDKL5 was assessed by western blotting using β-actin as a loading control (Figure 3.2D). Similarly to mouse cultured neurons, CDKL5 is expressed in rat neurons in culture at different time points and this seems to be developmentally regulated, although additional replicates would be necessary to obtain a conclusive result. Although CDKL5 can be found in both excitatory and inhibitory mouse neurons (Rusconi *et al.*, 2011; Ricciardi *et al.*, 2012; Tang *et al.*, 2019), primary hippocampal cultures mostly consist of excitatory neurons and, as a result, we did not proceed further with an analysis of the CDKL5 expression with respect to the neuronal type.

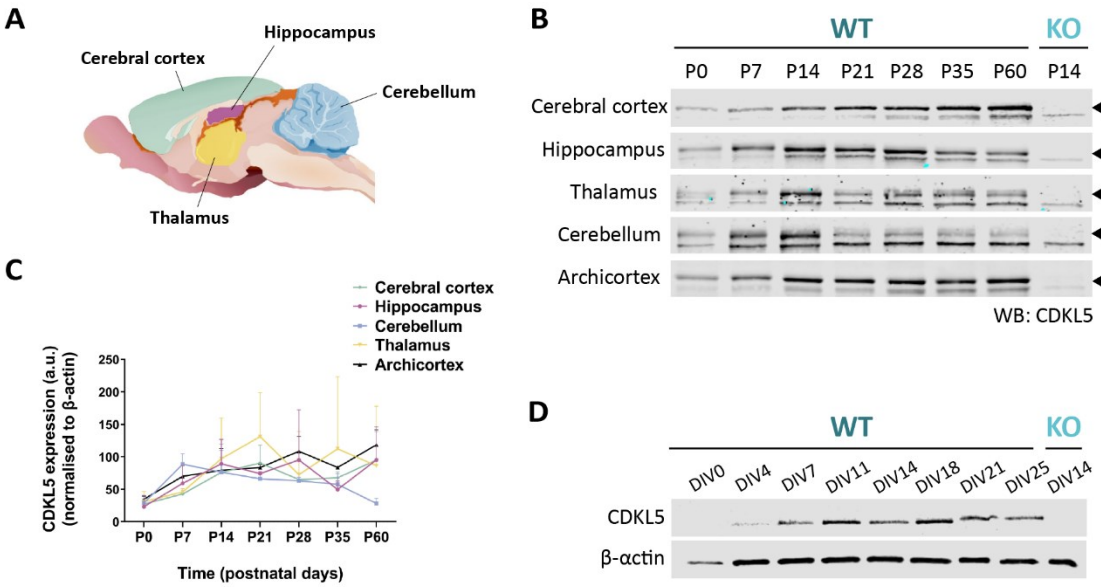

Figure 3.2 Time course analysis of CDKL5 expression in different brain regions and neuronal lysates

(**A**) Schematic representation of anatomical brain regions in a sagittal plane of the rat brain that were dissected and homogenised for time course analysis of CDKL5 expression. (**B**) Western blot analysis of CDKL5 expression in rat brain lysates postnatally. Different brain areas including cerebral cortex, hippocampus, cerebellum, thalamus, and archicortex, were dissected and lysed in RIPA buffer at the indicated time points. The protein concentration was quantified and adjusted to 1 mg/ml. The level of β-actin was used as loading control. A sample from KO brain lysate was also included in the analysis to indicate the presence of CDKL5 in the WT lysates. (**C**) Quantification of the CDKL5 expression in various brain areas of the rat brain at different postnatal days normalised to β-actin. CDKL5 is progressively expressed during the early postnatal time points and is maintained relatively constant throughout adulthood. Data indicate mean ± SD. n = 2 animals

per time point. (**D**) Western blot analysis of CDKL5 expression in mouse hippocampal neuronal lysates at different days in culture. Neurons were lysed in RIPA buffer at the indicated time points. Lysates were concentrated and the total protein amount was measured and adjusted to 1 mg/ml. The expression level of β-actin was used as a loading control.

3.2.3 CDKL5 is sorted into nerve terminals

The subcellular distribution of a protein can be informative for both its functional role as well as its regulation and potential interactions. CDKL5 is considered to be primarily sorted into the neuronal cytoplasm and, to a lesser extent, the nucleus (Rusconi *et al.*, 2011; Wang *et al.*, 2012; Schroeder *et al.*, 2019). In the cytoplasm, CDKL5 can be found at the postsynaptic density of dendritic spines (Ricciardi *et al.*, 2012; Zhu *et al.*, 2013), but it is likely to be widely sorted throughout the neuron including the axon and nerve terminals. Indeed, previous studies have demonstrated that CDKL5 colocalises with the presynaptic vesicular glutamate transporter 1 (VGLUT1) in mouse glutamatergic neurons (Ricciardi *et al.*, 2012; Wang *et al.*, 2021). To examine the distribution of CDKL5 to the presynapse, we double-stained rat hippocampal neurons fixed at 15 DIV for endogenous CDKL5 and the presynaptic marker SV2A (Figure 3.3A). We then determined the degree of colocalization between CDKL5- and SV2A-positive puncta in various fields of view per image by calculating the Pearson correlation coefficient excluding cell bodies from the

analysis (Figure 3.3B)[3]. The histogram of the Pearson correlation coefficient values indicated that there was colocalisation between CDKL5 and SV2A-positive boutons with most fields of view falling within the range 0.4-0.55 (Figure 3.3C). Although CDKL5 can be found in presynaptic boutons, it was not enriched there, as the overlap of SV2A with CDKL5 is characterised by lower Pearson correlation coefficient values than with the presynaptic transporter VGLUT1 (Figure 3.3D). Since primary hippocampal neurons are not merely glutamatergic, the Pearson correlation coefficient for the SV2A and VGLUT1 overlap was lower than 1, but it was roughly similar to what has been previously reported in the rat brain (Bragina *et al.*, 2011). This evidence recommends that CDKL5 is sorted into the presynaptic terminal in rat hippocampal neurons, but it is not an exclusively presynaptic kinase.

Given that staining for CDKL5 was not optimal due to the limited efficacy of the CDKL5 antibody for immunolabelling, we further tested the presynaptic localisation of CDKL5 by subcellular fractionation. Adult rat brain was homogenised and subjected to differential fractionation to generate distinct subcellular fractions including a synaptosome- (P2) and an SV-enriched (LP2) fraction according to Huttner *et al.* (1983). The P2 and LP2 fractions together with intermediate fractions were analysed by fluorescent western blotting to test for the presence of CDKL5 in the presynaptic compartment and the vicinity of SVs represented largely by the LP2 fraction as indicated by the accumulation of the presynaptic protein synaptophysin 1 (Syp1). Syp1 is an integral SV glycoprotein that is widely used as a marker of nerve terminals (Wiedenmann & Franke, 1985; Takamori *et al.*, 2006). The distribution of PSD95 was also examined as a postsynaptic marker. We observed that CDKL5 is

[3] The scatter plot was generated by Python 3.8 using a code provided by Marios Kalomenopoulos (University of Edinburgh).

present at the LP2 fraction and also seems to be enriched there compared to the synaptosomal fraction in contrast to the purification profile of PSD95 (Figure 3.3E). Similar distribution profile for CDKL5 was also obtained in the case of a mouse brain (Appendix - Supplementary Figure 1). The LP2 fraction was crudely purified in this study and thus it is not unlikely other vesicle populations, such as presynaptic endosomes and lysosomes, to be also present in this fraction but only at low levels (Lee *et al.*, 2001; Corera *et al.*, 2009). Likewise, the very low levels of PSD95 detected in the LP2 do not support a considerable contamination with postsynaptic elements. This confirms that CDKL5 localises at the presynapse where it possibly associates with or is adjacent to SVs.

Both immunolabelling and subcellular fractionation indicate a presynaptic sorting of CDKL5 within the neuronal cytoplasm. For this reason, we next examined whether CDKL5 is targeted exclusively to some nerve terminals or displays a diffuse axonal distribution by coefficient of variance (CV) analysis. A low CV value indicates that the distribution of a protein along the axon is homogeneous in contrast to a punctate localization that is characterised by higher values. Since CDKL5 is N-terminally tagged with mCer, we labelled fixed hippocampal neurons overexpressing CDKL5 with a GFP antibody to amplify the mCer fluorescence (Figure 3.3F). Neurons transfected with either mCer or Syp1-mCer were used as controls. Syp1-mCer is targeted to the presynaptic boutons (Li & Murthy, 2001; Pennuto *et al.*, 2002) and, as a result, it is expected to have a punctate distribution along axons and a high CV value. Quantification of the distribution profile of CDKL5 in axonal segments (> 15 μm) by CV analysis indicated that CDKL5 had a CV value similar to mCer (Figure 3.3G) pointing that CDKL5 is diffusely distributed along the axon and is present but not enriched in presynaptic terminals.

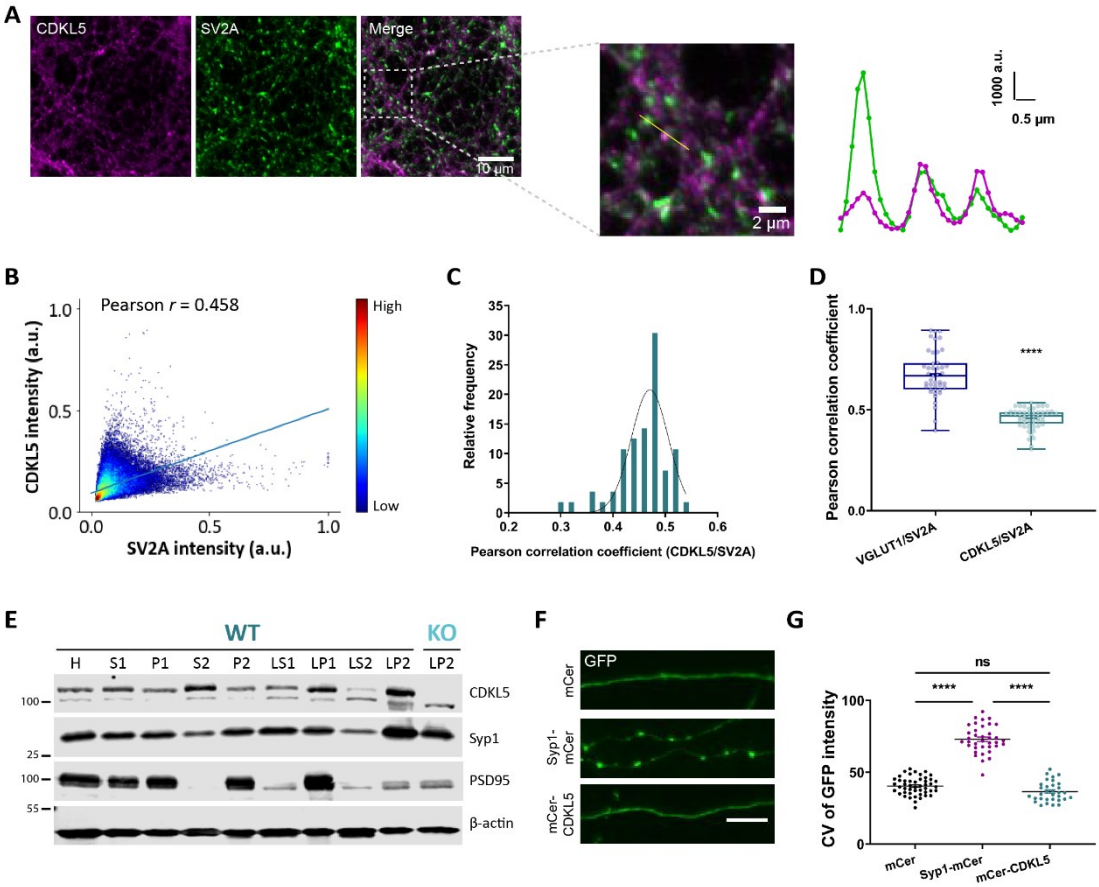

Figure 3.3 Endogenous CDKL5 localises at the nerve terminal

(**A**) Rat hippocampal neurons were fixed at 15 DIV and stained for endogenous CDKL5 and the presynaptic marker SV2A. Representative fields of view that were analysed for determining colocalisation between CDKL5 and SV2A and merged image. Scale bar, 10 µm. The histogram of the pixel values in a selected ROI (yellow bar in zoomed image; scale bar, 2 µm) indicates colocalisation of CDKL5 with SV2A-positive boutons. (**B**) Example scatter plot of the Pearson correlation coefficient for CDKL5 and SV2A. (**C**) Example histogram of the Pearson correlation coefficient values of all the fields of view analysed indicates that they mostly range between 0.4-0.55. (**D**) Quantification of the Pearson correlation coefficient for

CDKL5/SV2A and VGLUT1/SV2A as positive control. Box plots present median with IQR indicating min-max whiskers. ****p < 0.001 by Mann-Whitney two-tailed t test. + indicates mean value. VGLUT1/SV2A *n* = 43, CDKL5/SV2A *n* = 56 fields of view from 3-4 independent preparations of neuronal cultures. (**E**) CDKL5 is detected in the synaptic vesicle fraction. An adult rat brain (H) was homogenised in sucrose/EDTA solution and fractionated for isolating a crude synaptosome (P2) and crude SV (LP2) fraction. Subsequent fractions of increased purity were adjusted to 1 mg/ml and analysed by immunoblotting. The intermediate fractions that include (P1) tissue debris, nuclei, and large myelin fragments, (S2) microsomes, some small mitochondria, and synaptosomes, (LP1) synaptic membrane, large mitochondria, and myelin fragments, and (LS2) synaptosomal cytoplasm were also analysed. CDKL5 is enriched in both the P2 and LP2 fractions. Following a similar fractionation protocol, a LP2 fraction derived from a CDKL5 KO rat brain was also generated and analysed by immunoblotting. CDKL5 was not detected in the CDKL5 KO LP2 fraction confirming that the top band (110 kDa) represents indeed CDKL5. Syp1 and PSD95 were used as a pre- and postsynaptic marker, respectively, and β-actin as a loading control. (**F**) Mouse hippocampal neurons overexpressing mCer, Syp1-mCer or mCer-CDKL5 were fixed at 15 DIV and stained for GFP. Examples of axonal segments > 15 μm that were selected for CV analysis. Scale bar, 5 μm. (**G**) The distribution pattern of CDKL5 was assessed by CV analysis of GFP fluorescence intensity along > 15 μm axonal segments. Scatter plots indicate mean ± SEM. ns, not significant, ****p < 0.0001 by one-way ANOVA followed by Tukey's multiple comparison test. mCer *n* = 48, Syp1 *n* = 37, CDKL5 *n* = 32 fields of view from 4 independent preparations of neuronal cultures.

3.2.4 CDKL5 deficiency does not alter the presynaptic integrity

The presence of CDKL5 in the presynaptic terminal indicates that it serves possibly a presynaptic role. Prior to addressing the potential role of CDKL5 in SV recycling, we investigated whether the absence of CDKL5 causes any defects in the presynaptic stability. For this reason, we examined two parameters that determine presynaptic integrity, including the total protein levels of different presynaptic proteins and the number of presynaptic boutons. Dysregulation of protein levels as well as altered synapse number have been both reported in mice lacking CDKL5 (Della Sala *et al.*, 2016; Ren *et al.*, 2019; Schroeder *et al.*, 2019; Tang *et al.*, 2019); however, whether this is the case for the presynaptic compartment in particular has not been addressed.

In the first case, we evaluated whether lysates obtained from WT and CDKL5 KO neurons display altered total amount of various presynaptic proteins by western blotting. We analysed a range of presynaptic molecules including proteins important for SV recycling, such as CHC, Dyn1, endophilin A1, and syndapin 1; integral SV proteins, such as Syp1, VGLUT1, and the v-type proton ATPase subunit B (ATP6V1B2); and phosphoproteins that have been implicated in the regulation of endocytosis, such as pGSK3α/β-S9/S21 and pAkt-S473. Besides, the PI3K/GSK3/Akt pathway is one of the most perturbed signalling cascades linked to CDKL5 deficiency (Wang *et al.*, 2012; Amendola *et al.*, 2014; Jiang *et al.*, 2019). We found that lack of CDKL5 did not alter the total protein amount or phosphorylation levels of any of them (Figure 3.4) inferring thus that CDKL5 loss does not dysregulate presynaptic protein levels in rat hippocampal neurons.

We next examined whether the loss of CDKL5 leads to vulnerable presynaptic terminals and, consequently a compromised neuronal network.

To examine any potential loss of presynaptic contacts upon CDKL5 absence, we double-stained WT and CDKL5 KO neurons for two distinct presynaptic markers, including SV2A and VGLUT1, to count the number of positive presynaptic boutons. Since glutamate is an excitatory neurotransmitter, staining for VGLUT1 can inform about the number of excitatory presynaptic boutons, while SV2A is a common presynaptic reporter. In this way, we can assess not only the total number of presynaptic boutons, but also their subpopulations. Stained presynaptic boutons were counted along multiple selections of around (50 x 15) μm^2 of dendrites for quantification of SV2A- and VGLUT1-positive puncta (Figure 3.5A). We found that the loss of CDKL5 did not alter the number of presynaptic boutons compared to WT neurons suggesting that CDKL5 deficiency does not cause degradation and/or defective biogenesis of nerve terminals in rat neurons (Figure 3.5B, C). These observations recommend that the integrity of the presynaptic compartment with respect to the parameters examined here was not affected upon CDKL5 deficiency in rat hippocampal neurons. Whether the presynaptic ultrastructure remains intact in neurons lacking CDKL5 remains to be assessed in order to have a more complete view of the presynapse status.

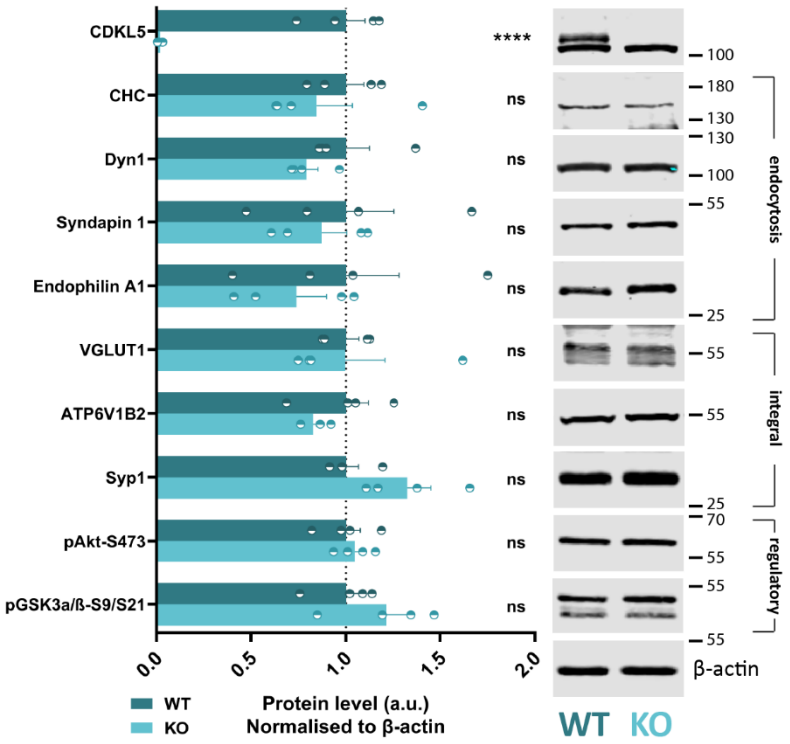

Figure 3.4 The level of presynaptic proteins is not altered in the absence of CDKL5 at hippocampal neurons

Hippocampal neurons were lysed at 14-15 DIV and analysed by fluorescent immunoblotting for different presynaptic proteins with a focus on endocytic molecules. Loss of CDKL5 does not result in any significant change in the total amount of any of these proteins. Quantification of protein level was performed by determining relative band intensities normalised to β-actin. Bars indicate mean ± SEM. ns, not significant, ****$p < 0.001$ by unpaired two-tailed t test. $n = 4$ neuronal lysates per genotype from 4 independent preparations of neuronal cultures.

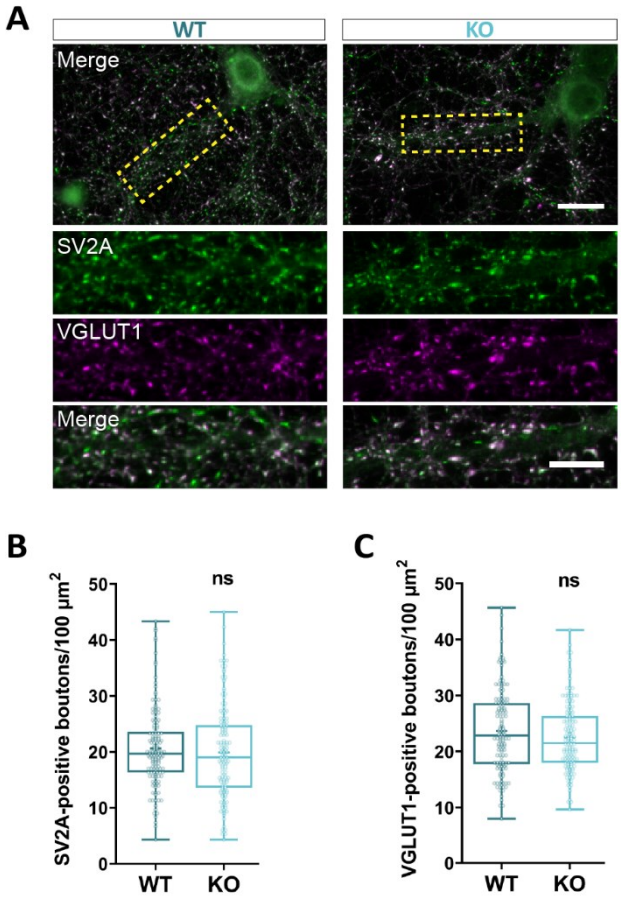

Figure 3.5 The number of presynaptic boutons is not altered in CDKL5 deficient neurons

(**A**) Hippocampal neurons derived from WT and CDKL5 KO rats were fixed at 15 DIV and stained for the presynaptic proteins SV2A and VGLUT1. The number of nerve terminals was quantified in (50 x 15) µm² selections along dendrites (dashed grey boxes) for both SV2A and VGLUT1. Scale bar, 20 µm (neurons), 10 µm (dendrites). (**B**) Quantification of the SV2A-positive boutons and (**C**) VGLUT1-positive boutons along WT and CDKL5 KO dendrites. Box plots present median with IQR indicating min-max whiskers. ns, not significant by two-tailed Mann-

Whitney test, + indicates mean value. WT n = 144, KO n = 142 neurons from 3 independent preparations of neuronal cultures.

3.2.5 CDKL5 deficient neurons display impaired SV recycling

3.2.5.1 CDKL5 deficiency impairs SV endocytosis kinetics

The presynaptic localisation of CDKL5 suggests that it might participate in SV recycling and thus neurotransmission. Indeed, phenotypes reported in rodents lacking CDKL5, such as altered frequency of sPSCs and mPSCs (Tang *et al.*, 2017; Wang *et al.*, 2021; Simões de Oliveira et al., in preparation), and aberrant paired-pulse facilitation (Tang *et al.*, 2019), point towards defects in synaptic transmission that could be due to unreliable SV recycling. To unravel any presynaptic deficits in SV recycling, we used the genetically-encoded pH-sensitive reporter sypHy. The pH-sensitive green fluorescent protein pHluorin (pKa ~7.1) is fused to an intravesicular loop of Syp1 to generate sypHy (Miesenbock *et al.*, 1998; Granseth *et al.*, 2006). Fluorescence of sypHy is dictated by differences in the pH of the environment with fluorescence being quenched in the acidic SV lumen (pH ~5.5), unquenched upon stimulus-dependent SV release and exposure to the neutral extracellular space (pH 7.4), and once again quenched following endocytosis and reacidification (Figure 3.6A). Importantly, the total amount of Syp was not altered in neurons lacking CDKL5 (as shown in 3.2.4 CDKL5 deficiency does not alter the presynaptic integrity) allowing the use of sypHy in our study.

Owning to the possible participation of CDKL5 in SV release that could explain the above phenotypes, we examined whether loss of CDKL5 results in

impaired SV exocytosis. Hippocampal neurons derived from either WT or CDKL5 KO rats were transfected with sypHy and stimulated at increasing frequencies including 5, 10 and 40 Hz (Figure 3.6B, E, H). To quantify for the extent of SV exocytosis, the sypHy fluorescence during stimulation was expressed as a portion of the total fluorescence revealed by perfusion with NH_4Cl. Since NH_4Cl is cell-permeable, this results in all sypHy signal to be unquenched allowing therefore an estimation of the total SV pool size. We found that the extent of SV exocytosis does not differ and across various stimulation frequencies between genotypes (Figure 3.6C, F, I).

Since CDKL5 absence does not impair SV fusion, we next focused on SV endocytosis. As reacidification is considered a rapid process (Atluri & Ryan, 2006), monitoring the sypHy fluorescence decay in time can be used to estimate SV endocytosis kinetics following stimulation (Sankaranarayanan & Ryan, 2000). The sypHy fluorescence was normalised to the stimulation peak to allow for comparison of endocytosis kinetics. To quantify the kinetics of SV retrieval, we measured the distance from the baseline at 180 s for 5 Hz stimulation or 152 s for 10 or 40 Hz stimulation as endocytosis was quite slow to allow for τ or rate decay estimation in certain cases. We observed that neurons lacking CDKL5 displayed slower SV endocytosis after evoked stimulation at various frequencies in comparison with WT neurons, suggesting that CDKL5 is important for SV endocytosis (Figure 3.6D, G, J). In addition, the extent of the slowing of SV retrieval tended to be milder as the stimulation frequency increased.

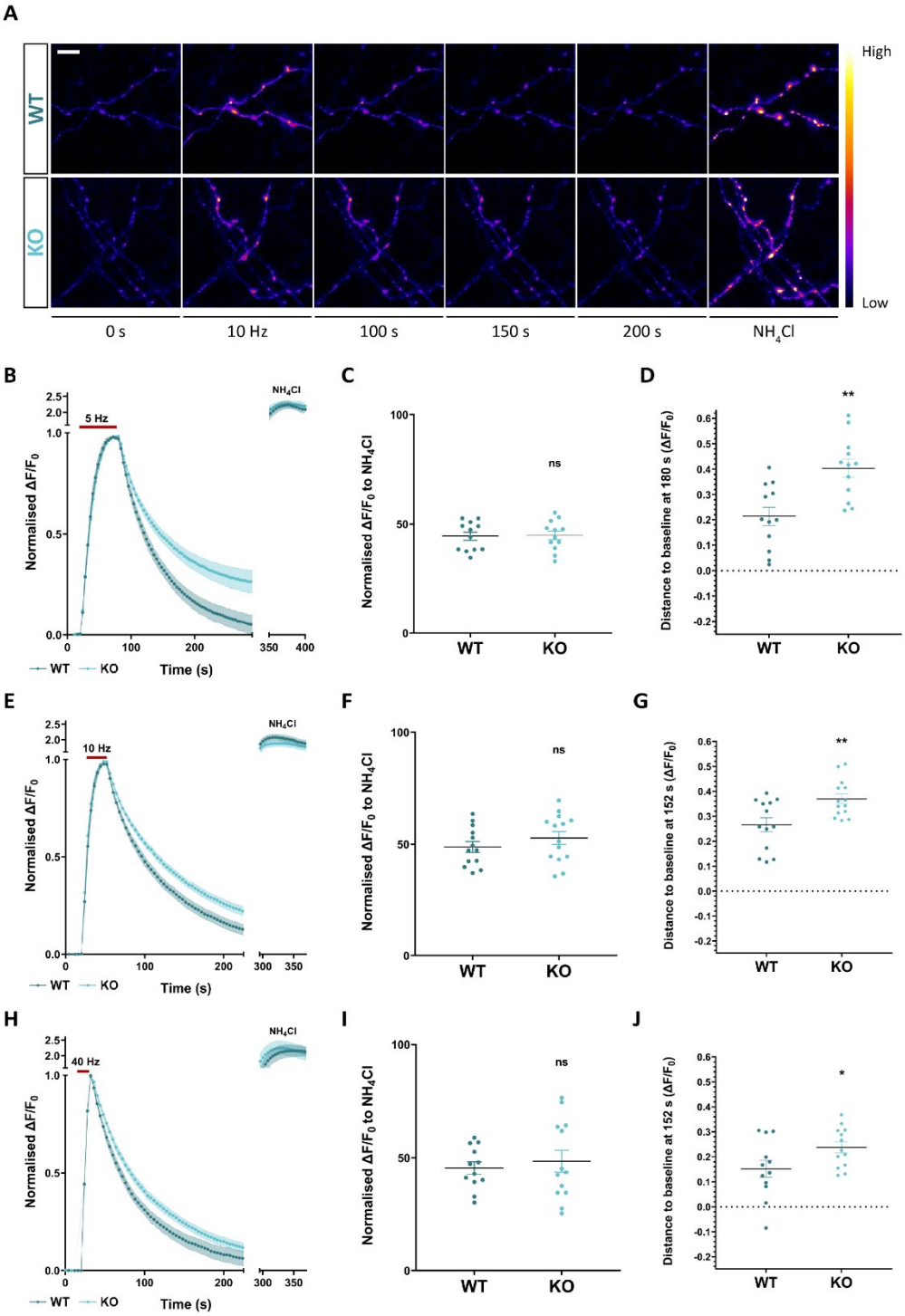

Figure 3.6 Loss of CDKL5 impairs the kinetics of synaptic vesicle endocytosis but not exocytosis

Primary hippocampal neurons from WT and CDKL5 KO rats were transfected with sypHy at 8-9 DIV and imaged at 13-14 DIV. (**A**) Example responses from sypHy-expressing axons that were subjected to 300 APs at 10 Hz and perfused with NH_4Cl solution. Representative image slices were selected from the whole time-course that was recorded from both WT (top) and CDKL5 KO neuronal cultures (bottom). (**B**) Mean sypHy response from neurons stimulated at 5 Hz for 60 s (red bar) normalised to the stimulation peak. (**C**) sypHy fluorescence at stimulation peak when total sypHy response is normalised to NH_4Cl. (**D**) sypHy fluorescence measuring the distance from baseline at 180 s. (**B-D**) WT $n = 12$, KO $n = 12$ coverslips from 4 independent preparations of neuronal cultures. (**E**) Mean sypHy response from neurons stimulated at 10 Hz for 30 s (red bar) normalised to the stimulation peak. (**F**) sypHy fluorescence at stimulation peak when total sypHy response is normalised to NH_4Cl. (**G**) sypHy fluorescence measuring the distance from baseline at 152 s. (**E-G**) WT $n = 13$, KO $n = 14$ coverslips from 4 independent preparations of neuronal cultures. (**H**) Mean sypHy response from neurons stimulated at 40 Hz for 10 s (red bar) normalised to the stimulation peak. (**I**) sypHy fluorescence at stimulation peak when total sypHy response is normalised to NH_4Cl. (**J**) sypHy fluorescence measuring the distance from baseline at 152 s. (**H-J**) WT $n = 12$, KO $n = 13$ coverslips from 4 independent preparations of neuronal cultures. Scatter plots indicate mean ± SEM. ns, not significant, *$p < 0.05$, **$p < 0.01$ by unpaired two-tailed t test.

3.2.5.2 CDKL5 deficiency does not affect SV exocytosis and total pool size

Whilst the sypHy imaging assay offers insight into the exocytosis kinetics, the sypHy fluorescence during stimulation is the net effect of exo- and endocytotic events. To assess the impact of CDKL5 loss on the fusion rate exclusively, we measured the rate of fluorescence increase during prolonged stimulation at 10 Hz for 90 s in the presence of 1 μM bafilomycin A1, a v-ATPase inhibitor, in WT and CDKL5 KO neurons expressing sypHy (Figure 3.7A). The antibiotic bafilomycin A1 blocks the reacidification of newly-generated SVs preventing thus the quenching of sypHy fluorescence following endocytosis (Sankaranarayanan & Ryan, 2001). In the presence of bafilomycin A1, the recycling pool can be depleted in a period shorter than 90 s with the sypHy signal reaching hence a plateau (Fernandez-Alfonso & Ryan, 2004). The sypHy fluorescence was normalised to the plateau allowing comparison of the SV fusion rate. No difference was observed between WT and CDKL5 KO neurons confirming that SV exocytosis was not altered upon CDKL5 loss (Figure 3.7B). We also estimated the total SV pool size that consists of the recycling pool that is entirely exhausted during stimulation in the presence of bafilomycin A1 and the remaining resting pool that emerges after perfusion with NH_4Cl. Similarly, no difference in total SV pool size was reported between genotypes (Figure 3.7C). Since the rate of SV fusion was not altered either in the presence or absence of bafilomycin A1 (as shown in 3.2.5.1 CDKL5 deficiency impairs SV endocytosis), we did not proceed measuring the endocytosis speed during neuronal activity with the likelihood any changes to be negligible.

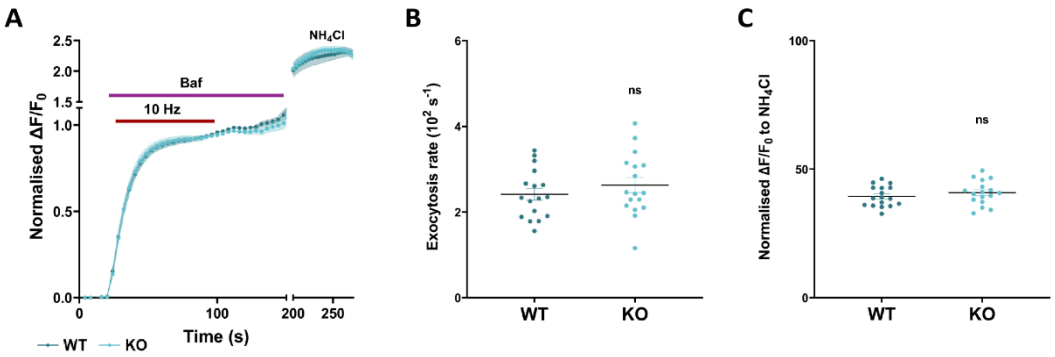

Figure 3.7 Loss of CDKL5 does not impact on SV exocytosis or total pool size

Primary hippocampal neurons from WT and CDKL5 KO rats were transfected with sypHy at 8-9 DIV and imaged at 13-14 DIV. (**A**) Mean sypHy response from neurons stimulated at 10 Hz for 90 s (red bar) in the presence of 1 μM bafilomycin A1 (purple bar) normalised to the plateau. (**B**) Mean exocytosis rate and (**C**) sypHy fluorescence at plateau when total sypHy response is normalised to NH_4Cl. WT *n* = 17, KO *n* = 17 coverslips from 4 independent preparations of neuronal cultures. Scatter plots indicate mean ± SEM. ns, not significant by unpaired two-tailed t test.

3.2.5.3 CDKL5 deficiency does not affect SV acidification

Since the sypHy signal depends on pH differences in the immediate environment, we next verified whether neurons deficient of CDKL5 displayed deceleration in SV retrieval rather than impaired reacidification dynamics. Since reacidification of newly-endocytosed SVs is a rapid process (Atluri & Ryan, 2006), the acquisition rate was set at 2 s as this offers sufficient temporal

resolution. WT and CDKL5 KO neurons expressing sypHy were initially perfused with acid buffer (pH 5.5) prior to stimulation resulting in all sypHy molecules residing on the neuronal membrane at resting conditions to be quenched. Next, neurons were stimulated at 10 Hz for 30 s and perfused once again with acid solution after the end of stimulation to quench fluorescence of sypHy molecules residing on the plasma membrane (Figure 3.8A). Therefore, all the newly-formed SVs (still basic intralumenally) contained sypHy molecules protected from the acidic surface environment. The fluorescence quenching of these sypHy molecules can be used to estimate reacidification kinetics. The reacidification rate was estimated by calculating the poststimulus rate decay. We reported no significant difference in the reacidification rate in neurons lacking CDKL5 compared to WT neurons implying that the slowing in SV endocytosis upon loss of CDKL5 does not result from impaired SV reacidification (Figure 3.8B).

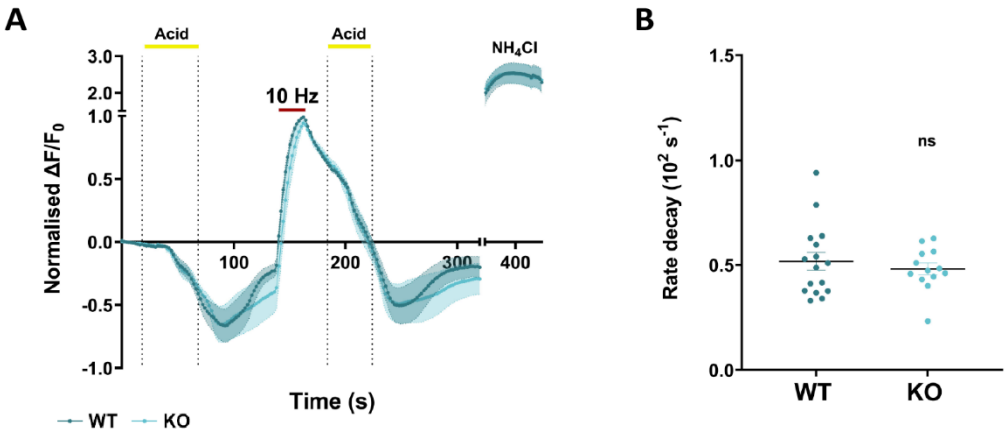

Figure 3.8 Loss of CDKL5 does not impair SV acidification rate

Primary hippocampal neurons from WT and CDKL5 KO rats were transfected with sypHy at 8-9 DIV and imaged at 13-14 DIV. (**A**) Mean sypHy response from neurons stimulated at 10 Hz for 30 s (red bar) normalised to the stimulation peak. Neurons were perfused with acid solution both pre- and post-stimulation (yellow bars). (**B**) Mean rate decay of acidification measured after applying a post-stimulus acid pulse. WT n = 16, KO n = 13 coverslips from 3 independent preparations of neuronal cultures. Scatter plots indicate mean ± SEM. ns, not significant by unpaired two-tailed t test.

3.2.6 CDKL5 deficiency does not affect ADBE

CDKL5 deficiency leads to slower SV endocytosis in rat hippocampal neurons after stimulation at both low and high frequencies. However, ADBE is the leading endocytic pathway during high frequency stimulation, which sypHy imaging fails to report (Nicholson-Fish *et al.*, 2015). Therefore, it is crucial to explore the impact of CDKL5 absence on ADBE to obtain a more complete insight on the role of CDKL5 during intense neuronal activity. Besides, molecules that have been implicated in ADBE, such as GSK3 and Akt, display altered phosphorylation levels upon CDKL5 loss (Fuchs *et al.*, 2014). To test whether CDKL5 deficiency disrupts ADBE, we used the fluid-phase marker TMR-dextran to count for presynaptic terminals that underwent ADBE. TMR-dextran is a fluorescently labelled polysaccharide of high molecular weight that can be endocytosed in a size-limiting manner during stimulation. Hence, TMR-dextran is selectively endocytosed by bulk endosomes following high frequency stimulation rather than SVs (Figure

3.9A). WT and CDKL5 KO hippocampal neurons at 13-14 DIV were stimulated at 40 Hz for 10 s in the presence of 50 μM TMR-dextran and z-stacks were acquired from fields of view of similar neuronal density. TMR-dextran-positive boutons were counted from maximum z-projections following thresholding (Figure 3.9B). Unstimulated controls were used to subtract background signal. We observed that there was a downward trend in the number of TMR-dextran-positive boutons in CDKL5-null compared to WT neurons albeit this finding did not reach statistical significance (Figure 3.9C). This indicates that ADBE was not impaired due to the loss of CDKL5 at the level of the neuronal population.

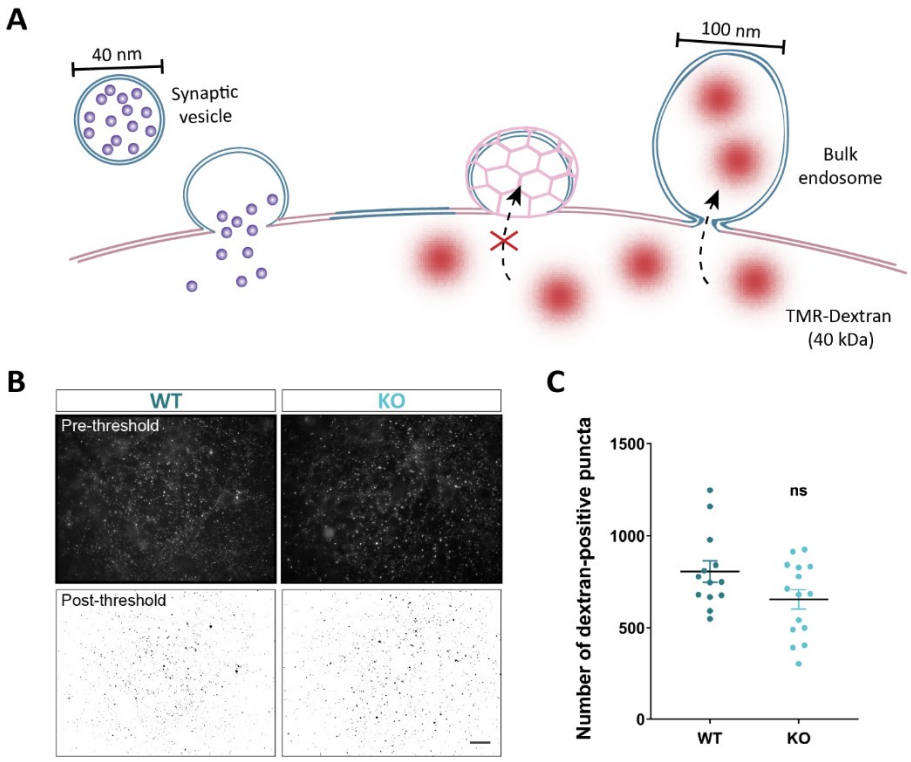

Figure 3.9 Loss of CDKL5 does not alter ADBE

(**A**) Schematic representation of TMR-dextran (40 kDa) uptake for the selective detection of ADBE. (**B**) Primary hippocampal neurons from WT and CDKL5 KO rats at 13-14 DIV were stimulated at 40 Hz for 10 s in the presence of 50 µM TMR-dextran followed by acquisition of z-stacks. Representative maximum z-projections of TMR-dextran-positive puncta (top) were subjected to thresholding (bottom). Scale bar, 20 µm. (**C**) Quantification of the number of presynaptic boutons that underwent ADBE in thresholded images. The number of TMR-dextran-positive presynaptic terminals from unstimulated controls were subtracted in all cases. WT n = 13, KO n = 15 coverslips from 3 independent preparations of neuronal cultures. Scatter plots indicate mean ± SEM. ns, not significant by unpaired two-tailed t test.

3.3 Discussion

3.3.1 CDKL5 expression in the rat brain

CDD is a monogenic developmental and epileptic encephalopathy with onset in early infancy that is caused by mutations in the *CDKL5* gene (Fehr *et al.*, 2013; Mangatt *et al.*, 2016). Autistic-like features are commonly reported in CDD patients; therefore, in this work, we used a novel CDKL5 KO rat model due to the social behaviour that rats exhibit in an attempt to pinpoint phenotypes upon loss of CDKL5 that were previously difficult to identify in various mouse models. In the rat brain, we found that CDKL5 is expressed in several regions, including the cortex, hippocampus, cerebellum, and thalamus. This pattern is similar to the expression profile of CDKL5 in the mouse brain (Rusconi *et al.*, 2008) and correlates with the multifocal and generalised type of seizures that are reported in CDD (Bahi-Buisson & Bienvenu, 2012; Fehr *et al.*, 2013).

At the same time, the expression of rat CDKL5 increases during the early developmental stages highlighting its importance for the early postnatal brain development and supporting thus the early-onset occurrence of CDD. Recent findings suggest that CDKL5 is essential not only for the developing but also for the aged brain (Mulcahey *et al.*, 2020; Terzic *et al.*, 2021). With the exception of the cerebellum, we indeed observed that all rat brain regions maintain CDKL5 expression throughout adulthood indicating that CDKL5 is important for fundamental biological processes that occur during and beyond the early developmental stages.

3.3.2 Primary rat hippocampal cultures as an experimental system to study the role of CDKL5 in SV recycling

The fact that SV release and regeneration are at risk in a number of neurodevelopmental disorders implies that presynaptic dysfunction might be the common denominator. To explore any potential presynaptic role of CDKL5, we selected primary hippocampal neurons derived from CDKL5 KO rats and WT littermate controls as model system for several reasons. Amongst the various experimental systems that have been employed to understand the processes that dictate the presynaptic biology and especially SV recycling, primary hippocampal neurons are one of the most well-studied (Gan & Watanabe, 2018). Second, pH-sensitive genetically tagged fluorescent probes can be used to label endogenous presynaptic proteins, such as Syp1, to study a number of parameters of SV recycling. Third, we observed that CDKL5 expression in cultured hippocampal neurons exhibits a comparable time course profile to the rat hippocampus making it a relevant system for CDKL5 research, which agrees with previous report (Schroeder *et al.*, 2019). Importantly, the hippocampus is characterised by high potential for synaptic plasticity and controls memory and learning, processes that are often disturbed upon CDKL5 deficiency (Wang *et al.*, 2012; Della Sala *et al.*, 2016).

3.3.3 CDKL5 localisation at the presynaptic terminal

CDKL5 is a ubiquitous neuronal kinase; yet little evidence exists for its presence in the presynaptic terminal, while it has been repeatedly reported at dendrites and spines (Ricciardi *et al.*, 2012; Zhu *et al.*, 2013). Therefore, this is the first study that focuses on describing its subcellular sorting into the

presynapse in more detail. Using an antibody generated against human CDKL5 that was initially validated by both western blotting and immunolabelling, we tested the degree of colocalisation of CDKL5 with the vesicular glycoprotein SV2A. The Pearson correlation coefficient indicated that CDKL5 colocalises with SV2A at several but not all presynaptic boutons in relation to the correlation of SV2A with the vesicular transporter VGLUT1. Given that SV2A staining cannot distinguish between excitatory and inhibitory neuronal subtypes, this might explain the proportional presence of CDKL5 in nerve terminals. In support of a presynaptic localisation, CDKL5 colocalises with the excitatory VGLUT1 both at the mRNA and protein levels (Ricciardi *et al.*, 2012; Wang *et al.*, 2021). Furthermore, despite its presence at the nerve terminal, CDKL5 is not a presynaptically enriched kinase but rather displays a diffuse distribution along the axon.

Following an alternative approach, we also examined the presence of CDKL5 in presynaptic terminals using a typical fractionation protocol to purify crude synaptosome and SV pellets from an adult rat brain. To our surprise, we reported that CDKL5 is enriched at the crude SV fraction. Presynaptic lysosomes and endosomes can be co-purified together with the crude SV faction (Lee *et al.*, 2001; Corera *et al.*, 2009), but there has been no evidence linking CDKL5 to the endolysosomal membrane trafficking network so far. However, since endosomal intermediates with attached budding vesicles have been also detected in LP2 pellets by electron microscopy (Takei *et al.*, 1996), it is not unlikely CDKL5 to associate with or surround SVs and/or sorting endosomes. Regardless of the vesicle population that CDKL5 relates with in the LP2 fraction, this data reinforces that CDKL5 is present throughout the neuronal cytoplasm from dendrites to axons and dendritic spines to presynaptic terminals.

3.3.4 The role of CDKL5 in SV retrieval and potential underlying mechanisms

The presynaptic distribution of CDKL5 led to the hypothesis that it might serve a role in SV recycling and thus neurotransmission. Using sypHy, we revealed that SV regeneration occurs more slowly in CDKL5 deficient rat neurons following stimulation at different frequencies, while SV exocytosis remains unaltered. The sypHy response at 10 Hz was examined either in the presence or absence of the antibiotic bafilomycin A1, an vATPase inhibitor, showing that during stimulation neither SV exocytosis nor endocytosis is altered in CDKL5 KO neurons limiting the impairment in SV endocytosis to the poststimulus phase. Since sypHy monitors pH changes through the neutralisation of the lumen of SVs during exocytosis and their subsequent acidification following endocytosis, it cannot discriminate whether the newly-generated non-acidified SVs originate directly from the plasma membrane, an intermediate endosome or both. Thus, the stage at which CDKL5 facilitates SV retrieval is not clear. However, the reacidification kinetics alone is not affected by the loss of CDKL5 indicating that CDKL5 participates in the SV reformation prior to reacidification. Overall, these findings support that CDKL5 participates in SV retrieval following evoked SV release at various frequencies. This is important since it is the first report to implicate CDKL5 in a purely presynaptic process inferring also that impaired SV recycling might contribute to the CDD pathogenesis.

There are several potential mechanisms that underlie the impact of CDKL5 deficiency on SV retrieval. To begin with, the most critical role of CDKL5 relies on its kinase activity. In fact, most pathogenic mutations identified in CDD patients are missense mutations within the CDKL5 kinase domain that result in its compromised phosphorylation activity. More than one targets may be

phosphorylated by CDKL5 to regulate SV regeneration either in a direct manner or not, although this pool of potential endocytic targets remains to be identified. Up to date, Amph1 is the only potential direct presynaptic substrate of CDKL5 in the presynaptic terminal, albeit *in vitro* (Sekiguchi *et al.*, 2013). Amph1 is a presynaptically enriched BAR-containing protein that is involved in SV regeneration. CDKL5-facilitated phosphorylation of Amph1 has been suggested to control its interaction for endophilin A1 pointing towards a mechanism through which the lack of CDKL5 may alter SV recycling (Sekiguchi *et al.*, 2013; Katayama *et al.*, 2015).

CDKL5 phosphorylates and/or interacts with various proteins that participate in gene expression and regulation (Amendola *et al.*, 2014; Trazzi *et al.*, 2016). Deleting CDKL5 though does not seem to affect the amount of key endocytic proteins, such as CHC, Dyn1, and endophilin A1, in our rat hippocampal cultures eliminating the possibility that defective SV retrieval is due to altered expression of the protein machinery that mediates different steps of SV regeneration. Furthermore, label-free mass spectrometry of WT and CDKL5 KO synaptosomes did not reveal quantitative differences between genotypes (personal communication, M. Trost, Newcastle University).

A few additional aspects should be considered for understanding the impact of the absence of CDKL5 in SV retrieval kinetics, although exploring their part in impairing SV endocytosis is the work of a future study. First, membrane composition and subsequent fluidity can support a slowing in SV endocytosis. Indeed, perturbed cholesterol profile is reported in CDD patients (Pecorelli *et al.*, 2015) indicating that altered membrane composition might modulate SV membrane trafficking in nerve terminals (Wasser *et al.*, 2007; Yue & Xu, 2015). Second, Ca^{2+} influx is essential for triggering SV release; however, evidence suggests that the presynaptic Ca^{2+} concentration remains an

important regulator in relation to SV endocytosis (Yao *et al.*, 2009; Leitz & Kavalali, 2011,2016) despite a number of studies challenging this (Miyano *et al.*, 2019; Orlando *et al.*, 2019). Aberrant Ca^{2+} accumulation in the nerve terminal resulting from defective mitochondrial Ca^{2+} uptake affects the rate of SV endocytosis (Marland *et al.*, 2016). At the same time, abnormal mitochondrial function has been observed in CDKL5-deficient mice (Jagtap *et al.*, 2019; Vigli *et al.*, 2019; Carli *et al.*, 2021) and, thus, it can possibly explain delayed SV endocytosis linked to the absence of CDKL5.

CDKL5 has been also linked to MT remodelling and cargo trafficking (Baltussen *et al.*, 2018; Barbiero *et al.*, 2019a), so the role of axonal MTs may be worth considering for SV recycling events (Bodaleo & Gonzalez-Billault, 2016; Bodaleo *et al.*, 2016). Amongst the cytoskeletal elements, actin filaments predominate in both orchestrating the SV cycle and organising distinct SV pools. However, some evidence supports that the MTs have a more decisive role to play in neurotransmission, albeit not directly on SV trafficking dynamics (Piriya Ananda Babu *et al.*, 2020). Despite being a matter of debate, presynaptic boutons have been shown to act as activity-dependent MT nucleation centres (Qu *et al.*, 2019) and it has been proposed that transport of cargos and local signalling rely on such initiation spots (Freal & Hoogenraad, 2019). This could be a mechanism that potentially affects SV recycling by impeding transport of elements that are necessary for SV endocytosis and/or affecting local signalling (Yagensky *et al.*, 2016).

3.3.5 Frequency-dependent activity of CDKL5

Another feature that emerges from our data is that the slowing in SV endocytosis kinetics in CDKL5 deficient neurons seems to be dependent on

the stimulation frequency with decreasing neuronal firing triggering more severe impairment. In accordance, little impact is observed on ADBE that occurs preferably at high frequency in CDKL5-depleted neurons. Remarkably, CDKL5 is not the only kinase of the CMGC group that has been reported to behave in an activity-dependent manner. For example, overexpression of Dyrk1A results in more augmented delay of SV endocytosis following 5 Hz stimulation rather than higher frequencies in hippocampal neurons (Kim *et al.*, 2010). Conversely, Cdk5 is rather required for SV endocytosis following prolonged release (Evans & Cousin, 2007).

Possible explanations of the frequency-dependent nature of the CDKL5-related defect in SV retrieval kinetics lie on its catalytic activity. The fraction of the SV releasable pool that is triggered at low stimulation frequency is smaller in comparison with more demanding activity rates. This is likely to provide enough time for CDKL5 to phosphorylate its putative target(s) at the presynapse. In accordance, CDKL5 may preferentially facilitate SV regeneration from the plasma membrane but not a sorting endosome, and assuming this step is faster and thus more time-critical due to rapid propagation of membrane tension following exocytosis (Perez *et al.*, 2021), lower frequencies would allow CDKL5 to have enough time to act. In contrast to CDKL5 being more functional at lower rates, the dephosphorylation activity of the phosphatase calcineurin might be compromised (Evans & Cousin, 2007). Calcineurin is responsible for dephosphorylating a number of endocytic proteins in an activity-dependent manner to enable the next round of neurotransmitter release. Providing that both enzymes share common targets or converged signalling pathways, the augmented catalytic activity of CDKL5, while calcineurin remains restricted, might inversely control the fate of SV

endocytosis at lower rates. Of course, similar explanations have been also proposed for the frequency-dependent activity of Dyrk1A (Kim *et al.*, 2010).

3.3.6 Lack of effect in SV exocytosis and ADBE in CDKL5-deficient neurons

Even though the slow time course of SV endocytosis in CDKL5-null neurons is not accompanied by any change in the rate of SV exocytosis, it is likely repetitive neuronal activity to lead to depression of SV release eventually. Besides, mice deficient of CDKL5 display altered frequency of spontaneous and miniature postsynaptic currents (Tang *et al.*, 2017; Wang *et al.*, 2021), and aberrant short-term plasticity (Tang *et al.*, 2019) that can result from dysfunctional SV recycling. On the other hand, CDKL5 acts preferably at lower stimulation frequency indicating that there is enough time for SV endocytosis to resupply the recycling SV pool even when its kinetics is impaired. In this case, the efficacy of synaptic transmission may depend on the quality of the newly-formed SVs with potential mislocalised SV cargo rendering them inefficient for a subsequent round of release. Although the protein levels of abundant cargo molecules, such as VGLUT1, Syp and ATP6V1B2, is not altered in CDKL5 lacking neurons indicating that the SV composition remains intact, we have not examined elements that are crucial for SV fusion, such as SNARE proteins. In support, the total SV population is preserved after CDKL5 deletion, although we have no information about their fine organisation and degree of clustering that could be added on the factors affecting SV release (Reshetniak & Rizzoli, 2021).

Loss of a functional protein can impact on neuronal health in a variety of ways. A common feature in CDKL5 deficient animal models is the loss of functional synapses that can result from inefficient synaptogenesis and/or

maintenance (Zhu & Xiong, 2019). Despite the lack of a time course analysis, the number of both SV2A- and VGLUT1-positive presynaptic boutons in mature cultured neurons is preserved after loss of CDKL5 and, therefore, it is reasonable to expect also similar number of inhibitory synapses across genotypes. This discrepancy may reflect that CDKL5 activity varies across species. On the other hand, since immunolabelling cannot distinguish between functional and inactive synapses, it is likely that the loss of functional synapses occurs in CDKL5 KO neurons without being able to be detected. Preliminary work using lumenal-directed Syt1 antibodies, as previously indicated (Ivanova *et al.*, 2021), suggests that there is no difference in the number of active synapses across genotypes, although this could be confirmed using the dye FM1-43.

In the above context, our last observation concerns the number of presynaptic boutons that undergo ADBE that is preserved upon loss of CDKL5 at the level of the neuronal network in culture. Accordingly, key signalling elements that are involved in ADBE regulation, such as the phosphorylation levels of Akt-S473 and GSK3α/β-S9/21, remained unaffected in contrast to previous studies in mice (Wang *et al.*, 2012; Amendola *et al.*, 2014). Despite the limitation of the dextran uptake assay to inform about the degree of ADBE that occurs in a single presynaptic terminal and the absence of an ultrastructural analysis, the lack of any changes in signalling molecules implicated in ADBE makes the likelihood ADBE to be overall altered in the absence of CDKL5 weaker agreeing thus with more limited CDKL5 activity at higher frequencies.

3.3.7 Conclusions

Overall, this chapter shows that CDKL5 is expresses widely in the rat brain and is required for proper postnatal development and throughout adulthood. In addition, our data describes the presynaptic localisation of CDKL5 in rat hippocampal neurons and provides evidence for a role of CDKL5 in SV endocytosis there possibly regulated in an activity-dependent manner. Furthermore, a number of parameters, such as SV exocytosis and reacidification, ADBE, the number of nerve terminals, and the total amount of various presynaptic proteins remains unaltered in CDKL5 deficiency.

Chapter 4: Investigating the role of CDKL5 in SV endocytosis

4.1 Introduction

Protein kinases are a large group of enzymes that modulate numerous cellular processes by catalysing the reversible phosphorylation of their physiological substrates. CDKL5 is a proline-directed S/T kinase with an N-terminal catalytic domain that bears signature motifs of the CMGC group of kinases. CDKL5 recognises its protein targets through the RPX(S/T)(A/G/P) consensus sequence (Canning *et al.*, 2018; Munoz *et al.*, 2018), albeit not all the reported CDKL5 substrates bear this motif. In addition to the kinase domain, CDKL5 consists of a long unstructured C-terminal tail that contributes to the neuronal performance of CDKL5 in various ways. It has been suggested that the C-terminal tail is important for the subcellular sorting (Rusconi *et al.*, 2008; Zhu *et al.*, 2013) and protein stability of CDKL5 (Lin *et al.*, 2005; Williamson *et al.*, 2012), mediates protein-protein interactions (Zhu *et al.*, 2013; Nawaz *et al.*, 2016), and contains putative phosphosites that are likely to regulate CDKL5 activity (Oi *et al.*, 2017; Munoz *et al.*, 2018). Moreover, several kinases possess distal interaction domains that interact with docking sites of the substrate to enhance specificity and affinity (Goldsmith *et al.*, 2007; Ubersax & Ferrell, 2007) and the C-terminal tail could act as a platform for such interactions. However, whether the C-terminal tail regulates the phosphorylation activity of CDKL5 and through which specific mechanisms is not largely understood.

So far, only a limited number of *in vivo* CDKL5 substrates has been identified that consists exclusively of MT-related proteins, such as MAP1S, EB2, CEP131, and DLG5 (Baltussen *et al.*, 2018; Munoz *et al.*, 2018). Moreover, a few proteins have been shown to serve as CDKL5 substrates *in vitro*, such as ARHGEF2 and DNMT1 (Kameshita *et al.*, 2008; Baltussen *et al.*, 2018). At the same time, the phosphorylation levels of additional proteins, often involved in signalling pathways, are dysregulated upon CDKL5 absence. For example, CDKL5 deficiency results in altered phosphorylation of GSK3 and Akt in mice (Fuchs *et al.*, 2014), although a direct association with the CDKL5 catalytic activity remains to be confirmed.

A liquid-phase isoelectric fractionation of mouse brain extracts together with *in vitro* kinase assays revealed Amph1-S293 as a phosphosite of CDKL5 (Sekiguchi *et al.*, 2013), which is the only potential presynaptic target of CDKL5 up to date. Amph1 acts mainly as an interface for various protein interactions during SV endocytosis with some of the most established ones to be that with endophilin A1, Dyn1, clathrin, and AP2. Deficiency of Amph1 results in occurrence of irreversible seizures in mice and it seems that signalling pathways modulated by CDKL5, such as the PI3K/AKT pathway, to be also affected by Amph1 indicating a convergence of the activities of the two proteins (Di Paolo *et al.*, 2002; Y. Chen *et al.*, 2020). Amph1 bears the consensus motif of an endogenous CDKL5 substrate with S293 residing within the sequence RPRS^{293}P. Furthermore, thanks to its position within the PRD of Amph1, the phosphorylation dynamics at S293 controls its affinity for endophilin A1 *in vitro* (Sekiguchi *et al.*, 2013) indicating its putative functional role in SV endocytosis. This agrees with mass spectrometric data showing that the S293 residue is abundantly phosphorylated in rat brain synaptosomes,

while it is dephosphorylated during neuronal activity and, thus, it is a phosphosite of high biological importance (Craft *et al.*, 2008).

As shown in Chapter 3, rat hippocampal neurons lacking CDKL5 display compromised SV endocytosis kinetics at different frequencies. The main objective of this chapter is to begin exploring the potential mechanism underlying this presynaptic deficit. Using primary hippocampal cultures, we followed a strategy of molecular replacements employing deletion mutants of CDKL5 to decipher the elements that may be important for SV endocytosis, such as its phosphorylation activity. In parallel, we tested the relevance of the SV endocytosis attenuation to CDD by examining CDKL5 mutations reported in CDD patients. Given that Amph1 is the only putative presynaptic substrate of CDKL5 that has been identified up to date, albeit *in vitro*, and for the reasons mentioned above, we hypothesised that CDKL5 exerts its effect on SV endocytosis through Amph1. To explore the relationship of CDKL5 with Amph1, we first investigated their potential interaction *in vivo*. We then studied the putative CDKL5-facilitated phosphorylation of Amph1 at S293 in rat hippocampal neurons using a phosphospecific antibody against Amph1-S293.

4.2 Results

4.2.1 Molecular replacements to restore the speed of SV endocytosis

4.2.1.1 SV endocytosis rate is restored by CDKL5 expression at 10 and 40 Hz

Rat hippocampal neurons deficient of CDKL5 display altered SV recycling due to decelerated SV endocytosis as shown in Chapter 3. This implies that supplying neurons with the missing kinase should restore the speed of SV endocytosis providing that the impairment is not an indirect effect. To verify that the loss of CDKL5 is responsible for compromising SV endocytosis performance, we co-transfected CDKL5 KO neurons with mCerC1-CDKL5 and sypHy. At the same time, we tested whether overexpression of mCerC1-CDKL5 in WT neurons influences SV endocytosis kinetics by either accelerating or decelerating the endocytosis speed. The CDKL5 variant that was used here (or hCDKL5_1 according to the established nomenclature) is the predominant isoform expressed in the human brain and refers to a protein product of 960 residues (Williamson *et al.*, 2012; Hector *et al.*, 2016). Due to its relevance to CDD, it was selected for all rescue experiments in this study. WT and CDKL5 KO neurons transfected with the mCerC1 empty vector acted as control groups. Neurons were stimulated either at 10 Hz for 30 s or at 40 Hz for 10 s. Analysis of the poststimulus sypHy response showed that expression of mCerC1-CDKL5 restored the kinetics of SV endocytosis to WT levels at 10 Hz, whereas overexpression of mCerC1-CDKL5 did not impact SV endocytosis kinetics (Figure 4.1A, B). In agreement, WT neurons overexpressing mCerC1-CDKL5 exhibited unaltered SV endocytosis kinetics

at 40 Hz, although a partial rescue was observed in the case of CDKL5 KO neurons due to mCerC1-CDKL5 expression (Figure 4.1C, D). The inability of CDKL5 to fully rescue the SV endocytosis slowing at 40 Hz is likely to result from limited activity of CDKL5 at higher frequencies or to be due to biological variance given that this was not always the case as presented in the following subsections. Therefore, these findings confirm that CDKL5 participates in SV endocytosis in rat hippocampal presynaptic terminals.

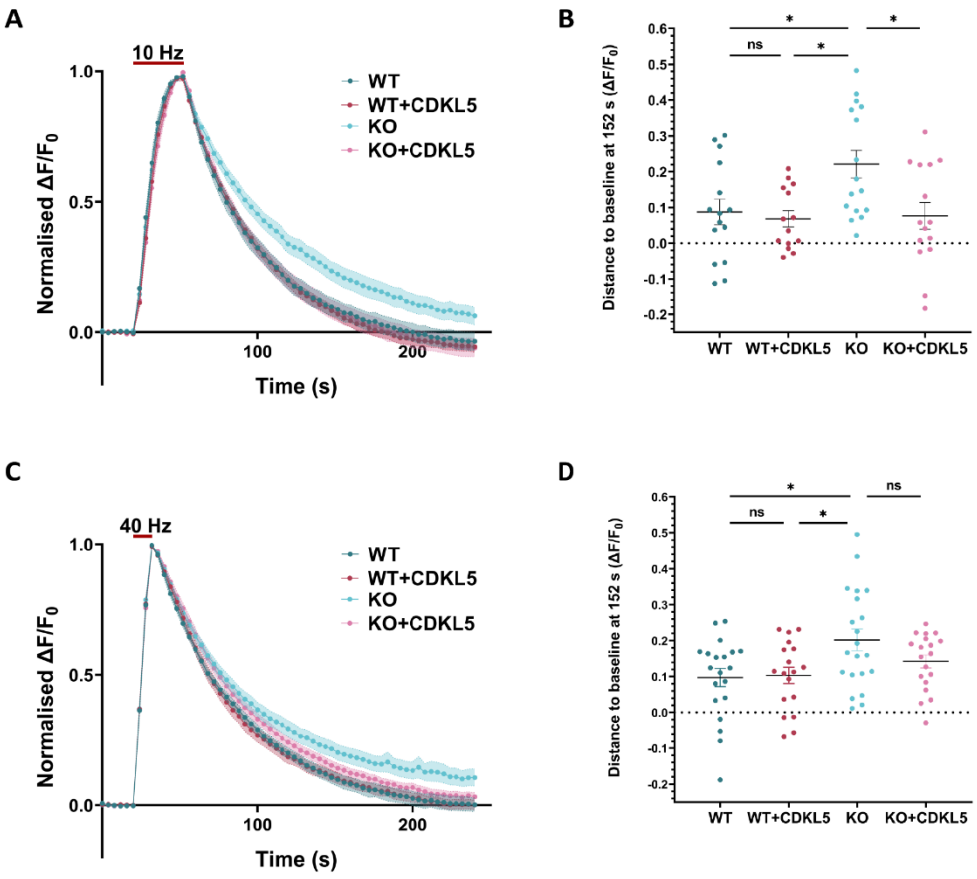

Figure 4.1 CDKL5 expression restores the speed of SV endocytosis but overexpression of CDKL5 does not impact SV endocytosis

Primary hippocampal neurons from WT and CDKL5 KO rats were co-transfected with sypHy and mCer (WT, dark turquoise; KO, dark pink) or hCDKL5_1 (WT+CDKL5, light turquoise; KO+CDKL5, light pink) at 8-9 DIV and imaged at 13-14 DIV. (**A**) Average sypHy fluorescence response from neurons stimulated at 10 Hz for 30 s (red bar) normalised to the stimulation peak. (**B**) Average sypHy fluorescence measuring the distance from baseline at 152 s. Scatter plots indicate mean ± SEM. ns, not significant, *p < 0.05 by two-way ANOVA followed by Tukey's multiple comparison test. WT n = 15, WT+CDKL5 n = 14, KO n = 16, KO+CDKL5 n = 15 coverslips from 4 independent preparations. (**C**) Average sypHy fluorescence response from neurons stimulated at 40 Hz for 10 s (red bar) normalised to the stimulation peak. (**D**) Average sypHy fluorescence measuring the distance from baseline at 152 s. Scatter plots indicate mean ± SEM. ns, not significant, *p < 0.05 by two-way ANOVA followed by Tukey's multiple comparison test. WT n = 20, WT+CDKL5 n = 18, KO n = 21, KO+CDKL5 n = 19 coverslips from 5 independent preparations.

4.2.1.2 The kinase activity of CDKL5 is important for regulating SV endocytosis

Structurally, CDKL5 consists of two distinct regions: an N-terminal kinase domain that has a well-defined tertiary structure and a long C-terminal tail that occupies the remaining two thirds of the protein and contains multiple intrinsically disordered regions. Functionally, the catalytic domain mediates the phosphorylation activity of CDKL5, while the C-terminal tail has been implicated in many functions possibly including that of supporting the catalytic activity of CDKL5. To understand the role of each domain in SV endocytosis and determine whether CDKL5 phosphorylation activity is important, we generated truncated constructs of CDKL5 comprising either the

kinase domain (ΔC; aa 1-297) or the C-terminal tail (Δkinase; aa 298-960) (Figure 4.2A). All constructs were tagged with mCer at their N-terminus.

Hippocampal CDKL5 KO neurons were co-transfected with sypHy and either full-length CDKL5 or one of the deletion mutants, whereas CDKL5 KO neurons transfected with the mCer empty vector acted as control. The expression level of these mutants is examined in 4.2.1.4 subsection. Their ability to restore SV endocytosis kinetics was assessed by sypHy imaging stimulating neurons at either 10 Hz for 30 s or at 40 Hz for 10 s. We observed that ΔC was sufficient to rescue the impairment in SV endocytosis similarly to full-length CDKL5 (Figure 4.2B-E). In contract, Δkinase was not able to fully rescue the SV endocytosis slowing suggesting that the C-terminal tail is less important for SV endocytosis. As a result, CDKL5-mediated phosphorylation is essential for SV retrieval in hippocampal nerve terminals.

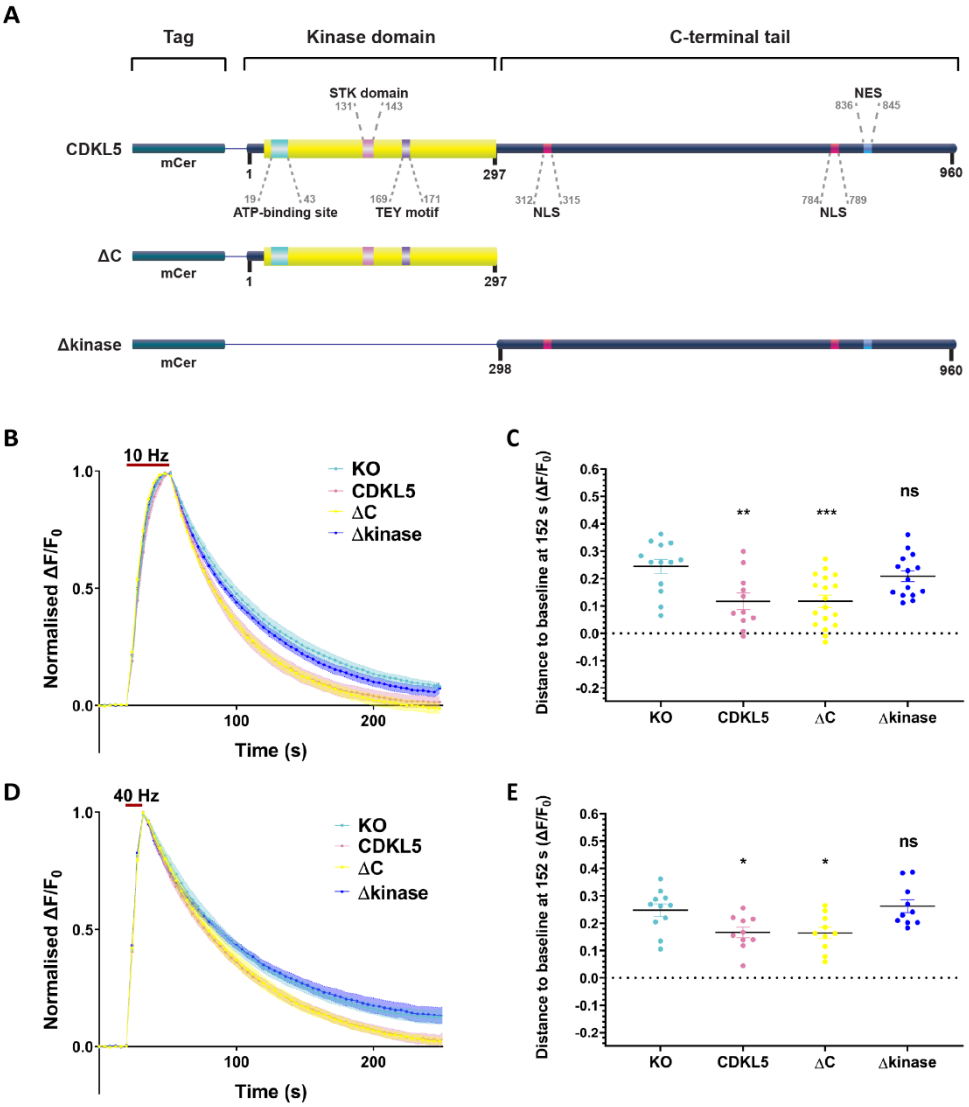

Figure 4.2 The kinase domain of CDKL5 is sufficient to restore the SV endocytosis kinetics

(**A**) Schematic representation of the structural domains of CDKL5. Truncated versions of CDKL5 were generated comprising either the kinase domain (ΔC) or the C-terminal tail (Δkinase). All constructs were tagged with mCer at their N-terminal end. The numbering refers to the human sequence. (**B**) Primary hippocampal neurons from CDKL5 KO rats were co-transfected with sypHy and

mCer (KO, light turquoise), hCDKL5_1 (CDKL5, light pink), the kinase domain (ΔC, yellow) or the C-terminal tail (Δkinase, blue) at 8-9 DIV and imaged at 13-14 DIV. Average sypHy fluorescence response from neurons stimulated at 10 Hz for 30 s (red bar) normalised to the stimulation peak. (**C**) Average sypHy fluorescence measuring the distance from baseline at 152 s. Scatter plots indicate mean ± SEM. ns, not significant, **p < 0.01, ***p < 0.001 by one-way ANOVA followed by Dunnett's multiple comparison test. KO *n* = 13, CDKL5 *n* = 11, ΔC *n* = 18, Δkinase *n* = 15 coverslips from 4 independent preparations of neuronal cultures. (**D**) Average sypHy fluorescence response from neurons stimulated at 40 Hz for 10 s (red bar) normalised to the stimulation peak. (**E**) Average sypHy fluorescence measuring the distance from baseline at 152 s. Scatter plots indicate mean ± SEM. ns, not significant, *p < 0.05 by one-way ANOVA followed by Dunnett's multiple comparison test. KO *n* = 11, CDKL5 *n* = 10, ΔC *n* = 10, Δkinase *n* = 10 coverslips from 3 independent preparations of neuronal cultures.

4.2.1.3 Impairment of SV endocytosis kinetics contributes to CDD pathogenicity

In CDD, most pathogenic mutations are found within the kinase domain and have been widely admitted resulting in loss of protein function (Hector *et al.*, 2017; Munoz *et al.*, 2018). So, we hypothesised that point mutations introduced within the kinase domain of CDKL5 are loss-of-function in terms of SV endocytosis. To address this question, we generated two mutated forms of full-length CDKL5 bearing the missense mutations K42R and R178P, respectively (Figure 4.3A). Although K42R has not been identified in a CDD patient to the best of our knowledge, it is a catalytically-inactive derivative of

CDKL5 blocking its ability to bind ATP (Lin *et al.*, 2005). On the other hand, R178P was initially reported in CDD patients of both sexes exhibiting severe neurological features (Elia *et al.*, 2008; Nemos *et al.*, 2009). Again, the expression level of these mutants is examined in 4.2.1.4 subsection. Neurons lacking CDKL5 were co-transfected with sypHy and either WT CDKL5 or one of the point mutants to evaluate SV endocytosis kinetics following stimulation at 10 Hz for 30 s or 40 Hz for 10 s. CDKL5 KO neurons transfected with the mCer empty vector were used as a control. We found that neither mutated version of CDKL5 was able to rescue the defect in SV endocytosis in contrast to WT CDKL5 (Figure 4.3B-E). These data further support that the phosphorylation activity of CDKL5 is essential for sustaining SV endocytosis kinetics and potentially indicate that defective SV endocytosis may contribute to the CDD pathogenicity.

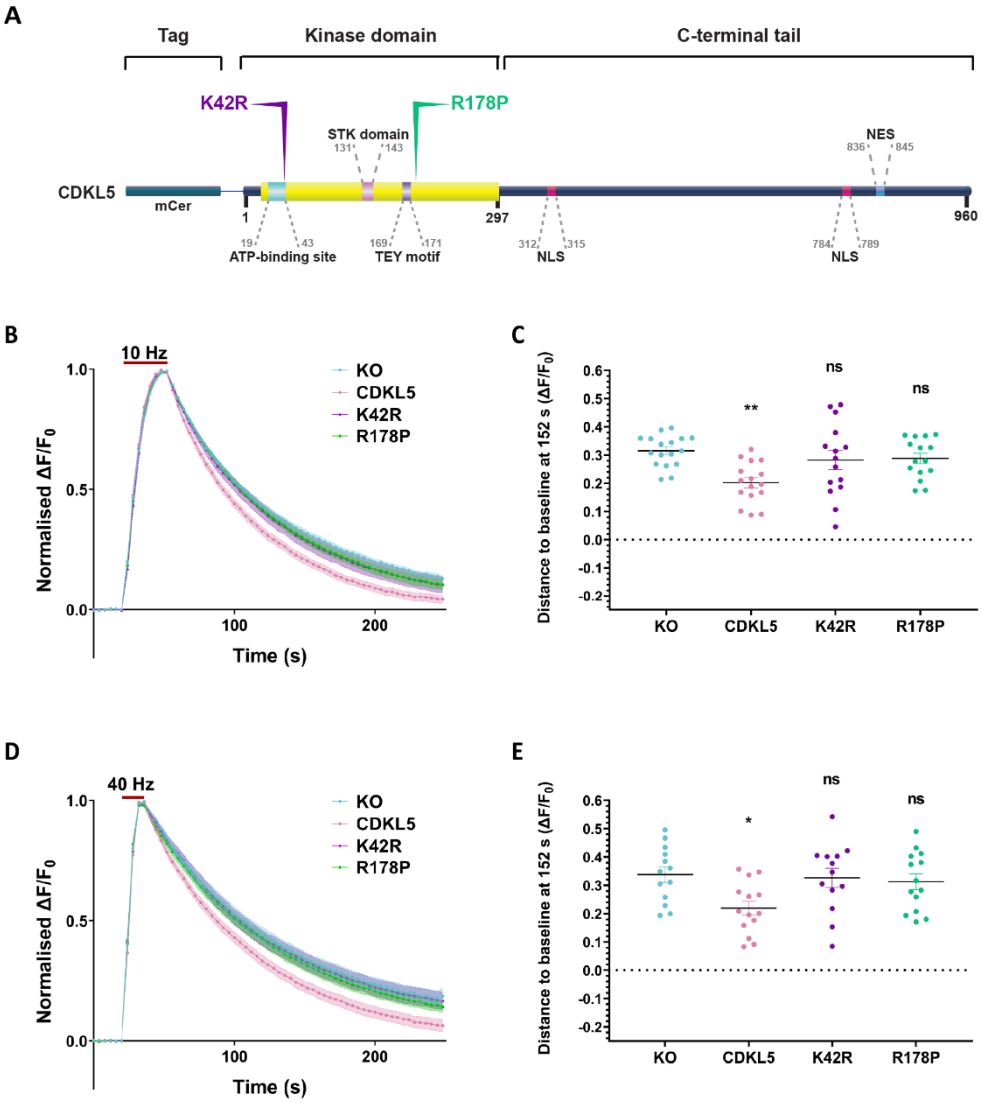

Figure 4.3 CDKL5 mutants are not able to restore the SV endocytosis kinetics

(**A**) Schematic representation of the structural domains of CDKL5. Point mutations were introduced into the kinase domain including K42R found within the ATP-binding region and R178P adjacent to the TEY motif. All constructs were tagged with mCer at their N-terminal end. The numbering refers to the human sequence. (**B-E**) Primary hippocampal neurons from CDKL5 KO rats were co-transfected with sypHy and mCer (KO, light turquoise), hCDKL5_1 (CDKL5, light pink), K42R

(purple) or R178P (green) at 8-9 DIV and imaged at 13-14 DIV. (**B**) Mean sypHy fluorescence response from neurons stimulated at 10 Hz for 30 s (red bar) normalised to the stimulation peak. (**C**) Mean sypHy fluorescence measuring the distance from baseline at 152 s. Scatter plots indicate mean ± SEM. ns, not significant, **p < 0.01 by one-way ANOVA followed by Dunnett's multiple comparison test. KO *n* = 17, CDKL5 *n* = 16, K42R *n* = 15, R178P *n* = 15 coverslips from 4 independent preparations of neuronal cultures. (**D**) Average sypHy fluorescence response from neurons stimulated at 40 Hz for 10 s (red bar) normalised to the stimulation peak. (**E**) Average sypHy fluorescence measuring the distance from baseline at 152 s. Scatter plots indicate mean ± SEM. ns, not significant, *p < 0.05 by one-way ANOVA followed by Dunnett's multiple comparison test. KO *n* = 13, CDKL5 *n* = 14, K42R *n* = 13, R178P *n* = 14 coverslips from 4 independent preparations of neuronal cultures.

4.2.1.4 Expression of CDKL5 mutants in hippocampal neurons

From all CDKL5 constructs examined in this chapter for their ability to restore the speed of SV retrieval, only the kinase domain is able to rescue the SV endocytosis defect in neurons lacking CDKL5. As a result, this raises the question whether the inability of the remaining CDKL5 constructs to rescue SV endocytosis impairment is due to their inadequate activity or a consequence of limited expression and/or defective subcellular redistribution. To study this, we initially assessed by immunolabelling the protein levels of CDKL5 expression for the full-length protein, its C-terminal tail as well as K42R and R178P. Primary hippocampal neurons from WT rats were

transfected with each CDKL5 construct at 8-10 DIV and fixed at 15 DIV prior to being labelled for CDKL5 and GFP (Figure 4.4A). WT neurons transfected with the mCerC1 empty vector acted as a control. The CDKL5 fluorescence intensity was measured within the region of cell bodies of transfected neurons, as identified by GFP staining, and normalised to that of untransfected cell bodies (usually average intensity of 5 cell bodies). Background intensity was subtracted from both transfected and untransfected neuronal bodies. We observed that all CDKL5 constructs were elevated with respect to the mCerC1 control with their protein levels being equivalent to WT CDKL5 or even higher in the case of the C-terminal tail (Figure 4.4B).

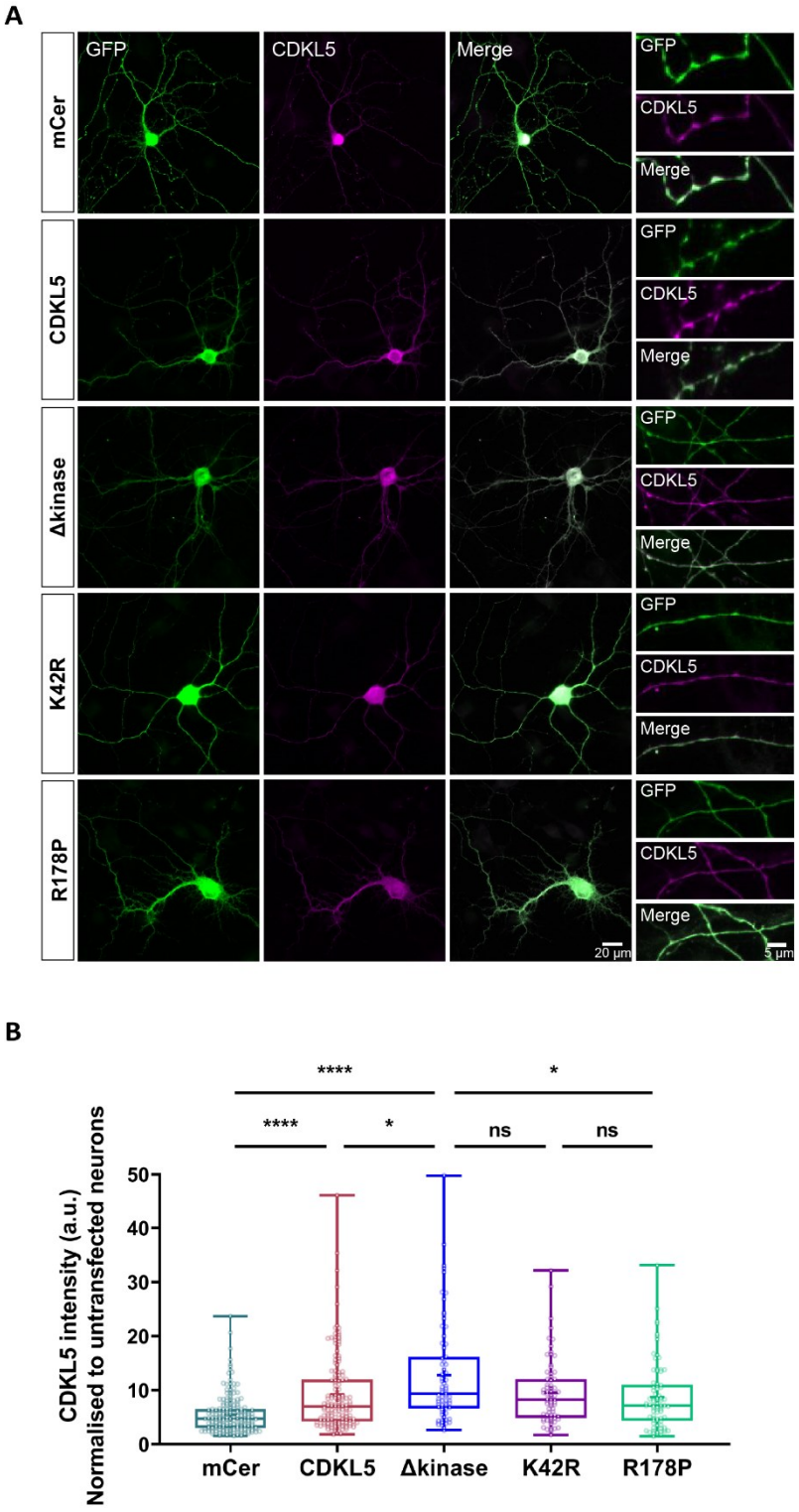

Figure 4.4 CDKL5 mutants are expressed in primary hippocampal cultures

(**A**) Primary cultures of hippocampal neurons were transfected at 8-10 DIV and fixed at 15 DIV. Representative images of neurons and axons expressing mCer (control) and various CDKL5 constructs labelled for GFP (green) and CDKL5 (magenta). Merged images of GFP and CDKL5. Scale bar, 20 μm (neurons) and 5 μm (axons). (**B**) Quantification of CDKL5 fluorescence intensity of cell bodies normalised to untransfected neurons. Background was subtracted in all cases. Box plots present median with IQR indicating min-max whiskers. ns, not significant, *p < 0.05, ****p < 0.0001 by Kruskal-Wallis test followed by Dunn's multiple comparison test, + indicates mean value. mCer *n* = 191, CDKL5 *n* = 149, Δkinase *n* = 71, K42R *n* = 71, R178P *n* = 78 neurons from 4 independent preparations of neuronal cultures.

4.2.2 CDKL5 interacts with Amph1 *in vivo*

One way to further understand the role of CDKL5 in SV recycling is to explore possible interactions with presynaptic proteins. We found previously that the phosphorylation activity of CDKL5 is essential for preserving the rate of SV endocytosis, which suggests that there is at least one CDKL5 substrate at the presynapse. While it is expected a potential substrate to serve also as an interacting partner of CDKL5, the opposite is not always necessary. In agreement, proteins that have been identified as potential interactors of CDKL5 through its C-terminal tail, such as PSD95, NGL1, and Rac1, have not been yet confirmed as substrates (Chen *et al.*, 2010; Ricciardi *et al.*, 2012; Zhu *et al.*, 2013). For this reason, we tested whether Amph1 interacts with CDKL5 given that it is an *in vitro* substrate of CDKL5 and the only presynaptic

candidate to be identified so far. To do that, an adult rat brain was homogenised and incubated with an antibody against either CDKL5 or Amph1. A random antibody against the endocytic protein EHD was used as a control. The homogenate was pre-cleaned prior to incubation with antibodies using appropriate amount of agarose beads to enhance specificity. We found that both Amph1 and CDKL5 were co-immunoprecipitated using a CDKL5 or Amph1 antibody, respectively (Figure 4.5). We also confirmed their interaction in the adult mouse brain (Appendix - Supplementary Figure 2). This indicates that CDKL5 binds to Amph1 *in vivo*, although their interaction seems to be weak in relation to the input level.

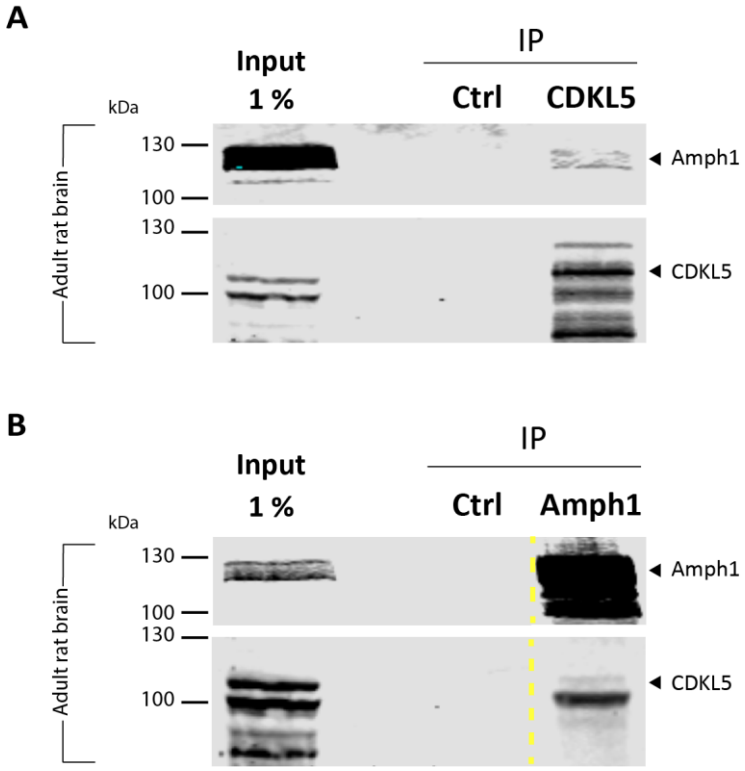

Figure 4.5 CDKL5 interacts with Amph1 ***in vivo***

(**A**) Immunoprecipitation from adult rat brain lysates with CDKL5. Samples were analysed by immunoblotting for CDKL5 and Amph1. A random antibody against EHD was used as control. CDKL5 reacted with Amph1 in the rat brain. (**B**) Immunoprecipitation from adult rat brain lysates with Amph1. Samples were analysed by immunoblotting for CDKL5 and Amph1. A random antibody against EHD was used as control. Amph1 reacted with CDKL5 in the rat brain. $n = 1$ animal.

4.2.3 Exploring the CDKL5-mediated phosphorylation of Amph1

4.2.3.1 Generation of a phosphospecific antibody targeting Amph1-S293

The identification of Amph1 as an *in vivo* interacting molecule of CDKL5 in the rodent brain in combination with previous studies revealing Amph1-S293 as an *in vitro* target of CDKL5 (Sekiguchi *et al.*, 2013; Katayama *et al.*, 2015) suggest that it is likely for CDKL5 to also facilitate phosphorylation of Amph1 *in vivo*. In order to explore the CDKL5-mediated phosphorylation of Amph1, we generated a rabbit polyclonal phosphospecific antibody against Amph1-S293 that is located within the Amph1 PRD and is part of the CDKL5 consensus motif (Figure 4.6A). For this, a rabbit was injected with the synthesised peptide PVRPR**S**^{293}PSQTRC to elicit an immune response and polyclonal phosphoantibodies were obtained from the serum. To test its specificity, we expressed recombinant GST-conjugated constructs of WT Amph1 (GST-Amph1) and two Amph1 phosphomutants including a null (GST-S293A) and a mimetic version (GST-S293E) in bacteria. Previous studies in the lab suggested that the N-bar domain of Amph1 makes its expression in bacteria difficult and, therefore, this domain was omitted in all cases. All GST-fused constructs of Amph1 were incubated with rat synaptosomal lysates and used as baits for pull-down assays that will be discussed in Chapter 5. A GST-containing empty vector was used as a control. The specificity of the pAmph1-S293 antibody was assessed by western blotting. This approach revealed that the pAmph1-S293 antibody reacted exclusively with the phosphomimetic GST-S293E version, although all GST-fused proteins were sufficiently expressed as the CBB staining indicated (Figure 4.6B). This confirms that the phosphoantibody is highly specific for Amph1-S293.

Amph1 is known to undergo dephosphorylation coupled to neuronal activity (Bauerfeind *et al.*, 1997; Micheva *et al.*, 1997b). Accordingly, Amph1-S293 is one of the phosphosites that is dephosphorylated following high frequency stimulation (Murakami *et al.*, 2006). So, we next focused on reassessing whether Amph1-S293 was dephosphorylated in an activity-dependent manner. To do this, we treated hippocampal neurons with 50 mM KCl for 2 min to induce neuronal depolarisation. We found that phosphorylation at Amph1-S293 was abolished upon stimulation suggesting also that the pAmph1-S293 antibody is a sufficient reporter for this. Since the stimulation-dependent dephosphorylation of various proteins in the nerve terminal is mediated by calcineurin (Nichols *et al.*, 1994; Bauerfeind *et al.*, 1997; Marks & McMahon, 1998; Cousin & Robinson, 2001), we next examined whether Amph1-S293 dephosphorylation occurs via calcineurin or another phosphatase. In addition to KCl-stimulation, neurons were treated with either 10 μM cyclosporin A or 100 nM calyculin A as an inhibitor of calcineurin and protein phosphatase 1 (PP1)/2A (PP2A), respectively. PP1 and PP2A are responsible for the main phosphatase activity in presynaptic terminals under basal and depolarising conditions, although the major dephosphorylation activity that is coupled to Ca^{2+} influx and, thus, neuronal activity is attributed to calcineurin (Sim *et al.*, 1991). We found that treatment with cyclosporin A prevented the activity-dependent dephosphorylation at Amph1-S293 demonstrating therefore that it is mediated by calcineurin (Figure 4.6C). In contrast, treatment with calyculin A failed to prevent Amph1-S293 dephosphorylation. The phosphorylation profile of Amph1-S293 was similar to that of pDyn1-S774, an established site that undergoes calcineurin- and activity-dependent dephosphorylation (Liu *et al.*, 1994; Tan *et al.*, 2003; Smillie & Cousin, 2005; Armbruster *et al.*, 2013). Overall, these findings suggest that

Amph1-S293 undergoes calcineurin-facilitated dephosphorylation linked to neuronal activity and its phosphorylation dynamics are efficiently reported by the pAmph1-S293 antibody.

Treatment with high KCl concentration represents an intense approach to trigger neuronal depolarisation. Alternatively, we examined electrical stimulation during which neurons were stimulated at either 10 Hz for 30 s or 40 Hz for 10 s in the presence or absence of 50 μM AP5 and 10 μM CNQX to prevent glutamate receptor activity. In this way, the experimental conditions could be also consistent with the stimulation parameters that were applied during our functional studies. Western blot analysis showed that Amph1-S293 was dephosphorylated after stimulation at both frequencies with the intensity of the upper band to be eliminated compared to the control (Figure 4.6D). In agreement, phosphorylation of the Dyn1-S774 was reduced, although not abolished. The presence of AP5/CNQX inhibitors did not have any impact on the dephosphorylation level of Amph1-S293 at either frequency implying that its (de)phosphorylation is independent of any postsynaptic activity or recurrent spontaneous activity in culture. Hence, depolarisation of primary hippocampal neurons by field-stimulation was able to reproduce the activity-dependent dephosphorylation that Amph1 undergoes at S293 at both 10 and 40 Hz stimulation frequencies similarly to KCl stimulation.

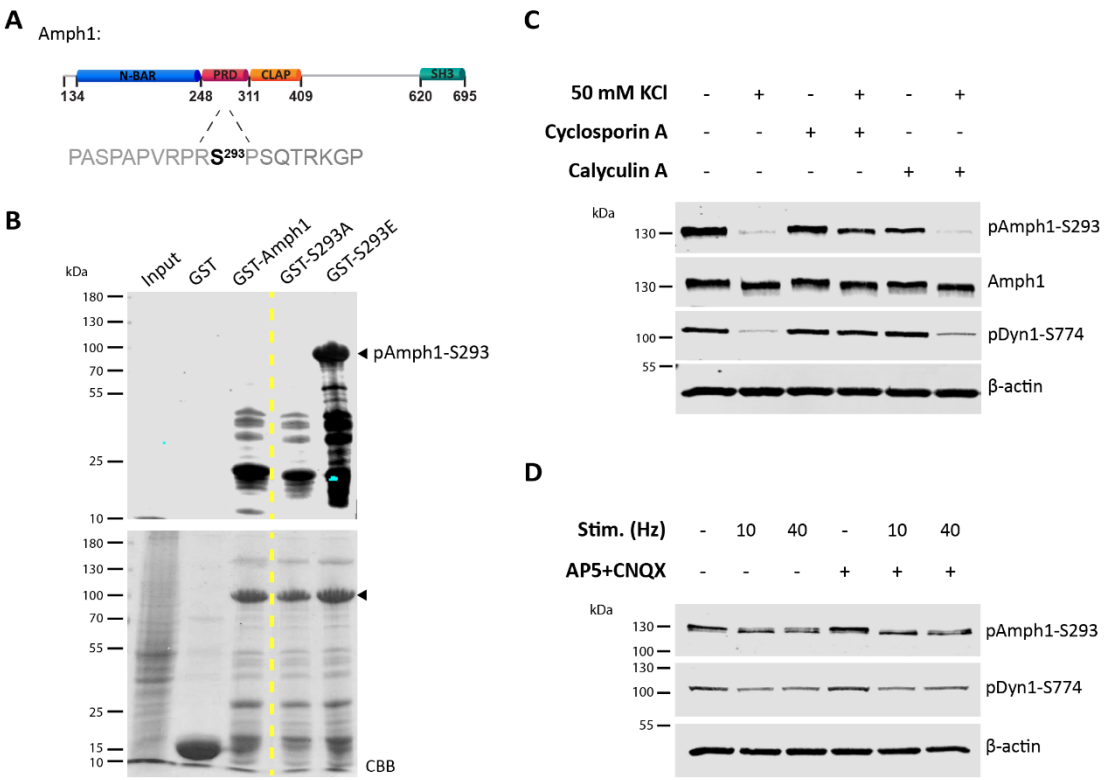

Figure 4.6 Validation of a phosphoantibody targeting Amph1-S293

The pAmph1-S293 antibody reports the phosphorylation dynamics of Amph1-S293 in primary hippocampal neurons. (**A**) Schematic representation of the structural domains of Amph1. The sequence PVRPRS[293]PSQTRC is located within the Amph1 PRD and was used as an antigen for the production of the pAmph1-S293 antibody. The numbering refers to the human sequence. (**B**) The GST-fused phosphomutants of Amph1 lacking the N-BAR and SH3 domains, S293A and S293E, were generated and expressed in *Escherichia coli*. The pAmph1-S293 antibody detects robustly only the phosphomimetic S293E fusion protein. All GST-fused proteins were adequately expressed as the CBB staining indicates. (**C**) Neuronal cultures at 14-15 DIV were stimulated with 50 mM KCl for 2 min to trigger neuronal depolarisation resulting in dephosphorylation of Amph1-S293. Neurons were treated with 10 μM

cyclosporin A, a calcineurin inhibitor, blocking the Amph1-S293 dephosphorylation. Treatment with 100 nM calyculin A, an inhibitor of PP1/PP2A phosphatases, failed to block dephosphorylation at Amph1-S293. The phosphorylation status at Dyn1-S774 was also tested as this site is known to undergo activity-dependent dephosphorylation mediated by calcineurin. (**D**) Neurons at 14-15 DIV were stimulated with 300 APs at 10 Hz or 400 APs at 40 Hz in the presence or absence of glutamate receptor inhibitors including 50 μM AP5 and 10 μM CNQX. Neuronal lysates were collected and analysed by western blotting. Dephosphorylation at Amph1-S293 occurs at both frequencies independently of AP5 and CNQX similarly to Dyn1-S774.

4.2.3.2 Phosphorylation of Amph1 at S293 occurs independently of CDKL5

Since the phosphorylation activity of CDKL5 plays a role in SV retrieval, we next focused on investigating the potential CDKL5-facilitated phosphorylation of Amph1, the only identified substrate of CDKL5 at the presynaptic terminal to date. A previous study determined Amph1-S293 as an *in vitro* phosphorylation site of CDKL5 (Sekiguchi *et al.*, 2013; Katayama *et al.*, 2015), while the phosphorylation dynamics at S293 is thought to control affinity for the presynaptic protein endophilin A1 (Murakami *et al.*, 2006; Sekiguchi *et al.*, 2013). This implies that the S293 residue is a potentially important target of CDKL5 at the presynapse. Indeed, S293 has been identified as the most abundant *in vivo* phosphosite on Amph1 highlighting the physiological importance of this site (Craft *et al.*, 2008). In support, S293 resides within the consensus motif that CDKL5 preferentially phosphorylates *in vivo*

(Baltussen *et al.*, 2018; Munoz *et al.*, 2018). Given that Amph1 regulates SV regeneration, we first examined whether CDKL5 phosphorylates Amph1 at S293 regulating thus SV endocytosis at the presynaptic terminal. WT and CDKL5 KO neurons at 14-15 DIV were treated with 50 mM KCl and left to repolarise for different periods of increased duration to determine whether the absence of CDKL5 impacted on rephosphorylation of this residue prior to lysis and analysis by western blotting (Figure 4.7A). Neuronal depolarisation was induced by KCl application to allow a complete dephosphorylation of S293, which provided the widest possible dynamic range to visualise changes in its rephosphorylation. The phosphoantibody against MAP1S-S900 was used as a positive control given that this site is an endogenous phosphosite of CDKL5 (Baltussen *et al.*, 2018; Munoz *et al.*, 2018). We found that the phosphorylation levels of Amph1-S293 were not altered between genotypes when normalised to the total Amph1 levels either pre- or post-stimulation (Figure 4.7B) supporting that Amph1-S293 is phosphorylated *in vivo* despite the absence of CDKL5.

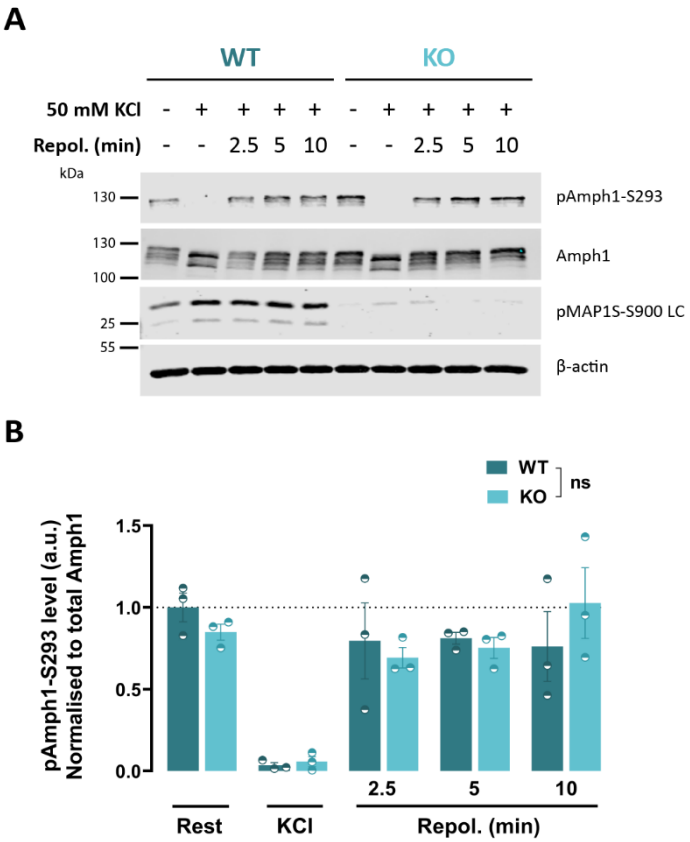

Figure 4.7 Amph1-S293 is subject to phosphorylation independently of CDKL5

(**A**) Primary hippocampal neurons from WT and CDKL5 KO rats were treated with KCl and allowed to be rephosphorylated for 2.5, 5, and 10 min. Neurons were lysed at 14-15 DIV and analysed by western blotting for pAmph1-S293, total Amph1, pMAP1S-S900 as a positive control, and β-actin as a loading control. The numbering refers to the human isoforms. (**B**) Quantification of the phosphorylation levels of Amph1 at S293 was performed by determining relative band intensities normalised to the total amount of Amph1. Background was subtracted in all cases. Bars indicate mean ± SEM. ns, not significant by two-way ANOVA followed by Sidak's multiple comparison test. *n* = 3 coverslips/condition per genotype from 3 independent preparations of neuronal cultures.

4.2.3.3 *Phosphorylation of distinct pools of Amph1 may be regulated differentially by CDKL5*

Biochemical studies suggest that Amph1 can be found both in association with SVs and as an unbound fraction within the presynaptic cytoplasm (Lichte *et al.*, 1992; Wigge *et al.*, 1997). These two pools of Amph1 at the presynapse are likely to be differentially regulated. Although Amph1-S293 gets phosphorylated despite the absence of CDKL5 in neuronal cultures suggesting that CDKL5 might not phosphorylate this site, these were homogenised and analysed without a prior separation of Amph1 distinct fractions. To test whether one of the pools of Amph1 undergoes phosphorylation by CDKL5, we performed subcellular fractionation of adult WT and CDKL5 KO rat brains to crudely purify a synaptosomal P2 and an SV-enriched LP2 fraction. Synaptosomal subfractions, including the membranous LP1 and cytosolic LS1 fractions, were analysed by fluorescent western blotting to evaluate the phosphorylation levels of Amph1-S293 between genotypes (Figure 4.8A). We found that the phosphorylation levels of Amph1-S293 in different subfractions vary between genotypes in those fractions containing cytoplasmic Amph1 when normalised to the total Amph1 levels (Figure 4.8B). This points towards the idea that cytoplasmic, but not membrane-associated Amph1 phosphorylation is likely to be regulated differentially by CDKL5, although additional replicates would be necessary to achieve a final conclusion.

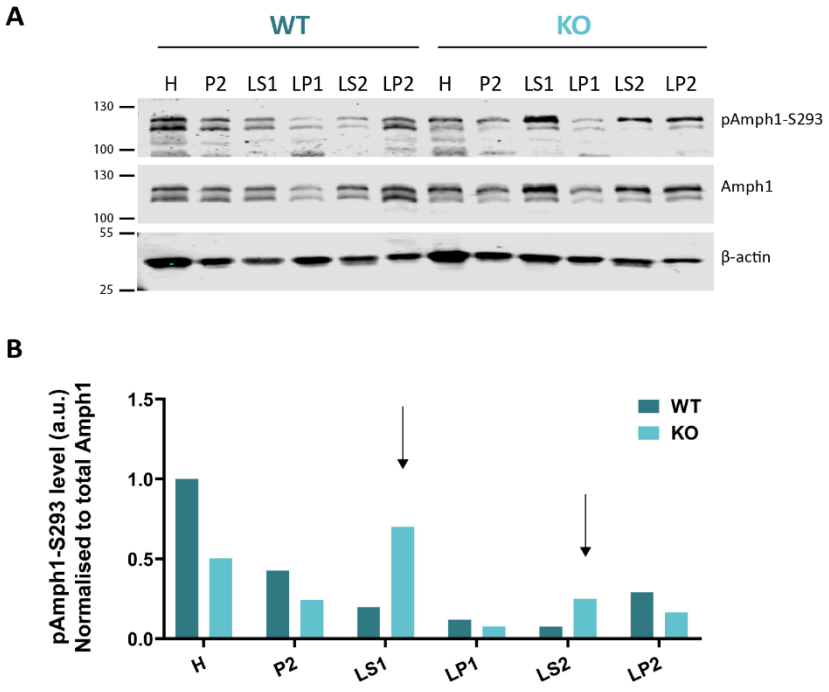

Figure 4.8 CDKL5 may regulate phosphorylation of cytosolic but not SV-bound Amph1 at presynaptic terminals

(**A**) WT and CDKL5 KO adult rat brains were homogenised in sucrose/EDTA and fractionated for the crude purification of LP2 pellets. Synaptosomal subfractions were analysed by western blotting for estimating the phosphorylation levels of Amph1-S293, total Amph1 levels, and β-actin as a loading control. (**B**) The levels of pAmph1-S293 were estimated by measuring band intensities and normalised to total Amph1. n = 1 animal per genotype.

4.2.3.4 Several kinases phosphorylate Amph1 at S293

The elevated phosphorylation levels of cytosolic Amph1-S293 in the absence of CDKL5 indicates that another kinase is responsible for its phosphorylation *in vivo*. The presence of several cytosolic kinases in the nerve terminal leads to the idea that Amph1-S293 might be phosphorylated by multiple kinases owning to the fact that this site is abundantly phosphorylated *in vivo* (Craft *et al.*, 2008). In agreement, a number of early studies showed that there are two kinases that possibly phosphorylate Amph1-S293 *in vitro* in addition to CDKL5, including Dyrk1A (Murakami *et al.*, 2006) and MAPK (Shang *et al.*, 2004), whereas Cdk5 (Floyd *et al.*, 2001; Liang *et al.*, 2007) is also reported as a kinase of Amph1 in mature neurons. In non-neuronal cells, casein kinase 2 (Doring *et al.*, 2006), and cdc2/cyclin B kinase complex (Floyd *et al.*, 2001) have been also indicated as possible Amph1 kinases.

In an attempt to unmask any potential phosphorylation of Amph1-S293 that is facilitated by CDKL5 in mature neurons and to determine whether other protein kinases substitute for CDKL5 in its absence, we treated WT and CDKL5 KO neurons at 14-15 DIV with 20 mM EGCG, 100 μM PD98059, and 50 μM roscovitine inhibitors to eliminate simultaneously the kinase activity of Dyrk1A, MAPK, and Cdk5, respectively (Figure 4.9A). Control WT and CDKL5 KO neurons were treated with appropriate amount of DMSO (< 1 %) to control for any neurotoxic effect. KCl-induced depolarisation of WT and CDKL5 KO neurons was followed by repolarisation for 10 min prior to lysis and analysis by western blotting (Figure 4.9B). We revealed that the phosphorylation levels of pAmph1-S293 were not altered between genotypes when normalised to the total Amph1 levels (Figure 4.9C). Moreover, the cocktail of kinase inhibitors abolished the rephosphorylation of Amph1-S293

post-stimulation, indicating that kinases other than CDKL5 phosphorylate this residue in culture and the contribution of CDKL5 to its phosphorylation is minor, if any. The phosphorylation of the endogenous substrate of CDKL5 pMAP1S-S900 (Baltussen *et al.*, 2018; Munoz *et al.*, 2018) in the presence of inhibitors excludes the possibility these inhibitors to act on CDKL5. Collectively, these data suggest that defective CDKL5-mediated phosphorylation of Amph1 at S293 is not responsible for impairing SV endocytosis.

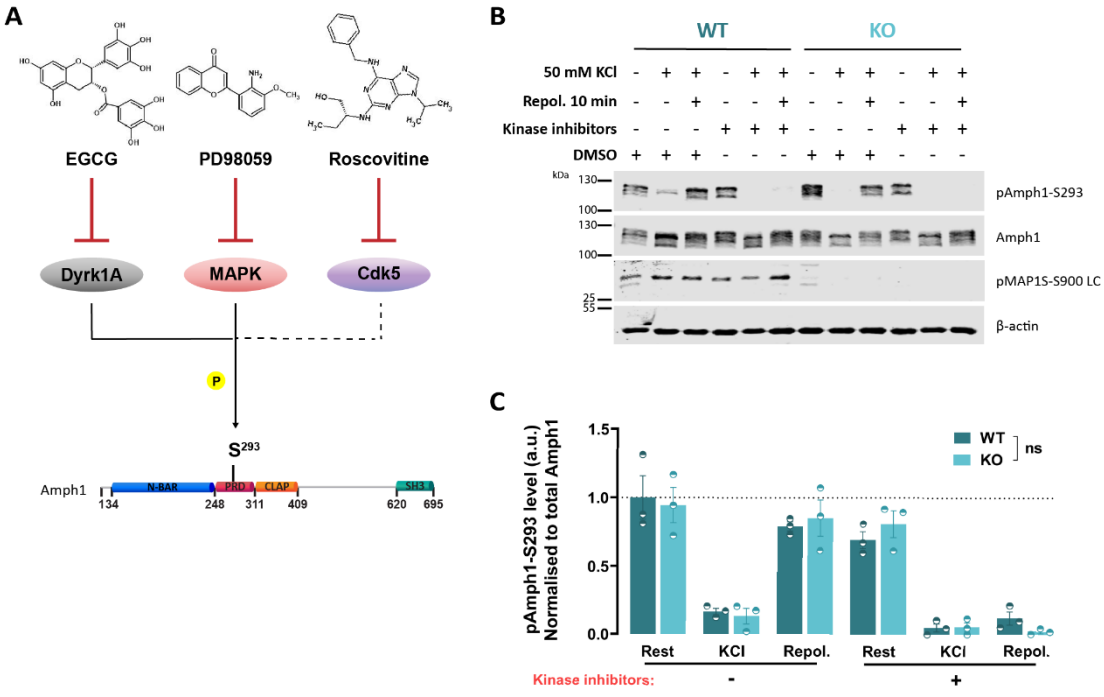

Figure 4.9 Amph1-S293 is phosphorylated by several kinases

(**A**) EGCG, PD98059, and roscovitine were combined to block the kinase activity of Dyrk1A, MAPK, and Cdk5, respectively. All three kinases phosphorylate Amph1

in neurons with Dyrk1A and MAPK (continuous lines) also targeting the residue S293 within the PRD, while it is likely the same residue to be also phosphorylated by Cdk5 (dashed line). The skeletal structures of the inhibitors were generated by ACD/ChemSketch, 2021.1.0. (**B**) Hippocampal neurons derived from WT and CDKL5 KO rats were treated with 50 mM KCl and allowed to be rephosphorylated for 10 min. Neurons were treated with the kinase inhibitor cocktail and lysed at 14-15 DIV to be analysed by western blotting for pAmph1-S293, total Amph1, pMAP1S-S900 as a positive control, and β-actin as a loading control. (**C**) Quantification of the phosphorylation levels of Amph1 at S293 was performed by determining relative band intensities normalised to the total amount of Amph1. Background was subtracted in all cases. Bars indicate mean ± SEM. ns, not significant by two-way ANOVA followed by Sidak's multiple comparison test. *n* = 3 coverslips/condition per genotype from 3 independent preparations of neuronal cultures.

4.3 Discussion

4.3.1 Elements that are critical for CDKL5-mediated SV endocytosis

CDKL5 is implicated in SV recycling in rat hippocampal neurons, since its absence results in slower rate of SV endocytosis kinetics as shown in Chapter 3. This deficit can be rescued at 10 Hz by restoring CDKL5 protein levels suggesting, therefore, that SV reformation requires the actual involvement of CDKL5 activity, and its impairment in the absence of CDKL5 is not a side effect. Overexpression of CDKL5 is also able to rescue the SV endocytosis impairment at 40 Hz, although partially, which might rise from the less

preferable activity that CDKL5 displays at higher frequencies. Considering that gene therapy attempts in order to replace the dysfunctional CDKL5 gene have already started (Gao *et al.*, 2020), it is critical to be aware of the risks that non-selective targeting at healthy neurons entails given that most CDD patients are heterozygous females. However, in the context of cultured hippocampal neurons where the SV retrieval-related phenotype is observed, overexpression of human CDKL5 in the WT background does not have any additional effect in relation to the SV endocytosis speed.

Since the impairment of SV endocytosis kinetics is specific to the loss of CDKL5, we examined a number of mutated versions of CDKL5 for their ability to restore the speed of SV retrieval in CDKL5 KO neurons in order to shed some light on the elements that are required for CDKL5 to perform its role in SV recycling. Immunolabelling analysis of the CDKL5 mutants suggests that their expression and localisation is not affected. To begin with, we first examined the role of a truncated mutant of CDKL5 that comprises its kinase domain. While a few studies investigating the role of the CDKL5 catalytic activity have selected an extended kinase sequence containing part of the C-terminal tail (1-352 aa) (Kameshita *et al.*, 2008; Sekiguchi *et al.*, 2013; Baltussen *et al.*, 2018), we focused on the shorter possible version (1-297 aa) for two reasons. Firstly, we avoided the risk to have a mislocalised product by including an NLS (312-315 aa). Secondly, we tried to determine the shortest CDKL5 kinase sequence that can be functional in our system considering its potential application for gene therapy to replace the mutated human CDKL5. Our data revealed that the kinase domain of CDKL5 alone when expressed in CDKL5-deficient neurons is sufficient to accelerate SV retrieval following stimulation at both 10 and 40 Hz. However, the CDKL5 kinase domain corrects

the SV retrieval deficit at 40 Hz only to a limited extent in agreement with our previous observations for a frequency-dependent CDKL5 activity.

Despite the physiological importance of the catalytic domain of CDKL5 as a kinase and its pathological relevance for CDD given that most patient mutations reside within the kinase domain, the C-terminal tail is also of importance. Not only it occupies the two thirds of CDKL5, but it also acts as a hub for interacting partners, controls its subcellular localisation, assists the catalytic activity of CDKL5, and, lastly, is where CDKL5 can autophosphorylate itself. For these reasons, the C-terminal tail was tested for its ability to correct the SV retrieval kinetics in the CDKL5 KO background. We found that the C-terminal tail of CDKL5 is not the most critical part of the protein in relation to its contribution to SV endocytosis, though there is a very limited extent of rescue presumably due to its role as an interface for potential interactions in the nerve terminal. However, our data also implies that the C-terminal tail is not required for assisting the phosphorylation activity of CDKL5. Overall, our findings support that the catalytic activity of CDKL5 is essential for its involvement in SV endocytosis independently of the presence of its C-terminus tail. This also endorses the frequency-dependent nature of CDKL5 activity as discussed in Chapter 3.

4.3.2 Inability of R178P and K42R human CDKL5 mutants to correct SV endocytosis

A large number of distinct missense mutations has been identified in CDD patients and, in their majority, are found within the kinase domain resulting in a dysfunctional CDKL5 product. Such an example is the missense mutation R178P that has been reported in patients of both sexes (Elia *et al.*, 2008; Nemos

et al., 2009). What is interesting about R178P mutant is that is accompanied by severity of symptoms especially in the case of the male subject, despite the fact that it is not localised within the characteristic motifs of the CDKL5 kinase domain. In addition to R178P, different substitutions of the residue R178, including R178Q and R178W, are also reported in CDD patients (MacKay *et al.*, 2021) indicating that it is a sensitive location on CDKL5 where multiple alterations can turn out to be pathogenic. Lastly, examining the role of a CDKL5 mutation that has been found in a male patient might be more relevant for our experimental system given that all neuronal cultures were produced from male rats. We revealed that expression of the full-length human CDKL5 bearing the missense mutation R178P in CDKL5 KO neurons is not able to correct the speed of SV endocytosis both at 10 and 40 Hz. In these experiments, we mutated the full-length CDKL5 in an attempt to mimic the disease conditions, although we would expect a mutated version of the kinase domain alone to behave in a similar way.

Given that CDKL5-mediated phosphorylation is critical for SV endocytosis, the inability of R178P to correct its kinetics suggests that it inhibits the catalytic activity of CDKL5. This occurs possibly by modulating the (auto)phosphorylation of the neighbouring TEY motif within the activation loop of the kinase (Lin *et al.*, 2005), although its (auto)phosphorylation is debatable (Katayama *et al.*, 2020). As the mechanism through which R178P abolishes the CDKL5 kinase activity is not clear, we also examined the kinase-inactive mutant K42R that prevents ATP binding to the substrate docking groove, despite that it has not been reported to a CDD patient to the best of our knowledge. The inability of K42R to rescue the SV endocytosis deficit at both 10 and 40 Hz stimulation frequencies confirms the significance of the kinase activity of CDKL5 for proper SV reformation from the plasma

membrane. Furthermore, the lack of rescue by both R178P and K42R highlights the potential contribution of defective SV recycling to CDD onset.

4.3.3 CDKL5-mediated phosphorylation at the central nerve terminal

CDKL5-dependent phosphorylation is necessary for SV reformation leading to the idea that CDKL5 has one or more potential substrates at the presynapse. As discussed in Chapter 3, there are several mechanisms underlying CDKL5-facilitated SV retrieval with the most prominent involving its phosphorylation activity towards candidates of the endocytosis protein machinery. Amph1 is the only well-established endocytic protein so far that is known to be an *in vitro* substrate of CDKL5 (Sekiguchi *et al.*, 2013; Katayama *et al.*, 2015). In support, using a co-immunoprecipitation assay, we demonstrated that CDKL5 and Amph1 interact also with each other in the rat as well as mouse brain. Amph1 bears the CDKL5 consensus motif within its PRD with S293 being the specific phosphosite targeted (Sekiguchi *et al.*, 2013). Mass spectrometric analysis of rat brains has revealed that S293 is abundantly phosphorylated *in vivo* emphasizing the significance of its phosphorylation for proper Amph1-mediated endocytosis possibly via controlling the formation of a complex with the endocytic protein endophilin A1 and recruiting it to the endocytic pit (Murakami *et al.*, 2006; Craft *et al.*, 2008; Sekiguchi *et al.*, 2013).

The study of the phosphorylation of Amph1-S293 upon loss of CDKL5 in rat hippocampal neurons required the generation of a phosphoantibody against Amph1-S293. The specificity of this phosphoantibody at detecting the phosphomimetic mutant of Amph1, S293E, in contrast to the phosphonull S293A, reinforces that it is a valid reporter of the phosphorylation status at Amph1-S293. Using this phosphoantibody, we also demonstrate that Amph1-

S293 phosphorylation is modulated by neuronal activity, since neuronal depolarisation induced by either KCl treatment or field stimulation at 10 and 40 Hz leads to its dephosphorylation independently of any postsynaptic or spontaneous presynaptic activity. Treatment with cyclosporin A, a calcineurin inhibitor, blocked S293 dephosphorylation induced by KCl in contrast to calyculin A, an inhibitor of PP1 and PP2A, indicating that calcineurin is responsible for mediating the activity-dependent Amph1-S293 dephosphorylation. This comes as no surprise given that Amph1 is known to undergo calcineurin-mediated dephosphorylation coupled to neuronal activity and other endocytosis proteins, such as Dyn1, are regulated in a similar manner (Bauerfeind *et al.*, 1997; Anggono *et al.*, 2006).

Analysis of the phosphorylation levels at Amph1-S293 shows that there is no change in CDKL5-deficient neurons before or after neuronal depolarisation with KCl. Similarly, no difference is observed after increasing periods of repolarisation following treatment with KCl. Moreover, neurons lacking CDKL5 undergo calcineurin-mediated dephosphorylation similarly to WT neurons and thus we expect the loss of CDKL5 not to affect either calcineurin levels or its dephosphorylation activity at the presynapse. Except for CDKL5, a number of other kinases has been reported to phosphorylate Amph1 including Dyrk1A, MAPK, Cdk5 with the first two possible targeting also the S293 residue according to *in vitro* assays and/or studies in non-neuronal cell lines (Tomizawa *et al.*, 2003; Shang *et al.*, 2004; Murakami *et al.*, 2006; Liang *et al.*, 2007). It is not unlikely therefore that loss of CDKL5 tiggers the activity of other kinases of Amph1-S293 that compensate for its absence. For example, CDKL5 deficiency has been suggested to enhance the activity of Dyrk1A providing a putative mechanism through which CDKL5 regulates SV endocytosis dynamics (Trovo *et al.*, 2020). Phosphorylation of several SV

recycling-related proteins have been attributed to Dyrk1A in addition to Amph1, such as synaptojanin, and AP180 (Murakami *et al.*, 2006; Murakami *et al.*, 2012; Chen *et al.*, 2014), while *de novo* mutations have been linked to autism and intellectual disability (van Bon *et al.*, 2016). Lastly, both kinases share a common preference for events occurring at mild neuronal activity (Kim *et al.*, 2010). A combination of three different inhibitors, including EGCG, PD98059 and roscovitine, blocked the activity of the above kinases and, as a result, the rephosphorylation of Amph1-S293 following KCl treatment remains compromised in WT neurons, albeit not completely eliminated as in the case of CDKL5-lacking neurons. Therefore, providing that CDKL5 indeed phosphorylates Amph1-S293, this occurs only to a very limited extent in primary neurons and other kinases normally undertake this role in the nerve terminal.

Overall, our work does not provide any evidence that prevents Amph1-S293 from being a CDKL5 endogenous substate in general. First, it is important to take into account that the potential CDKL5-facilitated phosphorylation of Amph1 at S293 was explored at a specific developmental stage when neurons reach maturity in culture. In addition, different brain regions or neuronal subpopulations, such as inhibitory neurons, may display different patterns of CDKL5 activity and, thus, Amph1-S293 phosphorylation is not unlikely to be critical for some neuronal networks more than others. Moreover, our preliminary data from analysis of synaptosomal subfractions proposes that the membranous and cytosolic pools of Amph1 may be differentially phosphorylated at S293 in rat nerve terminals, although this is not conclusive yet. Lastly, CDKL5 exerts its function preferably at milder depolarising conditions; however, neurons were treated with KCl, which is a strong way to induce depolarisation. Nevertheless, one thing is certain that CDKL5-

facilitated phosphorylation of Amph1 at S293 does not underlie the involvement of CDKL5 in SV retrieval from the plasma membrane at hippocampal boutons. Thus, the underlying mechanism remains the subject of a future study as the identification of putative endogenous substrates of CDKL5 in the nerve terminal.

4.3.4 Conclusions

In conclusion, this chapter reveals that the phosphorylation activity of CDKL5 is critical for its role in SV endocytosis at central nerve terminals. In addition, our findings demonstrate that point mutations within the CDKL5 kinase domain are loss-of-function in relation to endocytosis suggesting that dysfunctional SV retrieval may contribute to CDD onset. Using a phosphoantibody against Amph1-S293, we show that several kinases phosphorylate Amph1-S293, whereas its phosphorylation levels remain unaltered upon loss of CDKL5. Therefore, we conclude that CDKL5-mediated phosphorylation of Amph1-S293 does not underlie defective SV retrieval upon loss of CDKL5.

Chapter 5: Revisiting Amph1-mediated SV recycling at central nerve terminals

5.1 Introduction

CME is a well-characterised pathway of vesicular cargo internalisation that neurons employ to maintain neurotransmission. To date, several components have been implicated in CME including Amph1, a hydrophilic protein significantly enriched at presynaptic terminals. The human neuron-specific isoform of Amph1 contains 695 residues and is assembled by an N-BAR, a PRD, a CLAP, and an SH3 domain. Amph1 participates in different stages during clathrin-dependent membrane retrieval. For instance, it facilitates cargo recruitment in clathrin-coated pits (Wang *et al.*, 1995), induces membrane fission (Snead *et al.*, 2019; Zhukovsky *et al.*, 2019), recruits Dyn and activates its GTPase activity (Takeda *et al.*, 2018), and possibly regulates actin dynamics during scission (Yamada *et al.*, 2009).

Evidence suggests that depletion of Amph1 results in various deficits in presynaptic boutons emphasizing its importance for reliable SV recycling and neurotransmitter release. Injection of human Amph-specific autoantibodies in the rat spinal cord leads to SV depletion and reduced number of CCVs and endosome-like structures upon high frequency stimulation in GABAergic terminals (Werner *et al.*, 2016). Furthermore, primary neuronal cultures treated with autoantibodies against Amph exhibit altered composition of vSNAREs with enhanced synaptobrevin 2 but downregulated synaptobrevin 7 SV

subpopulations after prolonged stimulation (Werner *et al.*, 2016). In agreement, mice lacking Amph1 display presynaptic defects including reduced number of SVs and endosome-like structures as well as less competent SVs for a repeated round of exocytosis (Di Paolo *et al.*, 2002). Lastly, Amph seems to control the speed of fusion of dense-core vesicles in a Ca^{2+}-dependent but Dyn1-independent manner with Amph favouring fast dilation and constriction events (Llobet *et al.*, 2008). Based on these findings, it is likely that Amph1-mediated SV endocytosis not only sustains but also defines neurotransmitter release by undertaking vigorous cargo sorting, ensuring the competency of newly-regenerated SVs during increased neuronal activity, and establishing the speed of fusion events. Therefore, it comes as no surprise that mice deficient of Amph1 are susceptible to seizures (Di Paolo *et al.*, 2002).

The involvement of Amph1 in SV regeneration is dictated by various domain-specific protein-protein and protein-lipid interactions supporting thus its main functions as a membrane curvature sensor and a scaffolding protein. To begin with, the N-BAR domain of Amph1 is characterised by the presence of long stretches of amphiphilic α-helices and can either homodimerize or form heterodimers with Amph2. Amph2 is a 90-kDa protein with similar tissue expression, subcellular distribution, and structural organization with Amph1 (Wigge *et al.*, 1997). Amphipathic helices-containing dimers of Amph sense highly-bend membranes and exhibit fission-inducing activity (Peter *et al.*, 2004; Snead *et al.*, 2019). The remaining domains of Amph1 interact with some of the most critical players in CME: endophilin A1 through its PRD; clathrin and AP2 through its CLAP domain; and lastly, Dyn1 and synaptojanin 1 through its SH3 domain (Wu *et al.*, 2009). Disruption of these Amph1-mediated complexes after activity-dependent cleavage of Amph1

leads to short-term depression in hippocampal slices and inhibition of SV endocytosis in neurons (Wu *et al.*, 2007).

The PRD of Amph1 binds with high affinity to the SH3 domain of endophilin A1 (Micheva *et al.*, 1997b) in a phosphorylation-dependent manner (Murakami *et al.*, 2006; Sekiguchi *et al.*, 2013), although the precise binding sequence within the Amph1 PRD has not been defined yet. Endophilin A1 is an additional N-BAR- and SH3-containing protein that acts as a scaffolding protein during SV endocytosis (Kjaerulff *et al.*, 2011). In addition, owning to its N-BAR domain, endophilin A1 is associated with membrane remodelling prior to scission (Gallop *et al.*, 2006), while it facilitates the uncoating of newly-generated vesicles following scission (Gad *et al.*, 2000; Milosevic *et al.*, 2011). Except for its role in CME, endophilin has been implicated in fast AP2- and clathrin-independent endocytosis as well as ultrafast endocytosis (Llobet *et al.*, 2011; Boucrot *et al.*, 2015; Watanabe *et al.*, 2018). Lastly, it has been linked to regulation of fusion kinetics in chromaffin cells, independently of its endocytic roles (Gowrisankaran *et al.*, 2020). However, the impact of the interaction between Amph1 and endophilin A1 on SV recycling has not been fully explored at central nerve terminals.

In the following chapter, we aim to characterise the Amph1-mediated SV recycling with respect to distinct interactions of Amph1 with various endocytic partners at hippocampal presynaptic boutons. Using GST pull-down assays, we initially re-assessed known domain-specific interactions of Amph1 *in vitro* for a holistic view of the Amph1-centric protein network. We next focused on describing the aspects that determine the interaction of Amph1 with endophilin A1 by mapping its previously unknown binding motif within the Amph1 PRD and also studying the phosphorylation dynamics at S293, as an important *in vivo* phosphosite that resides within the

PRD. Using sypHy live-cell imaging, SV retrieval kinetics was measured in mouse nerve terminals where expression of Amph1 was silenced. Subsequently, we pursued a molecular replacement strategy to examine Amph1 mutants that are capable of fully eliminating interactions with CHC, AP2, SH3, and endophilin A1 in order to untangle the function of domain-specific Amph1 complexes in SV recycling at hippocampal boutons.

5.2 Results

5.2.1 Amph1 interacts with different endocytic proteins through distinct sites

Prior to exploring the function of Amph1 complexes in SV recycling, we verified known interactions of Amph1 with CHC, α-AP2, and Dyn1. The binding sites of CHC and α-AP2 that have been previously identified within the CLAP domain of Amph1 (Slepnev *et al.*, 2000; Olesen *et al.*, 2008) were used in this study in order to generate recombinant GST-tagged Amph1 mutants. The point mutations ^{323}FFE^{325}→SSR (GST-SSR) were introduced into rat Amph1 to test its binding to α-AP2, whereas the substitutions ^{353}DLD^{355}→HSR and ^{382}WD^{383}→SR (GST-HSR/SR) were tested together as the binding site of CHC. Given that Amph1 comprises both a PRD and an SH3 domain, it has been hypothesised that an intramolecular interaction is likely to develop in-between preventing each domain from binding to its ligands (Farsad *et al.*, 2003). In order to test any potential intramolecular binding, we generated constructs that either contain or lack the SH3 domain. At the same time, since Amph1 binds to Dyn1 through its SH3 domain (David *et al.*, 1996; Rosendale *et al.*, 2019), we expected their interaction to be blocked in the case of Amph1

deletion mutants lacking SH3 (ΔSH3). The N-BAR domain was excised from all Amph1 mutants to avoid any complications during their bacterial expression. The reason why we generated constructs devoid of the N-BAR domain is because BAR-containing proteins have not been reported in prokaryotes and thus their heterologous expression is likely to disturb membrane dynamics (Ren *et al.*, 2006; Bohuszewicz *et al.*, 2016). All Amph1 mutants together with the WT sequence (GST-WT) are depicted in Figure 5.1A.

Recombinant GST-fused Amph1 baits were bound to GSH-sepharose and incubated with rat brain synaptosomal lysates in order to perform pull-down assays. A GST-containing empty vector was included as a control for any unspecific binding to GST. The bacterial expression of all constructs was visualised by CBB staining and the potential interactions of Amph1 with CHC, α-AP2 subunits, Dyn1, and endophilin A1 were then assessed by immunoblotting (Figure 5.1B). The abnormal separation of α-AP2 subunits resulted possibly from the high protein content of the SH3-lacking GST-Amph1 constructs that run at a similar molecular weight (~100 kDa). The amount of the endocytic molecules that interacted with Amph1 was measured by densitometry and normalised to the total GST-tagged protein in the sample as revealed following CBB staining. We observed that the Amph1-HSR/SR mutation is sufficient to block interaction with CHC independently of the presence of the SH3 domain (Figure 5.1C). Accordingly, Amph1-SSR lost its ability to bind to α-AP2 subunits, whereas the binding of α-AP2 to Amph1 was compromised in constructs lacking the SH3 domain (Figure 5.1D). Furthermore, either mutation within the CLAP domain influenced the binding of both CHC and AP2 by abolishing the attachment of one and weakening the binding of the other. We also found that Amph1 devoid of SH3 was incapable of binding to Dyn1 supporting that their association occurs exclusively via the

SH3 domain (Figure 5.1E). Whilst both Amph1-SSR and Amph1-HSR/SR could bind to endophilin A1 similarly to Amph1-WT as the PRD domain remained intact (Figure 5.1F), their interaction was weaker in all constructs comprising the SH3 domain indicating possibly the formation of intramolecular bonds. These findings confirm the binding sites on Amph1 through which it associates with CME-related partners enabling therefore the study of Amph1-mediated interactions in SV recycling.

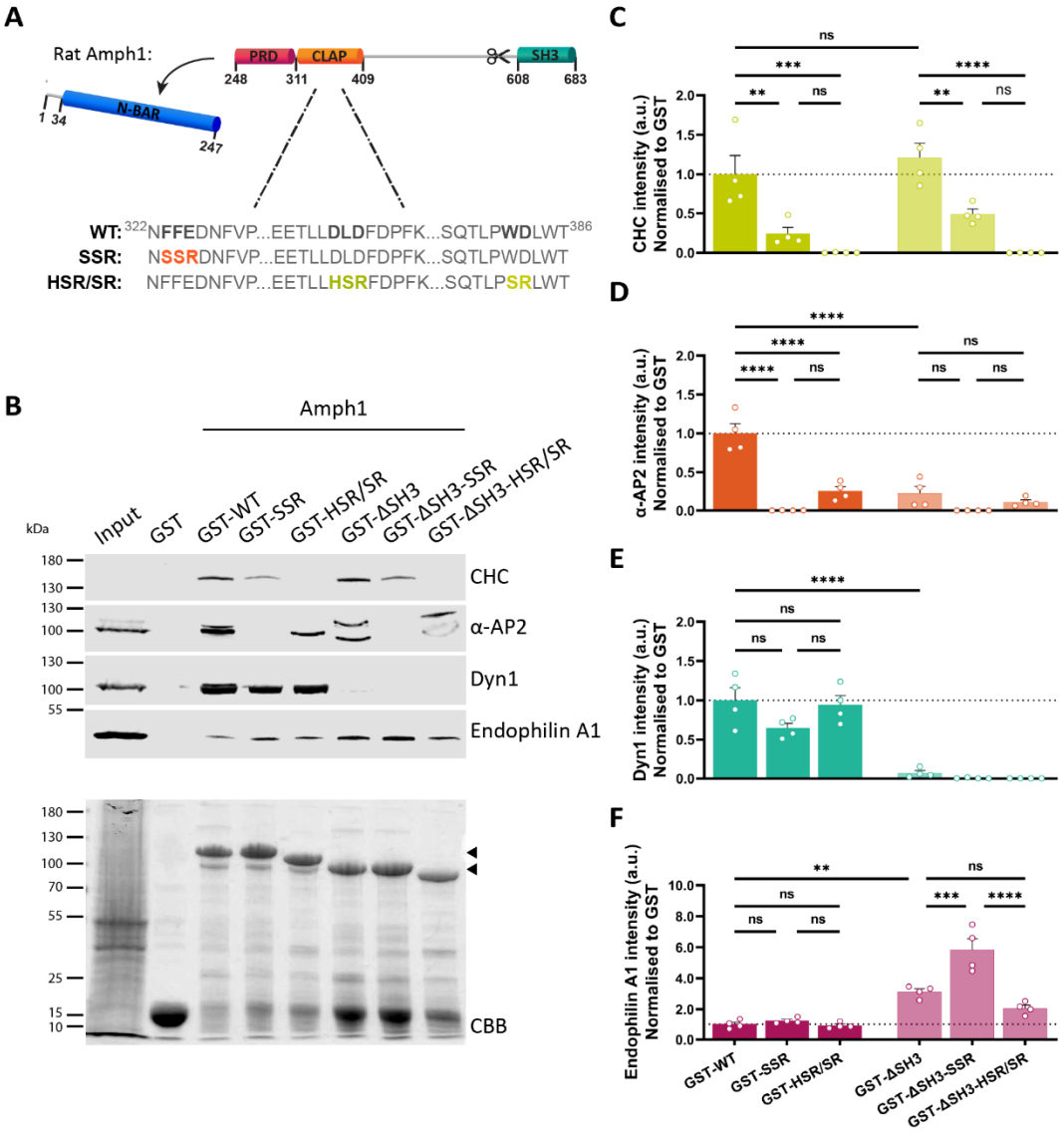

Figure 5.1 Mutations within the CLAP domain of Amph1 compromise its binding to CHC and α-AP2 subunits, while the SH3 domain controls interactions with Dyn1 and endophilin A1

(**A**) Schematic representation of the structural domains of Amph1 that were used for generating GST-fused mutants. Point mutations were introduced within the CLAP domain including FFE to SSR for the α-AP2 binding site (orange substitutions) and DLD to HSR and WD to SR for the CHC binding sites (yellow

substitutions). Constructs lacking the SH3 domain (ΔSH3) were also produced, whereas the N-BAR domain was omitted in all cases to facilitate bacterial expression. The residue numbering refers to the rat Amph1 protein. (**B**) Pull-down experiments were performed using synaptosomal lysates from rat brains and GST-tagged fusion proteins of Amph1 either including or not the SH3 domain. The binding affinity of purified endocytic proteins including endophilin A1, CHC, α-AP2 subunits, and Dyn1 was assessed by immunoblotting. A CBB staining was performed in parallel to control for GST-fused protein level. (**C**) Quantification of the binding efficacy of CHC, (**D**) α-AP2 subunits, (**E**) Dyn1, and (**F**) endophilin A1 was performed by determining relative band intensities by densitometry normalised to the level of the total GST-fused proteins. Bars indicate mean ± SEM. ns, not significant, **p < 0.01, ***p < 0.001, and ****p < 0.0001 by one-way ANOVA followed by Tukey's multiple comparison test. n = 4 synaptosomal lysates from 4 rat brains.

5.2.2 Validation of an Amph1 shRNA

A common way to evaluate the function of a protein is to assess the effects caused by its absence in the neuron. Silencing or downregulating its gene expression and blocking or modifying its protein activity are some methods widely exploited to untangle the activity of a protein. To assess the function of Amph1 in SV recycling, we generated an shRNA vector against mouse Amph1 (shAmph1) in order to downregulate its expression in primary hippocampal neurons at the post-transcriptional level. Given that it would be used for sypHy live-cell imaging, shAmph1 was designed to also express sypHy in

order to avoid additional transfections. We initially validated shAmph1 for its ability to block Amph1 expression by immunofluorescence using a scrambled vector as a control. Primary neuronal cultures derived from WT mouse hippocampi were transfected with shAmph1 or the scrambled control at 8-10 DIV and fixed at 15 DIV prior to labelling for Amph1 and GFP (Figure 5.2A). Quantification of Amph1 fluorescence intensity of transfected cell bodies, as indicated by GFP staining, normalised to the intensity of untransfected cell bodies showed that shAmph1 led to around 25 % reduction of Amph1 expression compared to the scrambled control (Figure 5.2B). In addition, we did not observe any profound morphological defects in our neuronal cultures following silencing of Amph1 expression.

To validate the impact of Amph1 in SV recycling and also explore whether the shAmph1-mediated decrease in Amph1 expression is sufficient to cause any defects in SV recycling, we transfected hippocampal neurons in culture with either shAmph1 or the scrambled control at 8-10 DIV and performed sypHy live-cell imaging at 14-15 DIV. Neurons were stimulated at 10 Hz for 30 s to trigger slow endocytosis that is mainly attributed to CME. The sypHy fluorescence was normalised to the stimulation peak to allow for comparison of endocytosis kinetics (Figure 5.2C). To quantify the kinetics of SV retrieval, we measured the distance from the baseline at 152 s, since endocytosis was quite slow to allow for τ or rate decay estimation in certain cases by fitting a monoexponential curve. We found that knocking down Amph1 expression results in slower SV retrieval kinetics following induced stimulation in comparison with the scrambled control (Figure 5.2D) confirming that Amph1 regulates SV endocytosis. To quantify for the extent of SV exocytosis, the sypHy fluorescence during stimulation was expressed as a portion of the total fluorescence revealed by perfusion with NH_4Cl that is equivalent to total SV

pool size. We found that the rate of SV exocytosis was compromised in neurons expressing less Amph1 compared to the scrambled (Figure 5.2E) implicating Amph1 in SV fusion. Taken together, these data show that Amph1 is essential for SV recycling and that the extent of shAmph1-facilitated reduction in Amph1 expression is sufficient to cause defects in the SV cycle.

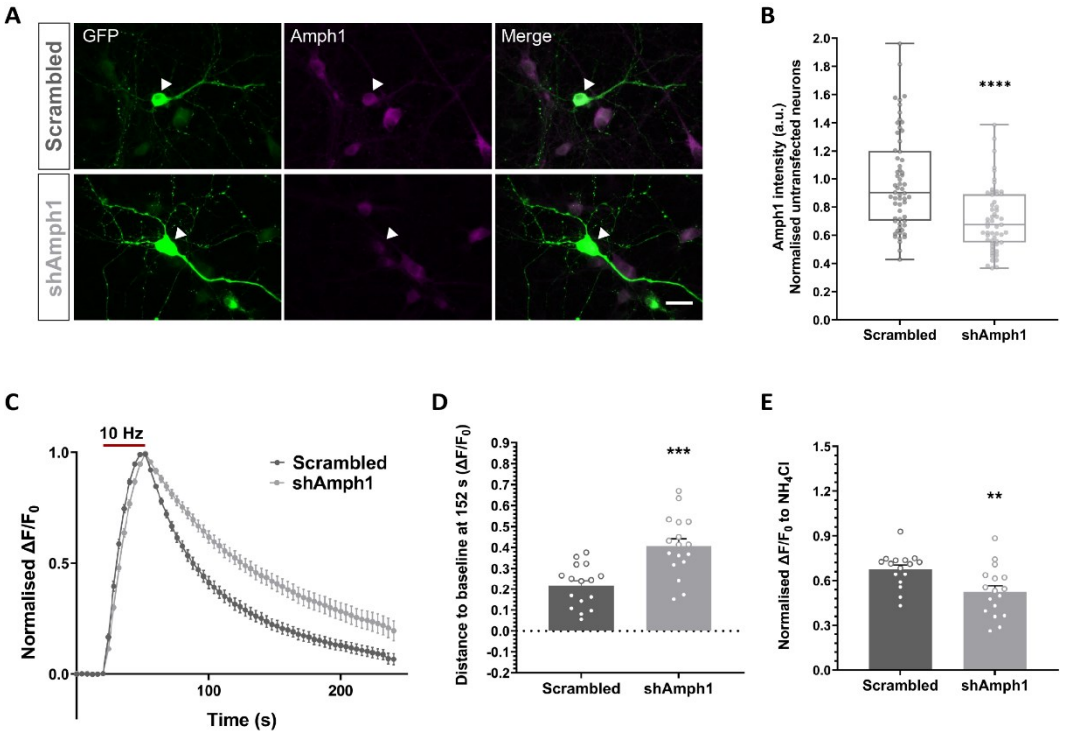

Figure 5.2 Validation of an shRNA construct to block Amph1 expression in mouse hippocampal neuron

(**A**) Primary hippocampal neurons were transfected with shAmph1 and a scrambled control expressing sypHy (scrambled, dark grey; shAmph1, light grey) at 8-10 DIV and fixed at 15 DIV. Representative images of neurons expressing scrambled and shAmph1 labelled for GFP (green) and Amph1 (magenta). Merged

images of GFP and Amph1. Scale bar, 20 μm. (**B**) Quantification of the mean cell body Amph1 fluorescence intensity normalised to untransfected neurons. Background was subtracted in all cases. Box plots present median with IQR indicating min-max whiskers. ****p < 0.001 by Mann-Whitney two-tailed t test. Scrambled n = 61, shAmph1 n = 55 neurons from 4 independent preparations of neuronal cultures. (**C**) Mean sypHy fluorescence response from neurons stimulated at 10 Hz for 30 s (red bar) normalised to the stimulation peak. (**D**) Mean sypHy fluorescence measuring the distance from baseline at 152 s. (**E**) Mean sypHy fluorescence normalised to the total pool after perfusion with NH_4Cl. Bars indicate mean ± SEM. **p < 0.01, ***p < 0.001 by unpaired two-tailed t-test. Scrambled n = 16, shAmph1 n =17 coverslips from 4 independent preparations of neuronal cultures.

5.2.3 Amph1 non-PRD mutants fail to restore SV endocytosis in Amph1-silenced neurons

Since downregulation of Amph1 results in defective SV regeneration and release, we hypothesised that this occurs due to restricted formation of Amph1-mediated complexes. To test this hypothesis, we examined our validated rat Amph1 missense mutants for their ability to restore recycling defects in neurons expressing less Amph1. To begin with, we used the Amph1 missense mutant SSR that is incapable of associating with α-AP2 and HSR/SR that blocks the interaction with CHC that were produced as previously described in subsection 5.2.1. Since we reported that lack of SH3 also affects interaction with other Amph1 partners in addition to Dyn1, we avoided truncating the SH3 domain in order to study the role of the Amph1-Dyn1

interaction. Instead, we introduced the point mutations ^{672}GLFP^{675}→RLFL within the SH3 domain that have been shown to eliminate the interaction with Dyn1 (Grabs *et al.*, 1997). As a result, all the constructs used for our functional experiments regarded the full-length Amph1 (Figure 5.3A).

Primary cultures of hippocampal neurons were transfected with the shAmph1 and one of the Amph1 missense mutants at 7-8 DIV and imaged at 13-15 DIV. All mutants were tagged with mCerN1 to allow for their visualisation during imaging and were adequately expressed in the shAmph1-silenced background as confirmed by immunolabelling (Figure 5.4A, B). Neurons transfected with mCerN1 were used as control. As previously, neurons were subjected to stimulation at 10 Hz for 30 s to evoke neurotransmitter release and subsequent SV regeneration. The sypHy fluorescence was normalised to the stimulation peak to allow for comparison of endocytosis kinetics (Figure 5.3B,E). We found that expression of the mutant HSR/SR in Amph1 knockdown neurons is able to restore the SV retrieval kinetics partially in comparison with WT Amph1, but it can fully rescue the defect in the rate of SV exocytosis following NH_4Cl perfusion (Figure 5.3C, D). Moreover, neither SSR nor RLFL mutants were able to restore the SV endocytosis speed in contrast to WT Amph1, but the rate of SV exocytosis returned almost to the WT levels (Figure 5.3F, G). Taken together, these findings indicate that Amph1-facilitated complexes with CHC, α-AP2 and Dyn1 are critical for SV retrieval but not exocytosis following a single stimulation.

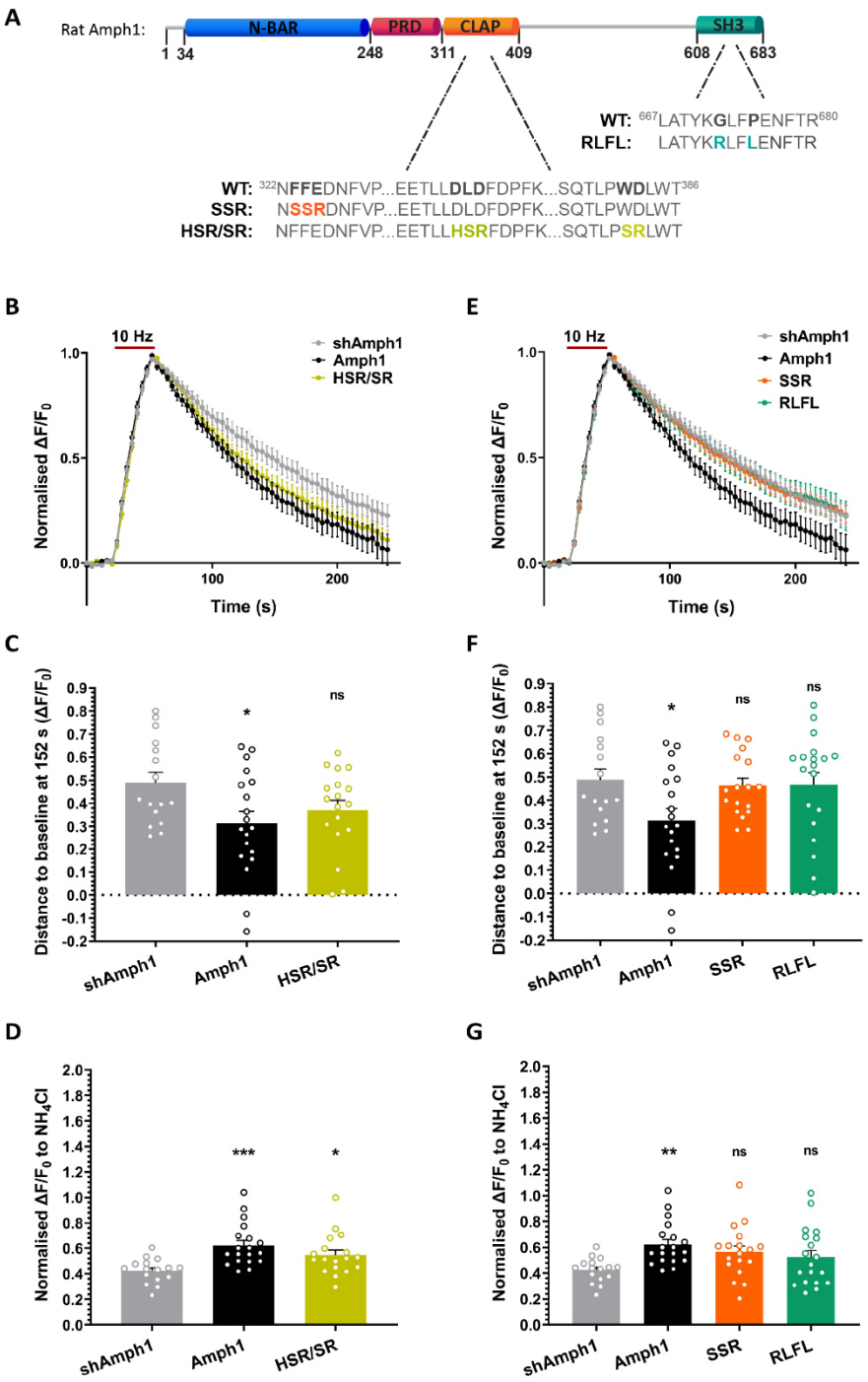

Figure 5.3 Amph1-mediated endocytosis occurs via interactions with multiple endocytic proteins

(**A**) Schematic representation of full length rat Amph1. Amph1 was mutated to block domain-specific interactions with AP2 (SSR; orange substitutions), CHC (HSR/SR; yellow substitutions), and Dyn1 (RLFL; green substitutions). (**B, E**) Primary hippocampal neurons from WT mice were co-transfected with shAmph1 and mCer (light grey), Amph1 (black), HSR/SR (yellow), SSR (orange), or RLFL (green) at 7-8 DIV and imaged at 13-15 DIV. Average sypHy fluorescence response from neurons stimulated at 10 Hz for 30 s (red bar) normalised to the stimulation peak. (**C, F**) Average sypHy fluorescence measuring the distance from baseline at 152 s and (**D, G**) after normalisation to the total pool following perfusion with NH_4Cl. Bars indicate mean ± SEM. ns, not significant, *p < 0.05, **p < 0.01, ***p < 0.001 by one-way ANOVA followed by Dunnett's multiple comparison test. shAmph1 n = 16, Amph1 n = 19, HSR/SR n = 18, SSR n = 18, RLFL n = 19 coverslips from 5 independent preparations.

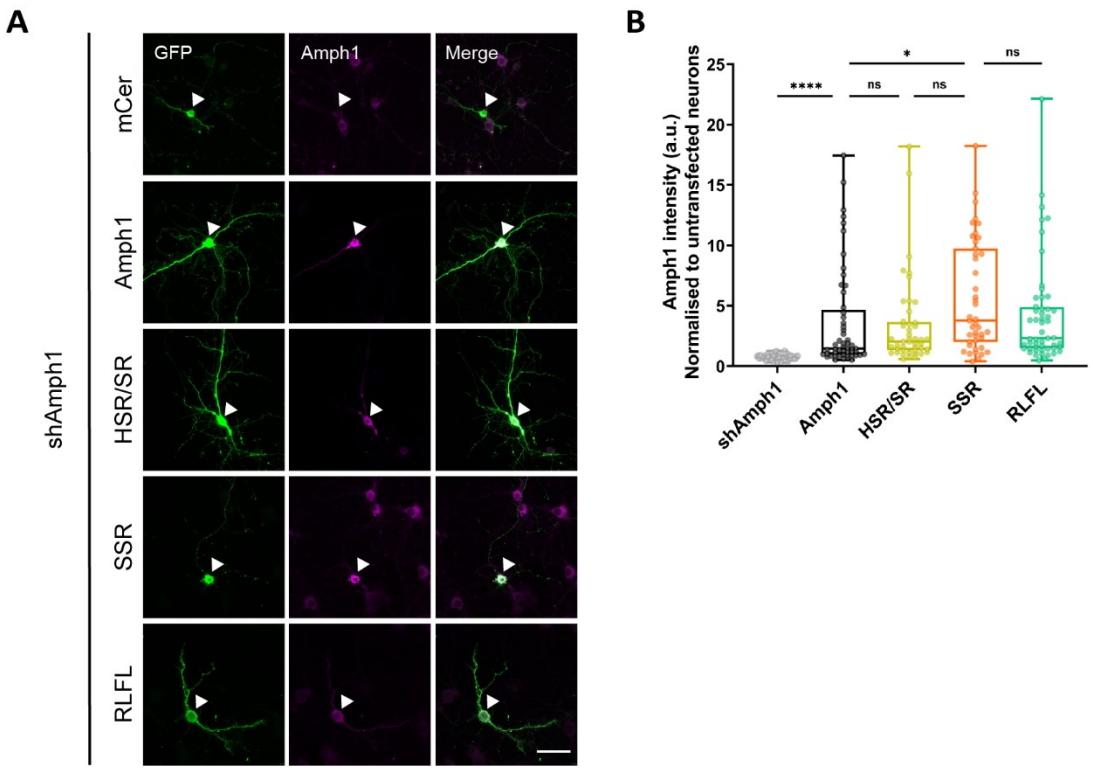

Figure 5.4 CLAP-related mutants of Amph1 are sufficiently expressed in neurons

(**A**) Primary cultures of hippocampal neurons were transfected at 8-10 DIV and fixed at 15 DIV. Representative images of neurons and axons expressing mCer (control) and various Amph1 constructs labelled for GFP (green) and Amph1 (magenta). Merged images of GFP and Amph1. Scale bar, 20 μm. (**B**) Quantification of Amph1 fluorescence intensity of cell bodies normalised to untransfected neurons. Background was subtracted in all cases. Box plots present median with IQR indicating min-max whiskers. ns, not significant, *p < 0.05, ****p < 0.0001 by Kruskal-Wallis test followed by Dunn's multiple comparison test. mCer *n* = 52, Amph1 *n* = 53, SR *n* = 45, SSR/HSR *n* = 43, RLFL *n* = 52 neurons from 3 independent preparations of neuronal cultures.

5.2.4 Amph1 interacts with endophilin A1 through a PPVPP motif within its PRD

Whilst Amph1 PRD interacts with the SH3 domain of endophilin A1 (Micheva *et al.*, 1997b), the specific interaction site on Amph1 remains unknown. To examine the role of the Amph1-endophiln A1 complex in SV recycling following a similar approach to the study of CLAP- and SH3-related interactions, it was essential to pinpoint the exact binding site on Amph1. In contrast to Amph1, the binding site of endophilin A1 on Amph2 has been mapped and consists of a RKGPPVPPLP motif within its PRD domain (Micheva *et al.*, 1997b). Amongst other roles, Amph1 and Amph2 share common interacting partners including endophilin A1 and, as a result, we hypothesised that Amph1 is likely to associate with endophilin A1 through an analogous motif. Indeed, a similar sequence is present within the PRD of Amph1 (^{298}RKGPPVPPLPK^{308}). To test the binding affinity of endophilin A1 for this motif, we generated three GST-conjugated mutants of Amph1 bearing the point mutations PPVPP→AAVAA (GST-$A_1A_2VA_3A_4$), PPV→AAV (GST-A_1A_2), and VPP→VAA (GST-A_3A_4).

Amph1 is a phosphoprotein with most of its potential phosphorylation sites located within the PRD, including S293 that consists its most abundant *in vivo* phosphosite (Craft *et al.*, 2008). We showed previously that Amph1-S293 undergoes calcineurin-mediated dephosphorylation coupled to neuronal activity indicating its functional importance. In addition, phosphorylation dynamics at S293 is critical for the formation of Amph1-endophilin A1 complex (Murakami *et al.*, 2006; Sekiguchi *et al.*, 2013). For these reasons, we generated two additional GST-fused constructs including a phosphonull and a phosphomimetic mutant bearing the missense mutation S293A (GST-S293A)

and S293E (GST-S293E), respectively. Although the sequence PPVPP is close to the S293 residue, we examined another PxxP motif that can be found in the vicinity of this phosphosite for its SH3 recognition potential (Cestra *et al.*, 1999). Therefore, we generated the GST-fused Amph1 mutant ^{288}PVRP^{291}→AVRA (GST-AVRA). All constructs that are depicted in Figure 5.5A were devoid of the N-BAR domain to facilitate bacterial expression as well as the SH3 domain to prevent the potential formation of an intramolecular loop as discussed in subsection 5.2.1.

Recombinant GST-tagged Amph1 versions were used as baits to perform pull-down assays from brain synaptosomal lysates. A GST-containing empty vector was included as a control for any unspecific binding to GST. The bacterial expression of all constructs was visualised by CBB staining and the potential interactions of Amph1 mutants with endophilin A1 as well as a number of other SH3-containing molecules were then assessed by immunoblotting (Figure 5.5B). The endophilin A1 binding to Amph1 was measured by densitometry and normalised to the total GST-tagged protein in the sample as revealed following CBB staining. We revealed that all three PPVPP-related mutants ($A_1A_2VA_3A_4$, A_1A_2, and A_3A_4) disrupt the binding to endophilin A1, whereas the mutant AVRA also exhibits compromised binding, albeit this did not reach statistical significance (Figure 5.5C). As a result, these data show that endophilin A1 preferentially interacts with the motif ^{301}PPVPP^{305} on Amph1 with all proline residues being critical. In addition, we observed that the phosphomimetic mutant S293E abolished the Amph1-endophilin A1 interaction, in contrast to the phosphonull substitution S293A, implying that the interplay between phosphorylation and dephosphorylation at S293 is key for regulating the formation of the Amph1-endophilin A1 complex. Lastly, we confirmed the specificity of these elements

for endophilin A1 binding as the association of Amph1 with other SH3-containing endocytosis proteins remained unaffected.

In agreement, co-immunoprecipitation of endophilin A1 from an adult mouse brain using either an antibody against Amph1 or the phosphoantibody pAmph1-S293 confirmed that while endophilin A1 interacted with Amph1 *in vivo*, their interaction was weaker in the case of phosphorylated Amph1 at S293 (Figure 5.6). A random antibody against EHD was used as a control and the homogenate was pre-cleaned prior to incubation with antibodies using appropriate amount of agarose beads to thus enhance specificity.

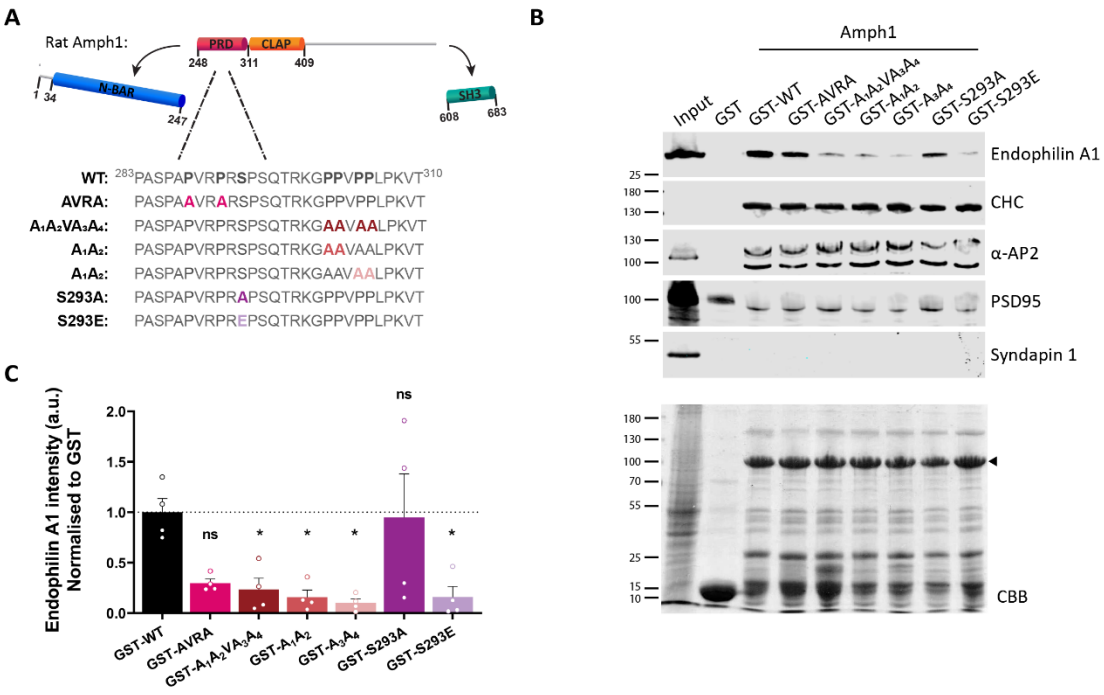

Figure 5.5 Endophilin A1 binds preferentially to the ^{301}PPVPP^{305} motif located within the Amph1 PRD and phosphorylation of Amph1 at S293 is critical for this binding

(**A**) Schematic representation of the structural domains of Amph1 that were used for generating GST-fused mutants. Point mutations were introduced within the PRD domain including substitutions of proline into alanine residues for AVRA, $A_1A_2VA_3A_4$, A_1A_2, and A_3A_4 mutants (pink- and red-shade substitutions). Also, substitution of S293 with an A or E residue resulted in the generation of the phosphonull S293A (purple substitution) and phosphomimetic S293E mutant (lilac substitution). All constructs lack the SH3 domain, whereas the N-BAR domain was omitted in all cases to facilitate bacterial expression. Residue numbering refers to the mouse Amph1 protein. (**B**) Pull-down experiments were performed using synaptosomal lysates from rat brains and GST-tagged fusion proteins of Amph1 lacking the SH3 domain. The binding ability of purified endophilin A1 and other

SH3-containing proteins, such as CHC, α-AP2, PSD95, and syndapin 1 was assessed by immunoblotting. A CBB staining was performed in parallel to control for GST-fused protein level. (**C**) Quantification of the endophilin binding efficacy was performed by determining relative band intensities by densitometry normalised to the level of the GST-fused proteins. Bars indicate mean ± SEM. ns, not significant, *p < 0.05 by one-way ANOVA followed by Dunnett's multiple comparison test. *n* = 4 synaptosomal lysates from 4 rat brains.

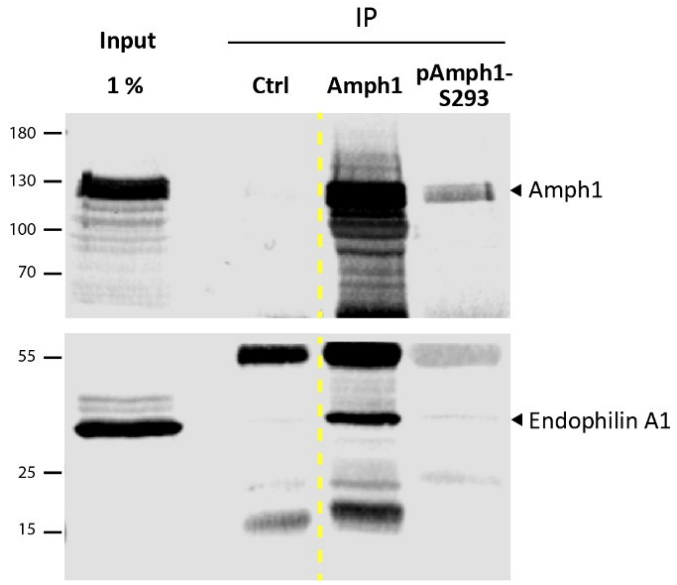

Figure 5.6 Amph1 interacts with endophilin A1, but its phosphorylation at S293 weakens their association

Co-immunoprecipitation from adult mouse brain lysates with Amph1 and pAmph1-S293. Samples were analysed by immunoblotting for Amph1 and

endophilin A1. A random antibody against EHD was used as control. Amph1 but not pAmph1-S293 reacted with endophilin A1 in the mouse brain. *n* = 1 animal.

5.2.5 Amph1 PRD-related mutants fail to restore SV endocytosis in Amph1-silenced neurons

The GST pull-down assay using different PRD-related mutants of Amph1 revealed putative elements that are responsible for the recognition of the SH3 domain of endophilin A1. Subsequently, the functional role of these mutants in regulating SV recycling was determined. For this, we tested whether Amph1 PRD-related mutants, presented in Figure 5.7A, were able to restore the defects in SV recycling in hippocampal neurons, where Amph1 was previously downregulated. Neurons were transfected at 7 DIV with sypHy-expressing shAmph1 and one of the PRD-related mutants or mCerN1 as a control prior to imaging at 13-15 DIV. All mutants were tagged with mCerN1 to allow for their visualisation during imaging and adequately expressed in the shAmph1-silenced background as confirmed by immunolabelling (Figure 5.9A, B). Neurons were subjected to stimulation at 10 Hz for 30 s and the sypHy fluorescence was normalised to the stimulation peak to allow for comparison of endocytosis kinetics (Figure 5.7B). To quantify the kinetics of SV retrieval, we measured the distance from the baseline at 152 s as previously. Except for AVRA, we found that no other PRD-related mutant was able to rescue the SV endocytosis delay in Amph1-knockdown neurons in contrast to WT Amph1 (Figure 5.7C). Intriguingly, $A_1A_2VA_3A_4$ together with A_3A_4 mutant resulted in more pronounced delay in SV endocytosis implying a potential

dominant negative role. Furthermore, we observed that both mutants caused slower SV exocytosis rate (Figure 5.7D), thus pointing towards the idea that the disruption of the Amph1-endophilin A1 complex may be required for neurotransmitter release as well as SV regeneration. Taken together, these data support that the association of Amph1 with endophilin A1 occurs primarily through the ^{301}PPVPP^{305} motif and this is required for proper SV endocytosis, whereas ^{301}PP^{302} is essential albeit secondary binding site.

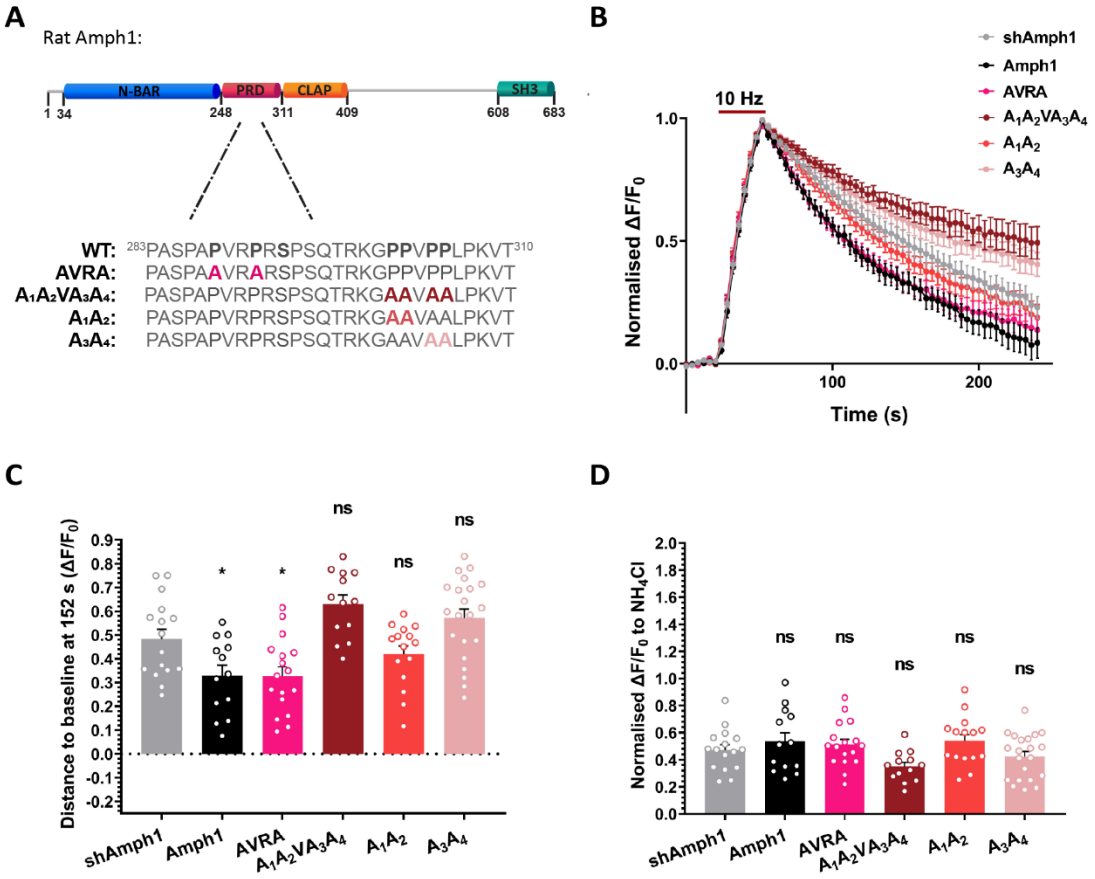

Figure 5.7 Amph1-mediated SV endocytosis occurs via its interaction with endophilin through the ^{301}PPVPP^{305} motif

(**A**) Schematic representation of full length rat Amph1. Proline residues (P) within the PRD of Amph1 were substituted by alanine (A) to generate various mutants. (**B**) Primary hippocampal neurons from WT mice were co-transfected with shAmph1 and mCer (light grey), Amph1 (black), AVRA (fuchsia), $A_1A_2VA_3A_4$ (cherry), A_1A_2 (rose), or A_3A_4 (salmon) mutant at 7 DIV and imaged at 13-15 DIV. Average sypHy fluorescence response from neurons stimulated at 10 Hz for 30 s (red bar) normalised to the stimulation peak. (**C**) Average sypHy fluorescence measuring the distance from baseline at 152 s and (**D**) after normalisation to the total pool following perfusion with NH_4Cl. Bars indicate mean ± SEM. ns, not significant, *p < 0.05 by one-way ANOVA followed by Dunnett's multiple comparison test. shAmph1 n = 16, Amph1 n = 13, AVRA n = 17, $A_1A_2VA_3A_4$ n = 13, A_1A_2 n = 15, A_3A_4 n = 21 coverslips from 5 independent preparations.

5.2.6 Phosphorylation at S293 is essential for Amph1 function in SV endocytosis

The two phosphomutants of Amph1 at S293 (Figure 5.8A), S293A and S293E, differ in their ability to bind to endophilin A1 implying that the phosphorylation dynamics at this site regulates SV recycling through the assembly/disassembly equilibrium of the Amph1-endophilin A1 complex. To test this hypothesis, neurons were initially co-transfected with sypHy and S293A, S239E or mCerN1 as a control to assess the impact of their expression on SV recycling following stimulation at 10 Hz for 30 s (Figure 5.8B). All mutants were tagged with mCerN1 to allow for their visualisation during imaging. We found that both SV endocytosis kinetics (Figure 5.8C) and the

rate of SV exocytosis (Figure 5.8D) remained unaffected in the presence of either excess S293A or S293E similarly to WT Amph1 eliminating the possibility of any dominant negative activity.

Next, neurons were co-transfected with sypHy-expressing shAmph1 to suppress Amph1 expression and one of the phosphomutants, Amph1 or mCerN1 as a control prior to imaging at 13-15 DIV. Neurons were subjected to stimulation at 10 Hz for 30 s to evoke SV release followed by SV regeneration (Figure 5.8E). We observed that neither S293A nor S293E was able to restore the speed of SV endocytosis in Amph1-silenced neurons in contrast to the partial rescue observed in the case of WT Amph1 (Figure 5.8F). In addition, we reported that all constructs seemed incapable of restoring the rate of SV exocytosis, although this needs to be examined further (Figure 5.8G). Their expression was examined in the shAmph1-silenced background by immunolabelling confirming that their levels were adequate (Figure 5.9A, B). Moreover, the Amph1-S293 phosphomutants did not appear to affect the localisation of Amph1 in agreement with previous findings in non-neuronal cells (Murakami *et al.*, 2006). Taken together, these data point towards the idea that the phosphorylation interplay at Amph1-S293 may be important for SV recycling at hippocampal synapses.

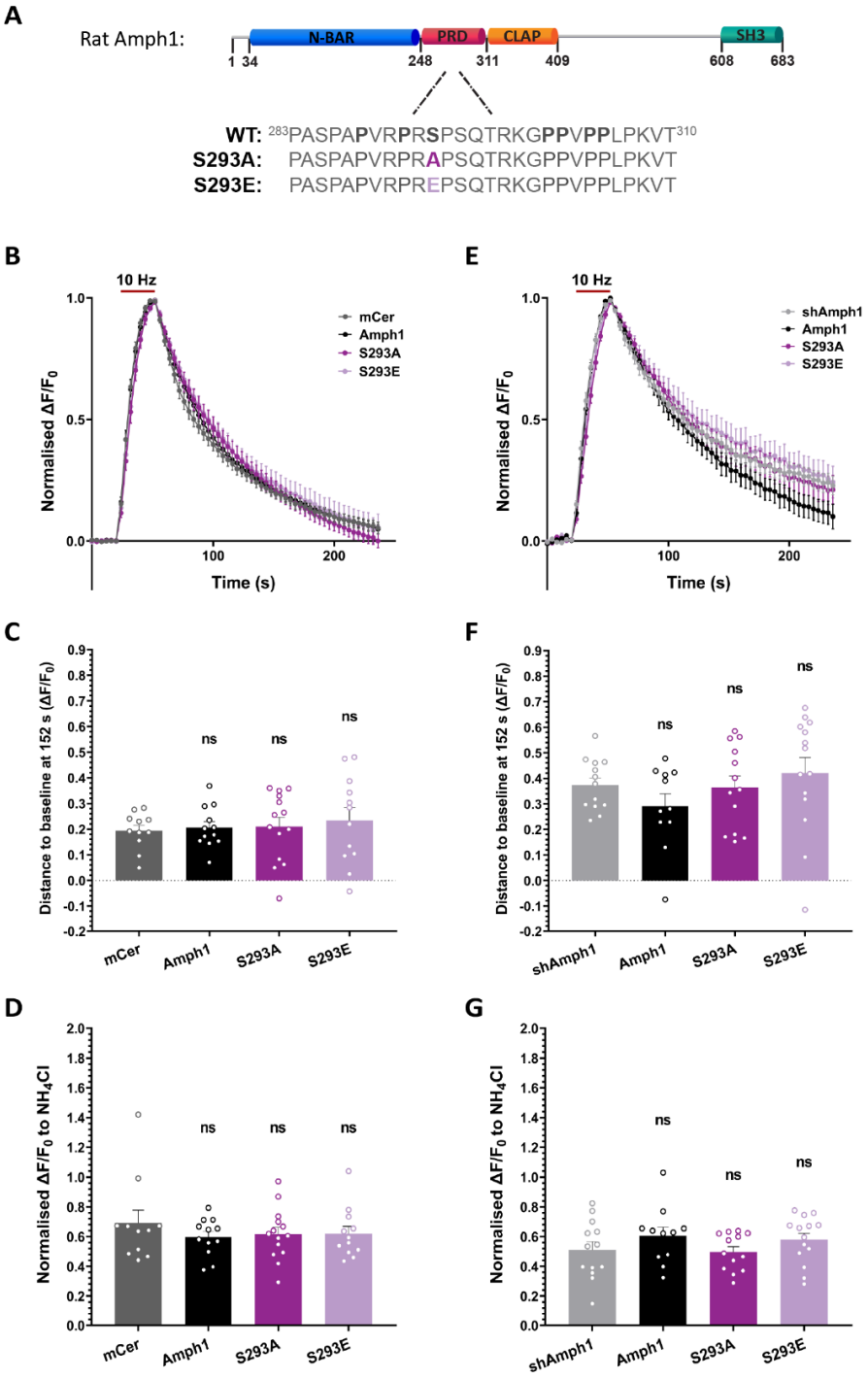

Figure 5.8 Phosphorylation at Amph1-S293 is critical for SV endocytosis

(**A**) Schematic representation of full length rat Amph1. Amph1 was modified at S293 to generate the phosphonull and phosphomimetic mutants, S293A and S293E, respectively. (**B**) Primary hippocampal neurons from WT mice were co-transfected with sypHy and mCer (dark grey), Amph1 (black), S293A (purple) or S293E (lilac) at 8-9 DIV and imaged at 13-15 DIV. Average sypHy fluorescence response from neurons stimulated at 10 Hz for 30 s (red bar) normalised to the stimulation peak. (**C**) Average sypHy fluorescence measuring the distance from baseline at 152 s and (**D**) after normalisation to the total pool following perfusion with NH_4Cl. Bars indicate mean ± SEM. ns, not significant by one-way ANOVA followed by Dunnett's multiple comparison test. mCer $n = 11$, Amph1 $n = 12$, S293A $n = 14$, S293E $n = 12$ coverslips from 5 independent preparations. (**E**) Primary hippocampal neurons from WT mice were co-transfected with shAmph1 and mCer (light grey), Amph1 (black), S293A (purple) or S293E (lilac) at 8-9 DIV and imaged at 13-15 DIV. Average sypHy fluorescence response from neurons stimulated at 10 Hz for 30 s (red bar) normalised to the stimulation peak. (**F**) Average sypHy fluorescence measuring the distance from baseline at 152 s and (**G**) after normalisation to the total pool following perfusion with NH_4Cl. Bars indicate mean ± SEM. ns, not significant by one-way ANOVA followed by Dunnett's multiple comparison test. mCer $n = 13$, Amph1 $n = 11$, S293A $n = 13$, S293E $n = 14$ coverslips from 4 independent preparations.

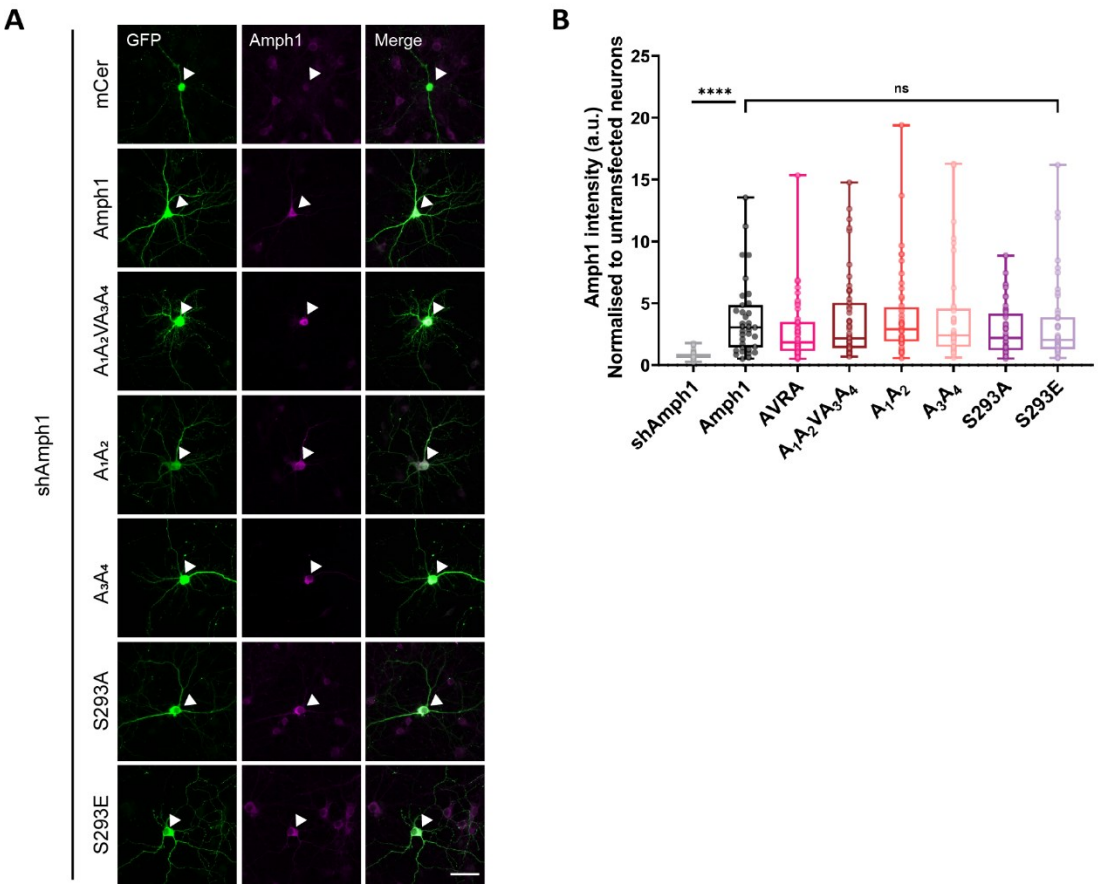

Figure 5.9 PRD-related mutants of Amph1 are sufficiently expressed in neurons

(**A**) Primary cultures of hippocampal neurons were transfected at 8-10 DIV and fixed at 15 DIV. Representative images of neurons and axons expressing mCer (control) and various Amph1 constructs labelled for GFP (green) and Amph1 (magenta). Merged images of GFP and Amph1. Scale bar, 20 μm. (**B**) Quantification of Amph1 fluorescence intensity of cell bodies normalised to untransfected neurons. Background was subtracted in all cases. Box plots present median with IQR indicating min-max whiskers. ns, not significant, ****$p < 0.0001$ by Kruskal-Wallis test followed by Dunn's multiple comparison test. mCer $n = 51$, Amph1 $n =$

35, AVRA n = 43, $A_1A_2VA_3A_4$ n = 51, A_1A_2 n = 48, A_3A_4 n = 36, S293A n = 49, S293E n = 47 neurons from 3 independent preparations of neuronal cultures.

5.3 Discussion

5.3.1 Amph1 as an interface for various interactions with presynaptic proteins

Several proteins have been reported to interact with Amph1 in a domain-specific manner, including some of the most well-established CME molecules, such as Dyn1, α-AP2, and CHC. Initially, we validated the specific binding locations for these interacting partners performing pull-down experiments with various GST-conjugated Amph1 mutants that were known to eliminate these interactions (Slepnev *et al.*, 2000). We confirmed that substitution of the motif ^{323}FFE^{325} within the CLAP domain eliminates the binding of Amph1 to α-AP2 but also reduces the binding affinity for CHC. Similarly, modification of the sequences ^{353}DLD^{355}/^{382}WD^{383} within the CLAP domain results in disruption of the Amph1-CHC complex as well as weakening of its association with α-AP2. These observations reinforce that Amph1-centric complexes are multi-protein and their formation occurs in a coordinated manner that entails the simultaneous binding of all three partners to ensure the optimal performance in CME (Slepnev *et al.*, 2000). At the same time, lack of the SH3 domain, that prevents the formation of the Amph1-Dyn1 complex, leads to compromised interaction with α-AP2 but not CHC, whereas Dyn1 is recruited independently of any prior interaction with either α-AP2 or CHC. In addition

to Dyn1, synaptojanin 1 also interacts with the SH3 domain of Amph1 (Micheva *et al.*, 1997a; Cestra *et al.*, 1999). Therefore, the interaction of a ligand with the Amph1 SH3 domain is critical for the association of α-AP2 that appears to be recruited later to the tertiary cluster.

Downregulation of Amph1 in primary neurons leads to defective SV recycling reminiscent of phenotypes that are observed in Amph1 KO mice (Di Paolo *et al.*, 2002). Examining the functional role of Amph1 mutants that are unable to form complexes with CHC, α-AP2 or Dyn1 in this context, we confirmed that they all play central role in Amph1-mediated SV endocytosis with the exception of the CHC mutant that restores SV endocytosis kinetics partially. Therefore, our data support distinct endocytic roles that have been attributed to Amph1-mediated interactions, including Dyn1 recruitment (Takei *et al.*, 1999; Meinecke *et al.*, 2013), Dyn1-mediated fission (Takeda et al., 2018), and the AP2-dependent cargo recognition at the plasma membrane. Since Amph1 has been reported to also interact with AP1 that acts in compartments other than the plasma membrane, such as the trans-Golgi surface (Huser *et al.*, 2013), it is likely that the interaction of Amph1 with CHC is of secondary importance and merely enhances the stabilisation of the tertiary assembly at the endocytic pit. In agreement, early observations reported that Amph1 is not enriched in a CCV fraction in contrast to clathrin and AP2 subunits proving that Amph1 is not a major component of CCVs (David *et al.*, 1996).

Lastly, our data indicate that the disruption of Amph1-mediated complexes does not alter the extent of SV exocytosis following a single neuronal stimulation, although this could be also confirmed by treatment with bafilomycin A1. One possible explanation is that the inability of Amph1 to form complexes with α-AP2, Dyn1 and, to a lesser extent, CHC may lead to

activation of other compensatory endocytosis routes, while it is likely an impairment in SV exocytosis to emerge only after repeated rounds of stimulation. In agreement, it has been proposed that disruption of the Amph1-AP2 complex may trigger alternative endocytosis pathways, such as clathrin-independent and AP3-dependent SV regeneration resulting in differentiated v-SNARE composition in GABAergic synapses (Werner *et al.*, 2016). Accordingly, downregulation of AP2 expression in primary neurons is functionally substituted by AP1 (Kim & Ryan, 2009).

5.3.2 Amph1 interacts with endophilin A1 to control SV endocytosis

Performing pull-down assay with GST-fused Amph1 mutants lacking the SH3 domain, we showed that its absence acts positively on the binding affinity of endophilin A1 possibly due to the prevention of an intramolecular interaction with the Amph1 PRD (Farsad *et al.*, 2003), although respective intermolecular interactions between Amph1/2 molecules cannot be excluded. Similar intramolecular loops have been reported in other endocytosis proteins, such as endophilin 2 and syndapin 1 (Chen *et al.*, 2003; Rao *et al.*, 2010). This mechanism that appears to be common amongst SH3-containing proteins can have an autoinhibitory role on BAR-mediated interactions of Amph1 with the plasma membrane that is blocked by the binding of Dyn1 to its SH3 domain (Rao *et al.*, 2010). Hence, it is likely the activity of Amph1 to be regulated in a similar way triggering the recruitment of endophilin A1 in the neck of the budding vesicle after the attachment of Dyn1 to its SH3 domain and subsequent release of its PRD to ensure timely completion of the Dyn-mediated fission (Hohendahl *et al.*, 2017). In support, depletion of Dyn1 results in compromised endophilin recruitment to membranes *in vitro* (Meinecke *et*

al., 2013). Since Dyn1 recruitment depends on the formation of multiple interactions with the Amph1 SH3 domain through distinct motifs (Rosendale *et al.*, 2019), the efficacy of autoinhibitory intramolecular loops to attract Dyn1, especially in an environment that Dyn1 molecules are not in favour stoichiometrically, needs to be assessed further.

Previous studies determined the motif PxxP (where x is any amino acid) with a positively-charged amino acid adjacent to either side as the SH3 domain binding consensus site (Ren *et al.*, 1993; Yu *et al.*, 1994). Based on the orientation of the positively-charged amino acid in relation to the PxxP motif, proline-enriched SH3-binding sites are categorised into two groups: class I (RxxPxxP) and class II (PxxPxR) (Teyra *et al.*, 2017). We showed that the binding of the endophilin A1 SH3 domain to the Amph1 PRD depends on the presence of a class I binding motif within the sequence ^{298}**R**KG**P**PV**P**PLPK^{308}, which coincides with that on Amph2 (Micheva *et al.*, 1997b). Mutagenesis of the sequence ^{301}PPVPP^{305} (underlined above) showed that both proline pairs, either separately or combined, affect the binding affinity for endophilin A1. In addition, our functional experiments indicate that the first pair ^{301}PP^{302} appears to be less critical than the second pair ^{304}PP^{305}, despite its location at the centre of the class I motif.

The above class I motif is the only canonical sequence that can be found within the PRD of Amph1. However, non-canonical sequences have been also reported to interact with SH3 modules (Teyra *et al.*, 2017), and therefore we investigated an additional PxxP-core motif, ^{288}**P**VR**P**RSP^{294}, for its ability to form a complex with endophilin A1. While its mutagenesis manages to weaken slightly its binding to endophilin A1 *in vitro*, the formation of the Amph1-endophilin A1 complex seems to occur regardless of the ^{288}**P**VR**P**^{291}

motif (underlined above). Indeed, sypHy fluorescence imaging agrees that it is not critical for either SV retrieval or exocytosis.

The same is not true for the neighbouring residue S293, however, that displays different ability to associate with endophilin A1 according to its phosphorylation status. Our data support previous observations that the phosphonull mutant S293A maintains its ability to associate with endophilin A1 in contrast to the phosphomimetic mutant S293E that fails to interact with it (Sekiguchi *et al.*, 2013). The regulation of Amph1-mediated interactions by phosphorylation is not limited to endophilin A1 as a similar mechanism has been also proposed for the binding of AP2 subunits, whereas other endocytic proteins, such as Dyn1 and syndapin 1, also form complexes that are dictated by phosphorylation (Shang *et al.*, 2004; Anggono *et al.*, 2006; Murakami *et al.*, 2012; Yuan *et al.*, 2019).

Despite the opposing roles of the two phosphomutants in relation to their binding to endophilin A1 *in vitro*, both S293A and S293E appear unable to restore either the kinetics of SV endocytosis or the SV exocytosis rate in neurons where Amph1 has been silenced. Although these data do not reach statistical significance, both S293A and S293E tend to have a loss-of-function effect in relation to SV retrieval. On the other hand, their overexpression in the WT background does not impact SV recycling. Since both phosphorylation states of Amph1-S293 seem to be loss-of-function, this suggests that the phosphorylation interplay at S293 is essential for sustaining subsequent rounds of SV recycling and this is regulated in a stimulus-dependent manner as shown in Chapter 4. Therefore, the phosphorylation-regulated assembly/disassembly equilibrium of the Amph1-endophilin A1 complex possibly determines the SV recycling performance overall in an activity-dependent manner via regulating clustering of endophilin A1 at the endocytic

pit (Werner *et al.*, 2016), controlling the availability of endophilin A1 to perform its roles in SV exocytosis, and coupling SV exocytosis to endocytosis (Chen *et al.*, 2003). This is also the case for Dyn, where both phosphonull and phosphomimetic versions are dominant negative in WT neurons (Anggono *et al.*, 2006; Clayton *et al.*, 2010).

5.3.3 Potential limitations

The inability of Amph1 to fully restore the defects in SV recycling in some datasets following shAmph1-mediated downregulation of its expression might originate from various causes. First, Amph1 forms both homodimers and heterodimers with Amph2 through their N-BAR domains. Although the N-BAR domain is well conserved between mouse and rat Amph1 with only a single mismatch at the protein level, this divergence may result in less optimal formation of complexes between exogenously expressed rat Amph1 and endogenous mouse Amph1 and/or Amph2. However, SV recycling remains unaltered when rat Amph1 is overexpressed in WT neurons. Second, the use of small interfering RNAs and subsequent silencing of protein expression can cause a degree of neurotoxicity that can impact membrane dynamics across presynaptic boutons. Indeed, from previous experience, it has been observed that unhealthy synapses expressing sypHy occasionally lack their ability to return to baseline following stimulation remaining thus to a neutral state indefinitely. Lastly, shAmph1 targets a sequence on mouse Amph1 mRNA that displays approximately 95 % identity with that of rat Amph1 indicating that shAmph1 might induce an off-target effect on rat Amph1. However, small interfering RNAs can distinguish between sequences that differ even by a single nucleotide (Schwarz *et al.*, 2006), therefore it is more likely shAmph1 to

suppress specifically the expression of mouse Amph1. In support, immunofluorescent analysis shows that both WT Amph1 and its modified versions are overexpressed in the shAmph1-silenced neurons.

Another parameter that is worth considering is that all our functional studies were performed at room temperature. As SV endocytosis is highly dependent on temperature with CME prevailing only at lower, non-physiological degrees at the nerve terminal (Sato *et al.*, 2009; Watanabe *et al.*, 2014), the inability of the Amph1 mutant HSR/SR (no binding to CHC) to restore the SV endocytosis kinetics at room temperature may argue either that Amph1-mediated SV endocytosis is clathrin-independent or that the interaction of Amph1 with CHC is not critical for CME to occur. However, our data indicate the importance of the Amph1-CHC complex for SV endocytosis rather than the absence of a role for clathrin in SV retrieval at room temperature. Firstly, HSR/SR achieves to rescue the speed of endocytosis only partially implying that the Amph1-CHC interaction has a role in SV endocytosis, albeit subtle. Secondly, the interaction of Amph1 with α-AP2, which relies in part on the interaction with CHC and is its major adaptor protein at the plasma membrane, is required for proper SV endocytosis despite the non-physiological temperature. Lastly, the changes observed in fluidity and protein conformation in the range between the room temperature to the physiological temperature are subtle (Chanaday & Kavalali, 2018). In support, the formation of the clathrin-coated pit can occur thermodynamically in a temperature-independent manner (Chanaday & Kavalali, 2018). Furthermore, clathrin maintains a role in SV endocytosis at physiological temperature, although this is limited to the regeneration of SVs from intermediate endosomes, highlighting that the functionality of the CME-related machinery is maintained at the presynaptic bouton (Watanabe *et al.*, 2014). On the other

hand, endophilin is important for clathrin-independent endocytic routes and fast neurotransmission (Llobet *et al.*, 2011; Boucrot *et al.*, 2015), inferring potentially an additional role for the Amph1-endophilin A1 complex. In conclusion, the role of Amph1-centric complexes needs to be further investigated considering the impact of factors that trigger different endocytosis routes (e.g. temperature, stimulation frequency) to fully untangle their involvement in neurotransmission.

5.3.4 Conclusions

In summary, this chapter offers a complete map of the most critical Amph1-centric interactions in brain synaptosomes, including confirmation of established interacting sites for CHC, α-AP2, and Dyn1 and identification of the endophilin A1 binding location. We also verify that downregulation of Amph1 in primary neurons results in compromised SV recycling. Following a molecular replacement strategy, we show that the domain-specific interactions of Amph1 are unable to restore defects in SV regeneration. Furthermore, we reveal that the Amph1-endophilin A1 complex is critical for SV retrieval at hippocampal synapses. Finally, we provide evidence that the phosphorylation interplay at S293 of Amph1 possibly controls the Amph1-mediated SV recycling via mediating its interaction with endophilin A1.

Chapter 6: Conclusions and future directions

CDKL5 has been previously implicated in various neuronal functions, including neurite outgrowth, MT remodelling, and cargo trafficking. However, our insight into the potential presynaptic roles of CDKL5 has been elusive. Overall, our findings support for the first time that CDKL5 is involved in SV recycling at the presynaptic terminal and that loss of CDKL5 results in presynaptic dysfunction that may contribute to the pathogenesis of CDD.

In Chapter 3, we used a novel CDKL5 KO rat model attempting to identify phenotypes associated with the loss of CDKL5 in the nerve terminal. After demonstrating that CDKL5 localises at the presynapse, we explored different aspects of SV recycling in rat hippocampal neurons. Using the fluorescently tagged reporter sypHy, we showed that loss of CDKL5 results in slower SV endocytosis kinetics across different stimulation conditions with more profound impairment reported at lower neuronal activity. Except for SV endocytosis, CDKL5 deficiency does not seem to affect any other presynaptic parameter, including the rate of SV exocytosis, the number of terminals undergoing ADBE, the levels of endocytic proteins, or the number of presynaptic boutons.

In Chapter 4, following a molecular replacement approach, we revealed that the kinase activity of CDKL5 is critical for reliable SV endocytosis. We hypothesised that CDKL5 is implicated in SV recycling through phosphorylating a protein that is directly related to the SV endocytosis machinery. Since the presynaptic protein Amph1 has been identified

previously as an *in vitro* substrate of CDKL5 at S293, we examined whether CDKL5 exerts its presynaptic role through phosphorylation of this site. Using a phosphospecific antibody for Amph1-S293, we showed that CDKL5-facilitated phosphorylation of Amph1-S293 does not regulate the kinetics of SV retrieval. Furthermore, we demonstrated that kinase-inactive mutants of CDKL5 reported in CDD patients fail to restore deficits in SV endocytosis kinetics.

Lastly, in Chapter 5, we explored the role of Amph1-related complexes in SV endocytosis in hippocampal neurons where Amph1 expression was downregulated. We confirmed that the interactions of Amph1 with AP2, CHC, and Dyn1 are critical for SV retrieval. Moreover, we showed that the PPVPP motif on Amph1 PRD is the binding site of endophilin A1 and that their interaction is required for SV endocytosis. Finally, we confirmed in primary neurons that the formation of the Amph1-endophilin A1 complex depends on the phosphorylation interplay at S293 with both phosphomimetic and phosphonull mutants of Amph1 being unable to restore the kinetics of SV endocytosis.

6.1 Compromised SV endocytosis and neurotransmission

Defective SV endocytosis can lead to synaptic dysfunction through different ways, such as SV depletion, formation of fusion-incompetent SVs or disturbance of the membrane equilibrium in the active zone. SV regeneration is critical for maintaining continuous neurotransmission through retrieval of both SV membrane and cargo that resupply subsequently the recycling vesicle pool. CDKL5 deficiency leads to slower SV regeneration indicating that this

might lead to SV shortage under conditions of prolonged neuronal activity decreasing potentially the number of functional release sites. Although we observed no difference in the rate of SV exocytosis upon loss of CDKL5 at both lower and higher stimulation frequencies, further studies are required to unravel whether SV exhaustion occurs eventually, such as investigating potential defects following multiple trains of stimuli (Kokotos *et al.*, 2019). However, our findings suggest that SVs that are reformed in CDKL5 KO neurons are competent for fusion suggesting that the endocytosis impairment is a global defect and not due to sorting of specific SV cargoes.

Slower SV retrieval might also influence the size of the active zone in CDKL5-depleted neurons. This parameter has been shown to strongly correlate with release probability (P_r) determining therefore the reliability of neurotransmission (Matz *et al.*, 2010). Accumulation of membrane and cargo in the active zone that results from slower endocytosis can impair SV fusion after sustained neuronal activity. Both reduction of functional release sites and altered P_r due to SV depletion and dysfunctional active zone homeostasis can explain the reduced frequency of mEPSCs reported in a mouse CDKL5 KO model as well as our rat model (Wang *et al.*, 2021; Simões de Oliveira et al., in preparation).

Altered paired-pulse ratio is an additional phenotype associated with CDKL5 deficiency that is mainly attributed to presynaptic mechanisms. In particular, paired-pulse depression is observed in mice where CDKL5 is depleted from forebrain excitatory neurons and, conversely, paired-pulse facilitation is reported in mice with CDKL5 deficient forebrain inhibitory neurons (Tang *et al.*, 2019; Wang *et al.*, 2021). This indicates that P_r is altered in the absence of CDKL5 as regards both the synapse and the intraneuronal network. Although the CDKL5 KO rat model does not exhibit altered paired-

pulse ratio (Simões de Oliveira *et al*., in preparation), it is likely that different neuronal subpopulations need to be assessed separately to untangle any potential changes. This discrepancy with our findings might originate from the fact that primary hippocampal neurons consist mainly of glutamatergic synapses and for this reason questions about defects in neurotransmission in CDKL5 deficiency are addressed in a less complex network. Considering the molecular mechanisms of epileptogenesis, the premise is that the onset of seizure activity results from an excitatory/inhibitory imbalance. Therefore, further work is required to explore SV endocytosis deficits in inhibitory synapses and in what way deficits in glutamatergic neurons might affect the signalling towards inhibitory neuronal populations.

6.2 Future work

The catalytic activity of CDKL5 proved to be essential for SV recycling, indicating that CDKL5 phosphorylates at least one substrate at the presynapse. Although we showed that the phosphorylation dynamics at Amph1-S293 control the interaction of Amph1 with endophilin and regulate the rate of SV recycling in hippocampal presynaptic terminals, our data support that CDKL5-facilitated phosphorylation of Amph1-S293 is unlikely to regulate the speed of endocytosis. As a result, it is critical for future research on presynaptic CDKL5 to pinpoint potential CDKL5 substrates in the nerve terminal that either can be involved directly in the recycling protein machinery or regulate processes that affect eventually SV endocytosis kinetics. Therefore, we propose that CDKL5 regulates SV endocytosis kinetics through phosphorylation of an endocytosis-related protein that facilitates SV retrieval

preferably from the plasma membrane and, to a lesser extent, an intermediate endosome; or a non-endocytosis protein that may be important for either mitochondrial function and regulation of intracellular Ca^{2+} accumulation in the cytoplasmic region adjacent to the periactive zone; or, finally, a non-endocytosis protein that is responsible for regulation of MT dynamics and trafficking of material necessary for SV endocytosis at axonal presynaptic terminals (Figure 6.1). Although there is an established CDKL5 consensus motif, it would be extremely challenging to predict putative CDKL5 substrates based only on this piece of information as many presynaptic proteins might contain it without being CDKL5 substrates necessarily. Besides, additional CDKL5 consensus motifs might exist that are yet unknown. Substrate profiling by mass spectrometry in combination with bioinformatic tools utilizing the CDKL5 consensus motif(s) can elucidate potential phosphorylation targets of CDKL5 presynaptically, including sites of autophosphorylation. This would be beneficial for elucidating further the basic biology of CDKL5 and, simultaneously, for generating potential biomarkers and/or druggable targets for CDD diagnosis and treatment.

Given that CDD onset is related to the disturbances at the circuit level, another angle of future research into CDKL5-mediated SV endocytosis has to focus on alternative systems in order to complement our findings with observations at higher levels of organisation. To begin with, it is necessary to dissect the impact of SV recycling deficits on excitatory and inhibitory neuronal populations to elicit any potential deregulation that could underlie neuronal hyperexcitability and synchronisation explaining thus any epileptiform activity. Exploiting the advances in the optogenetic toolbox or other technologies, such as nanoparticles, it would be interesting to explore the reliability of neurotransmission between the hippocampus and

neighbouring brain regions in CDKL5 KO rats to unmask altered neuronal interactions (Benfenati & Lanzani, 2021; Mahn *et al.*, 2021). However, as there are few CDD cases that display CDD-related symptoms but no seizures this suggests that epilepsy is not a de facto clinical feature in CDD (MacKay *et al.*, 2020). Therefore, focusing on the hypersynchrony in CDKL5 research while disregarding other phenotypes that are linked to neurodevelopmental delay and intellectual disability would be a restricting approach. Lastly, when research is conducted in rodent models that differ in brain structure and complexity in comparison to the human brain, any extrapolation of the preclinical outcomes to the human neurophysiology should be treated with precaution. A way to overcome this limitation is to perform further research on patient-derived iPSCs or organoids that could be enlightening with respect to its relevance to humans, despite these systems being relatively unstable and thus not directly comparable to primary neurons (Mertens *et al.*, 2016; Amin & Pasca, 2018).

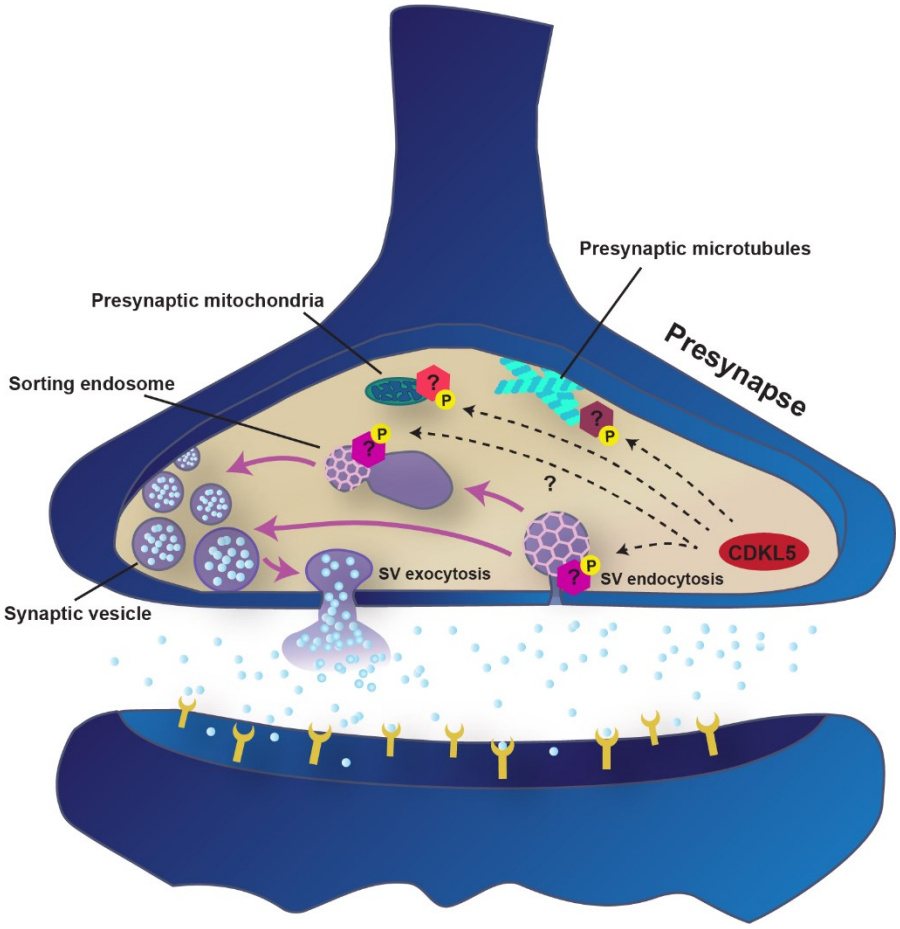

Figure 6.1 Proposed model of the impact of CDKL5-facilitated phosphorylation on SV endocytosis

CDKL5-mediated phosphorylation is vital for SV regeneration in hippocampal nerve terminals. Due to its frequency-dependent activity, we speculate that CDKL5 facilitates retrieval from the plasma membrane and, to a lesser extent, a sorting endosome via phosphorylation of an endocytic protein. Alternatively, CDKL5-mediated phosphorylation of a non-endocytic protein either associated with mitochondrial function or presynaptic microtubule dynamics might regulate SV

endocytosis indirectly through controlling presynaptic Ca^{2+} concentration or trafficking of endocytosis material, respectively.

6.3 Translational perspective

Today, CDD is currently untreatable with conventional methods including administration of antiepileptic drugs (Moseley *et al.*, 2012; Fehr *et al.*, 2016b), natural products, such as cannabidiol (Devinsky *et al.*, 2018; Dale *et al.*, 2019), and ketogenic diet therapy (Lim *et al.*, 2017). Moreover, translational read-through (TR)-inducing drugs, such as ataluren and aminoglycosides, that represent an RNA-based therapeutic approach to suppress *CDKL5* nonsense mutations have not been successful (Fazzari *et al.*, 2019; Devinsky *et al.*, 2021). Therefore, it is more than necessary for CDKL5-related research to have a translational orientation especially considering the severity of CDD.

The main finding of this work that CDKL5 is implicated in SV endocytosis also means that a novel monogenic disorder, CDD, is added to the long list of NDs that are associated with defective SV recycling. Despite the broad phenotypic range of CDD, understanding the basic biology of CDKL5 in the nerve terminal can enhance our insight into the occurrence of conserved and relevant phenotypes across distinct NDs conditions. This is critical not only to develop new pharmacological targets for diagnosis and treatment of CDD but also make use of already available options to subside epileptic activity and related comorbidities. Moreover, the description of a novel role of CDKL5 in axonal terminals can contribute to our understanding of the impact of gene replacement strategies for CDD treatment. For instance, we found that a

shorter version of human CDKL5 encompassing only the CDKL5 kinase domain can reverse the slowing in SV retrieval in CDKL5 KO neurons. We also demonstrated that additional CDKL5 does not harm healthy neurons in relation to SV recycling. Nevertheless, given moral, accessibility, and cost concerns that come with gene therapy application in combination with scientific limitations such as the insufficient delivery, non-target effects, and impact on healthy neurons, it would be reasonable to also aim in the development of more traditional strategies in parallel.

On this basis, one of the benefits of using embryonic hippocampal neurons as a preclinical model of epileptic conditions is that they grow into a functional network in culture within 2 weeks approximately. Seeking CDKL5-associated phenotypes, as the SV retrieval dysfunction reported in the absence of CDKL5, in such a system can have a valuable contribution on translational efforts because it can untangle molecular and cellular mechanisms of CDKL5 with limited confounding factors. At the same time, this system can be utilised as a primary method for screening drugs, neuroprotective compounds, or even natural products in a rapid manner (Spicer *et al.*, 2018). In addition, the identification and characterisation of novel substrates of CDKL5 in the nerve terminal can be beneficial for biomarker and/or drug development. Independently of the translation approach, this study achieves to enhance our insight on the activity of CDKL5 in the neuron and, in particular, at the presynaptic terminal paving hence the pathway for novel therapeutic treatments in CDD.

References

Aimar, P., Meireles, M., & Sanchez, V. (1990). A contribution to the translation of retention curves into pore size distributions for sieving membranes. *Journal of Membrane Science, 54*(3), 321-338. doi:10.1016/s0376-7388(00)80618-3

Aitman, T., Dhillon, P., & Geurts, A. M. (2016). A RATional choice for translational research? *Dis Model Mech, 9*(10), 1069-1072. doi:10.1242/dmm.027706

Amendola, E., Zhan, Y., Mattucci, C., Castroflorio, E., Calcagno, E., Fuchs, C., *et al.* (2014). Mapping pathological phenotypes in a mouse model of CDKL5 disorder. *PLoS One, 9*(5), e91613. doi:10.1371/journal.pone.0091613

Amenduni, M., De Filippis, R., Cheung, A. Y., Disciglio, V., Epistolato, M. C., Ariani, F., *et al.* (2011). iPS cells to model CDKL5-related disorders. *Eur J Hum Genet, 19*(12), 1246-1255. doi:10.1038/ejhg.2011.131

American Psychiatric Association. (2017). *Diagnostic and statistical manual of mental disorders : DSM-5*. Arlington, VA: American Psychiatric Association.

Amin, N. D., & Pasca, S. P. (2018). Building Models of Brain Disorders with Three-Dimensional Organoids. *Neuron, 100*(2), 389-405. doi:10.1016/j.neuron.2018.10.007

Andersson, F., Jakobsson, J., Low, P., Shupliakov, O., & Brodin, L. (2008). Perturbation of syndapin/PACSIN impairs synaptic vesicle recycling evoked by intense stimulation. *J Neurosci, 28*(15), 3925-3933. doi:10.1523/JNEUROSCI.1754-07.2008

Anggono, V., Smillie, K. J., Graham, M. E., Valova, V. A., Cousin, M. A., & Robinson, P. J. (2006). Syndapin I is the phosphorylation-regulated dynamin I partner in synaptic vesicle endocytosis. *Nat Neurosci, 9*(6), 752-760. doi:10.1038/nn1695

Antonescu, C. N., Aguet, F., Danuser, G., & Schmid, S. L. (2011). Phosphatidylinositol-(4,5)-bisphosphate regulates clathrin-coated pit initiation, stabilization, and size. *Mol Biol Cell, 22*(14), 2588-2600. doi:10.1091/mbc.E11-04-0362

Antonny, B., Burd, C., De Camilli, P., Chen, E., Daumke, O., Faelber, K., *et al.* (2016). Membrane fission by dynamin: what we know and what we need to know. *EMBO J, 35*(21), 2270-2284. doi:10.15252/embj.201694613

Ariel, P., Hoppa, M. B., & Ryan, T. A. (2012). Intrinsic variability in Pv, RRP size, Ca(2+) channel repertoire, and presynaptic potentiation in individual synaptic boutons. *Front Synaptic Neurosci, 4*, 9. doi:10.3389/fnsyn.2012.00009

Arkhipov, A., Yin, Y., & Schulten, K. (2009). Membrane-bending mechanism of amphiphysin N-BAR domains. *Biophys J, 97*(10), 2727-2735. doi:10.1016/j.bpj.2009.08.051

Armbruster, M., Messa, M., Ferguson, S. M., De Camilli, P., & Ryan, T. A. (2013). Dynamin phosphorylation controls optimization of endocytosis for brief action potential bursts. *Elife, 2*, e00845. doi:10.7554/eLife.00845

Atluri, P. P., & Ryan, T. A. (2006). The kinetics of synaptic vesicle reacidification at hippocampal nerve terminals. *J Neurosci, 26*(8), 2313-2320. doi:10.1523/JNEUROSCI.4425-05.2006

Bahi-Buisson, N., & Bienvenu, T. (2012). CDKL5-Related Disorders: From Clinical Description to Molecular Genetics. *Mol Syndromol, 2*(3-5), 137-152. doi:10.1159/000331333

Bahi-Buisson, N., Villeneuve, N., Caietta, E., Jacquette, A., Maurey, H., Matthijs, G., *et al.* (2012). Recurrent mutations in the CDKL5 gene: genotype-phenotype relationships. *Am J Med Genet A, 158A*(7), 1612-1619. doi:10.1002/ajmg.a.35401

Baker, K., Gordon, S. L., Melland, H., Bumbak, F., Scott, D. J., Jiang, T. J., *et al.* (2018). SYT1-associated neurodevelopmental disorder: a case series. *Brain, 141*(9), 2576-2591. doi:10.1093/brain/awy209

Baldelli, P., Fassio, A., Valtorta, F., & Benfenati, F. (2007). Lack of synapsin I reduces the readily releasable pool of synaptic vesicles at central inhibitory synapses. *J Neurosci, 27*(49), 13520-13531. doi:10.1523/JNEUROSCI.3151-07.2007

Baltussen, L. L., Negraes, P. D., Silvestre, M., Claxton, S., Moeskops, M., Christodoulou, E., *et al.* (2018). Chemical genetic identification of CDKL5 substrates reveals its role in neuronal microtubule dynamics. *EMBO J, 37*(24). doi:10.15252/embj.201899763

Barbiero, I., De Rosa, R., & Kilstrup-Nielsen, C. (2019a). Microtubules: A Key to Understand and Correct Neuronal Defects in CDKL5 Deficiency Disorder? *Int J Mol Sci, 20*(17). doi:10.3390/ijms20174075

Barbiero, I., Peroni, D., Siniscalchi, P., Rusconi, L., Tramarin, M., De Rosa, R., *et al.* (2019b). Pregnenolone and pregnenolone-methyl-ether rescue neuronal defects caused by dysfunctional CLIP170 in a neuronal model of CDKL5 Deficiency Disorder. *Neuropharmacology, 164*, 107897. doi:10.1016/j.neuropharm.2019.107897

Barbiero, I., Peroni, D., Tramarin, M., Chandola, C., Rusconi, L., Landsberger, N., *et al.* (2017a). The neurosteroid pregnenolone reverts microtubule derangement induced by the loss of a functional CDKL5-IQGAP1 complex. *Hum Mol Genet, 26*(18), 3520-3530. doi:10.1093/hmg/ddx237

Barbiero, I., Valente, D., Chandola, C., Magi, F., Bergo, A., Monteonofrio, L., *et al.* (2017b). CDKL5 localizes at the centrosome and midbody and is required for faithful cell division. *Sci Rep, 7*(1), 6228. doi:10.1038/s41598-017-05875-z

Bauerfeind, R., Takei, K., & De Camilli, P. (1997). Amphiphysin I is associated with coated endocytic intermediates and undergoes stimulation-dependent dephosphorylation in nerve terminals. *J Biol Chem, 272*(49), 30984-30992. doi:10.1074/jbc.272.49.30984

Benfenati, F., & Lanzani, G. (2021). Clinical translation of nanoparticles for neural stimulation. *Nature Reviews Materials, 6*(1), 1-4. doi:10.1038/s41578-020-00267-8

Blood, P. D., & Voth, G. A. (2006). Direct observation of Bin/amphiphysin/Rvs (BAR) domain-induced membrane curvature by means of molecular dynamics simulations. *Proc Natl Acad Sci U S A, 103*(41), 15068-15072. doi:10.1073/pnas.0603917103

Bodaleo, F. J., & Gonzalez-Billault, C. (2016). The Presynaptic Microtubule Cytoskeleton in Physiological and Pathological Conditions: Lessons from Drosophila Fragile X Syndrome and Hereditary Spastic Paraplegias. *Front Mol Neurosci, 9*, 60. doi:10.3389/fnmol.2016.00060

Bodaleo, F. J., Montenegro-Venegas, C., Henriquez, D. R., Court, F. A., & Gonzalez-Billault, C. (2016). Microtubule-associated protein 1B (MAP1B)-deficient neurons show structural presynaptic deficiencies in vitro and altered presynaptic physiology. *Sci Rep, 6*, 30069. doi:10.1038/srep30069

Bohuszewicz, O., Liu, J., & Low, H. H. (2016). Membrane remodelling in bacteria. *J Struct Biol, 196*(1), 3-14. doi:10.1016/j.jsb.2016.05.010

Boucrot, E., Ferreira, A. P., Almeida-Souza, L., Debard, S., Vallis, Y., Howard, G., *et al.* (2015). Endophilin marks and controls a clathrin-independent endocytic pathway. *Nature, 517*(7535), 460-465. doi:10.1038/nature14067

Boucrot, E., Pick, A., Camdere, G., Liska, N., Evergren, E., McMahon, H. T., *et al.* (2012). Membrane fission is promoted by insertion of amphipathic helices and is restricted by crescent BAR domains. *Cell, 149*(1), 124-136. doi:10.1016/j.cell.2012.01.047

Boumil, R. M., Letts, V. A., Roberts, M. C., Lenz, C., Mahaffey, C. L., Zhang, Z. W., *et al.* (2010). A missense mutation in a highly conserved alternate exon of dynamin-1 causes epilepsy in fitful mice. *PLoS Genet, 6*(8). doi:10.1371/journal.pgen.1001046

Bragina, L., Fattorini, G., Giovedi, S., Melone, M., Bosco, F., Benfenati, F., *et al.* (2011). Analysis of Synaptotagmin, SV2, and Rab3 Expression in Cortical Glutamatergic and GABAergic Axon Terminals. *Front Cell Neurosci, 5*, 32. doi:10.3389/fncel.2011.00032

Bykhovskaia, M. (2011). Synapsin regulation of vesicle organization and functional pools. *Semin Cell Dev Biol, 22*(4), 387-392. doi:10.1016/j.semcdb.2011.07.003

Candiello, E., Kratzke, M., Wenzel, D., Cassel, D., & Schu, P. (2016). AP-1/sigma1A and AP-1/sigma1B adaptor-proteins differentially regulate neuronal early endosome maturation via the Rab5/Vps34-pathway. *Sci Rep, 6*, 29950. doi:10.1038/srep29950

Canning, P., Park, K., Goncalves, J., Li, C., Howard, C. J., Sharpe, T. D., *et al.* (2018). CDKL Family Kinases Have Evolved Distinct Structural Features and Ciliary Function. *Cell Rep, 22*(4), 885-894. doi:10.1016/j.celrep.2017.12.083

Carli, S., Chaabane, L., Butti, C., De Palma, C., Aimar, P., Salio, C., *et al.* (2021). In vivo magnetic resonance spectroscopy in the brain of Cdkl5 null mice reveals a metabolic profile indicative of mitochondrial dysfunctions. *J Neurochem*. doi:10.1111/jnc.15300

Carouge, D., Host, L., Aunis, D., Zwiller, J., & Anglard, P. (2010). CDKL5 is a brain MeCP2 target gene regulated by DNA methylation. *Neurobiol Dis, 38*(3), 414-424. doi:10.1016/j.nbd.2010.02.014

Cestra, G., Castagnoli, L., Dente, L., Minenkova, O., Petrelli, A., Migone, N., *et al.* (1999). The SH3 domains of endophilin and amphiphysin bind to the proline-rich region of synaptojanin 1 at distinct sites that display an unconventional binding specificity. *J Biol Chem, 274*(45), 32001-32007. doi:10.1074/jbc.274.45.32001

Chanaday, N. L., Cousin, M. A., Milosevic, I., Watanabe, S., & Morgan, J. R. (2019). The Synaptic Vesicle Cycle Revisited: New Insights into the Modes and Mechanisms. *J Neurosci, 39*(42), 8209-8216. doi:10.1523/JNEUROSCI.1158-19.2019

Chanaday, N. L., & Kavalali, E. T. (2018). Time course and temperature dependence of synaptic vesicle endocytosis. *FEBS Lett, 592*(21), 3606-3614. doi:10.1002/1873-3468.13268

Chen, C. K., Bregere, C., Paluch, J., Lu, J. F., Dickman, D. K., & Chang, K. T. (2014). Activity-dependent facilitation of Synaptojanin and synaptic vesicle recycling by the Minibrain kinase. *Nat Commun, 5*, 4246. doi:10.1038/ncomms5246

Chen, Q., Zhu, Y. C., Yu, J., Miao, S., Zheng, J., Xu, L., *et al.* (2010). CDKL5, a protein associated with rett syndrome, regulates neuronal morphogenesis via Rac1 signaling. *J Neurosci, 30*(38), 12777-12786. doi:10.1523/JNEUROSCI.1102-10.2010

Chen, X., Wu, X., Wu, H., & Zhang, M. (2020). Phase separation at the synapse. *Nat Neurosci, 23*(3), 301-310. doi:10.1038/s41593-019-0579-9

Chen, Y., Cao, W., Wang, L., & Zhong, T. (2020). AMPH1 functions as a tumour suppressor in ovarian cancer via the inactivation of PI3K/AKT pathway. *J Cell Mol Med, 24*(13), 7652-7659. doi:10.1111/jcmm.15400

Chen, Y., Deng, L., Maeno-Hikichi, Y., Lai, M., Chang, S., Chen, G., *et al.* (2003). Formation of an endophilin-Ca2+ channel complex is critical for clathrin-mediated synaptic vesicle endocytosis. *Cell, 115*(1), 37-48. doi:10.1016/s0092-8674(03)00726-8

Cheung, G., & Cousin, M. A. (2012). Adaptor protein complexes 1 and 3 are essential for generation of synaptic vesicles from activity-dependent bulk endosomes. *J Neurosci, 32*(17), 6014-6023. doi:10.1523/JNEUROSCI.6305-11.2012

Cheung, G., & Cousin, M. A. (2013). Synaptic vesicle generation from activity-dependent bulk endosomes requires calcium and calcineurin. *J Neurosci, 33*(8), 3370-3379. doi:10.1523/JNEUROSCI.4697-12.2013

Cheung, G., & Cousin, M. A. (2019). Synaptic vesicle generation from activity-dependent bulk endosomes requires a dephosphorylation-dependent dynamin-syndapin interaction. *J Neurochem, 151*(5), 570-583. doi:10.1111/jnc.14862

Cheung, G., Jupp, O. J., & Cousin, M. A. (2010). Activity-dependent bulk endocytosis and clathrin-dependent endocytosis replenish specific synaptic vesicle pools in central nerve terminals. *J Neurosci, 30*(24), 8151-8161. doi:10.1523/JNEUROSCI.0293-10.2010

Choudhury, M., Kleiner, O., Chung, R., Barden, L., Morgan, L., Patel, T. R., *et al.* (2008). Amphiphysin I phosphorylation on residue threonine 260 in a pentylenetetrazole-induced seizure model. *Neurosci Lett, 444*(3), 245-249. doi:10.1016/j.neulet.2008.08.055

Clayton, E. L., Anggono, V., Smillie, K. J., Chau, N., Robinson, P. J., & Cousin, M. A. (2009). The phospho-dependent dynamin-syndapin interaction triggers activity-dependent bulk endocytosis of synaptic vesicles. *J Neurosci, 29*(24), 7706-7717. doi:10.1523/JNEUROSCI.1976-09.2009

Clayton, E. L., & Cousin, M. A. (2009). Quantitative monitoring of activity-dependent bulk endocytosis of synaptic vesicle membrane by fluorescent dextran imaging. *J Neurosci Methods, 185*(1), 76-81. doi:10.1016/j.jneumeth.2009.09.016

Clayton, E. L., Evans, G. J., & Cousin, M. A. (2008). Bulk synaptic vesicle endocytosis is rapidly triggered during strong stimulation. *J Neurosci, 28*(26), 6627-6632. doi:10.1523/JNEUROSCI.1445-08.2008

Clayton, E. L., Sue, N., Smillie, K. J., O'Leary, T., Bache, N., Cheung, G., *et al.* (2010). Dynamin I phosphorylation by GSK3 controls activity-dependent bulk endocytosis of synaptic vesicles. *Nat Neurosci, 13*(7), 845-851. doi:10.1038/nn.2571

Corera, A. T., Doucet, G., & Fon, E. A. (2009). Long-term potentiation in isolated dendritic spines. *PLoS One, 4*(6), e6021. doi:10.1371/journal.pone.0006021

Cortes-Saladelafont, E., Lipstein, N., & Garcia-Cazorla, A. (2018). Presynaptic disorders: a clinical and pathophysiological approach focused on the synaptic vesicle. *J Inherit Metab Dis, 41*(6), 1131-1145. doi:10.1007/s10545-018-0230-z

Costa-Mattioli, M., & Monteggia, L. M. (2013). mTOR complexes in neurodevelopmental and neuropsychiatric disorders. *Nat Neurosci, 16*(11), 1537-1543. doi:10.1038/nn.3546

Cousin, M. A., & Robinson, P. J. (2001). The dephosphins: dephosphorylation by calcineurin triggers synaptic vesicle endocytosis. *Trends Neurosci, 24*(11), 659-665. doi:10.1016/s0166-2236(00)01930-5

Craft, G. E., Graham, M. E., Bache, N., Larsen, M. R., & Robinson, P. J. (2008). The in vivo phosphorylation sites in multiple isoforms of amphiphysin I from rat brain nerve terminals. *Mol Cell Proteomics, 7*(6), 1146-1161. doi:10.1074/mcp.M700351-MCP200

Crawford, D. C., & Kavalali, E. T. (2015). Molecular underpinnings of synaptic vesicle pool heterogeneity. *Traffic, 16*(4), 338-364. doi:10.1111/tra.12262

Custer, K. L., Austin, N. S., Sullivan, J. M., & Bajjalieh, S. M. (2006). Synaptic vesicle protein 2 enhances release probability at quiescent synapses. *J Neurosci, 26*(4), 1303-1313. doi:10.1523/JNEUROSCI.2699-05.2006

Dale, T., Downs, J., Olson, H., Bergin, A. M., Smith, S., & Leonard, H. (2019). Cannabis for refractory epilepsy in children: A review focusing on CDKL5 Deficiency Disorder. *Epilepsy Res, 151*, 31-39. doi:10.1016/j.eplepsyres.2019.02.001

Daumke, O., Roux, A., & Haucke, V. (2014). BAR domain scaffolds in dynamin-mediated membrane fission. *Cell, 156*(5), 882-892. doi:10.1016/j.cell.2014.02.017

David, C., McPherson, P. S., Mundigl, O., & de Camilli, P. (1996). A role of amphiphysin in synaptic vesicle endocytosis suggested by its binding to dynamin in nerve terminals. *Proc Natl Acad Sci U S A, 93*(1), 331-335. doi:10.1073/pnas.93.1.331

David, C., Solimena, M., & De Camilli, P. (1994). Autoimmunity in stiff-Man syndrome with breast cancer is targeted to the C-terminal region of human amphiphysin, a protein similar to the yeast proteins, Rvs167 and Rvs161. *FEBS Lett, 351*(1), 73-79. doi:10.1016/0014-5793(94)00826-4

De Camilli, P., Thomas, A., Cofiell, R., Folli, F., Lichte, B., Piccolo, G., *et al.* (1993). The synaptic vesicle-associated protein amphiphysin is the 128-kD autoantigen of Stiff-Man syndrome with breast cancer. *J Exp Med, 178*(6), 2219-2223. doi:10.1084/jem.178.6.2219

De Jesus-Cortes, H. J., Nogueras-Ortiz, C. J., Gearing, M., Arnold, S. E., & Vega, I. E. (2012). Amphiphysin-1 protein level changes associated with tau-mediated neurodegeneration. *Neuroreport, 23*(16), 942-946. doi:10.1097/WNR.0b013e32835982ce

Deciphering Developmental Disorders, S. (2017). Prevalence and architecture of de novo mutations in developmental disorders. *Nature, 542*(7642), 433-438. doi:10.1038/nature21062

Della Sala, G., Putignano, E., Chelini, G., Melani, R., Calcagno, E., Michele Ratto, G., *et al.* (2016). Dendritic Spine Instability in a Mouse Model of CDKL5 Disorder Is Rescued by Insulin-like Growth Factor 1. *Biol Psychiatry, 80*(4), 302-311. doi:10.1016/j.biopsych.2015.08.028

Demarest, S., Pestana-Knight, E. M., Olson, H. E., Downs, J., Marsh, E. D., Kaufmann, W. E., *et al.* (2019). Severity Assessment in CDKL5 Deficiency Disorder. *Pediatr Neurol, 97*, 38-42. doi:10.1016/j.pediatrneurol.2019.03.017

Devinsky, O., King, L., Bluvstein, J., & Friedman, D. (2021). Ataluren for drug-resistant epilepsy in nonsense variant-mediated Dravet syndrome and CDKL5 deficiency disorder. *Ann Clin Transl Neurol*. doi:10.1002/acn3.51306

Devinsky, O., Verducci, C., Thiele, E. A., Laux, L. C., Patel, A. D., Filloux, F., *et al.* (2018). Open-label use of highly purified CBD (Epidiolex(R)) in patients with CDKL5 deficiency disorder and Aicardi, Dup15q, and Doose syndromes. *Epilepsy Behav, 86*, 131-137. doi:10.1016/j.yebeh.2018.05.013

Dhindsa, R. S., Bradrick, S. S., Yao, X., Heinzen, E. L., Petrovski, S., Krueger, B. J., *et al.* (2015). Epileptic encephalopathy-causing mutations in DNM1 impair synaptic vesicle endocytosis. *Neurol Genet, 1*(1), e4. doi:10.1212/01.NXG.0000464295.65736.da

Di Paolo, G., Sankaranarayanan, S., Wenk, M. R., Daniell, L., Perucco, E., Caldarone, B. J., *et al.* (2002). Decreased synaptic vesicle recycling efficiency and cognitive deficits in amphiphysin 1 knockout mice. *Neuron, 33*(5), 789-804. doi:10.1016/s0896-6273(02)00601-3

Dolphin, A. C., & Lee, A. (2020). Presynaptic calcium channels: specialized control of synaptic neurotransmitter release. *Nat Rev Neurosci, 21*(4), 213-229. doi:10.1038/s41583-020-0278-2

Doring, M., Loos, A., Schrader, N., Pfander, B., & Bauerfeind, R. (2006). Nerve growth factor-induced phosphorylation of amphiphysin-1 by casein kinase 2 regulates clathrin-amphiphysin interactions. *J Neurochem, 98*(6), 2013-2022. doi:10.1111/j.1471-4159.2006.04037.x

Dulac, O. (2001). Epileptic encephalopathy. *Epilepsia, 42 Suppl 3*, 23-26. doi:10.1046/j.1528-1157.2001.042suppl.3023.x

Dulubova, I., Lou, X., Lu, J., Huryeva, I., Alam, A., Schneggenburger, R., *et al.* (2005). A Munc13/RIM/Rab3 tripartite complex: from priming to plasticity? *EMBO J, 24*(16), 2839-2850. doi:10.1038/sj.emboj.7600753

Eggermann, E., Bucurenciu, I., Goswami, S. P., & Jonas, P. (2011). Nanodomain coupling between Ca(2)(+) channels and sensors of exocytosis at fast mammalian synapses. *Nat Rev Neurosci, 13*(1), 7-21. doi:10.1038/nrn3125

Elia, M., Falco, M., Ferri, R., Spalletta, A., Bottitta, M., Calabrese, G., *et al.* (2008). CDKL5 mutations in boys with severe encephalopathy and early-onset intractable epilepsy. *Neurology, 71*(13), 997-999. doi:10.1212/01.wnl.0000326592.37105.88

Ellenbroek, B., & Youn, J. (2016). Rodent models in neuroscience research: is it a rat race? *Dis Model Mech, 9*(10), 1079-1087. doi:10.1242/dmm.026120

Emperador-Melero, J., & Kaeser, P. S. (2020). Assembly of the presynaptic active zone. *Curr Opin Neurobiol, 63*, 95-103. doi:10.1016/j.conb.2020.03.008

Erez, A., Patel, A. J., Wang, X., Xia, Z., Bhatt, S. S., Craigen, W., *et al.* (2009). Alu-specific microhomology-mediated deletions in CDKL5 in females with early-onset seizure disorder. *Neurogenetics, 10*(4), 363-369. doi:10.1007/s10048-009-0195-z

Etholm, L., Bahonjic, E., Walaas, S. I., Kao, H. T., & Heggelund, P. (2012). Neuroethologically delineated differences in the seizure behavior of synapsin 1 and synapsin 2 knock-out mice. *Epilepsy Res, 99*(3), 252-259. doi:10.1016/j.eplepsyres.2011.12.004

Evans, G. J., & Cousin, M. A. (2007). Activity-dependent control of slow synaptic vesicle endocytosis by cyclin-dependent kinase 5. *J Neurosci, 27*(2), 401-411. doi:10.1523/JNEUROSCI.3809-06.2007

Evans, J. C., Archer, H. L., Colley, J. P., Ravn, K., Nielsen, J. B., Kerr, A., *et al.* (2005). Early onset seizures and Rett-like features associated with

mutations in CDKL5. *Eur J Hum Genet, 13*(10), 1113-1120. doi:10.1038/sj.ejhg.5201451

Evergren, E., Marcucci, M., Tomilin, N., Low, P., Slepnev, V., Andersson, F., *et al.* (2004). Amphiphysin is a component of clathrin coats formed during synaptic vesicle recycling at the lamprey giant synapse. *Traffic, 5*(7), 514-528. doi:10.1111/j.1398-9219.2004.00198.x

Fahmi, M., Yasui, G., Seki, K., Katayama, S., Kaneko-Kawano, T., Inazu, T., *et al.* (2019). In Silico Study of Rett Syndrome Treatment-Related Genes, MECP2, CDKL5, and FOXG1, by Evolutionary Classification and Disordered Region Assessment. *Int J Mol Sci, 20*(22). doi:10.3390/ijms20225593

Fallah, M. S., & Eubanks, J. H. (2020). Seizures in Mouse Models of Rare Neurodevelopmental Disorders. *Neuroscience*. doi:10.1016/j.neuroscience.2020.01.041

Farsad, K., Slepnev, V., Ochoa, G., Daniell, L., Haucke, V., & De Camilli, P. (2003). A putative role for intramolecular regulatory mechanisms in the adaptor function of amphiphysin in endocytosis. *Neuropharmacology, 45*(6), 787-796. doi:10.1016/s0028-3908(03)00306-x

Farsi, Z., Jahn, R., & Woehler, A. (2017). Proton electrochemical gradient: Driving and regulating neurotransmitter uptake. *Bioessays, 39*(5). doi:10.1002/bies.201600240

Fassio, A., Fadda, M., & Benfenati, F. (2016). Molecular Machines Determining the Fate of Endocytosed Synaptic Vesicles in Nerve Terminals. *Front Synaptic Neurosci, 8*, 10. doi:10.3389/fnsyn.2016.00010

Fazzari, M., Frasca, A., Bifari, F., & Landsberger, N. (2019). Aminoglycoside drugs induce efficient read-through of CDKL5 nonsense mutations, slightly restoring its kinase activity. *RNA Biol, 16*(10), 1414-1423. doi:10.1080/15476286.2019.1632633

Fehr, S., Downs, J., Ho, G., de Klerk, N., Forbes, D., Christodoulou, J., *et al.* (2016a). Functional abilities in children and adults with the CDKL5 disorder. *Am J Med Genet A, 170*(11), 2860-2869. doi:10.1002/ajmg.a.37851

Fehr, S., Wilson, M., Downs, J., Williams, S., Murgia, A., Sartori, S., *et al.* (2013). The CDKL5 disorder is an independent clinical entity associated with early-onset encephalopathy. *Eur J Hum Genet, 21*(3), 266-273. doi:10.1038/ejhg.2012.156

Fehr, S., Wong, K., Chin, R., Williams, S., de Klerk, N., Forbes, D., *et al.* (2016b). Seizure variables and their relationship to genotype and functional abilities in the CDKL5 disorder. *Neurology, 87*(21), 2206-2213. doi:10.1212/WNL.0000000000003352

Fernandez-Alfonso, T., & Ryan, T. A. (2004). The kinetics of synaptic vesicle pool depletion at CNS synaptic terminals. *Neuron, 41*(6), 943-953. doi:10.1016/s0896-6273(04)00113-8

Fernandez-Alfonso, T., & Ryan, T. A. (2008). A heterogeneous "resting" pool of synaptic vesicles that is dynamically interchanged across boutons in mammalian CNS synapses. *Brain Cell Biol, 36*(1-4), 87-100. doi:10.1007/s11068-008-9030-y

Fernandez-Chacon, R., Konigstorfer, A., Gerber, S. H., Garcia, J., Matos, M. F., Stevens, C. F., *et al.* (2001). Synaptotagmin I functions as a calcium regulator of release probability. *Nature, 410*(6824), 41-49. doi:10.1038/35065004

Fichou, Y., Nectoux, J., Bahi-Buisson, N., Chelly, J., & Bienvenu, T. (2011). An isoform of the severe encephalopathy-related CDKL5 gene, including a novel exon with extremely high sequence conservation, is specifically expressed in brain. *J Hum Genet, 56*(1), 52-57. doi:10.1038/jhg.2010.143

Floor, E., Leventhal, P. S., & Schaeffer, S. F. (1990). Partial purification and characterization of the vacuolar H(+)-ATPase of mammalian synaptic vesicles. *J Neurochem, 55*(5), 1663-1670. doi:10.1111/j.1471-4159.1990.tb04954.x

Floyd, S., Butler, M. H., Cremona, O., David, C., Freyberg, Z., Zhang, X., *et al.* (1998). Expression of amphiphysin I, an autoantigen of paraneoplastic neurological syndromes, in breast cancer. *Mol Med, 4*(1), 29-39.

Floyd, S., Porro, E. B., Slepnev, V. I., Ochoa, G. C., Tsai, L. H., & De Camilli, P. (2001). Amphiphysin 1 binds the cyclin-dependent kinase (cdk) 5 regulatory subunit p35 and is phosphorylated by cdk5 and cdc2. *J Biol Chem, 276*(11), 8104-8110. doi:10.1074/jbc.M008932200

Ford, M. G., Mills, I. G., Peter, B. J., Vallis, Y., Praefcke, G. J., Evans, P. R., *et al.* (2002). Curvature of clathrin-coated pits driven by epsin. *Nature, 419*(6905), 361-366. doi:10.1038/nature01020

Ford, M. G., Pearse, B. M., Higgins, M. K., Vallis, Y., Owen, D. J., Gibson, A., *et al.* (2001). Simultaneous binding of PtdIns(4,5)P2 and clathrin by

AP180 in the nucleation of clathrin lattices on membranes. *Science, 291*(5506), 1051-1055. doi:10.1126/science.291.5506.1051

Fossati, M., Assendorp, N., Gemin, O., Colasse, S., Dingli, F., Arras, G., *et al.* (2019). Trans-Synaptic Signaling through the Glutamate Receptor Delta-1 Mediates Inhibitory Synapse Formation in Cortical Pyramidal Neurons. *Neuron, 104*(6), 1081-1094 e1087. doi:10.1016/j.neuron.2019.09.027

Fowler, M. W., & Staras, K. (2015). Synaptic vesicle pools: Principles, properties and limitations. *Exp Cell Res, 335*(2), 150-156. doi:10.1016/j.yexcr.2015.03.007

Freal, A., & Hoogenraad, C. C. (2019). Neuronal Cytoskeleton: Presynaptic Boutons as Hotspots for Activity-Dependent Microtubule Nucleation. *Curr Biol, 29*(24), R1307-R1309. doi:10.1016/j.cub.2019.11.011

Frost, A., Unger, V. M., & De Camilli, P. (2009). The BAR domain superfamily: membrane-molding macromolecules. *Cell, 137*(2), 191-196. doi:10.1016/j.cell.2009.04.010

Fuchs, C., Gennaccaro, L., Ren, E., Galvani, G., Trazzi, S., Medici, G., *et al.* (2019a). Pharmacotherapy with sertraline rescues brain development and behavior in a mouse model of CDKL5 deficiency disorder. *Neuropharmacology*, 107746. doi:10.1016/j.neuropharm.2019.107746

Fuchs, C., Medici, G., Trazzi, S., Gennaccaro, L., Galvani, G., Berteotti, C., *et al.* (2019b). CDKL5 deficiency predisposes neurons to cell death through the deregulation of SMAD3 signaling. *Brain Pathol, 29*(5), 658-674. doi:10.1111/bpa.12716

Fuchs, C., Rimondini, R., Viggiano, R., Trazzi, S., De Franceschi, M., Bartesaghi, R., *et al.* (2015). Inhibition of GSK3beta rescues hippocampal development and learning in a mouse model of CDKL5 disorder. *Neurobiol Dis, 82*, 298-310. doi:10.1016/j.nbd.2015.06.018

Fuchs, C., Trazzi, S., Torricella, R., Viggiano, R., De Franceschi, M., Amendola, E., *et al.* (2014). Loss of CDKL5 impairs survival and dendritic growth of newborn neurons by altering AKT/GSK-3beta signaling. *Neurobiol Dis, 70*, 53-68. doi:10.1016/j.nbd.2014.06.006

Fukata, Y., & Fukata, M. (2017). Epilepsy and synaptic proteins. *Curr Opin Neurobiol, 45*, 1-8. doi:10.1016/j.conb.2017.02.001

Gad, H., Ringstad, N., Low, P., Kjaerulff, O., Gustafsson, J., Wenk, M., *et al.* (2000). Fission and uncoating of synaptic clathrin-coated vesicles are perturbed by disruption of interactions with the SH3 domain of endophilin. *Neuron, 27*(2), 301-312. doi:10.1016/s0896-6273(00)00038-6

Gallop, J. L., Jao, C. C., Kent, H. M., Butler, P. J., Evans, P. R., Langen, R., *et al.* (2006). Mechanism of endophilin N-BAR domain-mediated membrane curvature. *EMBO J, 25*(12), 2898-2910. doi:10.1038/sj.emboj.7601174

Gan, Q., & Watanabe, S. (2018). Synaptic Vesicle Endocytosis in Different Model Systems. *Front Cell Neurosci, 12*, 171. doi:10.3389/fncel.2018.00171

Gao, Y., Irvine, E. E., Eleftheriadou, I., Naranjo, C. J., Hearn-Yeates, F., Bosch, L., *et al.* (2020). Gene replacement ameliorates deficits in mouse and human models of cyclin-dependent kinase-like 5 disorder. *Brain, 143*(3), 811-832. doi:10.1093/brain/awaa028

Garcia, C. C., Blair, H. J., Seager, M., Coulthard, A., Tennant, S., Buddles, M., *et al.* (2004). Identification of a mutation in synapsin I, a synaptic vesicle protein, in a family with epilepsy. *J Med Genet, 41*(3), 183-186. doi:10.1136/jmg.2003.013680

Geppert, M., Goda, Y., Hammer, R. E., Li, C., Rosahl, T. W., Stevens, C. F., *et al.* (1994). Synaptotagmin I: a major Ca2+ sensor for transmitter release at a central synapse. *Cell, 79*(4), 717-727. doi:10.1016/0092-8674(94)90556-8

Goldsmith, E. J., Akella, R., Min, X., Zhou, T., & Humphreys, J. M. (2007). Substrate and docking interactions in serine/threonine protein kinases. *Chem Rev, 107*(11), 5065-5081. doi:10.1021/cr068221w

Gowrisankaran, S., Houy, S., Del Castillo, J. G. P., Steubler, V., Gelker, M., Kroll, J., *et al.* (2020). Endophilin-A coordinates priming and fusion of neurosecretory vesicles via intersectin. *Nat Commun, 11*(1), 1266. doi:10.1038/s41467-020-14993-8

Gowrisankaran, S., & Milosevic, I. (2020). Regulation of synaptic vesicle acidification at the neuronal synapse. *IUBMB Life, 72*(4), 568-576. doi:10.1002/iub.2235

Grabs, D., Bergmann, M., & Rager, G. (2000). Developmental expression of amphiphysin in the retinotectal system of the chick: from mRNA to protein. *Eur J Neurosci, 12*(5), 1545-1553. doi:10.1046/j.1460-9568.2000.00043.x

Grabs, D., Slepnev, V. I., Songyang, Z., David, C., Lynch, M., Cantley, L. C., *et al.* (1997). The SH3 domain of amphiphysin binds the proline-rich domain of dynamin at a single site that defines a new SH3 binding consensus sequence. *J Biol Chem, 272*(20), 13419-13425. doi:10.1074/jbc.272.20.13419

Gramlich, M. W., & Klyachko, V. A. (2017). Actin/Myosin-V- and Activity-Dependent Inter-synaptic Vesicle Exchange in Central Neurons. *Cell Rep, 18*(9), 2096-2104. doi:10.1016/j.celrep.2017.02.010

Granseth, B., Odermatt, B., Royle, S. J., & Lagnado, L. (2006). Clathrin-mediated endocytosis is the dominant mechanism of vesicle retrieval at hippocampal synapses. *Neuron, 51*(6), 773-786. doi:10.1016/j.neuron.2006.08.029

Guerrini, R., & Parrini, E. (2012). Epilepsy in Rett syndrome, and CDKL5- and FOXG1-gene-related encephalopathies. *Epilepsia, 53*(12), 2067-2078. doi:10.1111/j.1528-1167.2012.03656.x

Hanson, P. I., Roth, R., Morisaki, H., Jahn, R., & Heuser, J. E. (1997). Structure and conformational changes in NSF and its membrane receptor complexes visualized by quick-freeze/deep-etch electron microscopy. *Cell, 90*(3), 523-535. doi:10.1016/s0092-8674(00)80512-7

Hector, R. D., Dando, O., Landsberger, N., Kilstrup-Nielsen, C., Kind, P. C., Bailey, M. E., *et al.* (2016). Characterisation of CDKL5 Transcript Isoforms in Human and Mouse. *PLoS One, 11*(6), e0157758. doi:10.1371/journal.pone.0157758

Hector, R. D., Kalscheuer, V. M., Hennig, F., Leonard, H., Downs, J., Clarke, A., *et al.* (2017). CDKL5 variants: Improving our understanding of a rare neurologic disorder. *Neurol Genet, 3*(6), e200. doi:10.1212/NXG.0000000000000200

Henne, W. M., Boucrot, E., Meinecke, M., Evergren, E., Vallis, Y., Mittal, R., *et al.* (2010). FCHo proteins are nucleators of clathrin-mediated endocytosis. *Science, 328*(5983), 1281-1284. doi:10.1126/science.1188462

Hohendahl, A., Talledge, N., Galli, V., Shen, P. S., Humbert, F., De Camilli, P., *et al.* (2017). Structural inhibition of dynamin-mediated membrane fission by endophilin. *Elife, 6*. doi:10.7554/eLife.26856

Holt, M., Cooke, A., Wu, M. M., & Lagnado, L. (2003). Bulk Membrane Retrieval in the Synaptic Terminal of Retinal Bipolar Cells. *The Journal of Neuroscience, 23*(4), 1329-1339. doi:10.1523/jneurosci.23-04-01329.2003

Homberg, J. R., Wohr, M., & Alenina, N. (2017). Comeback of the Rat in Biomedical Research. *ACS Chem Neurosci, 8*(5), 900-903. doi:10.1021/acschemneuro.6b00415

Hosoya, O., Tsutsui, K., & Tsutsui, K. (2004). Localized expression of amphiphysin Ir, a retina-specific variant of amphiphysin I, in the ribbon synapse and its functional implication. *Eur J Neurosci, 19*(8), 2179-2187. doi:10.1111/j.0953-816X.2004.03340.x

Hui, E., Johnson, C. P., Yao, J., Dunning, F. M., & Chapman, E. R. (2009). Synaptotagmin-mediated bending of the target membrane is a critical step in Ca(2+)-regulated fusion. *Cell, 138*(4), 709-721. doi:10.1016/j.cell.2009.05.049

Huser, S., Suri, G., Crottet, P., & Spiess, M. (2013). Interaction of amphiphysins with AP-1 clathrin adaptors at the membrane. *Biochem J, 450*(1), 73-83. doi:10.1042/BJ20121373

Huttner, W. B., Schiebler, W., Greengard, P., & De Camilli, P. (1983). Synapsin I (protein I), a nerve terminal-specific phosphoprotein. III. Its association with synaptic vesicles studied in a highly purified synaptic vesicle preparation. *J Cell Biol, 96*(5), 1374-1388. doi:10.1083/jcb.96.5.1374

Ivanova, D., Dobson, K. L., Gajbhiye, A., Davenport, E. C., Hacker, D., Ultanir, S. K., *et al.* (2021). Control of synaptic vesicle release probability via VAMP4 targeting to endolysosomes. *Sci Adv, 7*(18). doi:10.1126/sciadv.abf3873

Jagtap, S., Thanos, J. M., Fu, T., Wang, J., Lalonde, J., Dial, T. O., *et al.* (2019). Aberrant mitochondrial function in patient-derived neural cells from CDKL5 deficiency disorder and Rett syndrome. *Hum Mol Genet, 28*(21), 3625-3636. doi:10.1093/hmg/ddz208

Jahn, R., & Fasshauer, D. (2012). Molecular machines governing exocytosis of synaptic vesicles. *Nature, 490*(7419), 201-207. doi:10.1038/nature11320

Jahne, S., Rizzoli, S. O., & Helm, M. S. (2015). The structure and function of presynaptic endosomes. *Exp Cell Res, 335*(2), 172-179. doi:10.1016/j.yexcr.2015.04.017

Jakimiec, M., Paprocka, J., & Smigiel, R. (2020). CDKL5 Deficiency Disorder-A Complex Epileptic Encephalopathy. *Brain Sci, 10*(2). doi:10.3390/brainsci10020107

Jenkins, N. A., Gilbert, D. J., Yamamoto, R., Kilimann, M. W., & Copeland, N. G. (1995). Amphiphysin (Amph) maps to the proximal region of mouse chromosome 13. *Genomics, 28*(2), 363-365. doi:10.1006/geno.1995.1161

Jiang, Z., Gong, T., & Wei, H. (2019). CDKL5 promotes proliferation, migration, and chemotherapeutic drug resistance of glioma cells via activation of the PI3K/AKT signaling pathway. *FEBS Open Bio*. doi:10.1002/2211-5463.12780

Kadam, S. D., Sullivan, B. J., Goyal, A., Blue, M. E., & Smith-Hicks, C. (2019). Rett Syndrome and CDKL5 Deficiency Disorder: From Bench to Clinic. *Int J Mol Sci, 20*(20). doi:10.3390/ijms20205098

Kaeser, P. S., & Regehr, W. G. (2017). The readily releasable pool of synaptic vesicles. *Curr Opin Neurobiol, 43*, 63-70. doi:10.1016/j.conb.2016.12.012

Kaksonen, M., & Roux, A. (2018). Mechanisms of clathrin-mediated endocytosis. *Nat Rev Mol Cell Biol, 19*(5), 313-326. doi:10.1038/nrm.2017.132

Kalscheuer, V. M., Tao, J., Donnelly, A., Hollway, G., Schwinger, E., Kubart, S., *et al.* (2003). Disruption of the serine/threonine kinase 9 gene causes severe X-linked infantile spasms and mental retardation. *Am J Hum Genet, 72*(6), 1401-1411. doi:10.1086/375538

Kameshita, I., Sekiguchi, M., Hamasaki, D., Sugiyama, Y., Hatano, N., Suetake, I., *et al.* (2008). Cyclin-dependent kinase-like 5 binds and phosphorylates DNA methyltransferase 1. *Biochem Biophys Res Commun, 377*(4), 1162-1167. doi:10.1016/j.bbrc.2008.10.113

Kapur, J. N., Sahoo, P. K., & Wong, A. K. C. (1985). A New Method for Gray-Level Picture Thresholding Using the Entropy of the Histogram. *Computer Vision Graphics and Image Processing, 29*(3), 273-285. doi:Doi 10.1016/0734-189x(85)90125-2

Kasprowicz, J., Kuenen, S., Miskiewicz, K., Habets, R. L., Smitz, L., & Verstreken, P. (2008). Inactivation of clathrin heavy chain inhibits synaptic recycling but allows bulk membrane uptake. *J Cell Biol, 182*(5), 1007-1016. doi:10.1083/jcb.200804162

Kasprowicz, J., Kuenen, S., Swerts, J., Miskiewicz, K., & Verstreken, P. (2014). Dynamin photoinactivation blocks Clathrin and alpha-adaptin recruitment and induces bulk membrane retrieval. *J Cell Biol, 204*(7), 1141-1156. doi:10.1083/jcb.201310090

Katayama, S., Sueyoshi, N., Inazu, T., & Kameshita, I. (2020). Cyclin-Dependent Kinase-Like 5 (CDKL5): Possible Cellular Signalling Targets and Involvement in CDKL5 Deficiency Disorder. *Neural Plast, 2020*, 6970190. doi:10.1155/2020/6970190

Katayama, S., Sueyoshi, N., & Kameshita, I. (2015). Critical Determinants of Substrate Recognition by Cyclin-Dependent Kinase-like 5 (CDKL5). *Biochemistry, 54*(19), 2975-2987. doi:10.1021/bi501308k

Kelly, B. T., Graham, S. C., Liska, N., Dannhauser, P. N., Honing, S., Ungewickell, E. J., *et al.* (2014). Clathrin adaptors. AP2 controls clathrin polymerization with a membrane-activated switch. *Science, 345*(6195), 459-463. doi:10.1126/science.1254836

Kilstrup-Nielsen, C., Rusconi, L., La Montanara, P., Ciceri, D., Bergo, A., Bedogni, F., *et al.* (2012). What we know and would like to know about CDKL5 and its involvement in epileptic encephalopathy. *Neural Plast, 2012*, 728267. doi:10.1155/2012/728267

Kim, S. H., & Ryan, T. A. (2009). Synaptic vesicle recycling at CNS snapses without AP-2. *J Neurosci, 29*(12), 3865-3874. doi:10.1523/JNEUROSCI.5639-08.2009

Kim, Y., Park, J., Song, W. J., & Chang, S. (2010). Overexpression of Dyrk1A causes the defects in synaptic vesicle endocytosis. *Neurosignals, 18*(3), 164-172. doi:10.1159/000321994

Kjaerulff, O., Brodin, L., & Jung, A. (2011). The structure and function of endophilin proteins. *Cell Biochem Biophys, 60*(3), 137-154. doi:10.1007/s12013-010-9137-5

Klein, K. M., Yendle, S. C., Harvey, A. S., Antony, J. H., Wallace, G., Bienvenu, T., *et al.* (2011). A distinctive seizure type in patients with CDKL5 mutations: Hypermotor-tonic-spasms sequence. *Neurology, 76*(16), 1436-1438. doi:10.1212/WNL.0b013e3182166e58

Koch, D., Spiwoks-Becker, I., Sabanov, V., Sinning, A., Dugladze, T., Stellmacher, A., *et al.* (2011). Proper synaptic vesicle formation and neuronal network activity critically rely on syndapin I. *EMBO J, 30*(24), 4955-4969. doi:10.1038/emboj.2011.339

Koh, T. W., Korolchuk, V. I., Wairkar, Y. P., Jiao, W., Evergren, E., Pan, H., *et al.* (2007). Eps15 and Dap160 control synaptic vesicle membrane retrieval and synapse development. *J Cell Biol, 178*(2), 309-322. doi:10.1083/jcb.200701030

Kokotos, A. C., Harper, C. B., Marland, J. R. K., Smillie, K. J., Cousin, M. A., & Gordon, S. L. (2019). Synaptophysin sustains presynaptic performance by preserving vesicular synaptobrevin-II levels. *J Neurochem, 151*(1), 28-37. doi:10.1111/jnc.14797

Kokotos, A. C., Peltier, J., Davenport, E. C., Trost, M., & Cousin, M. A. (2018). Activity-dependent bulk endocytosis proteome reveals a key presynaptic role for the monomeric GTPase Rab11. *Proc Natl Acad Sci U S A, 115*(43), E10177-E10186. doi:10.1073/pnas.1809189115

Kononenko, N. L., Puchkov, D., Classen, G. A., Walter, A. M., Pechstein, A., Sawade, L., *et al.* (2014). Clathrin/AP-2 mediate synaptic vesicle reformation from endosome-like vacuoles but are not essential for membrane retrieval at central synapses. *Neuron, 82*(5), 981-988. doi:10.1016/j.neuron.2014.05.007

Kwon, S. E., & Chapman, E. R. (2011). Synaptophysin regulates the kinetics of synaptic vesicle endocytosis in central neurons. *Neuron, 70*(5), 847-854. doi:10.1016/j.neuron.2011.04.001

La Montanara, P., Rusconi, L., Locarno, A., Forti, L., Barbiero, I., Tramarin, M., *et al.* (2015). Synaptic synthesis, dephosphorylation, and degradation: a novel paradigm for an activity-dependent neuronal control of CDKL5. *J Biol Chem, 290*(7), 4512-4527. doi:10.1074/jbc.M114.589762

Lai, M. M., Luo, H. R., Burnett, P. E., Hong, J. J., & Snyder, S. H. (2000). The calcineurin-binding protein cain is a negative regulator of synaptic vesicle endocytosis. *J Biol Chem, 275*(44), 34017-34020. doi:10.1074/jbc.C000429200

Lai, Y., Choi, U. B., Leitz, J., Rhee, H. J., Lee, C., Altas, B., *et al.* (2017). Molecular Mechanisms of Synaptic Vesicle Priming by Munc13 and Munc18. *Neuron, 95*(3), 591-607 e510. doi:10.1016/j.neuron.2017.07.004

Lasser, M., Tiber, J., & Lowery, L. A. (2018). The Role of the Microtubule Cytoskeleton in Neurodevelopmental Disorders. *Front Cell Neurosci, 12*, 165. doi:10.3389/fncel.2018.00165

Lee, C., Kim, S. R., Chung, J. K., Frohman, M. A., Kilimann, M. W., & Rhee, S. G. (2000). Inhibition of phospholipase D by amphiphysins. *J Biol Chem, 275*(25), 18751-18758. doi:10.1074/jbc.M001695200

Lee, K. Z., & Liao, W. (2018). Loss of CDKL5 disrupts respiratory function in mice. *Respir Physiol Neurobiol, 248*, 48-54. doi:10.1016/j.resp.2017.11.010

Lee, S. H., Valtschanoff, J. G., Kharazia, V. N., Weinberg, R., & Sheng, M. (2001). Biochemical and morphological characterization of an intracellular membrane compartment containing AMPA receptors. *Neuropharmacology, 41*(6), 680-692. doi:10.1016/s0028-3908(01)00124-1

Leitz, J., & Kavalali, E. T. (2011). Ca(2)(+) influx slows single synaptic vesicle endocytosis. *J Neurosci, 31*(45), 16318-16326. doi:10.1523/JNEUROSCI.3358-11.2011

Leitz, J., & Kavalali, E. T. (2016). Ca2+ Dependence of Synaptic Vesicle Endocytosis. *Neuroscientist, 22*(5), 464-476. doi:10.1177/1073858415588265

Li, D., Shao, L., Chen, B. C., Zhang, X., Zhang, M., Moses, B., *et al.* (2015). ADVANCED IMAGING. Extended-resolution structured illumination imaging of endocytic and cytoskeletal dynamics. *Science, 349*(6251), aab3500. doi:10.1126/science.aab3500

Li, Z., & Murthy, V. N. (2001). Visualizing postendocytic traffic of synaptic vesicles at hippocampal synapses. *Neuron, 31*(4), 593-605. doi:10.1016/s0896-6273(01)00398-1

Liang, J. S., Huang, H., Wang, J. S., & Lu, J. F. (2019). Phenotypic manifestations between male and female children with CDKL5 mutations. *Brain Dev, 41*(9), 783-789. doi:10.1016/j.braindev.2019.05.003

Liang, S., Wei, F. Y., Wu, Y. M., Tanabe, K., Abe, T., Oda, Y., *et al.* (2007). Major Cdk5-dependent phosphorylation sites of amphiphysin 1 are implicated in the regulation of the membrane binding and endocytosis. *J Neurochem, 102*(5), 1466-1476. doi:10.1111/j.1471-4159.2007.04507.x

Lichte, B., Veh, R. W., Meyer, H. E., & Kilimann, M. W. (1992). Amphiphysin, a novel protein associated with synaptic vesicles. *EMBO J, 11*(7), 2521-2530.

Lim, Z., Wong, K., Olson, H. E., Bergin, A. M., Downs, J., & Leonard, H. (2017). Use of the ketogenic diet to manage refractory epilepsy in CDKL5 disorder: Experience of >100 patients. *Epilepsia, 58*(8), 1415-1422. doi:10.1111/epi.13813

Lin, C., Franco, B., & Rosner, M. R. (2005). CDKL5/Stk9 kinase inactivation is associated with neuronal developmental disorders. *Hum Mol Genet, 14*(24), 3775-3786. doi:10.1093/hmg/ddi391

Lindy, A. S., Stosser, M. B., Butler, E., Downtain-Pickersgill, C., Shanmugham, A., Retterer, K., *et al.* (2018). Diagnostic outcomes for genetic testing of 70 genes in 8565 patients with epilepsy and neurodevelopmental disorders. *Epilepsia, 59*(5), 1062-1071. doi:10.1111/epi.14074

Liu, J. P., Sim, A. T., & Robinson, P. J. (1994). Calcineurin inhibition of dynamin I GTPase activity coupled to nerve terminal depolarization. *Science, 265*(5174), 970-973. doi:10.1126/science.8052858

Livide, G., Patriarchi, T., Amenduni, M., Amabile, S., Yasui, D., Calcagno, E., *et al.* (2015). GluD1 is a common altered player in neuronal differentiation from both MECP2-mutated and CDKL5-mutated iPS cells. *Eur J Hum Genet, 23*(2), 195-201. doi:10.1038/ejhg.2014.81

Llobet, A., Gallop, J. L., Burden, J. J. E., Camdere, G., Chandra, P., Vallis, Y., *et al.* (2011). Endophilin drives the fast mode of vesicle retrieval in a ribbon synapse. *J Neurosci, 31*(23), 8512-8519. doi:10.1523/JNEUROSCI.6223-09.2011

Llobet, A., Wu, M., & Lagnado, L. (2008). The mouth of a dense-core vesicle opens and closes in a concerted action regulated by calcium and amphiphysin. *J Gen Physiol, 132*(4), i3. doi:10.1085/JGP1324OIA3

Lo Martire, V., Alvente, S., Bastianini, S., Berteotti, C., Silvani, A., Valli, A., *et al.* (2017). CDKL5 deficiency entails sleep apneas in mice. *J Sleep Res, 26*(4), 495-497. doi:10.1111/jsr.12512

Lynch, B. A., Lambeng, N., Nocka, K., Kensel-Hammes, P., Bajjalieh, S. M., Matagne, A., *et al.* (2004). The synaptic vesicle protein SV2A is the binding site for the antiepileptic drug levetiracetam. *Proc Natl Acad Sci U S A, 101*(26), 9861-9866. doi:10.1073/pnas.0308208101

MacKay, C. I., Bick, D., Prokop, J. W., Munoz, I., Rouse, J., Downs, J., *et al.* (2020). Expanding the phenotype of the CDKL5 deficiency disorder: Are seizures mandatory? *Am J Med Genet A, 182*(5), 1217-1222. doi:10.1002/ajmg.a.61504

MacKay, C. I., Wong, K., Demarest, S. T., Benke, T. A., Downs, J., & Leonard, H. (2021). Exploring genotype-phenotype relationships in the CDKL5 deficiency disorder using an international dataset. *Clin Genet, 99*(1), 157-165. doi:10.1111/cge.13862

Mahn, M., Saraf-Sinik, I., Patil, P., Pulin, M., Bitton, E., Karalis, N., *et al.* (2021). Efficient optogenetic silencing of neurotransmitter release with a

mosquito rhodopsin. *Neuron, 109*(10), 1621-1635 e1628. doi:10.1016/j.neuron.2021.03.013

Mangatt, M., Wong, K., Anderson, B., Epstein, A., Hodgetts, S., Leonard, H., *et al.* (2016). Prevalence and onset of comorbidities in the CDKL5 disorder differ from Rett syndrome. *Orphanet J Rare Dis, 11*, 39. doi:10.1186/s13023-016-0418-y

Maortua, H., Martinez-Bouzas, C., Calvo, M. T., Domingo, M. R., Ramos, F., Garcia-Ribes, A., *et al.* (2012). CDKL5 gene status in female patients with epilepsy and Rett-like features: two new mutations in the catalytic domain. *BMC Med Genet, 13*, 68. doi:10.1186/1471-2350-13-68

Mari, F., Azimonti, S., Bertani, I., Bolognese, F., Colombo, E., Caselli, R., *et al.* (2005). CDKL5 belongs to the same molecular pathway of MeCP2 and it is responsible for the early-onset seizure variant of Rett syndrome. *Hum Mol Genet, 14*(14), 1935-1946. doi:10.1093/hmg/ddi198

Marie, B., Sweeney, S. T., Poskanzer, K. E., Roos, J., Kelly, R. B., & Davis, G. W. (2004). Dap160/intersectin scaffolds the periactive zone to achieve high-fidelity endocytosis and normal synaptic growth. *Neuron, 43*(2), 207-219. doi:10.1016/j.neuron.2004.07.001

Marks, B., & McMahon, H. T. (1998). Calcium triggers calcineurin-dependent synaptic vesicle recycling in mammalian nerve terminals. *Curr Biol, 8*(13), 740-749. doi:10.1016/s0960-9822(98)70297-0

Marland, J. R., Hasel, P., Bonnycastle, K., & Cousin, M. A. (2016). Mitochondrial Calcium Uptake Modulates Synaptic Vesicle Endocytosis in Central Nerve Terminals. *J Biol Chem, 291*(5), 2080-2086. doi:10.1074/jbc.M115.686956

Marsh, J., & Alifragis, P. (2018). Synaptic dysfunction in Alzheimer's disease: the effects of amyloid beta on synaptic vesicle dynamics as a novel target for therapeutic intervention. *Neural Regen Res, 13*(4), 616-623. doi:10.4103/1673-5374.230276

Martens, S., Kozlov, M. M., & McMahon, H. T. (2007). How synaptotagmin promotes membrane fusion. *Science, 316*(5828), 1205-1208. doi:10.1126/science.1142614

Massol, R. H., Boll, W., Griffin, A. M., & Kirchhausen, T. (2006). A burst of auxilin recruitment determines the onset of clathrin-coated vesicle uncoating. *Proc Natl Acad Sci U S A, 103*(27), 10265-10270. doi:10.1073/pnas.0603369103

Matz, J., Gilyan, A., Kolar, A., McCarvill, T., & Krueger, S. R. (2010). Rapid structural alterations of the active zone lead to sustained changes in neurotransmitter release. *Proc Natl Acad Sci U S A, 107*(19), 8836-8841. doi:10.1073/pnas.0906087107

McMahon, H. T., & Boucrot, E. (2011). Molecular mechanism and physiological functions of clathrin-mediated endocytosis. *Nat Rev Mol Cell Biol, 12*(8), 517-533. doi:10.1038/nrm3151

McPherson, P. S. (1999). Regulatory role of SH3 domain-mediated protein-protein interactions in synaptic vesicle endocytosis. *Cell Signal, 11*(4), 229-238. doi:10.1016/s0898-6568(98)00059-x

McPherson, P. S., Garcia, E. P., Slepnev, V. I., David, C., Zhang, X., Grabs, D., *et al.* (1996). A presynaptic inositol-5-phosphatase. *Nature, 379*(6563), 353-357. doi:10.1038/379353a0

Meinecke, M., Boucrot, E., Camdere, G., Hon, W. C., Mittal, R., & McMahon, H. T. (2013). Cooperative recruitment of dynamin and BIN/amphiphysin/Rvs (BAR) domain-containing proteins leads to GTP-dependent membrane scission. *J Biol Chem, 288*(9), 6651-6661. doi:10.1074/jbc.M112.444869

Melani, F., Mei, D., Pisano, T., Savasta, S., Franzoni, E., Ferrari, A. R., *et al.* (2011). CDKL5 gene-related epileptic encephalopathy: electroclinical findings in the first year of life. *Dev Med Child Neurol, 53*(4), 354-360. doi:10.1111/j.1469-8749.2010.03889.x

Melikishvili, G., Epitashvili, N., Tabatadze, N., Chikvinidze, G., Dulac, O., Bienvenu, T., *et al.* (2019). New insights in phenomenology and treatment of epilepsy in CDKL5 encephalopathy. *Epilepsy Behav, 94*, 308-311. doi:10.1016/j.yebeh.2019.02.013

Mertens, J., Marchetto, M. C., Bardy, C., & Gage, F. H. (2016). Evaluating cell reprogramming, differentiation and conversion technologies in neuroscience. *Nat Rev Neurosci, 17*(7), 424-437. doi:10.1038/nrn.2016.46

Messina, S., Onofri, F., Bongiorno-Borbone, L., Giovedi, S., Valtorta, F., Girault, J. A., *et al.* (2003). Specific interactions of neuronal focal adhesion kinase isoforms with Src kinases and amphiphysin. *J Neurochem, 84*(2), 253-265. doi:10.1046/j.1471-4159.2003.01519.x

Micheva, K. D., Kay, B. K., & McPherson, P. S. (1997a). Synaptojanin forms two separate complexes in the nerve terminal. Interactions with endophilin

and amphiphysin. *J Biol Chem, 272*(43), 27239-27245. doi:10.1074/jbc.272.43.27239

Micheva, K. D., Ramjaun, A. R., Kay, B. K., & McPherson, P. S. (1997b). SH3 domain-dependent interactions of endophilin with amphiphysin. *FEBS Lett, 414*(2), 308-312. doi:10.1016/s0014-5793(97)01016-8

Miesenbock, G., De Angelis, D. A., & Rothman, J. E. (1998). Visualizing secretion and synaptic transmission with pH-sensitive green fluorescent proteins. *Nature, 394*(6689), 192-195. doi:10.1038/28190

Miller, S. E., Mathiasen, S., Bright, N. A., Pierre, F., Kelly, B. T., Kladt, N., *et al.* (2015). CALM regulates clathrin-coated vesicle size and maturation by directly sensing and driving membrane curvature. *Dev Cell, 33*(2), 163-175. doi:10.1016/j.devcel.2015.03.002

Milosevic, I. (2018). Revisiting the Role of Clathrin-Mediated Endoytosis in Synaptic Vesicle Recycling. *Front Cell Neurosci, 12*, 27. doi:10.3389/fncel.2018.00027

Milosevic, I., Giovedi, S., Lou, X., Raimondi, A., Collesi, C., Shen, H., *et al.* (2011). Recruitment of endophilin to clathrin-coated pit necks is required for efficient vesicle uncoating after fission. *Neuron, 72*(4), 587-601. doi:10.1016/j.neuron.2011.08.029

Milovanovic, D., Wu, Y., Bian, X., & De Camilli, P. (2018). A liquid phase of synapsin and lipid vesicles. *Science, 361*(6402), 604-607. doi:10.1126/science.aat5671

Mirzaa, G. M., Paciorkowski, A. R., Marsh, E. D., Berry-Kravis, E. M., Medne, L., Alkhateeb, A., *et al.* (2013). CDKL5 and ARX mutations in males with early-onset epilepsy. *Pediatr Neurol, 48*(5), 367-377. doi:10.1016/j.pediatrneurol.2012.12.030

Miyano, R., Miki, T., & Sakaba, T. (2019). Ca-dependence of synaptic vesicle exocytosis and endocytosis at the hippocampal mossy fibre terminal. *J Physiol, 597*(16), 4373-4386. doi:10.1113/JP278040

Montini, E., Andolfi, G., Caruso, A., Buchner, G., Walpole, S. M., Mariani, M., *et al.* (1998). Identification and Characterization of a Novel Serine–Threonine Kinase Gene from the Xp22 Region. *Genomics, 51*(3), 427-433. doi:10.1006/geno.1998.5391

Morton, A., Marland, J. R., & Cousin, M. A. (2015). Synaptic vesicle exocytosis and increased cytosolic calcium are both necessary but not sufficient for

activity-dependent bulk endocytosis. *J Neurochem, 134*(3), 405-415. doi:10.1111/jnc.13132

Moseley, B. D., Dhamija, R., Wirrell, E. C., & Nickels, K. C. (2012). Historic, clinical, and prognostic features of epileptic encephalopathies caused by CDKL5 mutations. *Pediatr Neurol, 46*(2), 101-105. doi:10.1016/j.pediatrneurol.2011.11.007

Mulcahey, P. J., Tang, S., Takano, H., White, A., Davila Portillo, D. R., Kane, O. M., *et al.* (2020). Aged heterozygous Cdkl5 mutant mice exhibit spontaneous epileptic spasms. *Exp Neurol, 332*, 113388. doi:10.1016/j.expneurol.2020.113388

Mundigl, O., Ochoa, G. C., David, C., Slepnev, V. I., Kabanov, A., & De Camilli, P. (1998). Amphiphysin I antisense oligonucleotides inhibit neurite outgrowth in cultured hippocampal neurons. *J Neurosci, 18*(1), 93-103.

Munoz, I. M., Morgan, M. E., Peltier, J., Weiland, F., Gregorczyk, M., Brown, F. C., *et al.* (2018). Phosphoproteomic screening identifies physiological substrates of the CDKL5 kinase. *EMBO J, 37*(24). doi:10.15252/embj.201899559

Murakami, N., Bolton, D. C., Kida, E., Xie, W., & Hwang, Y. W. (2012). Phosphorylation by Dyrk1A of clathrin coated vesicle-associated proteins: identification of the substrate proteins and the effects of phosphorylation. *PLoS One, 7*(4), e34845. doi:10.1371/journal.pone.0034845

Murakami, N., Xie, W., Lu, R. C., Chen-Hwang, M. C., Wieraszko, A., & Hwang, Y. W. (2006). Phosphorylation of amphiphysin I by minibrain kinase/dual-specificity tyrosine phosphorylation-regulated kinase, a kinase implicated in Down syndrome. *J Biol Chem, 281*(33), 23712-23724. doi:10.1074/jbc.M513497200

Nawaz, M. S., Giarda, E., Bedogni, F., La Montanara, P., Ricciardi, S., Ciceri, D., *et al.* (2016). CDKL5 and Shootin1 Interact and Concur in Regulating Neuronal Polarization. *PLoS One, 11*(2), e0148634. doi:10.1371/journal.pone.0148634

Negraes, P. D., Trujillo, C. A., Yu, N. K., Wu, W., Yao, H., Liang, N., *et al.* (2021). Altered network and rescue of human neurons derived from individuals with early-onset genetic epilepsy. *Mol Psychiatry*. doi:10.1038/s41380-021-01104-2

Nemos, C., Lambert, L., Giuliano, F., Doray, B., Roubertie, A., Goldenberg, A., *et al.* (2009). Mutational spectrum of CDKL5 in early-onset encephalopathies: a study of a large collection of French patients and review of the literature. *Clin Genet, 76*(4), 357-371. doi:10.1111/j.1399-0004.2009.01194.x

Nguyen, T. H., Maucort, G., Sullivan, R. K., Schenning, M., Lavidis, N. A., McCluskey, A., *et al.* (2012). Actin- and dynamin-dependent maturation of bulk endocytosis restores neurotransmission following synaptic depletion. *PLoS One, 7*(5), e36913. doi:10.1371/journal.pone.0036913

Nichols, R. A., Suplick, G. R., & Brown, J. M. (1994). Calcineurin-mediated protein dephosphorylation in brain nerve terminals regulates the release of glutamate. *J Biol Chem, 269*(38), 23817-23823.

Nicholson-Fish, J. C., Kokotos, A. C., Gillingwater, T. H., Smillie, K. J., & Cousin, M. A. (2015). VAMP4 Is an Essential Cargo Molecule for Activity-Dependent Bulk Endocytosis. *Neuron, 88*(5), 973-984. doi:10.1016/j.neuron.2015.10.043

Oi, A., Katayama, S., Hatano, N., Sugiyama, Y., Kameshita, I., & Sueyoshi, N. (2017). Subcellular distribution of cyclin-dependent kinase-like 5 (CDKL5) is regulated through phosphorylation by dual specificity tyrosine-phosphorylation-regulated kinase 1A (DYRK1A). *Biochem Biophys Res Commun, 482*(2), 239-245. doi:10.1016/j.bbrc.2016.11.048

Okuda, K., Kobayashi, S., Fukaya, M., Watanabe, A., Murakami, T., Hagiwara, M., *et al.* (2017). CDKL5 controls postsynaptic localization of GluN2B-containing NMDA receptors in the hippocampus and regulates seizure susceptibility. *Neurobiol Dis, 106*, 158-170. doi:10.1016/j.nbd.2017.07.002

Okuda, K., Takao, K., Watanabe, A., Miyakawa, T., Mizuguchi, M., & Tanaka, T. (2018). Comprehensive behavioral analysis of the Cdkl5 knockout mice revealed significant enhancement in anxiety- and fear-related behaviors and impairment in both acquisition and long-term retention of spatial reference memory. *PLoS One, 13*(4), e0196587. doi:10.1371/journal.pone.0196587

Olesen, L. E., Ford, M. G., Schmid, E. M., Vallis, Y., Babu, M. M., Li, P. H., *et al.* (2008). Solitary and repetitive binding motifs for the AP2 complex alpha-appendage in amphiphysin and other accessory proteins. *J Biol Chem, 283*(8), 5099-5109. doi:10.1074/jbc.M708621200

Olson, H. E., Demarest, S. T., Pestana-Knight, E. M., Swanson, L. C., Iqbal, S., Lal, D., *et al.* (2019). Cyclin-Dependent Kinase-Like 5 Deficiency Disorder: Clinical Review. *Pediatr Neurol, 97*, 18-25. doi:10.1016/j.pediatrneurol.2019.02.015

Onofri, F., Giovedi, S., Kao, H. T., Valtorta, F., Bongiorno Borbone, L., De Camilli, P., *et al.* (2000). Specificity of the binding of synapsin I to Src homology 3 domains. *J Biol Chem, 275*(38), 29857-29867. doi:10.1074/jbc.M006018200

Orenbuch, A., Shalev, L., Marra, V., Sinai, I., Lavy, Y., Kahn, J., *et al.* (2012). Synapsin selectively controls the mobility of resting pool vesicles at hippocampal terminals. *J Neurosci, 32*(12), 3969-3980. doi:10.1523/JNEUROSCI.5058-11.2012

Orlando, M., Schmitz, D., Rosenmund, C., & Herman, M. A. (2019). Calcium-Independent Exo-endocytosis Coupling at Small Central Synapses. *Cell Rep, 29*(12), 3767-3774 e3763. doi:10.1016/j.celrep.2019.11.060

Pechstein, A., Tomilin, N., Fredrich, K., Vorontsova, O., Sopova, E., Evergren, E., *et al.* (2020). Vesicle Clustering in a Living Synapse Depends on a Synapsin Region that Mediates Phase Separation. *Cell Rep, 30*(8), 2594-2602 e2593. doi:10.1016/j.celrep.2020.01.092

Pecorelli, A., Belmonte, G., Meloni, I., Cervellati, F., Gardi, C., Sticozzi, C., *et al.* (2015). Alteration of serum lipid profile, SRB1 loss, and impaired Nrf2 activation in CDKL5 disorder. *Free Radic Biol Med, 86*, 156-165. doi:10.1016/j.freeradbiomed.2015.05.010

Peden, A. A., Park, G. Y., & Scheller, R. H. (2001). The Di-leucine motif of vesicle-associated membrane protein 4 is required for its localization and AP-1 binding. *J Biol Chem, 276*(52), 49183-49187. doi:10.1074/jbc.M106646200

Pennuto, M., Dunlap, D., Contestabile, A., Benfenati, F., & Valtorta, F. (2002). Fluorescence resonance energy transfer detection of synaptophysin I and vesicle-associated membrane protein 2 interactions during exocytosis from single live synapses. *Mol Biol Cell, 13*(8), 2706-2717. doi:10.1091/mbc.e02-01-0036

Perera, R. M., Zoncu, R., Lucast, L., De Camilli, P., & Toomre, D. (2006). Two synaptojanin 1 isoforms are recruited to clathrin-coated pits at different stages. *Proc Natl Acad Sci U S A, 103*(51), 19332-19337. doi:10.1073/pnas.0609795104

Perez, C. G., Dudzinski, N. R., Rouches, M., Machta, B., Zenisek, D., & Karatekin, E. (2021). Rapid propagation of membrane tension at a presynaptic terminal. *bioRxiv*, 2021.2005.2026.445801. doi:10.1101/2021.05.26.445801

Peter, B. J., Kent, H. M., Mills, I. G., Vallis, Y., Butler, P. J., Evans, P. R., *et al.* (2004). BAR domains as sensors of membrane curvature: the amphiphysin BAR structure. *Science, 303*(5657), 495-499. doi:10.1126/science.1092586

Piriya Ananda Babu, L., Wang, H. Y., Eguchi, K., Guillaud, L., & Takahashi, T. (2020). Microtubule and Actin Differentially Regulate Synaptic Vesicle Cycling to Maintain High-Frequency Neurotransmission. *J Neurosci, 40*(1), 131-142. doi:10.1523/JNEUROSCI.1571-19.2019

Pizzo, R., Gurgone, A., Castroflorio, E., Amendola, E., Gross, C., Sassoe-Pognetto, M., *et al.* (2016). Lack of Cdkl5 Disrupts the Organization of Excitatory and Inhibitory Synapses and Parvalbumin Interneurons in the Primary Visual Cortex. *Front Cell Neurosci, 10*, 261. doi:10.3389/fncel.2016.00261

Pucadyil, T. J., & Schmid, S. L. (2008). Real-time visualization of dynamin-catalyzed membrane fission and vesicle release. *Cell, 135*(7), 1263-1275. doi:10.1016/j.cell.2008.11.020

Qu, X., Kumar, A., Blockus, H., Waites, C., & Bartolini, F. (2019). Activity-Dependent Nucleation of Dynamic Microtubules at Presynaptic Boutons Controls Neurotransmission. *Curr Biol, 29*(24), 4231-4240 e4235. doi:10.1016/j.cub.2019.10.049

Quan, A., & Robinson, P. J. (2013). Syndapin--a membrane remodelling and endocytic F-BAR protein. *FEBS J, 280*(21), 5198-5212. doi:10.1111/febs.12343

Rademacher, N., Hambrock, M., Fischer, U., Moser, B., Ceulemans, B., Lieb, W., *et al.* (2011). Identification of a novel CDKL5 exon and pathogenic mutations in patients with severe mental retardation, early-onset seizures and Rett-like features. *Neurogenetics, 12*(2), 165-167. doi:10.1007/s10048-011-0277-6

Ramjaun, A. R., Micheva, K. D., Bouchelet, I., & McPherson, P. S. (1997). Identification and characterization of a nerve terminal-enriched amphiphysin isoform. *J Biol Chem, 272*(26), 16700-16706. doi:10.1074/jbc.272.26.16700

Rao, Y., Ma, Q., Vahedi-Faridi, A., Sundborger, A., Pechstein, A., Puchkov, D., *et al.* (2010). Molecular basis for SH3 domain regulation of F-BAR-mediated membrane deformation. *Proc Natl Acad Sci U S A, 107*(18), 8213-8218. doi:10.1073/pnas.1003478107

Ren, E., Roncace, V., Trazzi, S., Fuchs, C., Medici, G., Gennaccaro, L., *et al.* (2019). Functional and Structural Impairments in the Perirhinal Cortex of a Mouse Model of CDKL5 Deficiency Disorder Are Rescued by a TrkB Agonist. *Front Cell Neurosci, 13*, 169. doi:10.3389/fncel.2019.00169

Ren, G., Vajjhala, P., Lee, J. S., Winsor, B., & Munn, A. L. (2006). The BAR domain proteins: molding membranes in fission, fusion, and phagy. *Microbiol Mol Biol Rev, 70*(1), 37-120. doi:10.1128/MMBR.70.1.37-120.2006

Ren, R., Mayer, B. J., Cicchetti, P., & Baltimore, D. (1993). Identification of a ten-amino acid proline-rich SH3 binding site. *Science, 259*(5098), 1157-1161. doi:10.1126/science.8438166

Renden, R., & von Gersdorff, H. (2007). Synaptic vesicle endocytosis at a CNS nerve terminal: faster kinetics at physiological temperatures and increased endocytotic capacity during maturation. *J Neurophysiol, 98*(6), 3349-3359. doi:10.1152/jn.00898.2007

Reshetniak, S., & Rizzoli, S. O. (2021). The vesicle cluster as a major organizer of synaptic composition in the short-term and long-term. *Curr Opin Cell Biol, 71*, 63-68. doi:10.1016/j.ceb.2021.02.007

Ricciardi, S., Kilstrup-Nielsen, C., Bienvenu, T., Jacquette, A., Landsberger, N., & Broccoli, V. (2009). CDKL5 influences RNA splicing activity by its association to the nuclear speckle molecular machinery. *Hum Mol Genet, 18*(23), 4590-4602. doi:10.1093/hmg/ddp426

Ricciardi, S., Ungaro, F., Hambrock, M., Rademacher, N., Stefanelli, G., Brambilla, D., *et al.* (2012). CDKL5 ensures excitatory synapse stability by reinforcing NGL-1-PSD95 interaction in the postsynaptic compartment and is impaired in patient iPSC-derived neurons. *Nat Cell Biol, 14*(9), 911-923. doi:10.1038/ncb2566

Rizo, J. (2018). Mechanism of neurotransmitter release coming into focus. *Protein Sci, 27*(8), 1364-1391. doi:10.1002/pro.3445

Rosendale, M., Van, T. N. N., Grillo-Bosch, D., Sposini, S., Claverie, L., Gauthereau, I., *et al.* (2019). Functional recruitment of dynamin requires

multimeric interactions for efficient endocytosis. *Nat Commun, 10*(1), 4462. doi:10.1038/s41467-019-12434-9

Rusconi, L., Kilstrup-Nielsen, C., & Landsberger, N. (2011). Extrasynaptic N-methyl-D-aspartate (NMDA) receptor stimulation induces cytoplasmic translocation of the CDKL5 kinase and its proteasomal degradation. *J Biol Chem, 286*(42), 36550-36558. doi:10.1074/jbc.M111.235630

Rusconi, L., Salvatoni, L., Giudici, L., Bertani, I., Kilstrup-Nielsen, C., Broccoli, V., *et al.* (2008). CDKL5 expression is modulated during neuronal development and its subcellular distribution is tightly regulated by the C-terminal tail. *J Biol Chem, 283*(44), 30101-30111. doi:10.1074/jbc.M804613200

Russo, S., Marchi, M., Cogliati, F., Bonati, M. T., Pintaudi, M., Veneselli, E., *et al.* (2009). Novel mutations in the CDKL5 gene, predicted effects and associated phenotypes. *Neurogenetics, 10*(3), 241-250. doi:10.1007/s10048-009-0177-1

Ryan, T. A. (1999). Inhibitors of myosin light chain kinase block synaptic vesicle pool mobilization during action potential firing. *J Neurosci, 19*(4), 1317-1323.

Saheki, Y., & De Camilli, P. (2012). Synaptic vesicle endocytosis. *Cold Spring Harb Perspect Biol, 4*(9), a005645. doi:10.1101/cshperspect.a005645

Sankaranarayanan, S., De Angelis, D., Rothman, J. E., & Ryan, T. A. (2000). The use of pHluorins for optical measurements of presynaptic activity. *Biophys J, 79*(4), 2199-2208. doi:10.1016/S0006-3495(00)76468-X

Sankaranarayanan, S., & Ryan, T. A. (2000). Real-time measurements of vesicle-SNARE recycling in synapses of the central nervous system. *Nat Cell Biol, 2*(4), 197-204. doi:10.1038/35008615

Sankaranarayanan, S., & Ryan, T. A. (2001). Calcium accelerates endocytosis of vSNAREs at hippocampal synapses. *Nat Neurosci, 4*(2), 129-136. doi:10.1038/83949

Sato, K., Ernstrom, G. G., Watanabe, S., Weimer, R. M., Chen, C. H., Sato, M., *et al.* (2009). Differential requirements for clathrin in receptor-mediated endocytosis and maintenance of synaptic vesicle pools. *Proc Natl Acad Sci U S A, 106*(4), 1139-1144. doi:10.1073/pnas.0809541106

Scala, E., Ariani, F., Mari, F., Caselli, R., Pescucci, C., Longo, I., *et al.* (2005). CDKL5/STK9 is mutated in Rett syndrome variant with infantile spasms. *J Med Genet, 42*(2), 103-107. doi:10.1136/jmg.2004.026237

Schikorski, T., & Stevens, C. F. (2001). Morphological correlates of functionally defined synaptic vesicle populations. *Nat Neurosci, 4*(4), 391-395. doi:10.1038/86042

Schindelin, J., Arganda-Carreras, I., Frise, E., Kaynig, V., Longair, M., Pietzsch, T., *et al.* (2012). Fiji: an open-source platform for biological-image analysis. *Nat Methods, 9*(7), 676-682. doi:10.1038/nmeth.2019

Schneider, C. A., Rasband, W. S., & Eliceiri, K. W. (2012). NIH Image to ImageJ: 25 years of image analysis. *Nat Methods, 9*(7), 671-675. doi:10.1038/nmeth.2089

Schroeder, E., Yuan, L., Seong, E., Ligon, C., DeKorver, N., Gurumurthy, C. B., *et al.* (2019). Neuron-Type Specific Loss of CDKL5 Leads to Alterations in mTOR Signaling and Synaptic Markers. *Mol Neurobiol, 56*(6), 4151-4162. doi:10.1007/s12035-018-1346-8

Schwarz, D. S., Ding, H., Kennington, L., Moore, J. T., Schelter, J., Burchard, J., *et al.* (2006). Designing siRNA that distinguish between genes that differ by a single nucleotide. *PLoS Genet, 2*(9), e140. doi:10.1371/journal.pgen.0020140

Sekiguchi, M., Katayama, S., Hatano, N., Shigeri, Y., Sueyoshi, N., & Kameshita, I. (2013). Identification of amphiphysin 1 as an endogenous substrate for CDKL5, a protein kinase associated with X-linked neurodevelopmental disorder. *Arch Biochem Biophys, 535*(2), 257-267. doi:10.1016/j.abb.2013.04.012

Serajee, F. J., & Huq, A. M. (2015). Homozygous Mutation in Synaptic Vesicle Glycoprotein 2A Gene Results in Intractable Epilepsy, Involuntary Movements, Microcephaly, and Developmental and Growth Retardation. *Pediatr Neurol, 52*(6), 642-646 e641. doi:10.1016/j.pediatrneurol.2015.02.011

Shang, W. H., Adachi, Y., Nakamura, A., Copeland, T., Kim, S. R., & Kamata, T. (2004). Regulation of amphiphysin1 by mitogen-activated protein kinase: its significance in nerve growth factor receptor-mediated endocytosis. *J Biol Chem, 279*(39), 40890-40896. doi:10.1074/jbc.M404527200

Shao, X., Fernandez, I., Sudhof, T. C., & Rizo, J. (1998). Solution structures of the Ca2+-free and Ca2+-bound C2A domain of synaptotagmin I: does Ca2+ induce a conformational change? *Biochemistry, 37*(46), 16106-16115. doi:10.1021/bi981789h

Shupliakov, O., Haucke, V., & Pechstein, A. (2011). How synapsin I may cluster synaptic vesicles. *Semin Cell Dev Biol, 22*(4), 393-399. doi:10.1016/j.semcdb.2011.07.006

Shupliakov, O., Low, P., Grabs, D., Gad, H., Chen, H., David, C., *et al.* (1997). Synaptic vesicle endocytosis impaired by disruption of dynamin-SH3 domain interactions. *Science, 276*(5310), 259-263. doi:10.1126/science.276.5310.259

Sim, A. T., Dunkley, P. R., Jarvie, P. E., & Rostas, J. A. (1991). Modulation of synaptosomal protein phosphorylation/dephosphorylation by calcium is antagonised by inhibition of protein phosphatases with okadaic acid. *Neurosci Lett, 126*(2), 203-206. doi:10.1016/0304-3940(91)90554-7

Simunovic, M., Voth, G. A., Callan-Jones, A., & Bassereau, P. (2015). When Physics Takes Over: BAR Proteins and Membrane Curvature. *Trends Cell Biol, 25*(12), 780-792. doi:10.1016/j.tcb.2015.09.005

Sinha, R., Ahmed, S., Jahn, R., & Klingauf, J. (2011). Two synaptobrevin molecules are sufficient for vesicle fusion in central nervous system synapses. *Proc Natl Acad Sci U S A, 108*(34), 14318-14323. doi:10.1073/pnas.1101818108

Sivilia, S., Mangano, C., Beggiato, S., Giuliani, A., Torricella, R., Baldassarro, V. A., *et al.* (2016). CDKL5 knockout leads to altered inhibitory transmission in the cerebellum of adult mice. *Genes Brain Behav, 15*(5), 491-502. doi:10.1111/gbb.12292

Slepnev, V. I., Ochoa, G. C., Butler, M. H., & De Camilli, P. (2000). Tandem arrangement of the clathrin and AP-2 binding domains in amphiphysin 1 and disruption of clathrin coat function by amphiphysin fragments comprising these sites. *J Biol Chem, 275*(23), 17583-17589. doi:10.1074/jbc.M910430199

Slepnev, V. I., Ochoa, G. C., Butler, M. H., Grabs, D., & De Camilli, P. (1998). Role of phosphorylation in regulation of the assembly of endocytic coat complexes. *Science, 281*(5378), 821-824. doi:10.1126/science.281.5378.821

Smillie, K. J., & Cousin, M. A. (2005). Dynamin I phosphorylation and the control of synaptic vesicle endocytosis. *Biochem Soc Symp*(72), 87-97. doi:10.1042/bss0720087

Smillie, K. J., & Cousin, M. A. (2012). Akt/PKB controls the activity-dependent bulk endocytosis of synaptic vesicles. *Traffic, 13*(7), 1004-1011. doi:10.1111/j.1600-0854.2012.01365.x

Snead, W. T., Zeno, W. F., Kago, G., Perkins, R. W., Richter, J. B., Zhao, C., *et al.* (2019). BAR scaffolds drive membrane fission by crowding disordered domains. *J Cell Biol, 218*(2), 664-682. doi:10.1083/jcb.201807119

Snyder, J. S., Choe, J. S., Clifford, M. A., Jeurling, S. I., Hurley, P., Brown, A., *et al.* (2009). Adult-born hippocampal neurons are more numerous, faster maturing, and more involved in behavior in rats than in mice. *J Neurosci, 29*(46), 14484-14495. doi:10.1523/JNEUROSCI.1768-09.2009

Sollner, T., Bennett, M. K., Whiteheart, S. W., Scheller, R. H., & Rothman, J. E. (1993). A protein assembly-disassembly pathway in vitro that may correspond to sequential steps of synaptic vesicle docking, activation, and fusion. *Cell, 75*(3), 409-418. doi:10.1016/0092-8674(93)90376-2

Sorre, B., Callan-Jones, A., Manzi, J., Goud, B., Prost, J., Bassereau, P., *et al.* (2012). Nature of curvature coupling of amphiphysin with membranes depends on its bound density. *Proc Natl Acad Sci U S A, 109*(1), 173-178. doi:10.1073/pnas.1103594108

Soykan, T., Kaempf, N., Sakaba, T., Vollweiter, D., Goerdeler, F., Puchkov, D., *et al.* (2017). Synaptic Vesicle Endocytosis Occurs on Multiple Timescales and Is Mediated by Formin-Dependent Actin Assembly. *Neuron, 93*(4), 854-866 e854. doi:10.1016/j.neuron.2017.02.011

Spicer, T. P., Hubbs, C., Vaissiere, T., Collia, D., Rojas, C., Kilinc, M., *et al.* (2018). Improved Scalability of Neuron-Based Phenotypic Screening Assays for Therapeutic Discovery in Neuropsychiatric Disorders. *Mol Neuropsychiatry, 3*(3), 141-150. doi:10.1159/000481731

Staley, K. (2015). Molecular mechanisms of epilepsy. *Nat Neurosci, 18*(3), 367-372. doi:10.1038/nn.3947

Stein, A., Weber, G., Wahl, M. C., & Jahn, R. (2009). Helical extension of the neuronal SNARE complex into the membrane. *Nature, 460*(7254), 525-528. doi:10.1038/nature08156

Stephen, L. J., & Brodie, M. J. (2018). Brivaracetam: a novel antiepileptic drug for focal-onset seizures. *Ther Adv Neurol Disord, 11*, 1756285617742081. doi:10.1177/1756285617742081

Sullivan, J. M. (2011). A surprisingly singular role for endophilin in synaptic vesicle recycling. *Neuron, 72*(4), 504-505. doi:10.1016/j.neuron.2011.10.025

Sutton, R. B., Fasshauer, D., Jahn, R., & Brunger, A. T. (1998). Crystal structure of a SNARE complex involved in synaptic exocytosis at 2.4 A resolution. *Nature, 395*(6700), 347-353. doi:10.1038/26412

Szule, J. A., Harlow, M. L., Jung, J. H., De-Miguel, F. F., Marshall, R. M., & McMahan, U. J. (2012). Regulation of synaptic vesicle docking by different classes of macromolecules in active zone material. *PLoS One, 7*(3), e33333. doi:10.1371/journal.pone.0033333

Takamori, S., Holt, M., Stenius, K., Lemke, E. A., Gronborg, M., Riedel, D., *et al.* (2006). Molecular anatomy of a trafficking organelle. *Cell, 127*(4), 831-846. doi:10.1016/j.cell.2006.10.030

Takeda, T., Kozai, T., Yang, H., Ishikuro, D., Seyama, K., Kumagai, Y., *et al.* (2018). Dynamic clustering of dynamin-amphiphysin helices regulates membrane constriction and fission coupled with GTP hydrolysis. *Elife, 7*. doi:10.7554/eLife.30246

Takei, K., Mundigl, O., Daniell, L., & De Camilli, P. (1996). The synaptic vesicle cycle: a single vesicle budding step involving clathrin and dynamin. *J Cell Biol, 133*(6), 1237-1250. doi:10.1083/jcb.133.6.1237

Takei, K., Slepnev, V. I., Haucke, V., & De Camilli, P. (1999). Functional partnership between amphiphysin and dynamin in clathrin-mediated endocytosis. *Nat Cell Biol, 1*(1), 33-39. doi:10.1038/9004

Tam, L. W., Ranum, P. T., & Lefebvre, P. A. (2013). CDKL5 regulates flagellar length and localizes to the base of the flagella in Chlamydomonas. *Mol Biol Cell, 24*(5), 588-600. doi:10.1091/mbc.E12-10-0718

Tan, T. C., Valova, V. A., Malladi, C. S., Graham, M. E., Berven, L. A., Jupp, O. J., *et al.* (2003). Cdk5 is essential for synaptic vesicle endocytosis. *Nat Cell Biol, 5*(8), 701-710. doi:10.1038/ncb1020

Tang, S., Terzic, B., Wang, I. J., Sarmiento, N., Sizov, K., Cui, Y., *et al.* (2019). Altered NMDAR signaling underlies autistic-like features in mouse

models of CDKL5 deficiency disorder. *Nat Commun, 10*(1), 2655. doi:10.1038/s41467-019-10689-w

Tang, S., Wang, I. J., Yue, C., Takano, H., Terzic, B., Pance, K., *et al.* (2017). Loss of CDKL5 in Glutamatergic Neurons Disrupts Hippocampal Microcircuitry and Leads to Memory Impairment in Mice. *J Neurosci, 37*(31), 7420-7437. doi:10.1523/JNEUROSCI.0539-17.2017

Tarpey, P. S., Stevens, C., Teague, J., Edkins, S., O'Meara, S., Avis, T., *et al.* (2006). Mutations in the gene encoding the Sigma 2 subunit of the adaptor protein 1 complex, AP1S2, cause X-linked mental retardation. *Am J Hum Genet, 79*(6), 1119-1124. doi:10.1086/510137

Taylor, M. J., Perrais, D., & Merrifield, C. J. (2011). A high precision survey of the molecular dynamics of mammalian clathrin-mediated endocytosis. *PLoS Biol, 9*(3), e1000604. doi:10.1371/journal.pbio.1000604

Terada, Y., Tsutsui, K., Sano, K., Hosoya, O., Ohtsuki, H., Tokunaga, A., *et al.* (2002). Novel splice variants of amphiphysin I are expressed in retina. *FEBS Lett, 519*(1-3), 185-190. doi:10.1016/s0014-5793(02)02763-1

Terzic, B., Cui, Y., Edmondson, A. C., Tang, S., Sarmiento, N., Zaitseva, D., *et al.* (2021). X-linked cellular mosaicism underlies age-dependent occurrence of seizure-like events in mouse models of CDKL5 deficiency disorder. *Neurobiol Dis, 148*, 105176. doi:10.1016/j.nbd.2020.105176

Teyra, J., Huang, H., Jain, S., Guan, X., Dong, A., Liu, Y., *et al.* (2017). Comprehensive Analysis of the Human SH3 Domain Family Reveals a Wide Variety of Non-canonical Specificities. *Structure, 25*(10), 1598-1610 e1593. doi:10.1016/j.str.2017.07.017

Thapar, A., Cooper, M., & Rutter, M. (2017). Neurodevelopmental disorders. *Lancet Psychiatry, 4*(4), 339-346. doi:10.1016/S2215-0366(16)30376-5

Thevenaz, P., Ruttimann, U. E., & Unser, M. (1998). A pyramid approach to subpixel registration based on intensity. *IEEE Trans Image Process, 7*(1), 27-41. doi:10.1109/83.650848

Tomizawa, K., Sunada, S., Lu, Y. F., Oda, Y., Kinuta, M., Ohshima, T., *et al.* (2003). Cophosphorylation of amphiphysin I and dynamin I by Cdk5 regulates clathrin-mediated endocytosis of synaptic vesicles. *J Cell Biol, 163*(4), 813-824. doi:10.1083/jcb.200308110

Traub, L. M. (2009). Tickets to ride: selecting cargo for clathrin-regulated internalization. *Nat Rev Mol Cell Biol, 10*(9), 583-596. doi:10.1038/nrm2751

Trazzi, S., Fuchs, C., Viggiano, R., De Franceschi, M., Valli, E., Jedynak, P., *et al.* (2016). HDAC4: a key factor underlying brain developmental alterations in CDKL5 disorder. *Hum Mol Genet, 25*(18), 3887-3907. doi:10.1093/hmg/ddw231

Trovo, L., Fuchs, C., De Rosa, R., Barbiero, I., Tramarin, M., Ciani, E., *et al.* (2020). The green tea polyphenol epigallocatechin-3-gallate (EGCG) restores CDKL5-dependent synaptic defects in vitro and in vivo. *Neurobiol Dis, 138*, 104791. doi:10.1016/j.nbd.2020.104791

Ubach, J., Lao, Y., Fernandez, I., Arac, D., Sudhof, T. C., & Rizo, J. (2001). The C2B domain of synaptotagmin I is a Ca2+-binding module. *Biochemistry, 40*(20), 5854-5860. doi:10.1021/bi010340c

Ubach, J., Zhang, X., Shao, X., Sudhof, T. C., & Rizo, J. (1998). Ca2+ binding to synaptotagmin: how many Ca2+ ions bind to the tip of a C2-domain? *EMBO J, 17*(14), 3921-3930. doi:10.1093/emboj/17.14.3921

Ubersax, J. A., & Ferrell, J. E., Jr. (2007). Mechanisms of specificity in protein phosphorylation. *Nat Rev Mol Cell Biol, 8*(7), 530-541. doi:10.1038/nrm2203

Valli, E., Trazzi, S., Fuchs, C., Erriquez, D., Bartesaghi, R., Perini, G., *et al.* (2012). CDKL5, a novel MYCN-repressed gene, blocks cell cycle and promotes differentiation of neuronal cells. *Biochim Biophys Acta, 1819*(11-12), 1173-1185. doi:10.1016/j.bbagrm.2012.08.001

van Bon, B. W., Coe, B. P., Bernier, R., Green, C., Gerdts, J., Witherspoon, K., *et al.* (2016). Disruptive de novo mutations of DYRK1A lead to a syndromic form of autism and ID. *Mol Psychiatry, 21*(1), 126-132. doi:10.1038/mp.2015.5

Verhage, M., Maia, A. S., Plomp, J. J., Brussaard, A. B., Heeroma, J. H., Vermeer, H., *et al.* (2000). Synaptic assembly of the brain in the absence of neurotransmitter secretion. *Science, 287*(5454), 864-869. doi:10.1126/science.287.5454.864

Verhage, M., & Sorensen, J. B. (2008). Vesicle docking in regulated exocytosis. *Traffic, 9*(9), 1414-1424. doi:10.1111/j.1600-0854.2008.00759.x

Verstreken, P., Koh, T. W., Schulze, K. L., Zhai, R. G., Hiesinger, P. R., Zhou, Y., *et al.* (2003). Synaptojanin is recruited by endophilin to promote synaptic vesicle uncoating. *Neuron, 40*(4), 733-748. doi:10.1016/s0896-6273(03)00644-5

Vigli, D., Rusconi, L., Valenti, D., La Montanara, P., Cosentino, L., Lacivita, E., *et al.* (2019). Rescue of prepulse inhibition deficit and brain mitochondrial dysfunction by pharmacological stimulation of the central serotonin receptor 7 in a mouse model of CDKL5 Deficiency Disorder. *Neuropharmacology, 144*, 104-114. doi:10.1016/j.neuropharm.2018.10.018

Vissers, L. E., Gilissen, C., & Veltman, J. A. (2016). Genetic studies in intellectual disability and related disorders. *Nat Rev Genet, 17*(1), 9-18. doi:10.1038/nrg3999

Vitezic, M., Bertin, N., Andersson, R., Lipovich, L., Kawaji, H., Lassmann, T., *et al.* (2014). CAGE-defined promoter regions of the genes implicated in Rett Syndrome. *BMC Genomics, 15*, 1177. doi:10.1186/1471-2164-15-1177

Voets, T., Toonen, R. F., Brian, E. C., de Wit, H., Moser, T., Rettig, J., *et al.* (2001). Munc18-1 promotes large dense-core vesicle docking. *Neuron, 31*(4), 581-591. doi:10.1016/s0896-6273(01)00391-9

Waites, C. L., & Garner, C. C. (2011). Presynaptic function in health and disease. *Trends Neurosci, 34*(6), 326-337. doi:10.1016/j.tins.2011.03.004

Wang, C., Wang, Y., Hu, M., Chai, Z., Wu, Q., Huang, R., *et al.* (2016). Synaptotagmin-11 inhibits clathrin-mediated and bulk endocytosis. *EMBO Rep, 17*(1), 47-63. doi:10.15252/embr.201540689

Wang, D., Zhou, Q., Ren, L., Lin, Y., Gao, L., Du, J., *et al.* (2019). Levetiracetam-induced a new seizure type in a girl with a novel SV2A gene mutation. *Clin Neurol Neurosurg, 181*, 64-66. doi:10.1016/j.clineuro.2019.03.020

Wang, H. T., Zhu, Z. A., Li, Y. Y., Lou, S. S., Yang, G., Feng, X., *et al.* (2021). CDKL5 deficiency in forebrain glutamatergic neurons results in recurrent spontaneous seizures. *Epilepsia, 62*(2), 517-528. doi:10.1111/epi.16805

Wang, I. T., Allen, M., Goffin, D., Zhu, X., Fairless, A. H., Brodkin, E. S., *et al.* (2012). Loss of CDKL5 disrupts kinome profile and event-related potentials leading to autistic-like phenotypes in mice. *Proc Natl Acad Sci U S A, 109*(52), 21516-21521. doi:10.1073/pnas.1216988110

Wang, L. H., Sudhof, T. C., & Anderson, R. G. (1995). The appendage domain of alpha-adaptin is a high affinity binding site for dynamin. *J Biol Chem, 270*(17), 10079-10083. doi:10.1074/jbc.270.17.10079

Wang, Y., Okamoto, M., Schmitz, F., Hofmann, K., & Sudhof, T. C. (1997). Rim is a putative Rab3 effector in regulating synaptic-vesicle fusion. *Nature, 388*(6642), 593-598. doi:10.1038/41580

Wasser, C. R., Ertunc, M., Liu, X., & Kavalali, E. T. (2007). Cholesterol-dependent balance between evoked and spontaneous synaptic vesicle recycling. *J Physiol, 579*(Pt 2), 413-429. doi:10.1113/jphysiol.2006.123133

Watanabe, S., Mamer, L. E., Raychaudhuri, S., Luvsanjav, D., Eisen, J., Trimbuch, T., *et al.* (2018). Synaptojanin and Endophilin Mediate Neck Formation during Ultrafast Endocytosis. *Neuron, 98*(6), 1184-1197 e1186. doi:10.1016/j.neuron.2018.06.005

Watanabe, S., Trimbuch, T., Camacho-Perez, M., Rost, B. R., Brokowski, B., Sohl-Kielczynski, B., *et al.* (2014). Clathrin regenerates synaptic vesicles from endosomes. *Nature, 515*(7526), 228-233. doi:10.1038/nature13846

Weaving, L. S., Christodoulou, J., Williamson, S. L., Friend, K. L., McKenzie, O. L., Archer, H., *et al.* (2004). Mutations of CDKL5 cause a severe neurodevelopmental disorder with infantile spasms and mental retardation. *Am J Hum Genet, 75*(6), 1079-1093. doi:10.1086/426462

Wenzel, E. M., Morton, A., Ebert, K., Welzel, O., Kornhuber, J., Cousin, M. A., *et al.* (2012). Key physiological parameters dictate triggering of activity-dependent bulk endocytosis in hippocampal synapses. *PLoS One, 7*(6), e38188. doi:10.1371/journal.pone.0038188

Werner, C., Pauli, M., Doose, S., Weishaupt, A., Haselmann, H., Grunewald, B., *et al.* (2016). Human autoantibodies to amphiphysin induce defective presynaptic vesicle dynamics and composition. *Brain, 139*(Pt 2), 365-379. doi:10.1093/brain/awv324

Wiedenmann, B., & Franke, W. W. (1985). Identification and localization of synaptophysin, an integral membrane glycoprotein of Mr 38,000 characteristic of presynaptic vesicles. *Cell, 41*(3), 1017-1028. doi:10.1016/s0092-8674(85)80082-9

Wigge, P., Kohler, K., Vallis, Y., Doyle, C. A., Owen, D., Hunt, S. P., *et al.* (1997). Amphiphysin heterodimers: potential role in clathrin-mediated endocytosis. *Mol Biol Cell, 8*(10), 2003-2015. doi:10.1091/mbc.8.10.2003

Williamson, S. L., Giudici, L., Kilstrup-Nielsen, C., Gold, W., Pelka, G. J., Tam, P. P., *et al.* (2012). A novel transcript of cyclin-dependent kinase-like 5 (CDKL5) has an alternative C-terminus and is the predominant transcript in brain. *Hum Genet, 131*(2), 187-200. doi:10.1007/s00439-011-1058-x

Winther, A. M., Jiao, W., Vorontsova, O., Rees, K. A., Koh, T. W., Sopova, E., *et al.* (2013). The dynamin-binding domains of Dap160/intersectin affect bulk membrane retrieval in synapses. *J Cell Sci, 126*(Pt 4), 1021-1031. doi:10.1242/jcs.118968

Wood, M., Daniels, V., Provins, L., Wolff, C., Kaminski, R. M., & Gillard, M. (2020). Pharmacological Profile of the Novel Antiepileptic Drug Candidate Padsevonil: Interactions with Synaptic Vesicle 2 Proteins and the GABAA Receptor. *J Pharmacol Exp Ther, 372*(1), 1-10. doi:10.1124/jpet.119.261149

Wu, W., & Wu, L. G. (2007). Rapid bulk endocytosis and its kinetics of fission pore closure at a central synapse. *Proc Natl Acad Sci U S A, 104*(24), 10234-10239. doi:10.1073/pnas.0611512104

Wu, X. S., Lee, S. H., Sheng, J., Zhang, Z., Zhao, W. D., Wang, D., *et al.* (2016). Actin Is Crucial for All Kinetically Distinguishable Forms of Endocytosis at Synapses. *Neuron, 92*(5), 1020-1035. doi:10.1016/j.neuron.2016.10.014

Wu, Y., Liang, S., Oda, Y., Ohmori, I., Nishiki, T., Takei, K., *et al.* (2007). Truncations of amphiphysin I by calpain inhibit vesicle endocytosis during neural hyperexcitation. *EMBO J, 26*(12), 2981-2990. doi:10.1038/sj.emboj.7601741

Wu, Y., Matsui, H., & Tomizawa, K. (2009). Amphiphysin I and regulation of synaptic vesicle endocytosis. *Acta Med Okayama, 63*(6), 305-323. doi:10.18926/AMO/31822

Wu, Y., O'Toole, E. T., Girard, M., Ritter, B., Messa, M., Liu, X., *et al.* (2014). A dynamin 1-, dynamin 3- and clathrin-independent pathway of synaptic vesicle recycling mediated by bulk endocytosis. *Elife, 3*, e01621. doi:10.7554/eLife.01621

Xu, W., Fang, F., Ding, J., & Wu, C. (2018). Dysregulation of Rab5-mediated endocytic pathways in Alzheimer's disease. *Traffic, 19*(4), 253-262. doi:10.1111/tra.12547

Xue, J., Graham, M. E., Novelle, A. E., Sue, N., Gray, N., McNiven, M. A., *et al.* (2011). Calcineurin selectively docks with the dynamin Ixb splice variant to regulate activity-dependent bulk endocytosis. *J Biol Chem, 286*(35), 30295-30303. doi:10.1074/jbc.M111.273110

Xue, M., Craig, T. K., Xu, J., Chao, H. T., Rizo, J., & Rosenmund, C. (2010). Binding of the complexin N terminus to the SNARE complex potentiates synaptic-vesicle fusogenicity. *Nat Struct Mol Biol, 17*(5), 568-575. doi:10.1038/nsmb.1791

Xue, M., Stradomska, A., Chen, H., Brose, N., Zhang, W., Rosenmund, C., *et al.* (2008). Complexins facilitate neurotransmitter release at excitatory and inhibitory synapses in mammalian central nervous system. *Proc Natl Acad Sci U S A, 105*(22), 7875-7880. doi:10.1073/pnas.0803012105

Yagensky, O., Kalantary Dehaghi, T., & Chua, J. J. (2016). The Roles of Microtubule-Based Transport at Presynaptic Nerve Terminals. *Front Synaptic Neurosci, 8*, 3. doi:10.3389/fnsyn.2016.00003

Yamada, H., Padilla-Parra, S., Park, S. J., Itoh, T., Chaineau, M., Monaldi, I., *et al.* (2009). Dynamic interaction of amphiphysin with N-WASP regulates actin assembly. *J Biol Chem, 284*(49), 34244-34256. doi:10.1074/jbc.M109.064204

Yamamoto, R., Li, X., Winter, S., Francke, U., & Kilimann, M. W. (1995). Primary structure of human amphiphysin, the dominant autoantigen of paraneoplastic stiff-man syndrome, and mapping of its gene (AMPH) to chromosome 7p13-p14. *Hum Mol Genet, 4*(2), 265-268. doi:10.1093/hmg/4.2.265

Yang, X., Cao, P., & Sudhof, T. C. (2013). Deconstructing complexin function in activating and clamping Ca2+-triggered exocytosis by comparing knockout and knockdown phenotypes. *Proc Natl Acad Sci U S A, 110*(51), 20777-20782. doi:10.1073/pnas.1321367110

Yao, C. K., Lin, Y. Q., Ly, C. V., Ohyama, T., Haueter, C. M., Moiseenkova-Bell, V. Y., *et al.* (2009). A synaptic vesicle-associated Ca2+ channel promotes endocytosis and couples exocytosis to endocytosis. *Cell, 138*(5), 947-960. doi:10.1016/j.cell.2009.06.033

Yao, C. K., Liu, Y. T., Lee, I. C., Wang, Y. T., & Wu, P. Y. (2017). A Ca2+ channel differentially regulates Clathrin-mediated and activity-dependent bulk endocytosis. *PLoS Biol, 15*(4), e2000931. doi:10.1371/journal.pbio.2000931

Yasumura, M., Yoshida, T., Lee, S. J., Uemura, T., Joo, J. Y., & Mishina, M. (2012). Glutamate receptor delta1 induces preferentially inhibitory presynaptic differentiation of cortical neurons by interacting with neurexins through cerebellin precursor protein subtypes. *J Neurochem, 121*(5), 705-716. doi:10.1111/j.1471-4159.2011.07631.x

Yennawar, M., White, R. S., & Jensen, F. E. (2019). AMPA Receptor Dysregulation and Therapeutic Interventions in a Mouse Model of CDKL5 Deficiency Disorder. *J Neurosci, 39*(24), 4814-4828. doi:10.1523/JNEUROSCI.2041-18.2019

Yoshida, Y., Kinuta, M., Abe, T., Liang, S., Araki, K., Cremona, O., *et al.* (2004). The stimulatory action of amphiphysin on dynamin function is dependent on lipid bilayer curvature. *EMBO J, 23*(17), 3483-3491. doi:10.1038/sj.emboj.7600355

Yu, H., Chen, J. K., Feng, S., Dalgarno, D. C., Brauer, A. W., & Schreiber, S. L. (1994). Structural basis for the binding of proline-rich peptides to SH3 domains. *Cell, 76*(5), 933-945. doi:10.1016/0092-8674(94)90367-0

Yuan, Y., Zhao, X., Wang, P., Mei, F., Zhou, J., Jin, Y., *et al.* (2019). PTENalpha regulates endocytosis and modulates olfactory function. *FASEB J, 33*(10), 11148-11162. doi:10.1096/fj.201900588RR

Yue, H. Y., & Xu, J. (2015). Cholesterol regulates multiple forms of vesicle endocytosis at a mammalian central synapse. *J Neurochem, 134*(2), 247-260. doi:10.1111/jnc.13129

Zhang, N., Gordon, S. L., Fritsch, M. J., Esoof, N., Campbell, D. G., Gourlay, R., *et al.* (2015). Phosphorylation of synaptic vesicle protein 2A at Thr84 by casein kinase 1 family kinases controls the specific retrieval of synaptotagmin-1. *J Neurosci, 35*(6), 2492-2507. doi:10.1523/JNEUROSCI.4248-14.2015

Zhou, Q., Lai, Y., Bacaj, T., Zhao, M., Lyubimov, A. Y., Uervirojnangkoorn, M., *et al.* (2015). Architecture of the synaptotagmin-SNARE machinery for neuronal exocytosis. *Nature, 525*(7567), 62-67. doi:10.1038/nature14975

Zhu, Y. C., Li, D., Wang, L., Lu, B., Zheng, J., Zhao, S. L., *et al.* (2013). Palmitoylation-dependent CDKL5-PSD-95 interaction regulates synaptic targeting of CDKL5 and dendritic spine development. *Proc Natl Acad Sci U S A, 110*(22), 9118-9123. doi:10.1073/pnas.1300003110

Zhu, Y. C., & Xiong, Z. Q. (2019). Molecular and Synaptic Bases of CDKL5 Disorder. *Dev Neurobiol, 79*(1), 8-19. doi:10.1002/dneu.22639

Zhukovsky, M. A., Filograna, A., Luini, A., Corda, D., & Valente, C. (2019). Protein Amphipathic Helix Insertion: A Mechanism to Induce Membrane Fission. *Front Cell Dev Biol, 7*, 291. doi:10.3389/fcell.2019.00291

Zoghbi, H. Y., & Bear, M. F. (2012). Synaptic dysfunction in neurodevelopmental disorders associated with autism and intellectual disabilities. *Cold Spring Harb Perspect Biol, 4*(3). doi:10.1101/cshperspect.a009886

Appendix

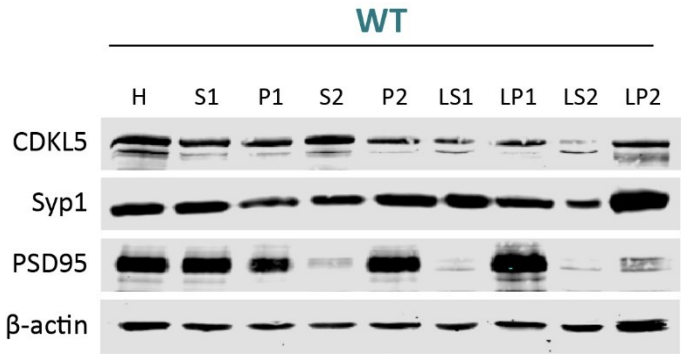

Supplementary Figure 1 CDKL5 is detected in the SV fraction derived from a mouse brain

An adult mouse brain (H) was homogenised in sucrose/EDTA solution and fractionated for isolating a crude synaptosome (P2) and crude SV (LP2) fraction. Subsequent fractions of increased purity were adjusted to 1 mg/ml and analysed by immunoblotting. CDKL5 is enriched in both the P2 and LP2 fractions. Syp1 and PSD95 were used as a pre- and postsynaptic marker, respectively, and β-actin as loading control.

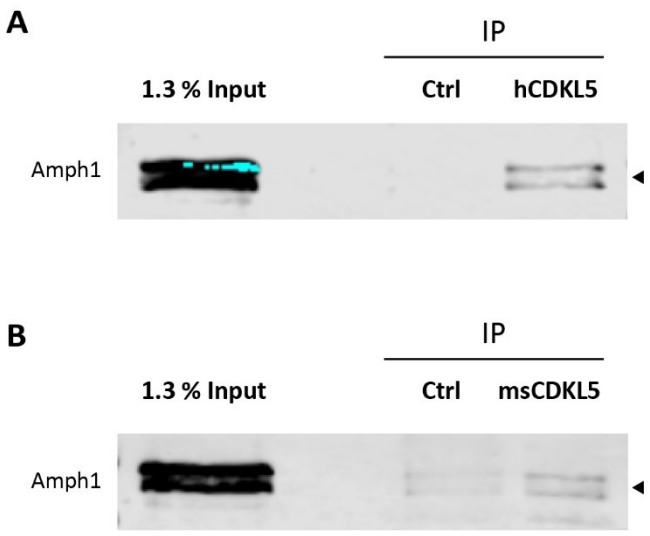

Supplementary Figure 2 Immunoprecipitation of Amph1 in the mouse brain

(**A**) Immunoprecipitation from adult rat brain lysates with CDKL5 antibody raised against a human and (**B**) a mouse epitope. Samples were analysed by immunoblotting for Amph1. A random antibody against EHD was used as control. Amph1 reacted with CDKL5 in the mouse brain.